Quantifying forest carbon stocks and changes in support of the Kyoto Protocol

Geneviève Patenaude

Linacre College

School of Geography and the Environment

University of Oxford



In fulfilment of the requirements for the

degree of Doctor of Philosophy

Hilary term 2005 [ie 2006] (LTS 31:06)

Quantifying forest carbon stocks and changes in support of the Kyoto Protocol

Geneviève Patenaude

Linacre College

School of Geography and the Environment

University of Oxford

In fulfilment of the requirements for the

degree of Doctor of Philosophy

Hilary term 2005 (i.e 2006)

This thesis brings together research conducted on field based, remote sensing and modelling approaches to meet reporting requirements set by the Kyoto Protocol. Parties are given the option to meet part of their greenhouse gases reduction requirements through the conservation and enhancement of the carbon stored in forest ecosystems. Two contrasting forests (Monks Wood, UK, 52°24' N, 0°14' W and Thetford UK, 52°30´ N, 0°30´ E) were selected for the development and assessment of the selected methods.

Field-based measurements were used to quantify carbon stocks in Monks Wood, providing the first exhaustive assessment of the carbon content held in a UK semi-natural woodland. The total carbon content of the stands varied from 346 to 616 tonnes per hectare (t ha^{-1}) and highlighted the importance of broadleaved woodlands as carbon stores in the UK. A quantitative appraisal of remote sensing methods was also provided. For land cover discrimination, both optical and radar remote sensing have been successful. For forest carbon stock estimation, LiDAR approaches may provide the only viable remote sensing tool for this purpose. As a result, a LiDAR-based method was developed and the results compared to field-based estimates. At the stand level, the agreement between the field-based and the LiDAR estimates was r=0.85. At the woodland level, due to the enhanced capability of LiDAR to monitor the natural variability of carbon across the woodland, the estimates were nearly 24% lower than those from the ground. Remote sensing of field-based approaches are unsuitable alone for quantifying below-ground carbon content and can be resource intensive. Process-based models enable an estimation of below-ground components to be made. Much uncertainty however arises from the lack of information available on model parameter values. The 3-PG model was used to simulate forest production in Thetford forest and a Bayesian calibration was applied. The results showed that this statistical approach could provide an overall framework for integrating and quantifying the uncertainty in the combined field based, remote sensing and modelling datasets, a result highly relevant in the context of the Kyoto Protocol.

Preface

This thesis brings together research conducted on a selection of methods for quantifying carbon content in UK forest ecosystems, in order to meet specific reporting requirements set by the Kyoto Protocol. This thesis is therefore fundamentally methodologically based.

Originally, I did not intend to work on such a variety of approaches. My aim was to explore the potential of optical data for meeting the reporting requirements for the UK and coupling remote sensing data with forest ecosystem modelling. The two study sites selected were ideal for this purpose, as for both sites, extensive remote sensing and field-based datasets were available from the Maestro (1989) and SHAC (2000) remote sensing campaigns. However, it became clear that optical remote sensing alone would have limited capability for quantifying forest carbon stocks at national scales, as confirmed by a large literature on this subject. In the UK context, the prevailing atmospheric conditions as well as the largely contextual spectral relationships with biomass would make it difficult to derive a relatively simple approach for use at such scales.

I hoped that my research would lead to important practical applications and possibly ease the task of reporting to the Kyoto Protocol: if the task of meeting the reporting commitments to the Protocol were straightforward and the costs for doing so reduced, political energy could be better spent on addressing the drivers of climate change instead of on the reporting logistics. I therefore decided to investigate several approaches to address this specific political issue. Too often, the political implications of scientific research are veiled behind scientific achievements, possibly because political and scientific needs are not always compatible. For instance, the forest definition provided by the Kyoto Protocol may not always meet that set by the scientific community, leading to large discrepancies in forest cover and thereby carbon store estimates. This incompatibility between definitions has led to considerable debate in the political process, exacerbated during the 7th Conference of the Parties (COP7) to the United Nations Framework Convention on Climate Change in Marrakesh (2001). This lack of compatibility has, on occasion, resulted in a deficiency of research aiming at addressing specific political aims.

As my knowledge of the political process evolved, and after field work was conducted in Monks Wood where a full carbon assessment was made, I realised that remote sensing could nevertheless become an important tool to meet specific reporting requirements, as this is probably the only means by which information can be collected repeatedly and with high frequency at national scales. Little information was then available about the appropriate approaches and costs to support the reporting to the Protocol. Consequently, I decided to address this by conducting a review of remote sensing approaches for meeting needs relevant to the Kyoto Protocol. As a consequence of this work, I was given the opportunity to contribute to the *Chapter 3: Supplementary methods and good practice guidance arising from the Kyoto Protocol* from the *Intergovernmental Panel on Climate Change (IPCC) Good practice guidance for land-use, land-use change and forestry* (IPCC 2003). To concentrate exclusively on this effort and on related contracts, I suspended my doctoral studies for several months.

After this review process and returning to full time studies, a research opportunity arose following discussions with remote sensing scientists at the Centre for Ecology and Hydrology in Monks Wood (UK), giving me access to processed LiDAR data to investigate the potential of this novel approach for the quantification of carbon in forests. At the start of the project, nothing had been published on this subject, even though LiDAR could perhaps become the most useful remote sensing approach for estimating forest carbon stocks and changes in forests (once available from satellite). I developed a method for quantifying above-ground carbon content in a UK forest ecosystem, explored the strengths and limitation of LiDAR, and identified ways in which this approach may become operational in the future.

The Protocol requires that estimates in all significant carbon pools be made. This was not possible using remote sensing alone, as although the technology enables large spatial and temporal coverage, it is not suitable for monitoring below-ground carbon stocks and changes in forest ecosystems. Field-based estimates would be practically impossible at national scales, whereas modelling approaches offered potential solutions. Additionally and in contrast to remote sensing approaches and field-based measurements, which can be thought of as empirical (determined by data collection), process-based models are fundamentally based on biological theory, thereby enabling us to assess and increase our understanding of these systems and the allocation of carbon to below-ground components.

I therefore decided to work with a well known light use efficiency process-based model. The 3-PG model provided the ideal framework for the integration of various datasets to quantify biomass and carbon content. The model had been tested in various ecosystems around the world, did not require excessive parameterisation, and was relatively simple in comparison with other process-based models. However, as all forest ecosystem modellers, I soon became confronted with the need to calibrate parameters in order to "fit" the data. Extensive discussions with Ronnie Milne and Marcel Van Oijen about the quantification of uncertainties led me to use a statistical paradigm increasingly used in science, but still relatively unknown to the field of ecology. Bayesian calibration enables the integration of various data sources for the reduction of uncertainty to parameters and model outputs. Instead of quantifying the uncertainty of a few components of a system (e.g. uncertainty of model outputs within a process-based model), the approach quantifies the uncertainty concerning the system as a whole. The Bayesian framework could provide an overall framework for integrating all available datasets pertaining to estimation and verification procedures. Indeed, an inventory of greenhouse gas emissions and removal remains incomplete until estimates of uncertainties can be made. The production of carbon stocks and change estimates at national scales necessarily involves using data of varied origins and certainty.

This thesis is submitted and formatted in accordance with the departmental guidelines set by the University of Oxford and the School of Geography and Environment. The format elected is that of at least four chapters submitted for publication in peer-reviewed journals. The following list presents the status of the papers at the time of the submission of this thesis:

Chapter 2:

Patenaude G., Milne R., Dawson T.P. (2005) Synthesis of remote sensing approaches for forest carbon estimation: reporting to the Kyoto Protocol. *Environmental Science and Policy* 8: 161-178

Chapter 3:

Patenaude G.L., Briggs B.D.J., Milne R., Rowland C.S., Dawson T.P., Pryor S.N. (2003) The carbon pool in a British semi-natural woodland. *Forestry* 76:109-119

Chapter 4:

Patenaude, G., Hill R.A., Milne R., Gaveau D.L.A., Briggs B.B.J., Dawson T.P. (2004) Quantifying forest above-ground carbon content using LiDAR remote sensing. *Remote Sensing of Environment* 93: 368-380

Chapter 5:

Patenaude G., Milne R., Van Oijen M., Dawson T.P. (Submitted) Using Bayesian calibration for the quantification of 3-PG parameter and output uncertainty: Applications for a UK Scots pine plantation *Ecological modelling*

Chapter 6:

Patenaude G., Milne R., Van Oijen M., Dawson T.P. (In prep.) The parameterisation of 3-PG for UK Corsican pine plantations using remote sensing data and Bayesian calibration (for submission in *Forest Ecology and Management)*

Acknowledgements

During my doctoral study, I had the chance to be advised by two exceptional supervisors, Ronald Milne and Terence Dawson, which provided complementary expertise into this work. Ronnie, I am forever indebted to you for sharing your expertise on carbon modelling and on the Kyoto Protocol. I am truly grateful for being always available for advice when I needed it. Terry, I would like to thank you for making this project reality. You have provided continual logistical support for the completion of this work and always offered cheerful thoughts.

Thanks are due to the British Atmospheric Data Centre for providing access to the Met Office Land Surface Observation Stations Data and to the Forestry Commission for granting me access to the GIS database for Thetford. I would like to thank the British National Space Centre - Link Carbon Offset Verification project, the Biffaward initiative and the Fonds Québécois de la Recherche sur la Nature et les Technologies for providing the funding to carry out this research.

Thanks to everyone at the Centre for Ecology and Hydrology (Edinburgh) and particularly Marcel Van Oijen and Peter Levy for their advice on statistics, Thomas Brown for his invaluable help in programming, and everyone in the lunch-time running club for helping me forget about the thesis, for a little while, everyday.

At the Centre for Ecology and Hydrology (Monks Wood), I would like to thank Clare Rowland for her early support while at the Environmental Change Institute, Oxford, Ross Hill for his contribution to the LiDAR work and Heiko Balzter and France Gerard for their generosity in providing a workspace during my visits to Monks Wood.

Very special thanks are due to Richard Waring (Oregon State University), Georgios Xenakis and Maurizio Mencuccini (University of Edinburgh) for sharing data and advice on 3-PG.

At the University of Oxford, I am grateful to Brian Briggs, for undertaking a remarkable undergraduate project which contributed to this work, to Peter Savill who provided advice on field work data collection and tree physiological characteristics and to Nick Brown for his academic input. I would like to thank Scott Henderson, Richard Pearson, Pam Berry and Rose Askew for their invaluable help with data collection.

Life as a PhD student would certainly not have been the same without the flamenco Babuchas. I am grateful to Saliha for her constant support and for bringing back the passion in me when everything seemed bleak, to Gema, Gemma, Erika, Scott and Suzana for transforming rainy Edinburgh into fiery Andalusia.

I am also grateful to Annie and Emilie "parce qu'ya un p'tit peu de chez nous la dedans", to Chiara, Daniela, Jeni, Sophie, Stephanie, and Tim for preparing real *Caffe*, for chatting about the ups and downs of PhD life, for the outings at the Cameo, or for simply making daily life extraordinary. In Oxford, thanks to Carter, Richard, James, Roby, Greger, Fran, Mandar, Jo and everyone who made my time there so special. I am forever indebted to you for support and cheerfulness throughout this PhD madness…

During the final moments, I would like to thank Bill, Elaine and Elly, without whom I would probably still be trying to debug Word.

Finally, I would like to thank my parents for being broadminded, fair, fun, adventurous, loving, thoughtful and always supportive, even in my most extravagant decisions. Sebastien, thanks for putting up with my endless silences and sleepless nights, for your consistent support and love, and for making me laugh, malgré tout, during the writing up period.

Abstract

This thesis brings together research conducted on a selection of methods to meet reporting requirements set by the Kyoto Protocol. The Protocol requires that signatory countries reduce their human-induced emissions of greenhouse gases by at least 5% below their emission levels of 1990 by 2008-2012. Parties ratifying the agreement are given the option to meet part of their reduction requirements through the conservation and enhancement of the carbon stored in forest ecosystems. To do this, they must estimate carbon stocks in 1990 and any changes since 1990 from all afforestation, reforestation and deforestation activities thus the UK will require additional monitoring and verification. To address this, three aims were defined in this thesis: (1) to design and investigate methodologies to help the UK build verification strategies of its forest carbon stocks and changes, (2) to investigate the potential for uniting methods and data sources within a process-based model framework, and (3) to find and assess an appropriate statistical approach to quantify uncertainty of a system as a whole. The methods discussed for this purpose were field-based approaches, remote sensing techniques, process-based modelling and Bayesian statistics. Two forests (Monks Wood deciduous semi-natural woodland UK, 52°24' N, 0°14' W and Thetford coniferous forest plantation UK, 52°30´ N, 0°30´ E), contrasting in terms of species composition, structure and management were selected for the development and assessment of methods. For both sites, extensive remote sensing and field-based datasets were available.

The carbon content of all significant above and below-ground forest components can only be properly estimated through ground estimation. Field-based measurements were used to quantify carbon stocks in Monks Wood, thereby providing the first exhaustive assessment of the carbon content held in a UK semi-natural woodland. The total carbon content of the five selected stands varied from 346 to 616 tonnes per hectare (t ha^{-1}). The mean carbon content of the forest components was approximately 2 t ha^{-1} for deadwood, 3 t ha^{-1} each for foliage and ground vegetation/litter, 18 t ha^{-1} for understorey shrubs and small trees, 28 tha^{-1} for all roots, 78 t ha^{-1} for overstorey trees, and 335 t ha^{-1} for soils. The results of this study suggest that if the stands sampled at Monks Wood were representative of broadleaved woodlands in the UK, they would contain 92.6 Mt carbon. This contrasts with a previous estimate of 61.9 Mt carbon, which excluded understorey vegetation, and highlights the importance of broadleaved woodlands as carbon stores.

Although exhaustive, field-based assessments are difficult to achieve at national scales. Remote sensing is a means by which information can be collected at such scales and repetitively in time. A quantitative appraisal of remote sensing methods with emphasis on their operational status was provided for (a) land cover discrimination to monitor deforestation and (b) above-ground forest carbon stocks estimation. For land cover discrimination, both optical and radar remote sensing have been successful. For forest carbon stock monitoring, radar is most appropriate until LiDAR is made available from satellite platforms. SAR backscatter techniques have been successful for the quantification of biomass in young and homogeneous coniferous woodlands but the signals saturate at high biomass. Conversely, LiDAR approaches do not suffer from this setback and may provide the only viable remote sensing tool for this purpose. The cost for acquiring space-borne optical or radar (for equal spatial coverage) is however considerably below that for acquiring airborne LiDAR data. The potential for merging low-cost, low resolution imagery with spatially resolved techniques should be further investigated until satellite missions especially designed for terrestrial carbon stock monitoring are operational.

As a result of this review, a LiDAR-based method for the quantification of forest carbon content in Monks Wood was developed. LiDAR data were acquired in June 2000, from which a digital canopy height model (DCHM) and a digital terrain model (DTM) were derived. A quantile-based approach was adopted to select a representative statistic of height per plot from which carbon content was estimated from an allometric model. Agreement of r=0.74 at the plot level was achieved between ground-based above-ground carbon content (AGCC) estimates and those derived from the DCHM. Using 20x20m grids superposed to the DCHM, the AGCC was estimated at the stand level and at the woodland level. At the stand level, the agreement between the plot data upscaled in proportion to area and the LiDAR estimates was r=0.85. At the woodland level, LiDAR estimates were nearly 24% lower than those from the upscaled plot data. This suggests that field-based approaches, which are not spatially exhaustive may not be adequate alone for carbon accounting over large areas. Conversely, the LiDAR 20x20 m grid approach has an enhanced capability of monitoring the natural variability of carbon across the woodland.

Remote sensing and field-based methods are unsuitable alone for quantifying below-ground carbon content. Although field-based methods may be suitable locally, destructive sampling

is highly resource intensive and not appropriate for national inventorying. For the quantification of below-ground carbon, remote sensing techniques are simply not applicable. Process-based models, fundamentally based on biological theory, enable an estimation of below-ground components to be made based on our understanding of the processes governing growth. Additionally, estimates of change in forest growth and carbon storage as a result of varying environmental conditions can be made, without the need for extensive data collection. Much uncertainty however arises in the use of these models especially at national scales, from the lack of information available on model parameter values. Although extensive datasets on model outputs have been collected (e.g. tree heights, stemwood biomass), often little is known about parameter values for specific case studies, as parameters may vary widely between ecosystem, species, or even genotypes, not withstanding differences arising from external environmental variability. In order to address the need to quantify biomass in above and below-ground forest ecosystems, the 3-PG model (Landsberg and Waring, 1997) was selected. This model was originally designed to address both scientific and practical needs and has been successfully applied to simulate forest production worldwide, but remained to be tested for many coniferous species in the UK. Thus the simulations were conducted for Thetford forest stands, whose management and species composition are characteristic of many coniferous ecosystems found in the UK.

For a quantification of uncertainty, a Bayesian calibration was applied. Bayesian calibration is a statistical approach enabling the quantification of uncertainty of a system as a whole, while calibrating parameters based on available data. Firstly, it provided the first full uncertainty assessment for 3-PG parameters and model outputs. Secondly, knowledge about species-specific physiological parameters was gained. Thirdly, an assessment of the model structure was made, along with suggestions as to how Bayesian calibration should be used to assess the reliability and suitability of models for providing estimates of biomass in various pools. Finally, this statistical approach provides an overall framework for integrating and quantifying the uncertainty in all available datasets, highly relevant in the context of the Kyoto Protocol.

Table of contents

Preface II
Acknowledgements VI
Abstract VIII
Table of contents XI
List of figures XV
List of tables XVII
List of acronyms and symbols XIX

CHAPTER 1
BACKGROUND AND THESIS STRUCTURE 1
1.1 ANTHROPOGENIC PERTURBATION OF THE CLIMATE SYSTEM 1
1.2 THE ROLE OF GLOBAL CLIMATE MODELS 2
1.3 UNCERTAINTY IN LAND-USE, LAND-USE CHANGE, AND FORESTRY ESTIMATES 4
1.4 THE POLITICAL RESPONSE TO CLIMATE CHANGE 7
1.5 THE UK GHG INVENTORY 10
1.5.1 The land-use change and forestry sector in the UK 11
1.5.2 Implications for the Kyoto Protocol 12
1.6 ASSUMPTIONS, AIMS AND OBJECTIVES 14
1.6.1 Assumptions 14
1.6.2 Aims 14
1.6.3 Objectives 15
1.7 STRUCTURE OF THE THESIS 16

CHAPTER 2
SYNTHESIS OF REMOTE SENSING APPROACHES FOR FOREST CARBON ESTIMATION: REPORTING TO THE KYOTO PROTOCOL 19
2.1 INTERNATIONAL AGREEMENTS AND REPORTING REQUIREMENTS: THE UK CASE STUDY 20
2.2 REMOTE SENSING FOR THE PROTOCOL 23
2.2.1 Meeting specific requirements 23
2.2.2 Inferring deforestation from land cover analyses 24
2.2.3 Quantifying forest above-ground carbon stocks 25
2.3 REMOTE SENSING FUNDAMENTALS FOR LUCF 26
2.3.1 Optical remote sensing 28
2.3.2 Radar remote sensing 31
2.3.3 LiDAR remote sensing 37
2.4 REMOTE SENSING SYNTHESIS FOR THE UK 40
2.4.1 Costs for meeting specific requirements 40
2.4.2 Reporting requirements 43
2.5 CONCLUSION AND FUTURE WORK 47

CHAPTER 3
THE CARBON POOL IN A BRITISH SEMI-NATURAL WOODLAND 50
3.1 INTRODUCTION 50

3.2 MATERIALS AND METHODS 51
3.2.1 Vegetation 53
3.2.2 Soils 55
3.2.3 Carbon content in British natural deciduous woodlands 55
3.3 RESULTS 56
3.3.1 Vegetation and soils 56
3.3.2 Carbon content in British natural deciduous woodlands 58
3.4 DISCUSSION 59
3.5 CONCLUSION 61

CHAPTER 4
QUANTIFYING FOREST ABOVE GROUND CARBON CONTENT USING LIDAR REMOTE SENSING 62
4.1 INTRODUCTION 62
4.2 DATA COLLECTION 64
4.2.1 Study area 64
4.2.2 Ground-based above-ground carbon content data (48 plots) 65
4.2.3 LiDAR ground elevation (1 m grid) and canopy elevation (1m grid) 66
4.2.4 Theodolite ground elevation (244 points) and canopy elevation (82 points) 68
4.2.5 Drymass density (49 trees) 69
4.3 MODELLING 71
4.3.1 Ground elevation (244 points) 71
4.3.2 Canopy height (82 points) 72
4.3.3 Basis for a carbon model 74
4.3.4 Stand and woodland above-ground carbon content 78
4.4 RESULTS AND DISCUSSION 78
4.5 CONCLUSIONS 83

CHAPTER 5
BAYESIAN CALIBRATION OF 3-PG FOR SCOTS PINE 85
5.1 INTRODUCTION 85
5.2 STRUCTURE OF THE 3-PG MODEL 87
5.2.1 Biomass production 87
5.2.2 Biomass allocation 88
5.2.3 Soil water balance 88
5.3 METHODS 88
5.3.1 Study site and climatic data 88
5.3.2 Model initialisation 90
5.3.3 Prescribed parameters 91
5.4 BAYESIAN CALIBRATION 91
5.4.1 The prior 92
5.4.2 The likelihood 95
5.4.3 Approximating the posterior 95
5.5 RESULTS: POSTERIOR DISTRIBUTION 97

5.5.1 Marginal posterior distributions of parameters *97*
5.5.2 Marginal posterior distributions of outputs *100*
5.5.3 Analysis of uncertainty *102*
5.6 DISCUSSION 103
5.6.1 Parameter marginal posterior distributions, θ_{MAPx}, and correlations between parameters *104*
5.6.2 Marginal posteriors distributions of outputs and analysis of uncertainty *108*
5.7 CONCLUSION 109

CHAPTER 6
BAYESIAN CALIBRATION THE 3-PG MODEL FOR CORSICAN PINE 111
6.1 METHODS 111
6.1.1 Study site, climatic data and available data *111*
6.2 BAYESIAN CALIBRATION 118
6.2.1 The prior *118*
6.2.2 The likelihood *121*
6.3 RESULTS: APPROXIMATING THE POSTERIOR DISTRIBUTION 124
6.3.1 Marginal posterior distributions of parameters and a posteriori probabilities *124*
6.3.2 Marginal posterior distributions of model outputs *134*
6.3.3 Analysis of uncertainty *141*
6.4 DISCUSSION 142
6.4.1 Marginal posterior distributions of parameters and correlations between parameters *142*
6.4.2 Marginal posterior distributions for the parameters: comparison with Scots pines *143*
6.4.3 Marginal posterior distribution of outputs: identification of key parameters and analysis of model structure *145*
6.5 CONCLUSION 148

CHAPTER 7
THESIS SUMMARY AND CONCLUSIONS 150
7.1 INTRODUCTION 150
7.2 ESTIMATING THE CARBON CONTENT OF SELECTED FOREST ECOSYSTEMS 150
7.2.1 Field-based measurements *150*
7.2.2 Remote sensing *152*
7.2.3 Process-based modelling *158*
7.3 THESIS CONCLUSION 161

REFERENCES 163

APPENDIX A
ADDITIONAL INFORMATION FOR THE SELECTED METHODS 182
8.1 EMPIRICAL FORESTRY METHODS 182
8.1.1 Carbon content of trees *182*
8.1.2 Carbon content in other pools *183*
8.2 ALTERNATIVE METHODS 184

8.2.1 Yield tables ... *184*
8.2.2 Carbon accounting models ... *185*
8.3 REMOTE SENSING ... 186
8.3.1 Overview ... *186*
8.3.2 LiDAR ... *189*
8.3.3 Hyperspectral ... *192*
8.4 ECOSYSTEM MODELLING ... 195
8.4.1 The 3-PG model ... *197*
8.5 BAYESIAN CALIBRATION ... 202
8.6 STUDY SITES ... 204
8.6.1 Monks Wood ... *205*
8.6.2 Thetford forest ... *206*
8.7 EXAMPLES OF COMMON BAND RATIOS USED FOR THE REMOTE SENSING OF VEGETATION USING MULTISPECTRAL SCANNERS ... 207
8.8 FACTORS AFFECTING THE SPECTRAL RESPONSE OF FOREST CANOPIES ... 208

APPENDIX B
LOCATION OF PLOTS AND STANDS IN MONKS WOOD AND PROPAGATION OF UNCERTAINTIES ... 209
9.1 STAND LOCATION IN MONKS WOOD ... 209
9.2 PLOT LOCATION IN MONKS WOOD ... 210
9.3 PROPAGATION OF UNCERTAINTIES ... 212

APPENDIX C
ADDITONAL INFORMATION FOR CHAPTER 4 ... 214
10.1 INTRODUCTION ... 214
10.2 THE IMPORTANCE OF SCALE: STANDS AS HOMOGENEOUS FOREST UNITS ... 215
10.3 PLOTS LOCATION ON THE DIGITAL CANOPY HEIGHT MODEL ... 217
10.3.1 Approach 1 - Parcel location using GPS data points ... *218*
10.3.2 Approach 2 - Parcel location using dominant tree heights and GPS data points ... *219*
10.3.3 Approach 3 - Parcel location using field-mapping ... *223*
10.4 HEIGHT AS A SURROGATE FOR VOLUME: VALIDATION OF THE ASSUMPTION ... 226
10.4.1 Comparison between average field-based dominant tree heights and LiDAR height metrics ... *227*
10.5 YIELD MODELS AS A BASIS FOR CARBON MODEL ... 228
10.6 WOOD DENSITY ... 229
10.7 QUANTIFYING CARBON CONTENT FROM LIDAR HEIGHT METRICS ... 230
10.7.1 AGCC from all pixels per parcel ... *231*
10.7.2 AGCC from a single DCHM canopy heights metric per parcel ... *232*

APPENDIX D
SOME USEFUL DEFINITIONS ... 240

List of Figures

Figure 1.1: Projected climatic responses to socio-economic emissions scenarios. 3
Figure 1.2: Global average annual carbon fluxes for the 1989-98 year periods 5
Figure 1.3 : The missing sink relative to the carbon budget 6
Figure 1.4: Carbon stocks in vegetation and soils across biomes 7
Figure 1.5 Thesis content outline 18
Figure 2.1: Monks Wood National Nature Reserve (UK, 157 ha) viewed from various remote sensing perspectives 27
Figure 3.1: Interval plot showing the carbon content per stand in Monks Wood. 57
Figure 3.2: Scatter plot showing above-ground carbon content and soil carbon content for the 5 stands. 58
Figure 4.1:a: Digital terrain model (DTM) against reference elevation data (m above sea level). b: Digital terrain model (DTM) residuals (m) 71
Figure 4.2: LiDAR against reference canopy height estimates (m) 73
Figure 4.3: Height distribution of plots from the five stands 76
Figure 4.4: a: Field-based AGCC and AGCC from optimised model against the LiDAR 80th height percentiles b: AGCC from optimised model against field-based estimates 77
Figure 4.5: AGCC per stand using all grid cells against AGCC from upscaled ground-based plot data 79
Figure 4.6: a: 3D view within the resulting DCHM. 80
Figure 5.1: Total woody biomass (stem, branches and bark, kg per tree) versus diameter at breast height (cm) 91
Figure 5.2: Examples of marginal posterior distributions resulting from the MCMC sampling 99
Figure 5.3: Similarity index (SRSE) between the θ_{MAPx} and the parameter vectors of highest probability 100
Figure 5.4: Mean and standard deviation (SD) of model outputs from the MCMC sample. 101
Figure 5.5: Partial correlations between parameters and model outputs 102
Figure 6.1: False color mosaicked hymap image with GIS overlay. 112
Figure 6.2: Visual contrast between (a.) normal and (b) noisy bands 114
Figure 6.3: Relationship between woody biomass and DBH. 117
Figure 6.4: Measured against heights derived from yield tables 121
Figure 6.5: Example of leaf area index change with stand growth. 122
Figure 6.6: Variance of LAI derived from remote sensing indices 124
Figure 6.7: Uncertainty reduction arising from the Bayesian calibration 126
Figure 6.8: Histograms from the sampled marginal posterior distributions for the parametersand MCMC steps 132
Figure 6.9: Histograms from the sampled marginal posterior distributions of the model outputs 138
Figure 6.10: Graphic summary of results from the MCMC sampling in comparison with available data. 140
Figure 6.11: "Fingerprint" of partial correlation between 3-PG parameters and model outputs 141
Figure 6.12: Mean model outputs from sampled marginal posterior distributions 147
Figure 6.13: Reduction of model output uncertainty from the available data. 147
Figure 6.14: Model output uncertainty as function of mean model output 147
Figure 8.1: *Pinus sylvestris* L. yield model for stemwood volume production per hectare as function of stand age. 185
Figure 8.2: Wavelengths of the electromagnetic spectrum 187
Figure 8.3: Operation of a Lidar system 190
Figure 8.4: Typical reflectance and absorption characteristics of green vegetation. 193
Figure 8.5: Hyperspectral remote sensing. Pixel values refer to the intensity of the reflectance. 194
Figure 8.6: 3-PG structure 198
Figure 8.7: A simplified example of Bayesian inference 203
Figure 8.8 Location of Monks wood and Thetford forest study sites in the UK 205

Figure 9.1: Location of each stand within the woodland 209
Figure 9.2: Plot location within each stand 212
Figure 10.1: Examples of resolutions selected to assess the spatial heterogeneity of Monks Wood. 216
Figure 10.2 Spatial heterogeneity within Monks Wood 217
Figure 10.3: Height per pixel within a circular parcel on the DCHM. 221
Figure 10.4: Selection of a suitable shape for the parcels 221
Figure 10.5: Location of the centre of the parcels 222
Figure 10.6 The sampling procedures for the selection of the parcel considering the GPS stated error. 223
Figure 10.7 Field-based above-ground carbon content against field-based average dominant tree height (a) per plot and (b) per stand 226
Figure 10.8: DCHM height metrics derived from the 20m diameter circular parcels against field-based average dominant tree height per plot. 227
Figure 10.9: Yield model selection based on DBH-age comparison between field collected tree cores and the SAB empirical yield models YC 4, 6 and 8. 229
Figure 10.10: Dry mass density from tree species in Monks Wood. 230
Figure 10.11: AGCC per parcel against AGCC per plot.. 232
Figure 10.12: Distribution of pixel heights in a 20x20m^2 circular parcel on the DCHM. 234
Figure 10.13: Approaches for scaling up the results to the woodland level 236
Figure 10.14: Replica of Figure 4.2, Chapter 4. 238
Figure 10.15: Residuals (a.) before and (b.) after the calibration of the digital canopy height model.. 238

List of Tables

Table 1.1: Total national emissions of CO_2 (Gg C) for the UK 10

Table 1.2: Emissions and removal of CO_2 (Gg C) from LUCF categories only 11

Table 1.3: Verification approaches suggested by the Intergovermental Panel on Climate Change in the *Good Practice Guidance for Land-use Land-use Change and Forestry* report (modified from IPCC 2003). 13

Table 2.1: Relevant land-use, land-use change and forestry definitions 22

Table 2.2: Synthetic Aperture Radar (SAR) biomass saturation values for various ecosystems and approaches 35

Table 2.3: Accuracy of the various SAR backscatter based models to derive stemwood volumes or biomass. 36

Table 2.4: Discrete and waveform LiDAR derived forest biomass and volume. 39

Table 2.5: Approximate magnitude of costs to acquire remote sensing and field-based data for monitoring AR since 1990, AR since 1940 and D activities in the UK. 42

Table 2.6: SAR biomass sensitivity zones for monitoring forest biomass in the UK based on P, L and C-band SAR saturation thresholds from Imhoff (1995). 45

Table 3.1: Description of the five contrasting stands in Monks Wood National Nature Reserve 52

Table 3.2: Summary of the methodology used for estimating the carbon content of the five stands 54

Table 3.3: Carbon content of all stand components (t ha^{-1}). 56

Table 3.4: Derivation of factors to convert stemwood to total carbon content. 59

Table 3.5: Bulk density and organic carbon content of Hanslope and Ragdale soils in the Melton Mowbray district in Britain (Thomasson 1971) compared with stand 1 and 4. 60

Table 4.1: Summary of the stand reference data 66

Table 4.2: Summary of the LiDAR and flight data 67

Table 4.3: Summary of 48 plots for calibration of the carbon model 70

Table 4.4: Summary statistics of residuals in the DTM and the DCHM 71

Table 4.5: Optimised model parameters for Monks Wood 77

Table 4.6; Sum of square errors (SSE) between modelled and field-based AGCC 78

Table 4.7: Total above-ground carbon content estimate of Monks Wood from different approaches 80

Table 5.1: Climate database for Thetford 90

Table 5.2: Definitions and units to the 35 3-PG parameters. 93

Table 5.3: Statistics from the MCMC sample summarising the full posterior distribution over the 19-D parameter space. 97

Table 5.4: Parameters for reduction in model output uncertainty 109

Table 6.1: Wavelength and spectral resolution of the Hyperspectral dataset. 115

Table 6.2: Definitions and units of the 3-PG parameters 119

Table 6.3: Parameters of Equation 10 as derived from PCA and NDVI 123

Table 6.4: Marginal distributions to the calibrated parameters 125

Table 6.5: Statistics from the MCMC summarising the full posterior distribution over the 22-D parameter space. 126

Table 6.6: Correlations between parameters. 133

Table 6.7: Descriptive statistics from the 60 000 MCMC models outputs sampling 139

Table 6.8: Partial correlations of $|r| > 0.6$ between parameters and model outputs 142

Table 6.9: Statistics from the marginal posterior distributions of Corsican and Scots pine parameters. 144

Table 8.1: Broad advantages and disadvantages of remote sensing approaches 188

Table 8.2: Specifications to selected airborne LiDAR systems. 191

Table 8.3: Component processes of a comprehensive ecosystem biochemical model 196

Table 10.1: Field-based metrics of dominant tree heights per plot 220

Table 10.2: British National Grid coordinates of parcel centres on the LiDAR DCHM. 225

Table 10.3: RMSE and bias calculated between DCHM height metrics and field-based average dominant tree height 228
Table 10.4: Parameters and SSE to the calibrated model at the pixel scale. 232
Table 10.5: Height statistics extracted per parcel. 233
Table 10.6: Parameters and sum of square errors resulting from the calibration of the carbon model with the given height statistic. 234

List of acronyms and symbols

Acronyms

3-PG	Physiological Processes Predicting Growth model
APAR	Photosynthetically Active Radiation Absorbed by the Canopy(PAR*fPAR)
AG	Above-Ground
AGB	Above-Ground Biomass
AGCC	Above-Ground Carbon Content
ALTM	Airborne Laser Terrain Mapper
AR	Afforestation and Reforestation
AVHRR	Advanced Very High Resolution Radiometre
BADC	British Atmospheric Data Centre
BLG	Below Ground
BNSC Earth-Observation Link	British National Space Centre programme launched in April 1995 which funds Earth Observation Systems based projects carried out by consortia consisting of at least one academic partner and at least one industrial partner
CEH	Center of Hydrology and Ecology (former Institute of Terrestrial Ecology)
COP	Conference of the Parties to the UNFCCC
DBH	Diametre at Breast Height (~1.4 metres)
DCHM	Digital Canopy Height Model
DEFRA	UK Department for Environment, Food and Rural Affairs
DGPS	Differential Global Positioning System
DHI	Directly Human-Induced
DRD	Discrete Return Device (LiDAR system)
DTM	Digital Terrain Model
FM	Forest Management
fPAR	(APAR/PAR) = dimensionless ratio corresponding to the fraction of PAR absorbed by canopy
GCM	Global Climate Model
GHG	Greenhouse Gas
GIS	Geographic Information System
GPP	Gross Primary Productivity
GPS	Global Positioning System

Gt C	Gigatonne Carbon
HyMap	Airborne Hyperspectral Scanner
INS	Inertial Navigation Units
IPCC	Intergovernmental Panel on Climate Change
LAI	Leaf Area Index (dimensionless); defined here as the projected one-sided area of leaf per ground area.
Landsat-TM	Landsat Thematic Mapper, sensor carried by Landsat 5
LiDAR	Ligth Detection And Ranging
LUCF	Land-Use Change and Forestry
LULUCF	Land-Use, Land-Use Change and Forestry
MAESTRO-1	Multi-frequency, multi-polarisation Synthetic Aperture Radar (SAR) campaign conducted in the UK in summer 1989 accompanied by a large campaign of ground data collection
MCMC	Markov Chain Monte Carlo
MIR	Middle Infrared
NDVI	Normalised Difference Vegetation Index
NIR	Near Infrared
NNR	National Nature Reserve
NPP	Net Primary Productivity
OS	Ordnance Survey
PAR	Photosynthetically Active Radiation in wavebands between 0.4 and 0.7 μm
PCA	Plant Canopy Analyzer (e.g. Li-Cor LAI-2000)
PCA	Principal Component Analysis
PEM	Production Efficiency Model
Pg C	Petagrams Carbon
RMSE	Root Mean Square Error
SAR	Synthetic Aperture Radar
SD	Standard Deviation
SHAC	SAR and Hyperspectral Airborne Campaign conducted in summer 2000 (during which extensive forestry field surveys were conducted)
SRSE	Sum of Normalised Root Square Errors
TM	Thematic Mapper
TRAC	Tracing Radiation and Architecture of Canopies instrument
UNFCCC	United Nations Framework Convention on Climate Change

VHF	Very High Frequencies - Radar system
VI	Vegetation Index
VPD	Vapour Pressure Deficit
WRD	Waveform Recording Device (LiDAR System)
YC	Yield Class

Symbols

a_S	Constant in stem mass *v* diam. Relationship
c_θ	Moisture ratio deficit which gives $f_\theta = 0.5$
f_{N0}	Value of f_N when $FR = 0$
FR	Fertility rating
g_B	Canopy boundary layer conductance (m s^{-1})
g_{Cx}	Maximum canopy conductance (m s^{-1})
i_{Rx}	Maximum fraction of rainfall intercepted by canopy
k	Extinction coefficient for PAR absorption by canopy
k_F	Number of days production lost for each frost day (days)
L_{Cx}	Canopy LAI for maximum canopy conductance (m^2 m^{-2})
L_{ix}	LAI for maximum rainfall interception (m^2 m^{-2})
m_0	Value of *m* when $FR = 0$
n_{age}	Power of relative age in f_{age}
n_{fN}	Power of (1-*FR*) in f_N
n_S	Power in stem mass *v* diam. Relationship
n_θ	Power of moisture ratio deficit in f_θ
p_2	Ratio of foliage:stem partitioning at $B = 2$ (cm)
p_{20}	Ratio of foliage:stem partitioning at $B = 20$ (cm)
r_{age}	Relative age to give $f_{age} = 0.5$
t_c	Age at full canopy cover (yr)
T_{max}	Maximum temperature for growth (°C)
T_{min}	Minimum temperature for growth (°C)
T_{opt}	Optimum temperature for growth (°C)
t_x	Maximum stand age used to compute relative age (year)
$t_{\gamma F}$	Age at which litterfall rate has median value (month)
t_σ	Age at which specific leaf area = $\frac{1}{2}(\sigma_0+\sigma_1)$ (yr)
y	Ratio NPP/GPP

α_{Cx}	Maximum canopy quantum efficiency (mol mol^{-1})
θ_{sx}	Maximum soil available water (mm)
γ_{F0}	Litterfall rate at $t = 0$ ($month^{-1}$)
γ_{F1}	Litterfall rate for mature stands ($month^{-1}$)
γ_{R}	Average monthly root turnover rate ($month^{-1}$)
η_{Rn}	Minimum fraction of NPP to roots
η_{Rx}	Maximum fraction of NPP to roots
σ_0	Specific leaf area at stand age 0 ($m^2\ kg^{-1}$)
σ_1	Specific leaf area for mature aged stands ($m^2\ kg^{-1}$)
λ	Wavelenght
P_n	Net primary production (t ha^{-1} d^{-1})
P_g	Gross primary production (t ha^{-1} d^{-1})
R_p	Rainfall per month (mm $month^{-1}$)
E_t	Evapotranspiration (mm $month^{-1}$)
i_r	Rainfall interception by the canopy (mm $month^{-1}$)
ϕ_{pa}	PAR intercepted by a stand (mol MJ^{-1})
θ_{MAP}	Parameter vector providing the maximum likelihood, given the data

Chapter 1

Background and thesis structure

This chapter sets out the scientific and political background to the thesis, underlines the aims and objectives of this work and provides a description of the thesis structure.

1.1 Anthropogenic perturbation of the climate system

The climate of the earth is variable and rapid climate changes have occurred in the past (e.g. Pfister *et al.* 1998, Cruz *et al.* 2005). Since the early 1980s, with the retrieval of isotope data from a Greenlandic ice core, it became possible to demonstrate that rapid climate change, at time-scales of human life, occurred in the past (Dansgaard *et al.* 1982, Dansgaard *et al.* 1993, Matrat *et al.* 2004, Cruz *et al.* 2005). During the Younger Dryas period (12,000-10,700 years ago), a warming of about 7 °C over a 50 years period has been estimated (Dansgaard *et al.* 1989, Houghton 2004). However, although climate change is a recurrent process, nearly always have abrupt changes considerably altered and transformed the biosphere, even leading to mass extinctions (e.g. Crowley and North, 1988).

Our climate is currently in a changing state. While it has been relatively stable for the past 10,000 years, since the 1800s, global temperatures have increased by 0.6 °C and by 2100, are expected to increase further by 1.4 to 5.8 °C (Houghton *et al.* 2001). This rapid change is beyond that believed to have occurred during the past 10,000 years (Houghton *et al.* 2001). The complete causes for the actual climate change are not well understood. However, there is an increasing scientific consensus that anthropogenic influences play an important role in the observed global warming (IPCC, 2001) (still debated, e.g. http://www.scientific-alliance.org or Bate 1998). Arguably, a principal cause for this change is anthropogenic emissions of greenhouse gases to the atmosphere. Of these, carbon dioxide (CO_2) is the most significant and abundantly human-induced. Along with other gases, it allows short-wave and visible radiation to pass through the atmosphere relatively unimpeded while trapping infrared radiation. By this process, near infrared radiation is partially absorbed or re-emitted back to the earth surface, thereby interfering with the natural radiative cooling process of the earth.

Carbon accounts for 10^{23}g of the entire $6x10^{27}$g mass of the earth and is one of the 6 principal constituents of every living organism (Schlesinger 1997). Along with hydrogen, oxygen, nitrogen and sulphur, it composes 95% of the entire biosphere and is found in the atmosphere, ocean, terrestrial vegetation and soil reservoirs. The atmosphere contains approximately 760 Petagrams Carbon (Pg C); the oceans, 39,000 Pg C; the terrestrial vegetation, 500 Pg C; and the soils, including organic detritus, 2500 Pg C (Bolin *et al.* 2000). Additionally, a very important accumulation of carbon is found as fossil organic carbon and carbonate minerals.

A small but significant portion of the carbon in these reservoirs circulates as a result of interactions between pools: a process referred to as the carbon cycle. For instance, through the processes of photosynthesis, carbon dioxide is withdrawn from the atmosphere. Conversely, through respiration processes from the vegetation itself (autotrophic respiration) and the decay of organic matter (heterotrophic respiration), CO_2 is re-emitted to the atmosphere. Circulation between reservoirs also results from interaction between vegetation and soils, as the decomposition of vegetation materials via heterotrophic activities transfers atmospheric carbon to soils. As a result of this process, soils contain globally approximately 4 times the amount of carbon held in vegetation (top 1m of soil, Watson *et al.* 2000).

Before the industrial era, and throughout the past millennium, variations in the concentration of atmospheric carbon dioxide (CO_2) were minimal and fluctuated between 275 and 285 ppmv (Ciais, 1999). Changes in atmospheric CO_2 seldom exceeded a few Pg C per decade (Ciais, 1999). However, since the dawn of the industrialised era, the extraction and burning of fossil fuels as a result of increasing demands for energy, industrial cement production, and deforestation activities have led to a consistent and rapid increase of CO_2 to 366 ppmv in 1998 (Keeling and Whorf, 1999). This consistent increase of CO_2 and other greenhouse gases has been linked to the observed increase in global mean temperature (Houghton and Skole, 1990, Houghton *et al.*, 2001).

1.2 The role of Global Climate Models

To further our understanding of the climate systems and processes controlling its variability, international efforts were made into the development of comprehensive climate models. This work, pioneered by Vilhem Bjerknes in the early 20th century, was to lead to

Global Climate Models (GCMs), which simulate mathematically the main components of the climate system (i.e. the atmosphere, oceans, land surfaces, cryosphere and biosphere) and interactions between them.

Strategies for understanding the anthropogenic influences on climate change and for making predictions involve simulating the current climate for several decades, or simulating past climates for which sufficient information has been collected, and exploring the impact of anthropogenic forcing (e.g doubled atmospheric CO_2 concentrations) on the climatic simulations. These simulations, compared with actual observations, available data or other independent simulations, enable the validation and assessment of the reliability of the GCMs. Once the reliability of the models are verified, predictions of climate change as a response to human activities can be made.

State of the art climate predictions have been conducted by the Intergovernmental Panel on Climate Change (IPCC) using various models (Houghton *et al.* 2001). These models were used to predict climate change under various scenarios of human-induced greenhouse gas emissions to inform policy making. Figure 1.1 a and b show the model predictions in global temperature and sea level change over the next century (Houghton *et al.* 2001). Under all scenarios, the models predict warmer global temperatures and higher sea levels over the next century.

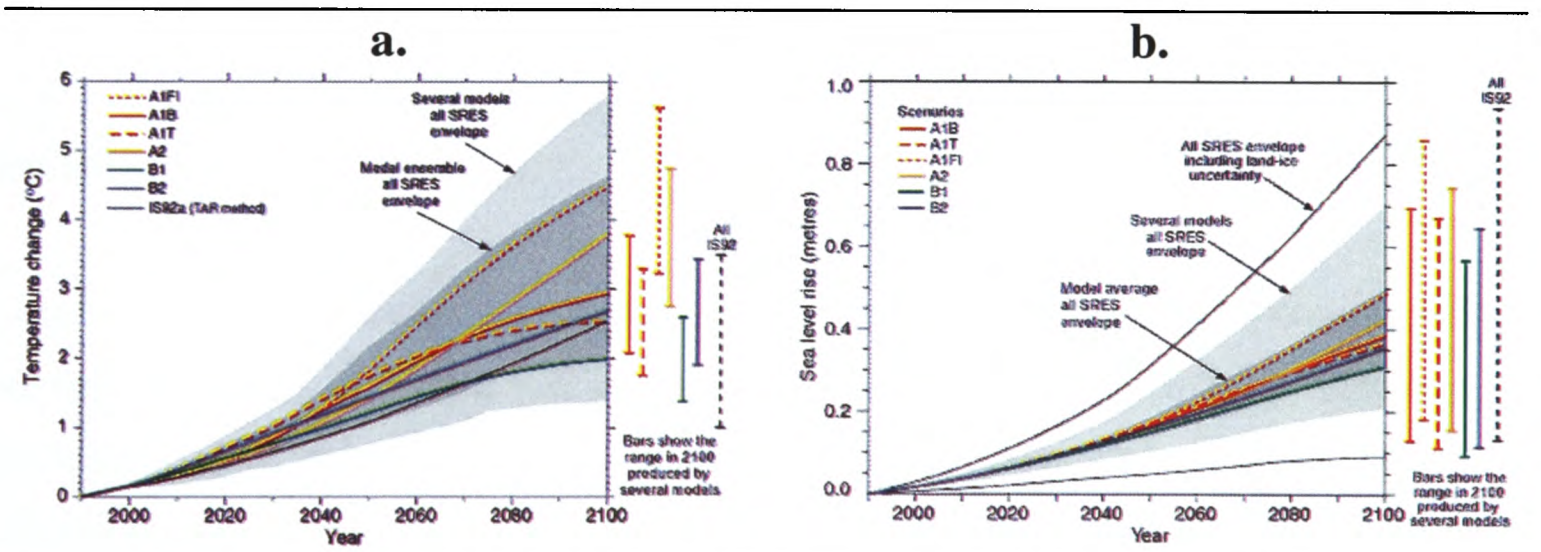


Figure 1.1: Projected climatic responses to socio-economic emissions scenarios. (adapted from Houghton *et al.* 2001).

(a) projected temperature and (b) sea level responses to socio-economic emission scenarios (adapted from Houghton *et al.* 2001). The socio-economic scenario (SRES) legend is shown in the upper left corner to each graph (A1F1 and others). In summary, these scenarios predict emissions under various economic and social circumstances. Further description of these scenarios is beyond the scope of this project. Details should be sought in Houghton *et al.* 2001. The "several models all SRES envelope" in (a) and (b) shows the sensitivity of the models to various climate variables. "All SRES envelopes" refer to the full range of 35 SRES scenarios. The "model average all SRES envelope" shows the average from these models for the range of given scenarios.

Additional predicted changes are as follow (McCarthy *et al.* 2001) :

- Increase of extremely high temperature events
- Increase in flooding in specific geographical regions
- Increase in drought, leading to extensive fires
- Increase in pest outbreak

And as clearly stated in the IPCC (McCarthy *et al.* 2001, p.65) :

> *"Observational evidence indicates that climate changes in the 20th century already have affected a diverse set of physical and biological systems. Examples of observed changes with linkages to climate include shrinkage of glaciers; thawing of permafrost; shifts in ice freeze and break-up dates on rivers and lakes; increases in rainfall and rainfall intensity in most mid- and high latitudes of the Northern Hemisphere; lengthening of growing seasons; and earlier flowering dates of trees, emergence of insects, and egg-laying in birds. Statistically significant associations between changes in regional climate and observed changes in physical and biological systems have been documented in freshwater, terrestrial, and marine environments on all continents."*

These changes could lead to disastrous consequences for ecosystems, human health and socio-economic sectors (Watson *et al.* 2000).

1.3 Uncertainty in Land-Use, Land-Use Change, and Forestry estimates

Large uncertainties remain in predicting the impact of anthropogenic activities on climate change, as shown in Figure 1.1. In this figure, different socio-economic scenarios are presented, which represent possible directions that societies might take in response to climate change. It should be noted that the "several models all SRES envelope" in Figure 1.1 (a) and (b) shows the sensitivity of the models to various climate variables. The resulting uncertainty (i.e. as to the position of the true response within the range of possible responses) is closely related to current deficiencies in our understanding of the climate system, including that of the carbon cycle, but also in the difficulty to predict how societies will react to the need to address climate change. While current emissions of CO_2 arising from the burning of fossil fuels or cement production can be assessed quite accurately, large

uncertainties remain in estimating sources and removal of CO_2 particularly from Land-use, Land-use Change, and Forestry activities (LULUCF). Poor agreement is reached by current approaches for estimating LULUCF fluxes (Prentice *et al.* 2001), to some extent as a result of differences in definitions of land cover types and in inconsistency between data sources. Until these uncertainties are addressed, our understanding of the carbon cycle will remain incomplete.

Figure 1.2 presents estimates of the average annual budget of CO_2 fluxes. Uncertainties in estimates of all emissions and removal categories over the 1989-1998 period are also given. Note that the largest uncertainty pertains to the removal of CO_2 from terrestrial ecosystems.

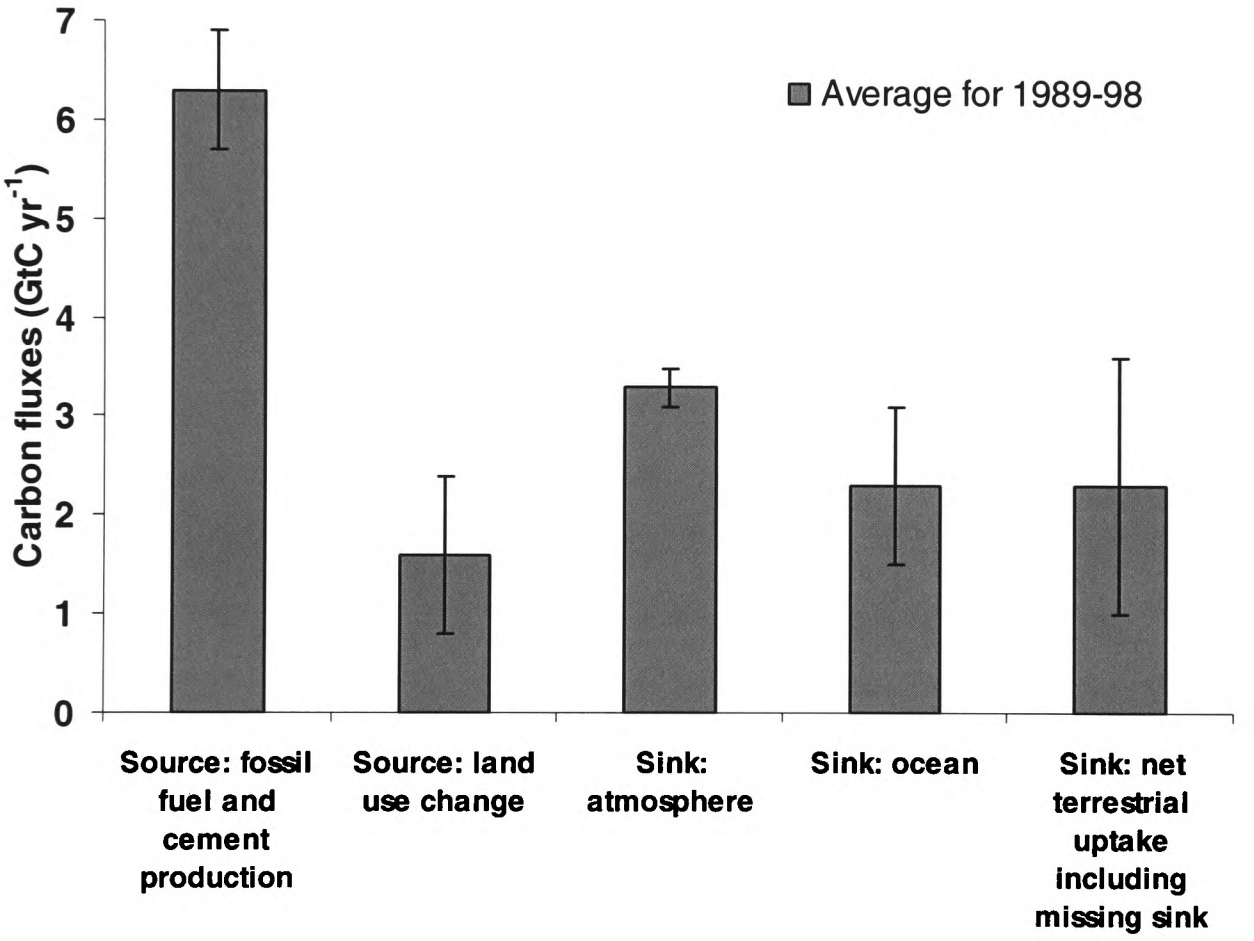


Figure 1.2: Global average annual carbon fluxes for the 1989-98 year periods(data from Watson *et al.* 2000). Error limits correspond to an estimated 90% confidence interval

Emissions from fossil fuel burning and cement production are about 6.3 Pg C annually. Of these, nearly 3.3 Pg C and 2.3 Pg C are absorbed by the atmosphere and the oceans respectively. The remaining 0.7 Pg C is attributed to a terrestrial uptake. However, if emissions from land-use change are also considered in the budget (1.7 Pg C annually), an equivalent sink or uptake of this order of magnitude is missing (Figure 1.3).

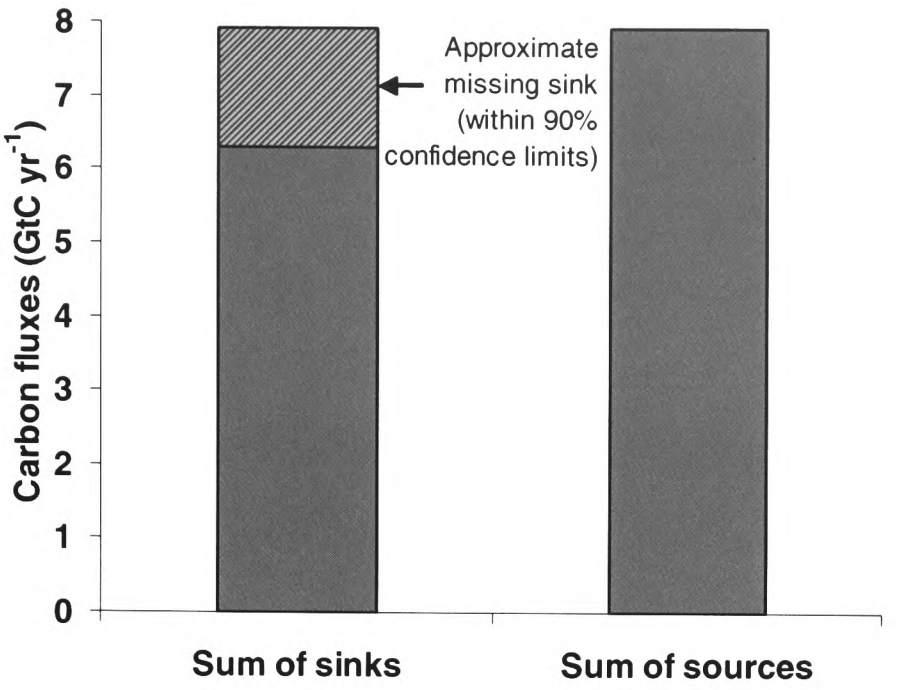


Figure 1.3 : The missing sink relative to the carbon budget (data from Watson *et al.* 2000)

There is considerable uncertainty about the magnitude of this missing sink but even larger uncertainty exists about its location. A probable location is in forest ecosystems (Malhi *et al.* 1999, Rayner *et al.* 1999, and Bousquet *et al.* 2000). Schimel *et al.* (2000) and Fehse *et al.* (2002) also suggested that many ecosystems currently in a regeneration state are not accounted for in the current budget. Other factors, such as carbon (Saxe *et al.* 1998, Norby *et al.* 1999) and nitrogen fertilisation (Vitousek *et al.* 1991, Vitousek *et al.* 1993) may also be associated with this missing sink. Difficulties in estimating emissions and removal of carbon from LULUCF activities arise from the fact that carbon stocks vary widely between the different biomes, as shown in Figure 1.4, and so does their contribution to atmospheric carbon fluxes. It should be noted that compared to other vegetation types, forests ecosystems represent the largest carbon store.

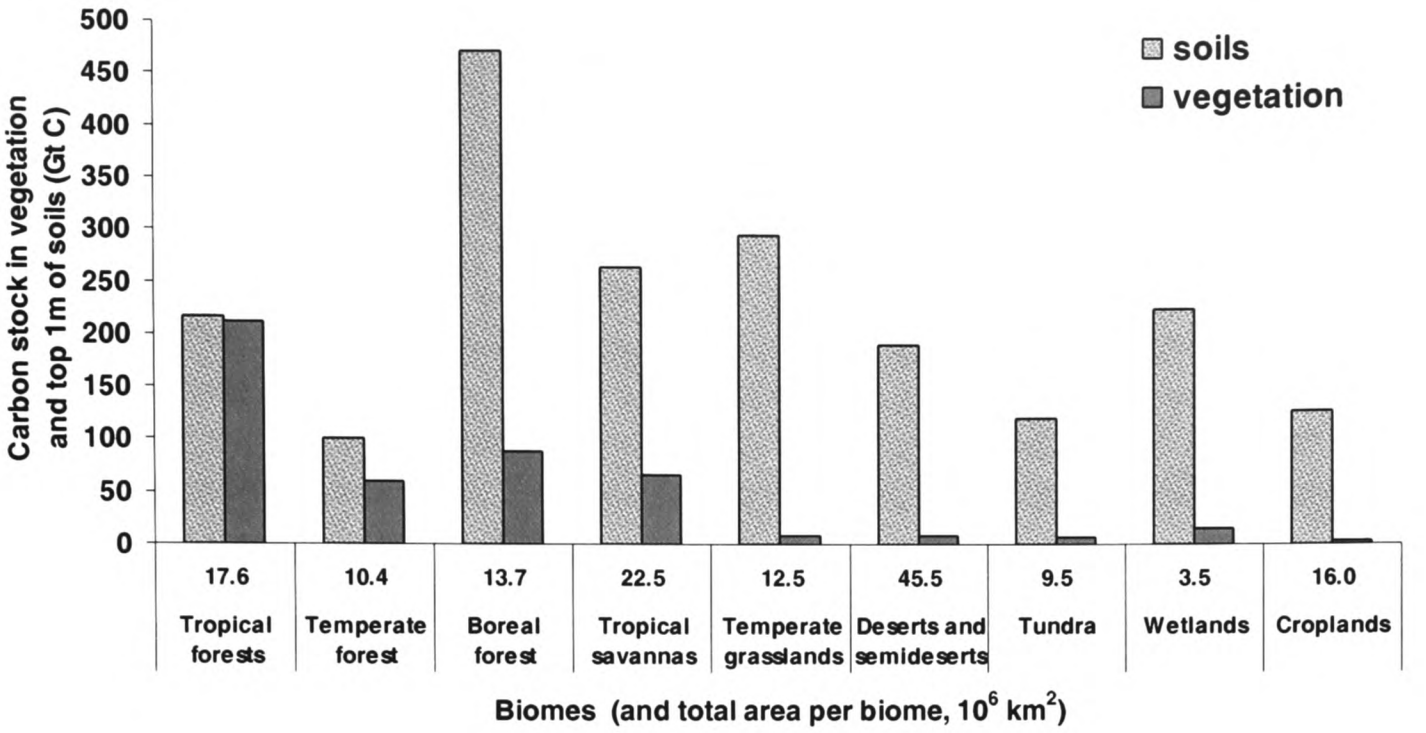


Figure 1.4: Carbon stocks in vegetation and soils across biomes (data from Watson *et al.* 2000).

1.4 The political response to climate change

Given the current and predicted climate change, there is a clear need to:

(i) Reduce anthropogenic emissions of CO_2

(ii) Conserve carbon stores and enhance carbon sinks from LULUCF activities

(iii) Reduce and quantify uncertainty in carbon stock and stock change estimates.

The fact that responsibility should be taken globally to address climate change and global warming was first recognised internationally at the Earth Summit in 1992. Since, several international agreements have come into force in order to address these needs. In particular, the United Nations Framework Convention on Climate Change (UNFCCC, 21st March 1994)[1] and the Kyoto Protocol (16th February 2005)[2] indicated an international recognition of the need to reduce emissions of carbon dioxide (CO_2) but also of methane (CH_4), nitrous oxide (NO_2), hydrofluorocarbons (HFCs), perfluorocarbons (PFCs) and sulphur hexafluoride (SF_6). Although under the UNFCCC parties are required to estimate annually their greenhouse gas emissions and removal, only the Kyoto Protocol is legally binding. Under the Protocol, countries are specifically required to reduce their directly human-induced (DHI) emissions by at least 5% below their 1990 level[3] by 2008-2012.

[1] Date of entry into force of the UNFCCC
[2] Date of entry into force of the Kyoto Protocol
[3] Each Party is assigned a specific reduction target (some Parties, such as Ireland, do not need to reduce their emissions). Overall, the reduction should be of 5% below the 1990 level.

In addition to reducing emissions, Article 3 Paragraphs 3 and 4 of the Kyoto Protocol allow for carbon sinks contained in the terrestrial vegetation to balance these emissions (UNFCCC, 1997):

> *"The net changes in greenhouse gas emissions by sources and removal by sinks resulting from direct human-induced land-use change and forestry activities, limited to afforestation, reforestation and deforestation since 1990, measured as verifiable changes in carbon stocks in each commitment period, shall be used to meet the commitments under this Article of each Party included in Annex I [of the UNFCCC]."*

and

> *" [...] The Conference of the Parties [...] shall [...] decide [...] which additional human-induced activities related to changes in greenhouse gas emissions by sources and removal by sinks in the agricultural soils and the land-use change and forestry categories shall be added to, or subtracted from, the assigned amounts for Parties included in Annex I. [...] A Party may choose to apply such a decision on these additional human-induced activities for its first commitment period, provided that these activities have taken place since 1990"*

The additional activities were subsequently defined as revegetation, forest, cropland and grazing land management (Table 2.1) (UNFCCC, 2001).

The Kyoto Protocol requires firstly that Parties take domestic actions for the purpose of meeting their emission limitation and reduction commitments. Secondly it provides "flexibility mechanisms" by which Parties can reduce the cost of curbing their emissions through lowering emissions or enhancing sinks abroad. This system is based on the premise that the impact of greenhouse gas emission reduction on the atmosphere is independent of the location where those reductions are achieved. The joint implementation mechanism (Article 6) allows countries listed in the Annex 1 to the UNFCCC to implement projects in other Annex 1 countries. The Clean Development Mechanism (Article 12) enables Annex 1 Parties to implement emissions reduction and afforestation and reforestation sink-enhancing projects in non-Annex 1 countries. Finally, emission trading (Article 17) entitles Annex 1 countries to trade units of emissions or removal of greenhouse gas with other Annex 1 countries.

Scientifically, this reporting raises a debate about the adequacy of methodologies available to monitor and report carbon stocks and stock changes in land vegetation. Although monitoring and modelling approaches have been designed to quantify emissions and

removal of CO_2 from LULUCF activities, these fluxes vary considerably in space and time and large discrepancies exist between estimates and results (Cramer *et al.* 1999, Watson *et al.* 2000, Prentice *et al.* 2001). However, as stated in Article 3.4 and 5.1 of the Protocol (UNFCCC, 1997):

> *"[...]each Party included in Annex I [of the UNFCCC] shall provide [...] data to establish its level of carbon stocks in 1990 and to enable an estimate to be made of its changes in carbon stocks in subsequent years."*

> *"[...]each Party included in Annex I [of the UNFCCC] shall have in place, no later than one year prior to the start of the first commitment period, a national system for the estimation of anthropogenic emissions by sources and removal by sinks of all greenhouse gases not controlled by the Montreal Protocol".*

To ensure that national estimates provided to the UNFCCC and the Kyoto Protocol are comprehensive, transparent, consistent, accurate, and verifiable as far as practicable, the IPCC provides methodological guidance for the development, update and publication of the national inventories (IPCC 1997a, 1997b, 1997c). Moreover, the *Good Practice and Uncertainty Management in National Greenhouse Gas Inventories* report (IPCC 2000) supplies assistance for reducing sources of uncertainties. Good practice in uncertainty management related to the Land-use Change and Forestry sector were dealt with in a separate guide: the *Good Practice Guidance for Land-use Land-use Change and Forestry* report (IPCC 2003), which includes additional guidance for meeting the reporting requirements specific to the Kyoto Protocol. These guidelines were designed to assist Parties to the UNFCCC in producing their annual inventories of greenhouse gas emissions and removal for 1990 onwards, including emissions and removal from LULUCF activities, but also serve as a basis for producing data relevant to the Kyoto Protocol.

In these guidelines, six sectors of anthropogenic activity generating significant atmospheric CO_2 emissions were defined (IPCC 1997a). In the UK, those where emissions and removals of CO_2 are significant are (numbers refer to the IPCC categories):

1. The energy sector
2. The industrial processes sector
5. The waste disposal and treatment sector
6. The land-use change and forestry sector

Two additional sectors, the solvent and other product use sector (3), and the agriculture sector (4) are not considered to contribute significantly to CO_2 emissions thus were not included here.

The energy sector (1) assembles fugitive emissions arising from coal mining, oil and gas operations but most importantly, emissions emerging from stationary (e.g. households or combustion plants) or mobile sources (e.g. vehicles) (IPCC 1997a, 1997b, 1997c). Emissions from industrial processes (2) include that from cement, lime, iron and steel production. The incineration or decomposition of industrial and municipal biomass waste also produce emissions of CO_2 and are considered under (5). Finally, emissions and removal of CO_2 from Land-use Change and Forestry (LUCF) activities (6) include that arising from changes in woody biomass stocks, forest and grassland conversion (e.g. deforestation) and changes in soil carbon.

1.5 The UK GHG inventory

The UK national estimates of emissions and removal are summarised in the latest national communication to the UNFCCC secretariat (DEFRA, 2001). Carbon dioxide emissions and removal from the significant sectors of anthropogenic activities and from categories within the LUCF sector are provided in Table 1.1 and Table 1.2.

Table 1.1: Total national emissions of CO_2 (Gg CO_2) for the UK (derived from DEFRA, 2001). Positive values are fluxes to the atmosphere; negative values represent uptake from the atmosphere.

	1990		**1999**	
Sector of activities	**Emissions**	**Removal**	**Emissions**	**Removal**
Energy	568,692	–	518,049	–
Industrial	14,123	–	13,480	–
Waste	663	–		–
LUCF	19,348	-10,556	16,271	-11,539

Table 1.2: Emissions and removal of CO_2 (Gg C) from LUCF categories only

	1990		1999	
LUCF categories	**Emissions**	**Removal**	**Emissions**	**Removal**
Changes in Forest and other biomass stock [a.]	–	-9,456	–	-10,439
CO_2 emissions and removal from soils [b.]	15,439	–	12,663	–
Others [c.]	3,908	-1,100	3,608	-1,100

[a.] Includes removal to forest litter and forest products.

[b.] Removal to soils due to set aside of arable land and emissions due to liming.

[c.] Includes emissions from soils due to upland drainage and peat extraction. Removal are from an increase in forest and other biomass.

The largest source of emissions is the energy sector. Emissions from this sector are at least one order of magnitude larger than that from all other sources. Emissions from the industrial sector and LUCF activities are of comparable magnitude to each other. The LUCF sector is, however, distinctive in that it produces both emissions and removal of CO_2.

1.5.1 The land-use change and forestry sector in the UK

In the UK, the following land-use change and forestry (LUCF) categories produce significant emissions and removal of atmospheric CO_2:

(i) Changes in forest and other woody biomass stocks: fluxes from an increase or reduction in forest biomass. This includes changes from forest growth, afforestation, reforestation, deforestation activities and forest management.

(ii) CO_2 emissions and removal from soils: fluxes associated with land-use change and management.

(iii)Others: fluxes arising from activities not included in the other LUCF categories.

Estimates of these emissions and removal are provided by the Centre for Ecology and Hydrology (http://www.nbu.ac.uk/ukcarbon/). Estimates of carbon uptake by growing forests planted since 1920 are made each year using a carbon accounting model based on forestry yield tables, growth rates, harvesting pattern and areas of newly planted forests provided by the Forestry Commission. There is the assumption that all harvested forests are restocked. The model calculates the carbon mass in trees, wood products, litter and soils. Estimates of removal and carbon fluxes to the soil carbon pool from afforestation and reforestation activities are also considered. Changes in soil stocks due to other land-use

change are estimated from a dynamic model of gain or loss of carbon and a matrix of land-use change for the UK.

1.5.2 Implications for the Kyoto Protocol

Although the UK has an inventorying framework, a system for the periodic monitoring and verification of UK forest carbon stocks and changes is required to establish the reliability and the accuracy of the national inventory. As stated in the Marrakech Accords: "*Inventory activities include [...] carrying out procedures for the verification of the inventory data at the national level [...]*" (UNFCCC, 2001).

Several approaches are currently being investigated for this purpose. Firstly, Forest Research has proposed the use of the National Inventory of Woodland and Trees (Forestry Commission, 2001), based on aerial photography and ground surveys. This inventory gathers information on the extent of forest cover, timber production, and wider environmental aspects of UK forests. Although exhaustive and partly based on ground surveys, the approach proposed for estimating carbon stocks and changes from these databases relies on the same forest production models and databases as that used in the current national inventory (Matthews and Broadmeadow 2003). This lack of independence could preclude the use of this approach for verification purposes.

Likewise, the Centre for Terrestrial Carbon Dynamics is investigating the potential for the fusions of technologies to measure gas exchanges between UK land surfaces and the atmosphere (http://www.shef.ac.uk/ctcd/, Grace *et al.* 2004). The technologies considered consist of field-based and remote sensing-derived land cover datasets, gas exchange models calibrated using eddy-covariance flux data for specific land-uses, and atmospheric gas concentration measured from European tall towers. Although a potentially promising approach, no results have yet been published and the reliability of the approach remains to be assessed. The need for representative samples of eddy covariance and tall tower gas measurements for specific land-uses is a foreseeable limitation of the approach. The temporal and spatial variability of these measurements may be large thus requiring a large statistical sample. Additionally, to upscale the results from local to national levels requires a full understanding of the uncertainties involved.

Table 1.3 categorises the verification approaches suggested by the IPCC (2004). Five broad categories have been identified. Approach 1 and 2 are not suitable for the UK as the current LULUCF inventory is based on the highest tier method. As such, global inventories and independent datasets are likely to be of lower resolution and accuracy as that currently used. Approaches 3, 4 and 5, or a combination of these, should therefore be considered.

Table 1.3: Verification approaches suggested by the Intergovermental Panel on Climate Change in the *Good Practice Guidance for Land-use Land-use Change and Forestry* report (modified from IPCC 2003).

	Approach 1 **Comparison with other inventories and other independent datasets**	**Approach 2** **Applying higher tier methods detailed in the GPG for LULUCF**	**Approach 3** **Direct measurements**	**Approach 4** **Remote sensing**	**Approach 5** **Modelling**
Land area	Suitable [a.]	Suitable [a.]	N.A.	Suitable	N.A.
Carbon pools					
ABG biomass	Suitable [a.]	Suitable [a.]	Suitable[b.]	Suitable[c.]	Suitable (regression ecosystem and growth models)
BLG biomass	Suitable [a.]	Suitable [a.]	Suitable[b.]	N.A.	Applicable (ecosystem and inventory-based models)
Dead Wood	Suitable [a.]	Suitable [a.]	Suitable[b.]	N.A.	Suitable (ecosystem and inventory-based models)
Litter	Suitable [a.]	Suitable [a.]	Suitable[b.]	N.A.	Suitable (ecosystem and inventory- based models
Soil organic matter	Suitable [a.]	Suitable [a.].	Suitable[b.]	N.A.	Suitable (ecosystem and inventory- based models
Emission factors	Suitable [a.]	Suitable [a.].	Suitable[b.]	N.A.	Suitable (ecosystem models)
Activity/land-based report					
Forest, grassland, cropland and other land-uses	Suitable [a.]	Suitable [a.]	Suitable[b.]	Suitable[d.]	Suitable (data intensive, can be an alternative approach when estimates from direct measurements and remote sensing are not available
ARD	Suitable [a.]	Suitable [a.]	Suitable[b.]	Suitable[d.]	Not practical

N.A. Not applicable, BLG: below ground, ABG: above ground, ARD: Afforestation, Reforestation and Deforestation activities

[a.] If data available

[b.] Resource intensive

[c.] Ground data needed

[d.] Particularly to identify land cover/land-use and their changes

1.6 Assumptions, aims and objectives

1.6.1 Assumptions

This thesis is based on the assumptions that:

Climate change is in part caused by external anthropogenic forcing, an assumption endorsed by the IPCC and through international agreements such as the Kyoto Protocol. Global warming is believed to be caused by greenhouse gases emissions in the atmosphere, including CO_2. A reduction in emissions of greenhouse gases can help to abate global warming.

The Protocol's first endeavour is to bind countries to reduce their greenhouse gas emissions. Forestry related activities have been included into the process as a means to increase terrestrial carbon stores and thereby, reduce atmospheric concentrations of carbon dioxide. Forest ecosystems, through the processes of photosynthesis, can store large amounts of carbon. Reducing deforestation activities and increasing the total forested surface area should help maintain/decrease the concentration of carbon dioxide in the atmosphere.

1.6.2 Aims

Within this context, this thesis has three principal aims.

1. To assess and develop methodologies to help build verification strategies for the UK, specifically for monitoring carbon stocks and stock changes in forest ecosystems. The methodologies proposed lie within the broader approaches 3-4-5 enumerated in Table 1.3.
2. To investigate a potential fusion of methodologies. At the national scale, the information available often originates from a wide variety of inadequate or incomplete datasets, thus methodologies should be combined for generating the inventory estimates.
3. To find and assess a statistical approach that enables the quantification of the joint uncertainty from combined datasets.

1.6.3 Objectives

In order to achieve these aims, the following objectives and sub-objectives were defined:

1. Estimate the carbon content of selected forest ecosystems from:

Field-based measurements

i. Comprehensively estimate the carbon content of a semi-natural, deciduous woodland, including that held in above and below-ground overstorey and understorey biomass, ground vegetation and litter, deadwood and soils. No such exhaustive quantification has been conducted in the UK.

ii. Discuss the implication of the results for verification purposes and for national inventory.

Remote sensing

iii. Review the potential of existing approaches (a.) for quantifying forest above-ground carbon content and (b.) for assessing forest to non forest land cover change.

iv. Provide estimates of costs to acquire remote sensing datasets, specifically to address the objectives iii (a.) and iii (b.).

v. Assess which remote sensing approach is currently most adequate for the quantification of above-ground carbon content in UK forests.

vi. Assess whether there exists new promising developments in the field, leading to nascent remote sensing techniques for this purpose.

vii. Based on (vi), develop a carbon quantification method from this approach, which can be applied to heterogeneous deciduous woodlands.

Forest ecosystem modelling

viii. Select a widely used, but relatively simple, process-based model for potential use by the wider community.

ix. Assess the potential of the selected model for quantifying above-ground biomass, from which carbon content and changes can be estimated.

2. Use the selected forest model as a framework for integration of various datasets.

3. Select a statistical approach for quantifying the uncertainty in biomass stock or change estimates when different sources of data were used to provide this estimate.

1.7 Structure of the thesis

Figure 1.5 outlines diagrammatically the structure of the thesis, which comprises 7 chapters.

Chapter 1 comprises introductory material to the thesis, introduces the rationale, aims and objectives of the research and provides a general outline of the manuscript. Readers unfamiliar with the approaches presented in this thesis can refer to Appendix A, which introduces the selected approaches and methodologies for quantifying carbon content.

Chapters 2, 3 and 4 specifically address aim #1. Chapter 2 reviews the potential of remote sensing approaches for meeting specific requirements to the Kyoto Protocol. A detailed description of existing techniques for quantifying above-ground carbon content and forest to non forest land-use change is presented to address UK reporting needs. This chapter is the first published quantitative review of remote sensing approaches for meeting explicit political challenges set by the Kyoto Protocol. Chapter 3 presents the field-based data collection and analysis conducted in Monks Wood NNR. In this chapter, the method for comprehensive estimation of carbon in all significant pools of the forest is presented. Implications of the results for national scale estimation of UK forest carbon stocks are discussed. Further details on the location of the surveyed stands and plots are provided in Appendix B. Chapter 4 presents the LiDAR-based quantification of above-ground carbon content in Monks Wood. The strengths and weaknesses of the methodology are discussed in comparison with the results in Chapter 3. Supplementary methodological details are provided in Appendix C.

Chapters 5 and 7 address the aims #2 and #3. The 3-PG process-based model for simulating forest production and biomass stocks is described and tested. The data available for Thetford forest enabled testing the suitability of the model for two coniferous species. In parallel, these chapters present a Bayesian calibration for uncertainty quantification which integrates various datasets such as remote sensing indices of leaf material, estimates of foliage, stem and root biomass and forestry yield tables. These chapters differ in their application of the Bayesian calibration. In Chapter 5, the approach is used to quantify uncertainty to parameters and outputs of 3-PG for simulating the growth of Scot pine

stands. Only a limited amount of data was available for the research. In Chapter 6, supplementary data on Corsican pine variables were available. Both chapters discuss the potential of the 3-PG model for estimating stand growth in a UK context and the strengths and limitations of using a Bayesian calibration for quantifying uncertainties.

Chapter 7 is the concluding chapter. It synthesises the contribution of this thesis to meet specific monitoring needs for the Kyoto Protocol. Areas of weaknesses in the methods presented, where further research is needed, are identified and discussed.

Finally, a list of useful definitions of specialised terms used in this thesis are provided in Appendix D.

Introduction

Chapter 1

- Introduces the political and scientific rationale of the thesis
- Defines the aims and objectives
- Describes the Monks Wood NNR and Thetford forests study sites.
- Describes the structure of the manuscript

Appendices A, B, C and D

- Introduces the various techniques and approaches discussed in the thesis
- Provides supplementary methodological information relevant to the methods used.

Field Sites

Remote sensing

Field-based measurements

Modelling and uncertainty assessment

Chapter 2 (in press)

- Describes existing remote sensing approaches
- Reviews their potential for meeting specific reporting requirements to the Kyoto Protocol
- Justifies the use of LiDAR remote sensing for the development of a carbon accounting method
- Appendix A provides additional information on optical remote sensing

Monks Wood NNR Site

Chapter 4 (published)

- Describes a novel approach for carbon accounting using LiDAR canopy height measurements and modelling approach
- Identifies the advantages and limitations of this approach.
- Appendix C provides supplementary methodological details

Chapter 3 (published)

- Describes the field data collection
- Integrates all carbon pools for a full assessment of the carbon content of Monks Wood NNR
- Determines the implications of these results for national inventory of UK forest carbon stocks
- Appendix B provides maps of the location of the stands and plots within the woodland

Thetford Forest Site

Chapter 5 (submitted) and 6 (in prep.)

- Describes the 3-PG process-based model
- Estimates biomass stock changes for coniferous species
- Quantifies uncertainty using a Bayesian approach
- Discusses the potential of the approach for verification

Conclusion

Chapter 7

The concluding chapter summarises the findings from the core chapters and emphasises the relevance of this research for the verification requirements to the Kyoto Protocol. The constraints and limitations to the research are considered and the future research directions, outlined.

Figure 1.5 Thesis content outline

Chapter 2

Synthesis of remote sensing approaches for forest carbon estimation: reporting to the Kyoto Protocol

Abstract

The Kyoto Protocol requires that signatory countries reduce their human-induced emissions of CO_2 by at least 5% below their emission levels of 1990 by 2008-2012. Parties ratifying the agreement are given the option to meet part of their reduction requirements through the conservation and enhancement of the carbon stored in forest ecosystems. To do this, they must estimate carbon stocks in 1990 and any changes since 1990 from all afforestation, reforestation and deforestation activities. In the UK, although some data are already available, the Protocol will require additional monitoring. To address this, we provide a quantitative assessment of remote sensing approaches for: (1) land cover discrimination to monitor deforestation; and (2) above-ground forest carbon stocks estimation. For land cover discrimination, both optical and radar remote sensing have been successful. For forest carbon stock monitoring, radar is most appropriate until LiDAR is made available from satellite platforms. While focusing on the requirements specific to the UK, our treatment is relevant for Parties having similar requirements. Finally, we stress the need for a synergetic use of approaches and for the launch of satellite missions designed especially for terrestrial carbon stock monitoring. We also highlight future requirements for improving the current forest inventory scheme.

Keywords

Remote sensing; Kyoto Protocol; Land-use Land-use Change and Forestry (LULUCF); Carbon; Biomass.

2.1 International agreements and reporting requirements: the UK case study

Two important international agreements address the pressing issue of reducing anthropogenic greenhouse gas (GHG) emissions in the atmosphere: the United Nations Framework Convention on Climate Change (UNFCCC) and the Kyoto Protocol[4]. Whereas the Convention does not explicitly stipulate levels to which Parties have to reduce their GHG emissions, under the Protocol they are specifically required to limit or reduce their directly human-induced (DHI) emissions of GHGs not controlled by the Montreal Protocol, by at least 5% below the 1990 levels by 2008-2012. The most significant of these gases is CO_2. Within this agreement, countries are allowed to meet part of their emission reduction requirements through the conservation and enhancement of the carbon stored in forest ecosystems (UNFCCC 1992, 1997). Vegetation, by the process of photosynthesis, transforms atmospheric CO_2 into carbohydrates. These are then stored in plant tissues during growth, some of which may also be transferred to the soil as dead organic matter.

To use the sink capacity of forests to help meet its reporting requirements to the Protocol, the UK must "*provide [...] data to establish its level of carbon stocks in 1990 and to enable an estimate to be made of its changes in carbon stocks in subsequent years*"(UNFCCC 1997). In Britain, 80 per cent of the carbon contained in the terrestrial vegetation is found in forests and woodlands (91.9 million tC) (Cannell and Milne 1995), with a similar percentage for Northern Ireland (Forestry Commission, 2002b). The monitoring of these ecosystems is thus highly relevant, particularly since the carbon sink provided by growing forests has increased since 1920 onwards (Cannell *et al.* 1999, Forestry Commission 2002a,b,c).

To produce estimates of carbon stocks and changes since 1990, some relevant data are already available. As a Party to the Convention, three national communications that include an inventory of anthropogenic emissions and removal of CO_2 from Land-use Change and Forestry (LUCF) activities are accessible. Estimates in those inventories (Cannell *et al.* 1999, Milne and Brown 2000), based on the Revised 1996 IPCC Guidelines (IPCC 1997a,

4. Subsequently referred to as the Convention and the Protocol respectively.

b, c), provide a basis for Kyoto reporting. However, the LUCF reporting requirements under the Protocol are supplementary to those of the Convention and more specific.

Under the Protocol,

> *"each Party [...] shall have in place, no later than one year prior to the start of the first commitment period [2008-2012], a national system for the estimation of anthropogenic emissions by sources and removal by sinks of all greenhouse gases not controlled by the Montreal Protocol"* (UNFCCC 1997 Art. 5.1).

This system must account for all DHI emissions and removal of CO_2 due to afforestation, reforestation (AR)[5] and deforestation activities that occurred since 1990. This reporting is mandatory (UNFCCC 1997). In addition, although not compulsory, Parties to the Protocol can elect to report emissions and removal from Article 3.4 activities, which include Forest Management (FM, Table 2.1). Finally, the Protocol requires that all estimates be verifiable (Article 3.3, Table 2.1). By verification, we mean the provision of estimates independent from those provided by the Parties, which allow a statistical evaluation of their reliability.

5. DHI Afforestation and Reforestation activities are treated equally for reporting and accounting under the Protocol.

Table 2.1: Relevant land-use, land-use change and forestry definitions.

UNFCCC: Relevant land-use change and forestry reporting categories as defined by the IPCC (1997a, b, c)	
5 A: Changes in forest and other woody biomass stocks	Emissions and removal of CO_2 from decreases or increases in biomass stocks due to forest management, logging, fuelwood collection, etc. Includes afforestation and reforestation activities.
5 B: Forest and grassland conversion	Emissions and removal of CO_2 from the conversion of existing forests and natural grasslands to other land-uses. Includes deforestation activities.
5 C: Abandonment of managed lands	Removal of CO_2 from the abandonment of formerly managed lands (e.g. croplands and pastures). Includes revegetation, not afforestation nor reforestation activities.
5 D: CO_2 emissions and removal from soil	Emissions and removal of CO_2 in soil associated with land-use change and management.
5 E: Other	Emissions and removal of CO_2 from land-use or land-use change activities, which cannot be included under the categories provided above.
Kyoto Protocol: Relevant land-use change and forestry reporting activities (UNFCCC 2001)	
Afforestation (AR)	Direct human-induced conversion of land that has not been forested for a period of a least 50 years to forested land through planting, seeding and/or the human-induced promotion of natural seed sources.
Reforestation (AR)	Direct human-induced conversion of non-forested land to forested land through planting, seeding and/or the human-induced promotion of natural seed sources, on land that was forested but that has been converted to non-forested land. For the first commitment period, reforestation activities will be limited to reforestation occurring on those lands that did not contain forest on the 31st of December 1989.
Deforestation (D)	Direct human-induced conversion of forested land to non-forested land. Implies a change in land-use.
Forest Management (FM)	System of practices for stewardship and use of forest land aimed at fulfilling relevant ecological (including biological diversity), economic and social functions of the forest in a sustainable manner.
Revegetation (RV)	Direct human-induced activity to increase carbon stocks on sites through the establishment of vegetation that covers a minimum area of 0.05 hectares and does not meet the definitions of afforestation and reforestation defined above.
Forest	Minimum area of land of 0.05-1.0 hectares with tree crown cover (or equivalent stocking level) of more than 10-30 per cent with trees with the potential to reach a minimum height of 2-5 metres at maturity *in situ*. A forest may consist either of closed forest formations where trees of various storeys and undergrowth cover a high proportion of the ground or open forest. Young natural stands and all plantations which have yet to reach a crown density of 10-30 per cent or tree height of 2-5 metres are included under forest, as are areas normally forming part of the forest area which are temporarily unstocked as a result of human intervention such as harvesting or natural causes but

	which are expected to revert to forest.
Forest definition elected by the UK	Land with a minimum of 0.1 ha under stands of trees with, or with the potential to achieve, tree crown cover of more than 20% (Forestry Commission, 2002a,b,c). Minimum width of a forest is 16m, thus to qualify as a forest a stand of trees must to be over 62.5m long (16m x 62.5m = 1000 m^2 = 0.1ha) (Steve Smith, Woodland Surveys, Forestry Commission, Edinburgh, UK, personal communication, 2003). Minimum tree height is expected to be 2 meters in the UK. This definition enables the selection of the remote sensing resolution required for monitoring forests.
Other relevant land-use, land-use change and forestry definitions	
Carbon stock	The amount of carbon stored in a pool at a specific time. In this manuscript, "carbon stock" refers predominantly to the carbon found in the above-ground biomass of forest ecosystems.
Estimation	Provision of figures based on empirical data or modelling approaches.
Verification	Comparison of estimates to data not used in the construction, or calibration of the approach or model used. Allows to establish the reliability of the data submitted by the Parties.
Accounting	Rules for comparing emissions and removal as reported by the Parties, with their assigned commitments. A system of accounting units has been designed to facilitate the trading mechanisms.
Reporting	Process of providing the estimates to the UNFCCC.
Land cover	The observed physical and biological cover of the earth's land, as vegetation or man-made features. Remote sensing only monitors land cover, from which interpretations of land-uses can be derived (Watson *et al.* 2000).
Land-use	The total of arrangements, activities, and inputs that people undertake in a certain land cover type (Watson *et al.* 2000).

2.2 Remote sensing for the Protocol

2.2.1 Meeting specific requirements

In light of these political considerations, our aim is to provide policy makers with an assessment of remote sensing approaches for meeting specific reporting requirements to the Protocol. Although the UK has been elected as a case study, this discussion is relevant for all other Parties having similar reporting and monitoring requirements. Remote sensing, the process of imaging the interactions between electromagnetic energy and matter at selected wavelengths, has the ability to monitor terrestrial ecosystems at various temporal and spatial scales and has been widely tested for land cover mapping and forestry applications. Rosenqvist *et al.* (2003) have reviewed qualitatively remote sensing techniques for use under the Protocol but have not provided an assessment of their operational status for use at national scales. We present a quantitative assessment (accuracy, comparative costs) of

existing and widely investigated optical, radar and *Li*ght *D*etection *A*nd *R*anging (LiDAR) remote sensing techniques, to address the following reporting needs:

(a) The detection of deforestation activities through land cover classification analyses

(b) The quantification of forest above-ground (AG) carbon stocks and changes arising from AR and FM

Remote sensing tools are explored for verifying rather than for producing the estimates. The costs to acquire remote sensing datasets are also discussed in this context. In our discussions, when possible, emphasis is given to satellite imagery as airborne acquisition is prohibitively expensive at the UK scale (Figure 2.1).

2.2.2 Inferring deforestation from land cover analyses

Unlike AR rates, which have been recorded in the UK since the 1920s, deforestation rates have not been consistently recorded (Forestry Commission 2002a). To address this, Levy and Milne (2004) compared rates derived from various data sources. Estimates from the different approaches vary between 18,353 to 449 hectares per year (Levy and Milne, 2004). Such discrepancies are attributed to the different spatial scales and the initial purpose for which the databases were created. This suggests the need for a reliable and accurate monitoring approach that specifically takes into consideration the spatial forest boundaries elected by the UK (Table 2.1).

Remote sensing may help to monitor such activities via the detection of forest to non-forest land cover change (Woodcock *et al.* 2001). However, the definition of deforestation provided in the Marrakesh Accords and the Protocol requires that it be specifically a DHI land-use change. This cannot be assessed via remote sensing alone. A non-DHI forest loss arising from natural fires does not constitute a DHI land-use change, nor does a harvested forest left to revert to a forest state represent a land-use change (Table 2.1). Thus, further ancillary data are required to assess a DHI land-use change from a remotely sensed land cover change. With this in mind, we will discuss in Sections 2.3.1.1, 2.3.2.1 and 2.3.3.1 the potential of remote sensing to discriminate between forests, non-forests and other land covers. In particular, we make reference to the hierarchical classification scheme defined by Anderson *et al.* (1976). At level I, general land cover classes (e.g. settlements, forests, non-forested land, agriculture) are discriminated. At level II, further segregation of specific land cover classes, such as broadleaved and coniferous forests, is made.

2.2.3 Quantifying forest above-ground carbon stocks

Estimation of carbon stock changes from AR activities is mandatory. In the UK it is expected that FM[6] will also be elected. For this, at a minimum, carbon stock changes arising from forest growth beyond that from AR since 1990, will need to be estimated and validated. Currently, estimations of carbon change from all forest growth (AR and FM) are made each year using the C-Flow carbon accounting model (Dewar and Cannell 1992, Cannell and Dewar 1995 and Milne *et al.* 1998). Using annual data on planting of conifers and broadleaves published by the UK Forestry Commission (2002a, b, c) and the Northern Ireland Department of Agriculture (2002), this model estimates the carbon uptake by forests using production tables (Milne 1992). Estimates of carbon in biomass other than stems and net changes in litter and soil carbon are also calculated. An assumption that all forest removal occurring on commercial forest land are restocked is made because current forestry policy has this aim. The approach however assumes that all coniferous forests are of Sitka spruce *Picea sitchensis* Carr. and all deciduous forests, of beech *Fagus sylvatica* Linn. (Cannell *et al.* 1999, Milne and Brown 2003). For each forest type, deciduous and coniferous, the management (e.g. spacing) and yield assumed are the same across the country, notwithstanding the spatial and temporal influences of climate (e.g. temperature, solar radiation, frost), soil fertility, nor changes in management practices (i.e. thinning) that affect growth processes.

Comparatively, direct estimation of carbon stocks via remote sensing could enable real time observation of forest ecosystems and as a result, account for these limiting factors. Although few studies relate remote sensing data to forest AG carbon stocks, many have related these to AG biomass or stemwood volume (hereafter referred to as volume), which are closely related to the AG carbon content. Conversion of volume or biomass to total carbon content can be achieved using ecosystems specific conversion and biomass expansion factors available in the literature (Milne 1992, Levy *et al* .2004, IPCC 2003); in mature forests, especially for coniferous species, often more than 90% of the AG biomass and carbon is contained within the main stem.

3. Although no formal decisions have been made yet about the use of Article 3.4 activities.

Once carbon stocks are estimated, change can be inferred either from consecutive carbon stock estimations –assuming that the signal of change is greater than the noise in the combined datasets (see Fuller *et al.* 2003 for a discussion on this subject) – or with ecosystem modelling (Running and Coughlan 1988, Running and Gower 1991, Landsberg and Waring 1997, Coops *et al.* 1998 and Waring and Running 1998). Another advantage of integrating modelling into a reporting scheme is that belowground components are difficult to assess and cannot be monitored using remote sensing alone. Soils contribute to approximately 25% of the total net CO_2 removal by UK forest ecosystems while 75% is absorbed by the remaining living biomass (Milne *et al.* 2003). Coupling soil models (e.g. Coleman and Jenkinson 1996, Sosanska *et al.* 2002 and Falloon *et al.* 2002) with remote sensing is thus highly pertinent.

2.3 Remote sensing fundamentals for LUCF

In selecting optical, radar or LiDAR approaches for estimating carbon stocks and for discriminating land covers, the following resolutions are predominantly relevant. The ***spatial resolution*** defines how well a sensor can discriminate between large and small-scale features and thus, how well it captures the smallest forest units as defined in Table 2.1. Figure 2.1 illustrates the compromise between spatial resolution and imagery costs. The ***temporal resolution*** refers to the elapsed time between captured images. The ***spectral resolution*** of optical approaches is the capacity to separate the continuum of electromagnetic wavelengths into separate intervals (or bands). High spectral resolution may enable leaf chemical and vegetation water content investigations thus providing enhanced information for biomass and land cover analyses.

In the next sections, each remote sensing approach is described in turn along with its capability for estimating AG biomass and classifying land cover. For a review of specific sensors operational for reporting to the Kyoto Protocol and their specifications, refer to Rosenqvist *et al.* (2003).

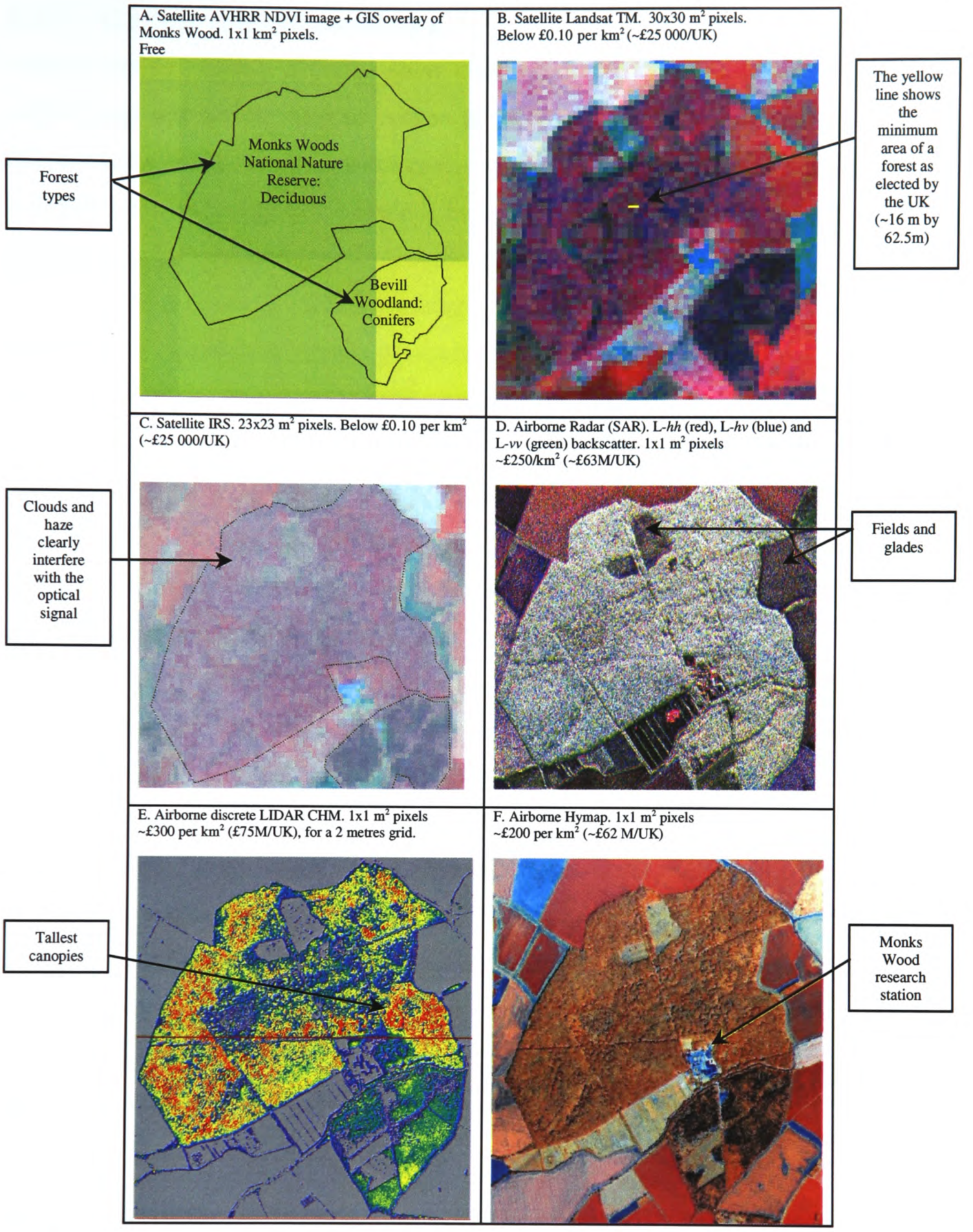


Figure 2.1: Monks Wood National Nature Reserve (UK, 157 ha) viewed from various remote sensing perspectives. The North is oriented upwards.

The images were acquired at various dates but all during summer seasons. Some images have been distorted for presentation purposes. A. NDVI image (see text) derived from images collected over a 10-days period by the Advanced Very High Resolution Radiometer (AVHRR) sensor. A GIS overlay shows the boundaries of the woodlands. The coniferous stand is too small to have a noticeable influence on the reflectance of the pixel. B. Landsat 1989 TM (see text) false colour composite image. In a false colour image, green vegetation appears red to the human eye. C. May 1998 False colour composite image from the Indian Remote Sensing Satellite (IRS). A vector layer has been added to help visualise the boundaries of the woodlands. Note that the atmospheric conditions (haze) clearly affect the quality of the image. D. June 2000 SAR image from the German Aerospace Research Establishment (DLR). The images shows a L-*hh, hv,vv* backscatter image (see text). The woodland is not fully covered by the imagery available. E. Canopy heights (CHM) derived from LIDAR discrete data collected in July 2000. Blue areas indicate canopy heights smaller than 10-m; green, larger than or equal to 10-m but smaller than 18-m; red, larger than or equal to 18-m. F. Airborne hyperspectral data (see text) false color image (green vegetation shown as red).

2.3.1 Optical remote sensing

Optical remote sensing captures solar energy reflected from the earth's surface in the visible, near and middle infrared portion of the electromagnetic spectrum (~ 0.4 to 2.5μm). Digital multispectral remote sensors record spectral information for a limited number (~ below 10) electromagnetic wavelengths for each pixel. Conversely, hyperspectral sensors record a greater number (tens to hundreds) of narrower bands. This information enables the derivation of a spectral profile for each pixel in the image. This profile or signature, compared to established signals of specific land covers, allows the classification of the pixels into land cover classes. Green vegetation exhibits a singular signature characterised by a strong reflectance in the green and in the infrared portions of the electromagnetic spectrum and by a strong absorbance in the red and some regions of the mid-infrared. Furthermore, variations in leaf internal cell structures, absorption levels of chlorophyll and variations in leaf water content (the latter measured using mid-infrared bands) enable the discrimination between vegetation types.

Various dimensionless ratios and indices, such as the widely used Normalised Differential Vegetation Index (NDVI, Jordan 1969), have been designed to optimise these vegetation signatures and to minimise the influence of soil reflectance and atmospheric attenuation (Jordan 1969, Rouse *et al.* 1974, Tucker 1979, Huete 1988). However, for proper application, vegetation indexes need to be selected carefully, consistent with individual sensors and specific applications (Gobron *et al.* 2000, Verstraete and Pinty 1996). An enumeration of existing indices for biophysical studies is provided by Treitz and Howarth (1999). For further information on the use of optical remote sensing for monitoring forests, see Wilkie and Finn (1996) and Gholz *et al.* (1997).

2.3.1.1 Inferring deforestation from land cover analyses

Optical techniques for land cover mapping have been successfully and widely used. Salajanu and Olson (2001) obtained 91.5% overall accuracy in the classification of 6 level-I classes using Spot multispectral (XS) imagery in Michigan, USA. When Landsat Thematic Mapper (TM) ^{7} channels 2,3,4 were used, 89.2% accuracy was obtained. Woodcock *et al.* (2001) used Landsat 7 Enhanced Thematic Mapper (ETM+) and Landsat TM images to monitor forest change over a 5 years period in the Oregon and Colorado States. For

monitoring large areas of forests, they used the concept of generalisation where a trained image classifier is applied to data not used in the calibration of the approach. The accuracy was comparable but less costly to current deforestation mapping methods. Wayman *et al.* (2001) classified forest and non-forest areas using Landsat images and compared two different approaches. Results ranged from 80% to 90% in accuracy. In Great Britain, two land cover maps were successfully derived using optical data. Accuracies of these maps ranged between 67 and 94%, depending on the classification approach and level (Fuller *et al.* 1994, Fuller *et al.* 2002). The potential for inferring change from these maps is discussed in Section 2.4.2.1. Bird *et al.* (2000) compared the accuracy of Spot PAN and Spot XS and showed that level-I classification accuracy using both sensors was good (96% and 87% respectively) but deteriorated at level-II (84% and 50%, respectively). Level II classification generally yields lower accuracies than level I (Fuller *et al.* 1994, Bird *et al.* 2000) and range approximately between 65 to 85% independently of the methods and sensors used (Holmgren and Thuresson 1998, Salajanu and Olson 2001). The use of mid-infrared bands, facilitating the differentiation of species and vegetation types from their leaf water content (Brockhaus and Khorram 1992, Fuller *et al.* 1994) and hyperspectral data (Ustin and Trabucco 2000), enabling the perception of subtle leaf chemistry differences between vegetation types, can improve the accuracy in forest and land cover mapping.

2.3.1.2 Quantifying forest above-ground carbon stocks

Optical remote sensing imagery provides two-dimensional views of forest canopy surfaces and as such, relate more appropriately to the percentage of canopy cover and leaf area index –a variable related to the amount of leaves available to capture sunlight energy for photosynthesis– than directly to biomass or carbon stocks. However, various studies have attempted to relate reflectance indices to AG biomass or volumes. Although the interpretation of reflectance data requires additional knowledge about the influence of soils and understorey on the signal, relationships between forest variables and spectral reflectance can nevertheless be generalised. As green leaf area increases, the reflectance in the green and near-infrared spectral region increases, whereas it decreases in the red and in some portions of the mid-infrared.

7. Landsat-TM5 has been in orbit for more than 10 years and is unlikely to carry on collecting data for much longer. Moreover, its successor, Landsat 7 (ETM), has recently developed a permanent malfunction and is now inadequate for LUCF monitoring.

The accuracy in deriving forest volume or biomass from optical data has been inconsistent and varied across case studies. The literature on this subject is extensive. Holmgren and Thuresson (1998) and Wulder (1998) provide wide perspectives on this subject but a sample of results is exemplified here. Trotter *et al.* (1997) investigated the potential of the Landsat TM sensor for estimating wood volumes in a coniferous plantation in New Zealand using various approaches. They showed that the models used could only explain 30% of the variance in wood volumes at the pixel scale. Such results are not uncommon. In comparing Spot XS and Landsat TM data for deriving basal area and stand age of a coniferous plantation in North Carolina, Brockhaus and Khorram (1992) showed that the correlations between various wavebands and these forest variables were too weak to develop predictive models. Likewise, Fazakas *et al.* (1999) used data from the Swedish national forest inventory, Landsat TM and a classification approach to estimate regional forest biomass and wood volumes. The accuracy of the approach was poor at the plot level. However, when the data were aggregated at the stand level, the results reached relatively low root mean square errors (RMSE) of 8.7% for biomass and 4.6% for wood volumes. Franklin *et al.* (1986) used another classification approach based on Landsat imagery and a digital terrain model to estimate the total volume for a large Californian forest. Their central result was that standard errors were comparable to those from conventional ground-based approaches. However, standard errors compare the precision of the approaches, not their accuracy. Conversely, Ahern *et al.* (1991) have found a highly significant relationship between net annual change in coniferous stemwood volume and vegetation condition spectral indices ($r^2>0.88$, $p<0.001$). Ripple *et al.* (1991) compared the relationships between forest wood volume and the log of reflectance data using Landsat TM images and Spot High Resolution Visible (HRV) images. Results showed a close correspondence between the model used and volumes (r^2 of 0.83 for Landsat TM channel 4 and of 0.89 for Spot HRV at the 0.01 significance level). Yet, in reviewing the paper from Ripple *et al.* (1991), Holmgren and Thuresson (1998) pointed out that for stands above 400-500 m^3 ha^{-1}, the information content in these images seemed negligible. It is not uncommon for the optical signal to saturate as leaf density increases as a result of growth (Spanner *et al.* 1994, Waring and Running 1998).

Such irregularity in the results reflects the inconsistency and inherent difficulty in using optical approaches for monitoring biomass across ecosystems. Notwithstanding the significant atmospheric attenuation in the UK (Fuller *et al.* 2003), a database of

relationships between biomass change and reflectance for different UK forest ecosystems would need to be developed for optical data to be exploitable at a national scale. This is not a trivial task, especially since "spectral response can only be related to structural variables when these present an homogeneous spatial distribution" (Baulies and Pons 1995). Forest ecosystems relatively homogeneous in terms of species composition and age may not be perceived as such when remotely sensed. These ecosystems may be contrasting in terms of their spectral characteristics, because several factors internal to the study sites such as the slope angle, tree spacing and density, and the soil optical properties, may interfere with the signal and contribute to their differentiation. Several other external factors such as cloud cover and sun elevation also impose a strong influence on the spectral responses of forest canopies (Guyot *et al.* 1989, Treitz and Howarth 1999). These emphasise the contextual nature of the relationships between biomass or volume and canopy reflectance, which makes the task of applying this at national scales difficult.

Nonetheless, optical remote sensing can provide useful means to monitor variables that strongly influence growth patterns. For example, several well-established growth models rely on remote sensing for deriving input variables such as the *leaf area index (LAI)* or the *fraction of photosynthetically active radiation (fPAR) absorbed by the canopy* – a variable related to the quantity of light absorbed by canopies for photosynthesis (Running and Coughlan 1988, Running and Gower 1991, Landsberg and Waring 1997, Coops *et al.* 1998).

2.3.2 Radar remote sensing

Radar systems are active remote sensors operating in the microwave portion of the electromagnetic spectrum (approximately between 1 cm to 10 m for VHF [8]). Active systems generate their own source of electromagnetic radiation allowing the capture of images independently from solar energy. Moreover, unlike optical wavelengths, the energy pathways in radar wavelengths are not impeded by moderate precipitation or cloud cover. Both scatterometers and imaging radars have been tested for forestry applications. Scatterometers have low spatial resolutions and those that are spaceborne, with resolutions in the order of tens of metres, are inadequate for forestry applications. Conversely, imaging

8. Very High Frequency, named from the perspective of much longer wavelengths.

radars have higher spatial resolution capabilities; of these, the Synthetic Aperture Radar (SAR) will be discussed.

When a pulse of microwave radiation is fired at the ground, radar systems detect and record the wave properties of the returned echoes from which three types of information can be retrieved. Most commonly, the amplitude of the returned echo (the backscatter amplitude) and the orientation of the electromagnetic wave (the polarisation) are measured. Polarisation configurations are designated as *v* for vertical and *h* for horizontal. A configuration of *vh* indicates that the sensor transmits energy vertically and receives horizontally. The horizontal or vertical distribution of the target (e.g., leaves, branches) will influence the backscattered response of the signal. Coherent techniques measure the stage of the wave cycle as the echo arrives (the phase). In particular, interferometry refers to the measurement of the difference in phase observed when a target is measured at different times or from slightly different locations. This technique can be used to derive topographic information. Balzter (2001) provides an overview of the potential and limits of interferometry for applications to forest mapping and monitoring. Recently, polarimetric SAR interferometry (PolInSAR) has received increasing interest for forest application and mapping (Cloude and Papathanassiou 1998, Balzter 2001, Woodhouse *et al.* 2002, Lee *et al.* 2003). Preliminary results are promising (Lee *et al.* 2003, Woodhouse *et al.* 2002) and with the future launch of the spaceborne L-Band TerraSAR sensor, methodologies could become available outside the research community. However, until further research is done, a judgement on the capabilities of these methods for reporting purposes would be premature. Accordingly, established techniques relying on backscatter amplitudes and polarisations will be discussed here.

In recent years, the use of SAR backscatter has been increasingly investigated for forest inventorying as radar wavelengths penetrate the vegetation, providing direct sensitivity to the vegetation structure and biomass. Most commonly the C, L and P-bands (or wavelengths) have been used for forestry applications since they are responsive to different components of the vegetation structure. The shorter wavelength, C-band (~5 cm wavelenght), is sensitive to small components of the canopy such as leaves and twigs. The longer wavelengths, L-Band (~24 cm), P-band (~70 cm) and the much longer VHF wavelengths (up to 100 cm) penetrate deeper into the canopy and are predominantly sensitive to larger tree branches and trunks.

Specific issues need to be considered prior to the selection of SAR for forest monitoring. Firstly, the geometry of SAR viewing angle, diagonal to the earth's surface, generates an effect known as lay-over, which restricts the applicability of SAR where the influence of topography is considerable. Secondly, the dielectric property of the surveyed surfaces, controlled primarily by their moisture content, also influences the signal such that light snow cover or varying soil moisture content will affect the backscattered response. These effects limit the application of SAR where these influences are considerable (Bayer *et al.* 1991, Vanzyl 1993, Pairman *et al.* 1997). Thirdly, a phenomenon referred to as speckle renders intricate the separation of the signal from noise in the data. To counteract this, temporal or spatial averaging is used (Porcello *et al.* 1976), the later reducing the effective spatial resolution of the resulting image by approximately three times its original resolution (Ian Woodhouse 2004, personal communication). Finally, the main external factor controlling the sensitivity of the SAR signal to biomass is the structural properties of the forest and its underlying surface. Given equal biomass, the radar backscatter response will be significantly different for a forest composed of sparse large trees versus one composed densely of young small trees (Dobson *et al.* 1995b). Nevertheless, the monitoring capabilities of SAR, which are independent of moderate precipitation, sunlight or cloud cover, offer advantages for forest monitoring in the UK, where atmospheric contamination is a chief limitation to the use of optical data.

For further information on the basic principles of radar see Nuesch and Kasischke (1989) and for its application to forestry, Kasischke *et al.* (1997).

2.3.2.1 Inferring deforestation from land cover analyses

Land cover classification using SAR has been successful in various locations. For a description of SAR classification methods, see Kasischke *et al.* (1997). Dobson *et al.* (1995b) achieved 94% overall accuracy in the classification of 6 land cover classes in Michigan, USA (bare surface, short vegetation and four different forest types) using Shuttle based multipolarimetric SAR and ancillary data. Pierce *et al.* (1994) tested a knowledge-based classification scheme on a spatially independent forest ecosystem (not used in designing the scheme) and reached level I accuracies in excess of 97 %. When the approach was tested for level II intra-species discrimination (aspen, pines and northern hardwood) the results were also excellent (>96%). Using a similar method, Dobson *et al.* (1995a) achieved

75%, 98% and 99% accuracy at level I using C-band (*hh*), L band (*hv*) and both bands combined respectively. Classification at level II for discriminating between deciduous and coniferous species yielded accuracies of 64%, 66% and 94% respectively for the same dataset. Similar results were reached by Ranson *et al.* (1995), which achieved classification accuracy for eight forest types in the order of 80%. Clear-cuts were correctly classified in 99% of cases. In a study comparing various combinations of frequency and polarisations, Hoekman and Quinones (2000) obtained highest accuracies when using multi-frequency data, especially when combining P(*hv*) and C(*vv*) bands. Combined L and C band, independently of the polarisation used, reached accuracies between 79% and 87%. The use of multi-frequency, multi-polarimetric SAR data clearly leads to successful classifications, in particular in discriminating forest from non-forest land covers (Dobson *et al.* 1995a). The use of single images for land classification is however limited, especially at C-band. Using this wavelength, differentiating between regenerating vegetation or crops from forests may be problematic, as these land surfaces have similar structural properties.

2.3.2.2 Quantifying forest above-ground carbon stocks

Several studies have investigated the potential of airborne, Space Shuttle-borne and satellite based radar systems for retrieving forest biomass or volumes. The following Table 2.2 and Table 2.3 summarise the results of eleven studies. For a given species or vegetation structural type, the backscatter coefficient or amplitude increases with biomass typically with a power law relationship. Thus, at high biomass, the potential of SAR to predict AG forest biomass is limited, as the signal saturates: increasing biomass does not necessarily yield an increase in the radar signal (Imhoff 1995). Table 2.2 presents the saturation level to these eleven studies. In Table 2.3 radar variables are related to forest biophysical variables (biomass or volume) derived from ground surveys to develop prediction equations. Some of these equations are then tested (validated) on independent forest stands or plots to evaluate their predictive capabilities.

Table 2.2: Synthetic Aperture Radar (SAR) biomass saturation values for various ecosystems and approaches.

Platform	Study number and ecosystem type	Band (polarisation)	Range [a.] of V (m^3ha^{-1}) or B ($t\ ha^{-1}$)	Saturation (V or B)	Sources
Airborne	1. Coniferous forests, Sweden	VHF	V: 0-625 B: 0-375	No saturation	(Fransson *et al.* 2000)
Airborne	2. Coniferous forests, UK	P-band (*hv*) L-band (*hv*)	V: 0-400	V: 120 V: 63	(Skinner 2002)
Airborne	3. Coniferous forests, Northern France	P-band (*hv*) L-band (*hv*)	B: 0-560	B: 200 B: 100	(Dobson *et al.* 1992)
Airborne	4. Deciduous and coniferous forests, Maine, USA.	P-band (*hv*) L-band (*hv*)	B: 0-350	B: 150 B: 150	(Ranson and Sun 1994)
Airborne	5. Tropical Broadleaved, Coniferous forests, Hawaii, Europe, North America.	P-band [b.] L-band [b.] C-band [b.]	B: 4-660	B: 100 B: 40 B: 20	(Imhoff 1995)
Satellite	6. Boreal coniferous forests, Sweden	L-band (*hh*) C-band (*vv*)	V: 0-300	V: 143 V: 64	(Fransson and Israelsson 1999)
Satellite	7. Tropical forests, Amazon, Brazil.	L-band (*hh*)	B: 0-400	B: 60	(Luckman *et al.* 1997, Luckman *et al.* 1998)
Satellite	8. Coniferous forests, Norfolk, UK	L-band (*hh*)	V: 0-400	V: 81	(Skinner 2002)
Shuttle	9. Boreal coniferous forests, Canada.	L-band C-band combined	B: 6-250	B: 200	(Ranson *et al.* 1995)
Shuttle	10. Deciduous and coniferous forests, Michigan, USA.	L-band C-band combined	B: 0-250	B: 250	(Dobson *et al.* 1995b)
Shuttle	11. Coniferous forests, Norfolk, UK	L-band (*hv*)	V: 0-400	V: 65	(Skinner 2002)

[a.] Range of B (Biomass) or V (Stemwood volume) found in the ecosystems under observation. [b.] For the four polarisations: *hh, vv, hv, v*h.

Table 2.3: Accuracy of the various SAR backscatter based models to derive stemwood volumes or biomass.

Study no [a]: Variable	**Band and polarisation**	**Variance explained by SAR backscatter model**	**Model validation**
1: Volume	VHF	$r^2 = 0.83$	n.a.
		RMSE 65.8 $m^3 ha^{-1}$	
2: Volume	P-band (*hv*)	$r^2 = 0.90$	$r^2 = 0.77$
	L-band (*hv*)	$r^2 = 0.86$	$r^2 = 0.63$
3: Biomass	P-band (*hv*)	$r^2 = 0.98$	n.a.
	L-band (*hv*)	$r^2 = 0.96$	
	C-band (*hv*)	$r^2 = 0.75$	
4: Biomass	P/C band (*hv*)[b.]	$r^2 = 0.83$	$r^2 = 0.74$
	L/C band (*hv*)[b.]	$r^2 = 0.79$	$r^2 = 0.62$
6: Volume	L-band (*hh*)	r^2(adjusted) = 0.51	r = 0.78
			RMSE 11 $m^3 ha^{-1}$
8. Volume	L-band (*hh*)	$r^2 = 0.77$	$r^2 = 0.53$
9: Biomass	L/C-band (*hv*)[b.]	$r^2 = 0.80$ [c.]	n.a.
		$r^2 = 0.82$ [d.]	
10:Biomass	L/C band (*hv*)[b.]	$r^2 = 0.64$ RMSE 23.8 t ha^{-1} [e.]	$r^2 = 0.96$ [f.]
		$r^2 = 0.96$ RMSE 6.2 t ha^{-1} [e.]	RMSE 14 t ha^{-1}
		$r^2 = 0.97$ RMSE 6.5 t ha^{-1} [e.]	
		$r^2 = 0.89$ RMSE 9.3 t ha^{-1} [e.]	
		$r^2 = 0.95$ RMSE 12.2 t ha^{-1} [e.]	
11:Volume	L-band (*hv*)	$0.77 \leq r^2 \leq 0.85$ [g.]	$0.50 \leq r^2 \leq 0.65$

Study numbers given in Table 2.3 refer to the relevant references in Table 2.2. [a.]Not all studies shown in Table 2.2. are presented in Table 2.3. [b.]A ratio between the longer and shorter wavelengths was used to derive the model. [c.]April data set. [d.]October data set. [e.]Models developed for each forest structural type (see text). r^2 values are given for Hardwood, Aspens, Lowland conifers, Upland Jack pine and Upland Red pine in descending order. [f.]All forest types combined. [g.] Multi-temporal analysis on various datasets.

Table 2.2 shows that the sensitivity to volume and biomass is greater for longer wavelengths. In particular, in the study by Fransson *et al.* (2000), no saturation was observed with the longer VHF bands. Unfortunately, the VHF and P-band frequencies interfere with radio communications and are unlikely to be deployed operationally in the UK. The saturation threshold of L-band, the lowest frequency planned in forthcoming satellites, remains on average below the levels of volumes and biomass found in mature UK woodlands where AG biomass levels between 200 to 400 t ha^{-1} are common (Cannell 1982, Patenaude *et al.* 2003). Table 2.3 shows that the coefficients of determination (r^2) between backscatter and AG biomass or volume vary between 0.51 and 0.98 and the predictive capabilities of the models, between 0.50 and 0.96, independently of the ecosystem type or methods used. For a given platform (shuttle and airborne), the accuracy of the backscatter

models for mixed deciduous woodlands was generally lower than that of coniferous. This is revealed by comparing results from study no. 4 to those from study no. 1, 2, and 3 (only study no. 3, C-band, is of similar magnitude) and by comparing the results from the mixed hardwood with all other woodland types in study no. 10. Dobson *et al.* (1995b) showed that mixed deciduous woodlands are particularly difficult to monitor using SAR because of their heterogeneous structure. *A priori* knowledge of the forest structural characteristics is required to analyse the SAR data adequately.

2.3.3 LiDAR remote sensing

The functioning of LiDAR is analogous to radar in that both are active remote sensing techniques. Using a pulse generated in the visible or the near infrared portion of the electromagnetic spectrum (900 to 1064 nm) LiDAR systems measure the travel time from the sensor to the target on the ground and back using ultra-accurate clocks, thus providing elevation information of targets. The precision of the timing is crucial as it determines the vertical precision (at the centimetre level). In contrast to optical and SAR systems, LiDAR collects samples along the flight path and as such, is not an imaging system. Interpolation between samples is required for thematic mapping. Although a promising technique for ecosystems studies (Hinsley *et al.* 2002), LiDAR systems are not yet available from satellite platforms.

There are currently two types of LiDAR systems: Discrete-return devices (DRD) and waveform recording devices (WRD) (Lefsky *et al.* 2002). Per pulse, DRD sample area from 5 to 90 cm diameter and record limited information about the returned waveform (e.g. only the first and last significant returned signal). However, these systems provide high pulse rates i.e. often more than one pulse per m^2. To derive estimates of canopy height, two surfaces need to be derived: a terrain model (TM) and a canopy surface model (CSM) (Nelson *et al.* 2000). The canopy height model (CHM) is then generated from the difference between the CSM and TM. See Hyyppä *et al.* (2000) and Lim *et al.* (2003) for methodologies.

WRD sample areas of 10-25 meters diameter per pulse and fully digitise the returned waveform, thus providing enhanced information on the vertical architecture of forests. Peaks in the waveform have been related to biomass or volume as these represent high intensity returns and often indicate a concentration of leaves, branches or trunks (Nilsson

1996, Lefsky *et al.* 1997, Lefsky *et al.* 1999b, Means *et al.* 1999). Although WRD have enhanced capabilities for forest structure characterisation, their operational status is likely to remain at the research stage until the launch of the Vegetation Canopy LiDAR (VCL) on a satellite platform. Unfortunately, NASA has suspended this project indefinitely. A description of an airborne version of this system, the Laser Vegetation Imaging Sensor (LVIS), is however available in Blair *et al.* (1999).

For further introduction to the functioning of LiDAR systems, the reader is referred to Flood and Gutelius (1997) and Wehr and Lohr (1999), while processing methods are summarised by Axelsson (1999). For the retrieval of forest parameters, see Lefsky *et al.* (2002). Companies providing systems and their operating costs can be found at www.airbornelasermapping.com.

2.3.3.1 Inferring deforestation from land cover analyses

Although not an imaging system – thus inadequate for land cover mapping alone – LiDAR may provide a direct and rapid verification tool for forest to non-forest land cover change detection using canopy height measurements. In the event that a LiDAR sensor suitable for forest monitoring were made accessible from satellite platforms, a systematic, stratified and georeferenced system could automatically detect areas where forests have been lost indicating areas where ancillary data are required for assessing deforestation.

2.3.3.2 Quantifying forest above-ground carbon stocks

The potential of LiDAR for direct estimation of AG biomass is promising (Table 2.4). WRD have the potential to record three-dimensional information on the forest structure in addition to elevation information. Relating the signal to biomass has yielded good results as shown by studies 6 to 8. Because WRD sample areas of 10-25 meters, the probability of hitting tree apexes and of encountering sufficient gaps in the canopy to sample ground elevation is improved.

Table 2.4: Discrete and waveform LiDAR derived forest biomass and volume.

Sensor Type [a.]	Ecosystem type	Variable estimated [a.]	Main driving variable	Variance explained	Validation	Sources
1. DRD	Pine and mixed hardwood, Georgia, USA	V_t B_t (Green)	Mean plot height [b.]	$r^2 = 0.53$ [c.] $r^2 = 0.54$ [c.]	$r^2 = 0.58$ $r^2 = 0.64$	(Nelson *et al.* 1988a)
2. DRD	Scots pines (Sp), Norway spruce (Ns), Norway	V_s	Mean per stand of largest tree height per 15x15m^2 grid cell.	r^2=0.456 Sp r^2=0.887 Ns	n.a.	(Naesset 1997b)
3. DRD	Douglas fir, Oregon, USA	Ln V_t	Height and canopy cover quantiles.	r^2=0.97	n.a.	(Means *et al.* 2000)
4. DRD	Norway spruce, Scots pines Norway	Ln V_s -Young -Mature, poor site -Mature, good site	Height quantiles and canopy density distributions.	 r^2=0.93 r^2=0.80 r^2=0.80	All stands [e.] r^2=0.91	(Naesset 2002)
5. DRD	Norway spruce Scots pine and Beech, Sweden	V_s	Height and canopy crown diameter	r^2=0.88 [f.]	n.a.	(Persson *et al.* 2002)
6. WRD	Scots pine, Sweden	B_t	Mean product of waveform area and laser height	r^2=0.78	n.a.	(Nilsson 1996)
7. WRD	Douglas fir, Western hemlock Oregon, USA	B_t	Filled canopy volume	r^2=0.91	n.a.	(Lefsky *et al.* 1997, Lefsky *et al.* 1999a)
8. WRD	Douglas fir, Western hemlock Oregon, USA	B_t	h_c	r^2 =0.90 [d.] r^2 =0.94 [d.] r^2 =0.96 [d.]		(Means *et al.* 1999)

[a.] DRD=discrete return recording device. WRD=Waveform recording device. V_t = Total above-ground volume. V_s =Stemwood volume. B_t = Total above-ground biomass. h_c = Mean canopy height. [b.] All pulses considered, including pulses to the ground. [c.] Best model presented. [d.] With h_c as driving variables for the three models. The latter two in descending order include one and two additional driving variables respectively. [e.] Equation transformed back to original scale. [f.] Square of the correlation coefficient.

Comparatively, systematic underestimation of tree height has been observed from DRD, as the signal tends to penetrate into the canopy prior to returning a significant signal (Nelson *et al.* 1988a, 1988b, Naesset 1997a, Gaveau and Hill 2003, Brandtberg *et al.*, 2003). Earlier, this has precluded reaching high accuracies in biomass or volume estimation. However, grid systems approaches such as that proposed by Naesset (1997a) and Magnussen and Boudewyn (1998) in which quantile estimators (e.g. max height) are used to approximate stand height have yielded good results especially in relatively homogeneous forest stands. Such approaches have been further used to estimate forest carbon content (Patenaude *et al.* 2004). More recently, the increased sampling densities capabilities of DRD coupled with 3-D individual tree modelling have made it possible to considerably reduce height underestimation and improve biomass estimates (e.g. study 5). Study 5 (Table 2.4) and results by Hyyppä *et al.* (2001), where tree heights were measured with sub meter accuracy, suggest that this approach is now suitable for forest inventories and biomass estimation. In these studies, the precision of the measurements was either comparable or better than that from standard inventory practices.

2.4 Remote sensing synthesis for the UK

2.4.1 Costs for meeting specific requirements

In Figure 2.1, approximate costs for acquiring various remote sensing images at the UK scale are given. In Table 2.5, the costs presented are for the acquisition of remote sensing and field-based data only, expressly for the monitoring of AR since 1990, AR since 1940 and deforestation in the UK. Costs estimates are given *per* forest surface area (km^2) *per* activity and were calculated using forestry statistics available for 2002 (Forestry Commission 2002a, 2002b) and by contacting various providers of remote sensing datasets. Figure 2.1 and Table 2.5 should however be interpreted with care, especially in regards to the radar and optical figures, as the processing of the remote sensing data implies additional costs (e.g. for the radiometric and topographic normalisation and for atmospheric and geometric correction). Additionally, in the UK, although nearly 50% of all forests are located in Scotland (Forestry Commission 2002b) their distribution is scattered across the country. Satellite images are usually acquired by scene, which may cover areas greater than those required. For a complete coverage of UK forests, the purchase of combined scenes may be necessary and final costs may be greater than those cited. Nevertheless, these

figures provide basic guidance but further research will be required for a comprehensive assessment of costs.

Table 2.5: Approximate magnitude of costs to acquire remote sensing and field-based data for monitoring AR since 1990, AR since 1940 and D activities in the UK. Data for 2002 annual planting statistics from the Forestry Commission (2002a) and the Northern Ireland Department of Agriculture (2002)

				Approximate costs [c.]			
			Ground survey [e.]	**Optical [d.]**		**Radar**	**LiDAR**
	Monitoring from remote sensing	**Forest area (km^2)**		**Satellite**	**Airborne**	**Satellite or Shuttle [d.]**	**Airborne**
				~ £0.10/km^2	**~ £250/km^2**	**~ £0.10/km^2**	**~ £300/km^2**
AGCC loss from Article 3.3 D activities	Total UK forest area plus AR since 1990	28,000	~ £ 3.5 millions	Less than ~ £ 3,000	~ £ 7 million	Less than ~ £ 3,000	~ £ 8.4 millions
AGCC gains from Article 3.3 AR activities (forest growth only)	All UK forest area planted after December 1989	4,500	~ £ 307,000	Less than ~£ 1000	~£ 615,000	Less than ~£ 1000	~£ 738,000
AGCC gains from Article 3.4 FM activities (forest growth only) [a.]	All UK forest area planted after 1940 [b.]	19,245	~ £ 1.8 millions	Less than ~£ 2,000	~£ 3.6 millions	Less than ~£ 2,000	~£ 4.3 millions

AGCC= above-ground carbon content. D= Deforestation. AR= Afforestation and Reforestation. FM= Forest Management. [a.] Only if FM elected by the UK. [b.] Based on the assumption that all forests above 50 years of age have reached maturity and do not contribute significantly to the carbon sink i.e., trees planted in 1970 contribute "significantly" as a sink for 30 years after 1990. [c.] Costs, rounded to the £1000, provide guidance only and are for image acquisition without processing. Costs are for acquiring one dataset only (i.e. for forest to non-forest land cover change detection, at least two datasets are required). [d.] Medium resolution (15-50 meters) [e.] Data collection only, no processing. Estimates based on costs for generating the Country Side Survey 2000, http://www.cs2000.org.uk/, (Steve Smith, 2004, personal communication).

Table 2.5 is structured as follow. Firstly, areas for which the quantification of forest AG carbon stock changes arising from Article 3.3. AR growth processes is required are given. For these activities, the total area necessitating monitoring is relatively small (4,500 km^2) because only AR areas since 1990 need to be included. Secondly, if FM activities are elected, the UK could benefit from the sinking capacity of forests planted prior to 1990. In this instance, all growing forests contributing significantly to a sink should be monitored. Assuming that all forests younger than 50 years of age contribute to a sink, while mature ones not significantly, all trees planted from 1940 onwards should be monitored. Planting years for all AR can be accessed from the UK Forestry Commission. This represents an area of about 19,000 km^2. Finally, to assess the extent of deforestation activities, the total area requiring monitoring is considerably larger. For this activity, all existing forest land units in 1990 as well as afforested and reforested areas since 1990 need to be monitored (28 000 km^2).

As all AR and existing forests larger or equal to 2 hectares are georeferenced (Forestry Commission, 2002c), this enables the provision of approximate costs for acquiring remote sensing and ground survey data per activity. Airborne LiDAR and radar approaches are by far the most expensive techniques, although these remain in the same order of magnitude to ground surveys. Comparatively, costs for satellite imagery are much lower, even though prices may vary given different providers and sensor specifications. If satellite imagery are acquired at the UK scale (Figure 2.1) for monitoring specific activities, the prices still remain considerably lower than those for ground surveys or airborne data, which cover appreciably smaller areas (Table 2.5).

2.4.2 Reporting requirements

2.4.2.1 Inferring deforestation from land cover analyses

Whereas LiDAR is not suitable alone, both radar and optical approaches are adequate for land cover classification. High accuracies have been reached, particularly in differentiating between forests and non-forests. However, although the approaches may be suitable for land cover classification, deriving land cover change from successive land cover maps raises the following issues.

For systematic derivation of change from successive land cover mapping exercises, methodological consistency is required. Land cover maps for Great Britain (e.g. 1990 and 1998, designated 2000) were successfully derived from optical data (Fuller *et al.* 1994,

Fuller *et al.* 2002). Unfortunately, their structural differences preclude their compatibility for land cover change analysis (Fuller *et al.* 2003). In 1990, *a per* pixel classification was used whereas in 1998, a per parcel classification was utilised. The *per* pixel approach classifies each pixel into one of selected target classes (Fuller *et al.* 1994). Conversely, in the *per* parcel approach, land area polygons were derived by segmenting the images into parcels of similar characteristics. Then the pixel data for each parcel were classified together (Fuller *et al.* 2002).

Additionally, for change to be detected accurately, the scale of change must be greater than the cumulative errors of the independent estimates (Fuller *et al.* 2003). For mapping change at national scales, very high accuracies are required to enable the detection of small changes. If only forest to non-forest discrimination is sought, such accuracies may be achievable. However extensive land cover change classification, entailing various land categories, may not be achievable at such scales with the methodologies available (Fuller *et al.* 2003). An accurate detection of change will clearly depend upon its nature and scale: extensive deforestation may be mapped accurately, but degradation may be difficult to detect.

2.4.2.2 Quantifying forest above-ground carbon stocks

For forest AG carbon stock estimation, optical sensors have produced inconsistent results thus are not suitable for national scale inventory. LiDAR techniques are comparatively promising, as no saturation is observed at high biomass levels. Unfortunately their operational status for reporting at such scales still depends largely on the future availability of sensors from satellite platforms. Until then, the accuracy and usefulness of a satellite-borne LiDAR for monitoring biomass at national scales as well as the effect of topography and atmospheric interference on the signal will remain to be fully tested.

Sufficient AG biomass estimations from Shuttle-borne and satellite-based SAR have been conducted to assess their capability for biomass estimation at national scales. In the context of the UK, its monitoring capacities, unaffected by moderate precipitation or cloud cover and independent of sunlight, offer clear advantages over other approaches. Additionally, results in biomass estimation from SAR approaches (longer wavelengths, cross-polarised) have been most successful in homogeneous coniferous ecosystems and especially in relatively young ones. Conveniently nearly 60% of UK forests are coniferous and this percentage is increasing as approximately 77 % of all AR occurring during last couple of

decades has been of such forests (Forestry Commission 2002a). Moreover, it is these young growing coniferous forests that contribute most significantly to the carbon storage by UK forest ecosystems. In planted temperate coniferous forests, the highest carbon storage rate occurs during the first 20-30 years (e.g. Edwards and Christie 1981).

Imhoff (1995) derived SAR biomass saturation values for P, L and C band across forests worldwide providing means to evaluate the potential usefulness for using SAR in the UK. Using these saturation values per band and the UK 1km map of forest carbon density provided by Milne and Brown (1997), Table 2.6 shows the total forest surface areas that could potentially be monitored in the UK.

Table 2.6: SAR biomass sensitivity zones for monitoring forest biomass in the UK based on P, L and C-band SAR saturation thresholds from Imhoff (1995).

Zone	Approximate biomass threshold ($t\ ha^{-1}$)	Total area (km^2)	% of total forest area	% of total forest biomass
Zone 1: C, L and P-Band	≤ 20	9357	34%	5%
Zone 2: L and P band	$20 < x \leq 40$	5079	18%	9%
Zone 3: P-band only	$40 < x \leq 100$	6714	24%	28%
Zone 4: Above saturation	> 100	6700	24%	57%

The three last columns indicate how much of the UK forests and above-ground biomass could be monitored under each threshold (estimated UK forest area and biomass). Methods used to derive these estimates are not presented in this paper.

If the saturation levels by Imhoff (1995) are suitable for the UK, nearly 52 % of the total UK forest areas could be monitored using satellite SAR C- and L-bands. Furthermore, some of the forests constituting the remainder 48% have already reached maturity and as such, may require less monitoring after 1990, as they are unlikely to contribute significantly to carbon fluxes. In 2002 for instance, approximately 59% of UK coniferous and 93% of UK deciduous woodlands were above 50 years of age, thus contributing less significantly to carbon fluxes than younger woodlands (Forestry Commission 2002a, 2002c Northern Ireland Department of Agriculture, 2002).

These estimates however do not consider that nearly 50% of all forests are located in Scotland, a region where the influence of topography could strongly impede on the application of SAR for biomass estimation. Furthermore, the estimated percentage of forest

AG biomass that can be monitored using SAR approaches is likely to decrease during the next decades if no solutions to the saturation problem are found. While current forests are ageing, AR activities have diminished in recent decades resulting in an increasing average biomass per unit of forested land (Forestry Commission 2002a).

2.4.2.3 Synthesis for the UK

While optical and SAR approaches could be operational for forest to non-forest land cover change detection at the UK scale, no remote sensing are yet fully operational for monitoring biomass change at such scales. Although suitable for local or regional estimations of biomass, several drawback still limit their potential for operational use at national scales. These limitations are:

(a) The limited availability or unavailability of satellite sensors adapted for this purpose.

(b) The external environment factors, inherently heterogeneous at national scales, which impede on the signals (atmospheric attenuation and environmental contamination).

(c) The intrinsic factors pertaining to the sensors and to current analytical methods, which limit their applicability for biomass monitoring (e.g. the saturation of the signal at high biomass).

If remote sensing is to be used in the future for national inventorying, the synergetic use of contrasting approaches and the fusion of complementary datasets to circumvent these limitations should be emphasised. Whereas low cost optical data can provide information on environmental variables or forest types, SAR and LiDAR can provide three-dimensional information on canopy architecture and structure. The fusion of low cost, low spatial resolution optical imagery (e.g.MODIS) with active sensors (radar-LiDAR) should be further investigated. However, to maximise costs/benefits and to minimise the processing requirements, research should prioritise on the synergy between LiDAR and radar approaches, as these combined may provide answers to both the forest to non-forests change detection as well as the biomass estimation requirements.

Ultimately, the selection of remote sensing techniques for reporting to the Protocol will depend on their role as an estimating or verifying tool. If remote sensing is used for providing estimates, then the use of higher resolution imagery involving higher costs may be justified for meeting the accuracy and the precision levels required. Conversely, such a stringency for a verification system, i.e. statistically powerful, georeferenced and providing

independent reassessments of all the figures, would be unrealistic. On the other hand, a flexible system involving perhaps the use of default figures (Smith, 2001) would likely yield considerable uncertainty. An intermediate solution would be preferable. Distinct estimates to those serving in the national communications are already available - such as the biomass estimates for all woodlands larger than two hectares (Forest Research 2001). Alas, these often rely on the same databases and production tables as those used for the national communications precluding their use as validating tools. Thus alternative intermediate solutions must be sought. If remote sensing is used for validation or for stratification purposes then lower costs imagery of lower resolution may be sufficient.

2.5 Conclusion and future work

In this paper we have discussed the potential of optical, radar and LiDAR remote sensing for direct AG forest carbon stock estimation and for forest to non-forest land cover change detection. Optical data, widely available at various spatial and temporal resolutions are inexpensive and have been widely and successfully used for land cover classification. However, this approach can be strongly impeded by atmospheric attenuation, limiting its potential application for LUCF monitoring in the UK. Additionally, for biomass estimation, the strength of the relationship between biomass and canopy reflectance is largely contextual.

LiDAR, while unsuitable alone for land cover mapping, will offer great capabilities for carbon stock and changes estimates when available from satellite platform, as the signal does not saturate at high biomass levels. However, until sensors are available from satellite platform, its capabilities for national inventory will remain untested. Additionally, the capture of an entire country with LiDAR data is clearly not feasible. Conversely, radar methods are not affected by light precipitation or cloud cover and are directly sensitive to biomass. As such, they have enhanced capabilities for carbon stock change estimation. Likewise, for forest to non-forest land cover discrimination, radar results have been very accurate. Because younger coniferous forests are those that contribute most significantly to the carbon storage of forest ecosystems and since these represent a large percentage of the UK forest cover, SAR approaches are best suited for the UK context. However, topography may limit its applicability to regional scales. Additionally, the current unavailability of appropriate hardware on satellite platform delays the proper application of radar for inventory and land cover mapping.

Future requirements to improve the reporting scheme are as follow. Firstly, additional reporting requirement will need to be addressed. If the UK elects to report Article 3.4 FM activities, direct human-induced degradation and devegetation activities may need to be considered and relevant monitoring methods developed. For instance, land units meeting the forest definition elected by the UK and having 70% tree crown cover will remain a forest even though its cover decreased to 25%. Such issues are extensively discussed in the GPG (IPCC 2003).

Moreover, future efforts should investigate the use of multi-temporal datasets and incremental databases to periodically quantify land cover and biomass change. For this purpose, we stress the need to develop image normalisation methods to allow the analysis of remote sensing images through time. Illumination differences (e.g. sun angle, view angle) need to be carefully normalised when multi-temporal analyses are being conducted.

Other potential uses of remote sensing for reporting include that of stratification. Stratification allows the classification of land into biomass and land cover categories, increasing the efficiency of inventory efforts. Global products such as the MODIS/MISR fPAR or LAI, although of relatively low spatial resolution, are already processed and are available regularly for monitoring larger scale deforestation. Integration of these products may help in the stratification of land covers and in the determination of subsequent datasets requirements.

Finally, there is a need for launching satellite sensors specifically designed for terrestrial carbon stock monitoring and particular that of a spaceborne LiDAR sensor. The fusion of sample data collected with a LiDAR sensor (providing "*in situ*", discrete point sampling) with other optical and/or SAR data (providing spatially extensive coverage) could allow extrapolation of discrete point biomass estimates across the landscape. Moreover, if LiDAR becomes available from a satellite platform, it may provide the only viable remote sensing tool, in terms of cost/benefits, for the verification of estimates of biomass change and forest cover loss.

Acknowledgements

Thanks are due to Craig Trotter (Landcare Research, New-Zealand) and Heiko Balzter (Centre for Ecology and Hydrology, UK) for their invaluable comments on this paper. The authors would also like to thank Clare Rowland and Ross Hill (Centre for Ecology and

Hydrology, UK) for providing the processed radar and LiDAR remote sensing images of Monks Wood NNR. This study was funded by the BNSC-Link Carbon Offset Verification project (UK), the Biffaward initiative (UK) and the FCAR foundation (Quebec, Canada).

Chapter 3

The carbon pool in a British semi-natural woodland

Summary

A comprehensive, generally non-destructive ground-based quantification of carbon in all significant above and below-ground forest components for five contrasting stands was undertaken in Monks Wood, South East Britain. The total carbon content of the five selected stands varied from 346 to 616 tonnes per hectare (t ha^{-1}). The mean carbon content of the forest components was approximately 2 t ha^{-1} for deadwood, 3 t ha^{-1} each for foliage and ground vegetation/litter, 18 t ha^{-1} for understorey shrubs and small trees, 28 t ha^{-1} for all roots, 78 t ha^{-1} for overstorey trees, and 335 t ha^{-1} for soils. The results of this study suggest that if the stands sampled at Monks Wood were representative of broadleaved woodlands in Great Britain and if understorey vegetation were considered, they would contain 92.6 Mt carbon. This contrasts with a previous estimate of 61.9 Mt carbon, which excluded understorey vegetation. The results highlight the importance of broadleaved woodlands as carbon stores and will be informative to current and future initiatives for developing British woodlands to offset greenhouse gas emissions.

3.1 Introduction

Since the beginning of the industrialised era, global atmospheric levels of carbon dioxide have risen from 280 to 367 ppm in 2000 and could reach between 478 to 1099 ppm by 2100 (IPCC 2000). This increase is attributable to fossil fuel combustion and land-use change such as deforestation. It is under this rationale that the UN Framework Convention on Climate Change recognises, along with a requirement to reduce carbon dioxide emissions, a need to preserve and enhance the amount of carbon stored in the terrestrial biosphere (UNFCCC 1997). In particular, Article 3.3 of the 1997 Kyoto Protocol allows changes in stored carbon, due to afforestation and reforestation, to be used to meet targets for net emission reductions.

In Great Britain, woodlands represent a considerable carbon store. Milne and Brown (1997) estimated that, although covering only 11% of the total rural land area (Barr *et al.* 1993), woodlands may hold as much as 80% of the total carbon contained in British terrestrial vegetation. However, these estimates only considered the carbon contained in the dominant

overstorey species. If shrubs and understorey trees were included, it would significantly increase the total store in broadleaved woodlands as the understorey vegetation can account for as much as 12% of the above-ground biomass (Satchell 1971).

Several European studies have provided data and methods for estimating biomass and carbon stored in overstorey and understorey trees, litterfall and deadwood of temperate forests ecosystems (i.e. Satchell 1971, Hamilton 1975, Swift *et al.* 1976, Cannell 1982, Vogt 1991, Matthews 1993). However, although Satchell (1971) estimated the total biomass of some forest components in Meathop wood (a woodland similar to Monks Wood in species composition and structure, located in Cumbria, Britain), there do not appear to be any comparable studies for semi-natural woodlands in Britain where the carbon content for all significant carbon pools, including soil, has been estimated and compiled. This paper presents a comprehensive and mainly non-destructive quantification of carbon in the overstorey, understorey, foliage, roots, ground vegetation/litter (GVL), deadwood and soils of a British deciduous woodland.

3.2 Materials and Methods

Fieldwork was undertaken in July 2000 at Monks Wood National Nature Reserve, a 157 ha temperate woodland located in Cambridgeshire, UK (52°24' N, 0°14' W). The dominant tree species are ash *Fraxinus excelsior L.*, oak *Quercus robur L.*, field maple *Acer campestre Linn.*, elm *Ulmus carpinifolia Gleditsh.* and aspen *Populus tremula Linn.*, whilst the dominant shrub species are hawthorn *Crataegus monogyna Jacq.*, hazel *Corylus avellana Linn.*, blackthorn *Prunus spinosa Linn.*, dogwood *Cornus sanguinea Linn.*, and wild privet *Ligustrum vulgare Linn.* The majority of overstorey trees are aged 70-80 years. The soils are Gleyed Brown Calcareous and Surface Water Gley resting on impervious clay (Hodge *et al.* 1973).

Five contrasting stands were selected, each defined as an identifiable spatial compartment of trees with relatively homogenous species composition, environmental characteristics and structure. The contrasting stands were chosen to be representative of the diversity of the wood (Table 3.1). Each stand was divided into 10 equal areas (8 in stand 5) and one sample plot of 20 m x 20 m (0.04 ha) was located randomly within each of these areas (Hamilton, 1975). This combined random and systematic sampling was intended to avoid sampling bias due to spatial trends and features (e.g. ridges or depressions).

Table 3.1: Description of the five contrasting stands in Monks Wood National Nature Reserve.[9]

Stand details -Total area of similar management within the wood.	**Vegetation structure and composition**	**Dry weight (t ha^{-1})**
Stand 1: 2.57 ha. Class: Non-interference. Total non-interference area : 34.14 ha.	Overstorey: field maple, oak, ash, well spaced and in equal numbers. Understorey: relatively mature consisting mainly of hawthorn, hazel, blackthorn and small privet schrubs.	271
Stand 2: 3.35 ha. Class: Non-interference. Total non-interference area: 34.14 ha.	Overstorey: field maple, ash, well spaced. Understorey: hawthorn and hazel.	233
Stand 3: 2.83 ha. Class: Field and glades. Total field and glades area: 9.00 ha.	Overstorey: few large trees, mixed composition: aspen, oak, field maple and ash occur at various stages of maturity. Understorey: large thickets of hawthorn and occasionally blackthorn.	148
Stand 4: 3.69 ha. Class: Woodland. Total woodland area: 57.89 ha.	Overstorey: ash and oak, fairly dense and closed canopy. Understorey: little understorey. Some privet shrubs and occasional hawthorn and hazel.	215
Stand 5: 0.84 ha. Class Mixed and coppiced. Total mixed and coppiced: 55.76 ha.	Overstorey: mostly elms, densely packed, which have escaped the Dutch elm disease. Understorey: understorey composed of elm saplings. Occasional hawthorn.	413
Belgium	Oak 120 years old with coppiced understorey of hazel	384
Former Czechoslovakia	Oak and ash 96 years old, with lime (*Tilia sp.)* and field maple understorey	360
Russia	Oak and ash 48 years old, Norway maple (*Acer platanoides Linn.*) understorey	261
Russia	Aspen and birch sp. 45-55 years old, some Norway spruce (*Picea abies Degen.*)	231
United Kingdom	Oak, ash, some birch, varying ages up to 81 years old, hazel understorey	203

The class indicates past treatments applied to the stands (Steele and Welch 1973). The table also includes the total dry weight (t ha^{-1}) of overstorey, understorey, roots and foliage for all stands in Monks Wood. Dry weight (t ha^{-1}) for woodlands of similar age (70-80) and

[9] See text for comparison between woodlands

species composition to Monks Wood located elsewhere in the world are also given (Cannell 1982).

3.2.1 Vegetation

Monks Wood is a National Nature Reserve and, as such, destructive measurements were prohibited. Therefore, standard forestry mensuration methods for estimating volumes and mass were adopted (Hamilton 1975). The species and diameter at 1.3 meters above-ground (DBH) were recorded in all plots for all woody stems of 7 cm DBH and above. A total of 2283 trees in 48 plots were measured. Trees were classified as overstorey (DBH $\geq$ 18 cm), understorey (7 $\leq$ DBH < 18 cm) or as saplings (DBH< 7 cm). Regression equations from Crockford (1987) were used to estimate the above-ground woody volume of each overstorey tree and total dry mass for all understorey trees. These regressions are based on destructive measurements of dominant species (ash, oak and beech) and a selection of understorey/coppiced trees across Britain. Proxy models were defined for overstorey tree species for which no regressions were available. For birch, aspen and elm overstorey trees, the regression for ash was used. For field maple, regressions for ash and beech were used and the results were averaged. Estimation of dry mass and carbon content was then achieved using conversion factors based on studies conducted in woodlands of similar soil type, vegetation composition, structure, and management to Monks Wood. Table 3.2 summarises the methodology and presents the conversion factors.

Foliage dry weights were obtained on a per species basis, as a percentage ratio of the above-ground woody dry weight for the respective species (Satchell 1971). The mean percentage ratio from oak, ash, birch and sycamore was used as proxy value for both ash and elm; sycamore was used as proxy value for field maple and hazel was used as proxy value for the understorey as no values were available for these species or components. Likewise, root dry weights were derived as a percentage ratio of the total above-ground woody dry weight. This conversion factor was derived from Cannell (1982) as the average ratio of roots to total above-ground dry weight of 26 European deciduous woodlands. A 1 m x 1 m square sample of living ground vegetation (including saplings) was also collected from the centre of each plot, together with all leaf and small woody litter. The sample was cut down to soil level, removed from the plot, air dried and weighed to estimate dry mass and carbon content. Finally, all deadwood was measured and counted to estimate volume and carbon content.

Table 3.2: Summary of the methodology used for estimating the carbon content of the five stands.

Forest Components	Species and unit measured	Volumes (m^3)	Conversion to Dry Weight (DW)	Conversion of Dry weight to Carbon Content (CC) (%)
Overstorey DBH ≥ 18 cm	Ash	Total AG Volume = 0.65002 - 0.063304.DBH + 0.0022603.DBH^2 (r^2 = 0.98)[a] Stemwood Volume = 0.48953-0.044703.DBH + 0.0014869. DBH^2 (r^2 = 0.93)	53	49.3[f]
	Field maple	Regressions for ash and beech used as proxy models. Results were averaged.	56	50.0
	Oak	Total AG Volume = 0.28191 - 0.031727.DBH + 0.0016827.DBH^2 (r^2 = 0.99) Stemwood Volume = -0.064351+0.00082257.DBH^2 (r^2 = 0.99)	49	49.0
	Birch	Regressions for ash used as proxy models.	53	48.8
	Aspen	Regressions for ash used as proxy models.	36[b]	49.9
	Elm	Regressions for ash used as proxy models.	43	50.2
	Beech	Total AG Volume = -0.2226 + 0.0014153.DBH^2 (r^2 = 0.97) Stemwood Volume = -0.34177+0.023826.DBH+0.00045029.DBH^2 (r^2 = 0.99)	N.A.	N.A.
			Woody aG DW/ Total volume (%)	
Understorey 7 cm ≤ DBH <18 cm	All species dealt with as one unit (total BA per plot).	Total AG Volume = 14.8 + 6.776. BA (r^2 = 0.96)[a]	Dry Weight = 9.59+ 3.522.BA. (r^2 = 0.93)[a]	49[g]
Foliage	Ash	----	2.5[c]	45[h]
	Field maple		3.1	
	Oak		2.9	
	Birch		2.5	
	Aspen		2.7	
	Elm		2.7	
	Hazel		3.7	
			Foliage DW / AG woody DW (%)	
Roots	----	----	28.5[d] Roots DW / AG woody DW (%)	For overstorey trees, see Species-specific CCs. For the understorey, see understorey CC.
Deadwood	Standing dead tree with crown	Dealt with as either overstorey or understorey depending upon DBH values.		
	Standing dead tree without crown	Height and DBH used to estimate volume.		
	Fallen branches: - Mid-diameter ≥ 7cm	Length and mid-diameter of pieces on the forest floor with mid-diameter ≥ 7 cm recorded per plot and used to calculate volume (Hamilton, 1975). Data for pieces > 3 m in length recorded as 3m sections.	26.7[e] Deadwood DW / Deadwood volume (%)	49[g]
	Fallen branches: - 4cm ≤ mid-diameter < 7cm	All fallen small branches, with mid-diameter between 4 and 7 cm counted and subsample used to derive mean dimensions of 5.5 cm diameter and 1 m length. Resulted in a volume of 0.0023 m^3 per branch.		
GVL	See text	See text	See text	45[h]

All conversion factors are shown to one decimal place only. GVL stands for Ground Vegetation and Litter; DBH for Diameter at Breast Height; BA for Basal Area; AG for Above-ground. There are no beech in Monks Wood but data required for proxy values; Units for DBH and BA are cm and cm^2 respectively. Sources: a. Crockford (1987) b. Hamilton (1975). No values available for aspen. Poplar used as proxy value. c. Satchell, (1971). d. Cannell (1982). e. The mean relative density of fallen dead wood obtained in Meathop Wood (Swift *et al.* 1976) f. Matthews (1993) g. Birdsley (1990) and Matthews (1993) h. Ajtay *et al.* (1979) and Vogt (1991).

3.2.2 Soils

Soils are spatially very heterogeneous (Brady 1990), so spatial variability of both carbon content and bulk density across the plots and through the soil profile may be large. Consequently, a comprehensive study of the soil carbon pools in Monks Wood was beyond the scope of this study. However, a preliminary analysis was conducted which included an estimate of the soil carbon pool to a depth of 50 cm. Thomasson (1971) analysed a soil of the Hanslope series (a soil similar to that of Monks Wood) under pasture-land and showed that carbon content decreases from 5.6% at 0-15 cm depth to 1.0% at 15-51 cm depth. A depth of 50 cm is therefore likely to contain a high proportion of the total carbon. A core of soil to a depth of 50 cm was collected from a random location within each plot using a soil auger of 2.5 cm diameter. The soil core from each plot was oven dried and 5 g subsamples ignited in a Muffle furnace, with loss on ignition used to calculate carbon content as a percentage of dry weight (Bengtsson and Enell 1986). The average bulk density of each soil type was calculated from the dry weight and volume of four independent soil cores, each 7 cm by 50 cm, taken from random locations within each stand. Bulk density was multiplied by the carbon content of each plot sample and the estimates for all plots within a stand were averaged and used to calculate carbon content per hectare to a depth of 50 cm.

3.2.3 Carbon content in British natural deciduous woodlands

Milne (1992) and Milne and Brown (1997) have estimated the total carbon content held in British woodlands using a Forestry Commission census of commercial woodlands in the state and private sectors (Locke 1987). Stemwood volumes per species were categorised in 10-year bands of forest age and divided by the equivalent land area. This provided average stemwood volumes per unit area for each age/species group. To convert stemwood volume to complete carbon content of trees (including roots), they estimated carbon density using a factor χ of 0.38 t m^{-3}. This factor was obtained as $\chi = \rho\omega\phi$ where ρ is the mean specific density of broadleaved species (0.55 t m^{-3}), ω is the mean ratio of total volume of wood to the stemwood volume (1.5) and ϕ is the fraction of wood mass which is carbon (0.46). However, this method does not differentiate between natural and commercial broadleaf woodlands. Consequently, to estimate a factor for natural broadleaf woodlands, results from the study in Monks Wood were used. Stemwood volumes (V_{stem}) and total volumes (V_{tot}) were calculated using the regressions presented in Crockford (1987) (Table 3.2), from which the mean ratio of total volume (V_{tot}, including roots) to stemwood volume (V_{stem}) was derived. Root volume was derived from above-ground vegetation volume using the

proportional relationship between root dry weight and above-ground vegetation dry weight (Table 3.2). Finally, a factor (χ) to convert stemwood volumes to carbon content was obtained using V_{stem} and the average carbon held in the vegetation of the five stands.

3.3 Results

3.3.1 Vegetation and soils

The highest carbon content per hectare, excluding soil, occurred in stand 5 (213 t ha^{-1}) and the lowest in stand 3 (78 t ha^{-1}), with a range of 135 t ha^{-1}. When the soil carbon pool to 50 cm depth is included, the range between the stands increases to 270 t ha^{-1} (Table 3.3). The quantity of carbon in the soil to a depth of 50 cm was considerably greater than the quantity of carbon in all other forest components combined. Forest components, in order of decreasing mean carbon pool size, were as follows: soils, overstorey wood, roots, understorey wood, GVL, foliage, deadwood. The smallest three carbon pools were approximately equal in size.

Table 3.3: Carbon content of all stand components (t ha^{-1}).

Stand	Overstorey			Understorey			DW	GVL	Sub Total	Soils	Total
	WAG	Fol	Rts	WAG	Fol	Rts					
1	85	2.2	24.3	16	0.9	4.5	0.9	4.6	138	346	484
2	70	1.6	19.9	18	0.6	5.0	1.6	3.1	119	331	450
3	38	1.0	10.9	18	0.6	5.0	2.5	2.3	78	268	346
4	53	1.3	15.1	27	0.9	7.8	1.7	3.4	111	327	437
5	143	3.5	40.7	14	1.7	4.0	3.4	3.1	213	402	616
Mean	78	1.9	22.2	19	0.9	5.3	2.0	3.3	132	335	467

WAG stands for Woody Above-ground; Fol for Foliage; Rts for Roots; DW for DeadWood and GVL for Ground Vegetation and Litter. All figures rounded to the integer or the first decimal in accordance to the resolution of the measurements.

Figure 3.1 shows interval plots for the carbon content of soils; of all components excluding soils; and of all components excluding soils, roots and foliage. Since only limited destructive sampling was possible, the estimates of carbon are generally based on allometric relationships developed for other woodlands. Hence, quantification of the overall error in the final carbon estimate is not possible. However, confidence limits at the 95% level are given for the carbon content of soils and for the carbon content of all components excluding soils, roots and foliage. No confidence limits are given for the carbon content of all components excluding soils, as root and foliage carbon contents were estimated as functions of other components. These confidence limits are based on the measurements collected at Monks Wood and do not include error introduced from other sources.

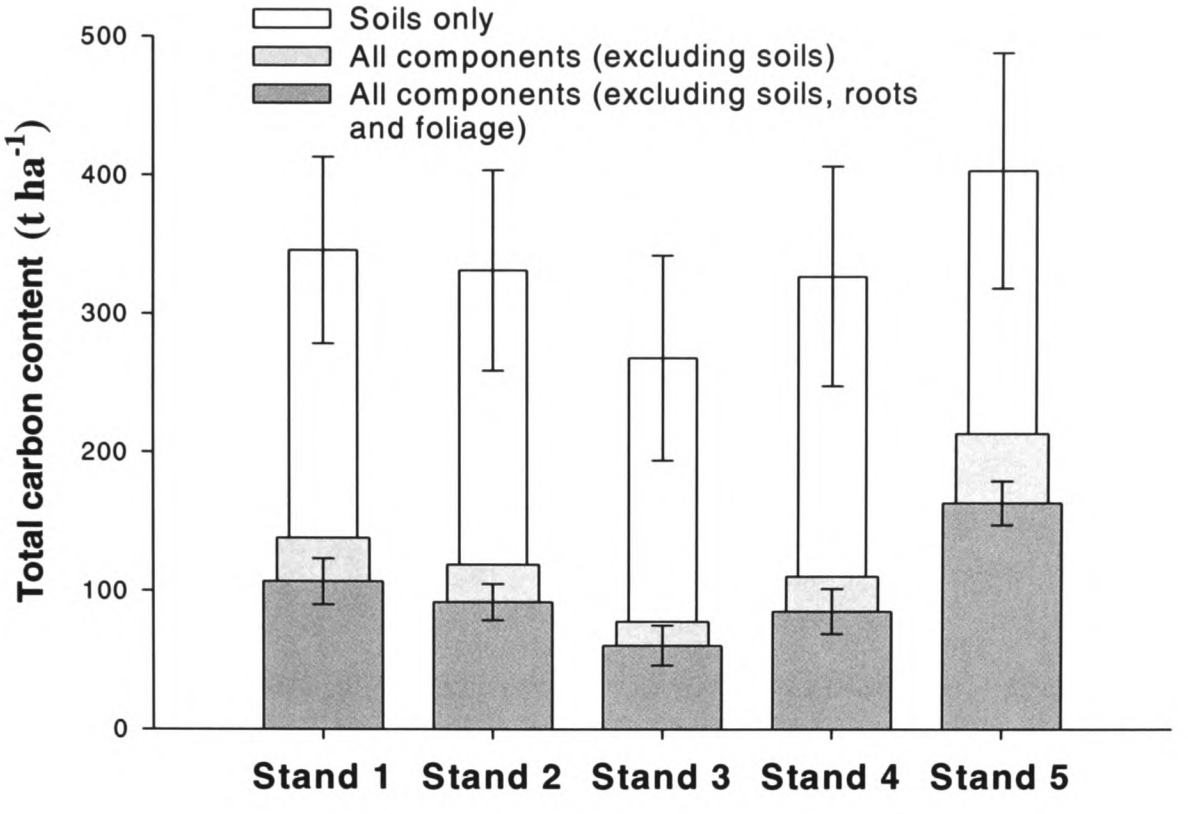


Figure 3.1: Interval plot showing the carbon content of soils; of all components excluding soils; and of all components excluding soils, roots and foliage (t ha^{-1}).

Figure 3.2 is a scatterplot showing above-ground carbon content and soil carbon content for each plot in the stands, along with stand averages (large, black symbols). The results show that at the stand scale, the size of the above-ground carbon pool is strongly correlated with the size of the soil carbon content (0.97, $p<0.05$). However, when all the plots from all the stands are considered, the correlation is still significant but much weaker (0.34, $p<0.05$), reflecting the heterogeneity within each stand.

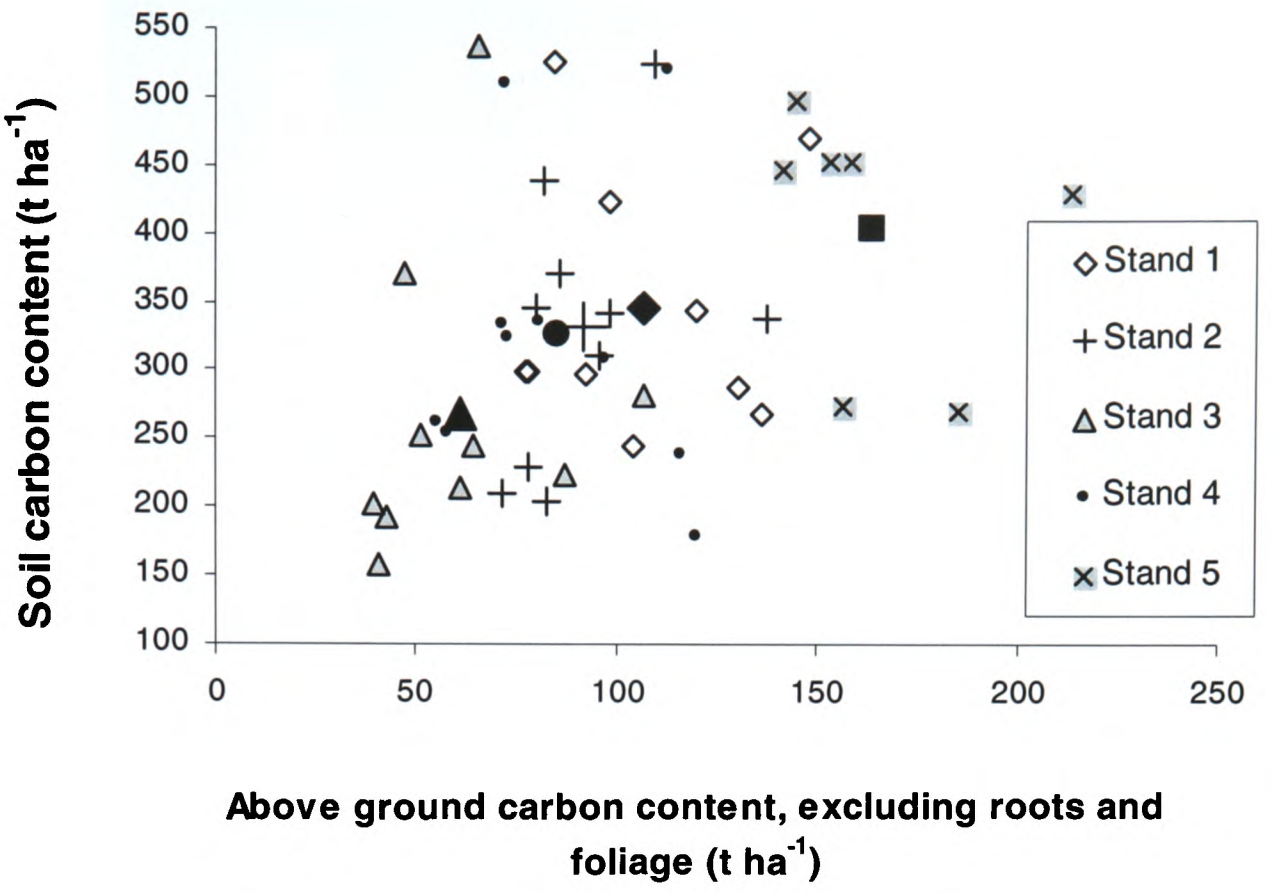


Figure 3.2: Scatter plot showing above-ground carbon content and soil carbon content for the 5 stands. Larger, black symbols represent stand averages

An estimate of the total carbon content of Monks Wood was obtained by weighting the carbon content per hectare per stand to the total area of the wood, falling within the same management class (Table 3.1). This suggests that Monks Wood contains a total of 79 ktonnes of carbon and 23 ktonnes if soils are excluded.

3.3.2 Carbon content in British natural deciduous woodlands

Finally, the biomass expansion factor for converting stemwood volumes to total volumes and the factor for converting stemwood volumes to carbon content per hectare are presented in Table 3.4. The mean ratio of total volume to stemwood volume (ω) is 2.12. Considering the overstorey, understorey, foliage, roots, GVL and deadwood components, the conversion factor from stemwood volumes to carbon content (χ) is 0.57.

Table 3.4: Derivation of factors to convert stemwood to total carbon content.

Stands	V_{stem} (m^3 ha^{-1})	V_{tot} [a] (m^3 ha^{-1})
1	190	482
2	215	422
3	67	279
4	194	387
5	494	888
Avg.	V_{stem} **=232**	V_{tot} **= 492**
CC_{tot} [b]	**132 t ha^{-1}**	
ω	**=** V_{tot} **/** V_{stem} **= 2.12**	
χ	**= 0.57 t m^{-3}** (CC_{tot} / V_{stem})	
	= 0.38 t m^{-3} (Milne,1992)	

a. Includes overstorey and understorey woody volumes (including roots). **b.** Includes all vegetation carbon

3.4 Discussion

Total dry weights of overstorey, understorey, roots and foliage for stands 1-5 in Monks Wood are generally within the observed range of European dry-biomass figures. However, stand 5 was slightly higher (Table 3.1). Differences between the dry-biomass estimates of the European woodlands and stands 1-5 reflect not only differences in species composition and age, but also in factors such as stem density, climate, and soil type or fertility.

Comparison of the carbon content and the bulk density of soils in Monks Wood with those of soils elsewhere show similar results (Table 3.5). In addition, 232 t ha^{-1} has been estimated as an average carbon content for soils in England and Wales (Milne and Brown 1997). The results for stands 1-5 fall within these values. Both the Ragdale woodland soil at Melton Mowbray and the Hanslope/Ragdale soil in Monks Wood have a higher average carbon content than the soils under pasture or grass. A woodland soil is expected to have a higher carbon content than a soil on pastureland, due to the transfer of leaf litter and deadwood residues to the soil (Brady 1990). The Monks Wood soil had a lower carbon content than the Ragdale soil under woodland. Soil type and woodland structure may account for these differences.

Table 3.5: Bulk density and organic carbon content of Hanslope and Ragdale soils in the Melton Mowbray district in Britain (Thomasson 1971) compared with stand 1 and 4.

Soil type and land-use	**Depth (cm)**	**Bulk density (g cm^{-3})**	**Carbon content (%)**
Ragdale under	0 - 23	0.8	Combined:
Oak/hazel woodland	23 - 43	1.2	5.6
	43 - 66	1.6	
Ragdale under pasture	0 - 18	1.2	4.3
	18 - 30	1.3	1.1
	30 - 56	1.4	N.A
Hanslope under pasture	0 - 15	1.1	5.6
	15 - 51	1.2	1.0
Hanslope temporarily	0 - 18	1.3	2.6
Under grass	18 - 33	1.5	0.8
	33 - 60	1.6	0.7
Stand 1	0 - 50	1.1	5.4
Hanslope/Ragdale complex			
Stand 4	0 - 50	1.1	4.7
Hanslope/Ragdale complex			

Bulk density and organic carbon content are also given for separate soil samples taken from stand 1 and 4 which fall into the Hanslope/Ragdale complex at Monks Wood. The mean organic carbon content was calculated separately from six and four samples each from stands 1 and 4 respectively. The mean bulk density was calculated from four samples taken from stands 1 and 4.

According to Cannell and Milne (1995), broadleaved woodlands account for 46.8% of the estimated total 113.8 MtC in British vegetation, despite covering just 4.1% of the total rural land area. Conifers cover 6.1% of the land area, but contain only 25.4% of the total carbon. These figures were calculated on the basis that broadleaved woodlands hold, on average, 61.9 tC ha^{-1} in trees compared with 21 tC ha^{-1} for conifer forests (Cannell and Milne 1995). The mean carbon content per hectare excluding soils for stands 1-5 in Monks Wood is 132 tC ha^{-1}, about 47 % greater than Cannell and Milne's (1995) average for broadleaved woods in Britain. Cannell and Milne's (1995) figures are based on a method (see Milne 1992, also

used by, Cannell 1999 and Milne and Brown 1997, 2000) which does not include the carbon present in the understorey, deadwood or GVL as it was designed to estimate the carbon content of commercial woodlands. For stands 1-5 in Monks Wood, these components averaged 30 t ha^{-1}, representing nearly 25% of the total carbon contained in the wood (soil excluded). When the average stemwood volume for stands 1-5 at Monks Wood (Table 3.4) is converted into carbon content using the Milne and Brown (1997) method, the result is 88.1 t ha^{-1}. This is close to the average they present for broadleaved trees aged 70-80 years (i.e. the majority of overstorey trees found in Monks Wood) of 76.8 t ha^{-1} but contrasts with our 132 t ha^{-1} average. This indicates that although an ω factor of 1.5 may be appropriate for commercial broadleaved woodlands, where the stemwood volume constitutes a high proportion of the total woody volume, this may not be the case for trees in more natural woodland where understorey trees and shrubs represent non-negligible standing carbon pools. Consequently, information on the proportions of natural and commercial broadleaf woodlands is required to accurately assess how the results of this study might affect estimates of the total stock of carbon in British woodlands.

3.5 Conclusion

The results of this study illustrate the importance of Monks Wood and similar woodlands as important carbon reservoirs. If trees are to be grown in the future with the aim of making a long-term contribution to carbon sequestration, then these results support current government policy which encourages the establishment of broadleaved woodland. Plantations plus their products can potentially equal the carbon storage of a mature woodland, but only if harvested timber and their products decay slowly (Cannell and Milne 1995). Broadleaved woodland is also of higher conservation and aesthetic value.

Acknowledgements

This study was supported by the BNSC-Link Carbon Offset Verification project, the Biffaward initiative and the FCAR foundation. The authors would like to thank Nick Brown, Peter Savill and Peter Darrah (University of Oxford) for their academic input; Heiko Balzter and Dave Hughes (CEH Monks Wood) for providing support and information about Monks Wood and Jane Houston, Scott Henderson, Richard Pearson, Pam Berry and Rose Askew (University of Oxford) for their invaluable help with data collection.

Chapter 4

Quantifying forest above-ground carbon content using LiDAR remote sensing

Summary

The UNFCCC and interest in the source of the missing terrestrial carbon sink are prompting research and development into methods for carbon accounting in forest ecosystems. Here we present a canopy height quantile-based approach for quantifying above-ground carbon content (AGCC) in a temperate deciduous woodland, by means of a discrete-return, small-footprint airborne LiDAR. Fieldwork was conducted in Monks Wood National Nature Reserve UK to estimate the AGCC of 5 stands from forest mensuration and allometric relations. In parallel, a digital canopy height model (DCHM) and a digital terrain model (DTM) were derived from elevation measurements obtained by means of an Optech Airborne Laser Terrain Mapper 1210. A quantile-based approach was adopted to select a representative statistic of height distributions per plot. A forestry yield model was selected as a basis to estimate stemwood volume per plot from these heights metrics. Agreement of r=0.74 at the plot level was achieved between ground-based AGCC estimates and those derived from the DCHM. Using 20x20m grids superposed to the DCHM, the AGCC was estimated at the stand level and at the woodland level. At the stand level, the agreement between the plot data upscaled in proportion to area and the LiDAR estimates was r=0.85. At the woodland level, LiDAR estimates were nearly 24% lower than those from the upscaled plot data. This suggests that field-based approaches alone may not be adequate for carbon accounting in heterogeneous forests. Conversely, the LiDAR 20x20 m grid approach has an enhanced capability of monitoring the natural variability of AGCC across the woodland.

4.1 Introduction

The need to increase the accuracy and the spatial coverage of carbon accounting in forest ecosystems has both political and scientific rationales. Politically, countries ratifying the Kyoto Protocol to the United Nations Framework Convention on Climate Change (UNFCCC) will be required to report annually their direct human-induced (DHI) emissions and removal of carbon dioxide (UNFCCC 1997). The reporting requirements include DHI emissions and removal of carbon dioxide from Land-use, Land-use Change and Forestry

activities, which comprise deforestation, afforestation, and reforestation activities (Article 3). In addition to the need to report nationally DHI emissions and removal of carbon dioxide, mechanisms in the Protocol allow countries to implement jointly projects aiming at reducing atmospheric carbon dioxide through Land-use, Land-use Change and Forestry activities (Article 4, Article 12). Estimating DHI carbon dioxide emissions from forestry related activities implies a prior knowledge of the carbon content of the land area, from which net carbon change can be inferred through subsequent carbon content estimations. However, large uncertainties remain in estimating carbon content both in the above and below-ground components of forests due to the spatial coverage of these ecosystems, their heterogeneity and the inherent difficulty to produce field-based inventories at national, continental and global scales. This need to improve carbon content estimates in forest ecosystem is also of scientific interest. Reducing these uncertainties may help in solving the missing terrestrial carbon sink, which is of the order of 1.9 Petagrams of Carbon (Pg C) annually (Houghton *et al.* 2001). Several studies suggest that it may be unaccounted for in the temperate and boreal forest regions (Rayner *et al.* 1999, Bousquet *et al.* 2000). Thus, accurate, rapid and cost efficient tools are required to improve the estimates of carbon content in temperate and boreal forest ecosystems and to enable countries, or any organisation involved in the nascent carbon-trading scheme to estimate accurately the carbon content of their national or project-related forested lands.

Although field-based carbon estimations remain necessary for these purposes, integrating remote sensing into carbon inventory schemes allows recovery of carbon content and spatial interpolation of estimates across landscapes, while reducing the total costs and the need for extensive field-based sampling. Several radar or passive optical remote sensing approaches have already proven adequate for quantifying above-ground biomass in relatively homogeneous and young forests (Franklin *et al.* 1986, Ahern *et al.* 1991, Ripple *et al.* 1991, Dobson *et al.* 1995, Ranson *et al.* 1995, Fransson and Israelsson 1999). Unfortunately, these are still inapt for monitoring biomass of mature or heterogeneous forest ecosystems (Imhoff 1995, Holmgren and Thuresson 1998). Radar and passive optical remote sensing suffer from a common setback: the signal-to-noise ratio or the sensitivity of these approaches decreases with increasing canopy structural heterogeneity and age. A comparatively recent, active remote sensing technique that operates on a principle called Light Detection And Ranging (LiDAR) has strong potential to monitor forest biomass and volumes across ecosystems and above-ground biomass ranges (Nilsson 1996, Lefsky *et al.* 1997, Lefsky *et al.* 1999a, Lefsky *et al.* 1999b, Means *et al.* 1999, Means *et al.* 2000). In addition to being less restricted by weather conditions and sun angle considerations than other optical remote

sensing approaches, LiDAR systems provide georeferenced digital elevation at high spatial resolution, with high accuracy and at relatively low costs (for approximate costs, see www.airbornelasermapping.com). However, in contrast to optical and radar systems, LiDAR devices collect samples along a flight path and as such, are not imaging systems. Interpolation between the sample points is required for thematic mapping. Flood and Gutelius (1997), Wehr and Lohr (1999), and www.airbornelasermapping.com provide good overviews of the conceptual basis and functioning of these systems. Methods for processing the collected data are summarised by Axelsson (1999).

For forestry application, two types of LiDAR systems can be differentiated: discrete-return devices (DRD) and waveform recording devices (WRD). The general specifications of these system types are detailed in Lefsky *et al.* (2002). Both DRDs and WRDs have been used worldwide for characterising forest structure (Lefsky *et al.* 1999a, Hyyppä *et al.* 2000, Hyyppä *et al.* 2001, Drake *et al.* 2002, Gaveau and Hill 2003). These technologies have successfully been used to retrieve tree height (Naesset 1997a, Magnussen and Boudewyn 1998, Magnussen *et al.* 1999), above-ground biomass and timber volumes (Naesset 1997b, Hyyppä *et al.* 2001) and crown properties (Naesset 2002, Naesset and Okland 2002). Lefsky *et al.* (2002) and Lim *et al.* (2003) review the potential of LiDAR devices for retrieving forest parameters. Although some studies have investigated their potential for forest carbon accounting (e.g. Drake *et al.* 2002, Nelson *et al.* 2003, Omasa *et al.* 2003), there is still a need to develop methods suitable for temperate and uneven-aged, mixed deciduous woodlands. In this paper, we present a method based on DRD LiDAR canopy height measurements for estimating forest above-ground carbon content (AGCC) in a semi-natural, deciduous woodland, for which extensive ground-based measurements were collected.

4.2 Data collection

4.2.1 Study area

Monks Wood National Nature Reserve (NNR) is a 157 ha semi-natural, partly managed, temperate deciduous woodland located at 52°24'N, 0°14'E in Cambridgeshire, UK. The dominant tree species are ash *Fraxinus excelsior* L., oak *Quercus robur* L., field maple *Acer campestre* Linn., with some occasional clusters of elm *Ulmus carpinifolia* Gleditsh. and aspen *Populus tremula* Linn. Dominant shrub species include hawthorn *Crataegus monogyna* Jacq., hazel *Corylus avellana* Linn., blackthorn *Prunus spinosa* Linn., dogwood *Cornus sanguinea* Linn., and wild privet *Ligustrum vulgare* Linn. Heavy felling was made

in the wood during and after the 1914-18 war so the majority of overstorey trees are estimated to be aged 70-80 years. The highest part of the reserve rises to about 46 metres above sea level with a maximum slope angle of 14.5° (Steele and Welch 1973).

4.2.2 Ground-based above-ground carbon content data (48 plots)

Fieldwork was undertaken in July 2000. Five contrasting stands falling under a specific management class and representative of the woodland were selected (Table 4.1). These were defined as compartments of trees with relatively homogenous species composition and structure. Each stand was divided into a grid of 10 equal areas (8 in stand 5). One 20mx20m sample plot was located randomly within each of these 10 gridded areas (8 in stand 5). This sampling approach yielded 10 20mx20m sample plots in 4 of the 5 stands, and 8 in stand 5. Only 8 sample plots were recorded in stand 5 because of its homogeneity and small size (Patenaude *et al.* 2003). The plots were selected following the methodology proposed by Hamilton (1975). Not all plots location could be recorded using a hand-held GPS. However, all were located using field-based quantitative description of plot centre locations (distance and orientation from path intersection and/or easily identifiable features).

Monks Wood NNR is a protected reserve so only limited destructive measurements were allowed. The approach summarised here relies primarily on non-destructive forestry mensuration methods and is detailed in Patenaude *et al.* (2003). For each plot, species and diameter at breast height (DBH) for all woody stems of at least 7cm DBH were recorded, totalling 2272 trees in 48 plots. Following the approach by Crockford (1987), trees of DBH larger than or equal to 18 cm were defined as overstorey, whereas trees and shrubs between 7-18 cm DBH were defined as understorey. A 1x1 m sample of ground vegetation and litter (including trees and shrubs < 7 cm DBH) was collected from the centre of each plot. This sample was air-dried and weighed to estimate dry mass (see Patenaude *et al.* 2003). Belowground vegetation components and soils were not considered here, as these components were not estimated from the LiDAR measurements.

For each overstorey tree per plot, total woody above-ground volume was calculated using species-specific regressions developed by Crockford (1987). Species-specific values for wood basic density and carbon content published by the UK Forestry Commission were then used to convert each stemwood volume into carbon content (Hamilton 1975). Proxy values were used when species-specific values were not available (see Patenaude *et al.* 2003 for details). Understorey species were dealt with as one unit in each plot and their total dry

weights for all shoots per plot were estimated using relationships based on basal area (Crockford 1987). A conversion figure of 0.49 was then used to convert understorey dry weight to carbon content (Birdsley 1990, Matthews 1993). Foliage dry weight was estimated by species for each overstorey tree. For the understorey, foliage dry weight was derived as a percentage of above-ground understorey wood dry weight. These foliage conversion factors were derived from a study conducted in an English wood similar to Monks Wood NNR in terms of species composition and environment (Satchell 1971). The carbon content for the foliage, ground vegetation and litter was then assumed to be 45% of dry weight, a figure commonly used for foliage, herbs and litterfall (Ajtay *et al.* 1979, Vogt 1991). Table 4.1 summarises the field data collection and the resulting AGCC estimates per stand. For further information on the ground-based AGCC estimation in Monks Wood, see Patenaude *et al.* (2003).

Table 4.1: Summary of the stand reference data (modified from Patenaude *et al.* 2003)

Stand no. [ha]	**Woodland area** [a.]	**Plots/stand [GPS located]** [b.]	**Trees per ha (dbh≥ 7cm)**	**Stand basal area (m^2 ha^{-1})**	**AGCC** [c.] **(t ha^{-1})**
1 [2.57]	17.07 NI	n=10 [7]	933	31.15	109 (8.2)
2 [3.35]	17.07 NI	n=10 [3]	1113	31.26	93 (6.3)
3 [2.83]	9.00 FG	n=10 [4]	1045	19.75	60 (7.1)
4 [3.69]	57.89 W	n=10 [6]	1008	30.92	86 (7.8)
5 [0.84]	55.76 MC	n=8 [5]	852	70.77	165 (8.8)
Total woodland:	156.79 ha	n=48 [25]	Avg. 990	Avg: 36.77	Total: 17.99 kt

a. Surface area (ha) of Monks Wood, which falls under similar vegetation structure and management class (Steele and Welch, 1973). NI= Non-interference; FG=Fields and glades; W=Woodland; MC=Mixed and coppiced.

b. Numbers in brackets correspond to the number of plots located using a global positioning system (GPS).

c. Integrates all woody above-ground and foliage components as well as ground vegetation and litter. Values are means. Standard errors are given in parentheses.

4.2.3 LiDAR ground elevation (1 m grid) and canopy elevation (1m grid)

On the 10th of June 2000, a DRD, small footprint Airborne Laser Terrain Mapper (Optech ALTM 1210) was flown over the Monks Wood NNR, in a north-south direction. The ALTM emits laser pulses at wavelength 1047 ηm (near infrared); part of the electromagnetic spectrum at which vegetation is highly reflective. The precision of the instrument was approximately 0.60 m in the *x* and *y* position and 0.15 in *z* (Gaveau and Hill 2003, www.optech.on.ca). Table 4.2 summarises the specifications of the ALTM flight and data collection. The scanning orientation, perpendicular to the flight direction, generated a saw-toothed sampling pattern. This, together with overlapping and combined flight paths

produced an irregular distribution of laser footprints (Table 4.2). For each point sample, only the first and last significant returns were considered, corresponding to the first and last part of the recorded signal.

Table 4.2: Summary of the LiDAR and flight data

System	Wavelength	Significant returns recorded	Footprint diameter at nadir	One ground canopy hit per:			Scan angle
				a. Min	b. Max	c. Mean	
Optech ALTM 1210	1047 ηm	First and last	0.25 m	2.80 m^2	6.50 m^2	4.83 m^2	± 10°

a. In areas scanned with overlapping flightlines
b. In areas sampled in one flightline
c. Mean across the woodland

Elevation attributes of the first and the last significant returns were treated as separate datasets. Interpolation of elevation attributes from the point-clouds of the first and last-returns to two spatially continuous surfaces was achieved in two stages. Firstly, a Triangulated Irregular Network (TIN) based on a Delaunay triangulation was applied to each dataset. Secondly a rectangular grid of pixels was extracted from each TIN using a linear interpolation method at a constant sampling interval of 1 m to generate the surfaces. This created a 1x1m spatial resolution raster for each surface. The surface layer created from the first return was assumed to approximate canopy surface elevations. The layer generated from the last return was assumed to be from ground surfaces or surfaces located beneath or within the canopy. From these, a Digital Canopy Height Model (DCHM) and a Digital Terrain Model (DTM) were generated as described below. A clear distinction between elevations and heights is made here. Whereas elevations are given in meters above sea level, height is the vertical distance between two points (e.g. ground and tree canopies).

To generate the DTM from the last return surface layer, differentiating between returns from the ground and surfaces located from within the canopy was crucial. Several methods have been proposed (e.g Kilian *et al.* 1996, Ruppert *et al.* 2000). Here, an adaptive morphological filter was applied to identify local minima, varying the filter size according to canopy structural heterogeneity. Enlarging the filter size where fewer canopy gaps were present increased the probability of locating local minima. Where the canopy was more open, smaller filter sizes were selected (Hill *et al.* 2003). A thin plate spline interpolation process was then applied to render a terrain surface from extrapolating between the

extracted local minima (Hill *et al.* 2003). This method of interpolation fits a smooth (continuous and differentiable) minimum curvature surface passing through all input point data. To generate the Digital Canopy Height Model, the DTM (corrected for bias, Section 4.3.2) was subtracted on a per pixel basis from the canopy elevation layer created from the first return.

4.2.4 Theodolite ground elevation (244 points) and canopy elevation (82 points)

Reference elevation data were recorded in June 2000 using a Pentax R-125N electronic total station (laser theodolite) which has a ranging distance, D (meters), of precision 0.005 + 0.003D. For each observation, the x, y and z position was calculated in relation to a permanent Ordnance Survey (OS) benchmark located at the Centre for Ecology and Hydrology (CEH) Monks Wood research station. The elevation values (z) were calculated in meters above sea level in relation to the OS 1936 Datum for Great Britain.

A total of 326 reference point measurements were collected, comprising 244 terrain elevation samples, recorded under the canopy and along exposed paths (rides), and 82 shrub and tree canopy elevation measurements. These three datasets (terrain, shrubs, trees) were collected in different locations due to the logistics of data collection. For the terrain and shrubs, the total station was operated from the ground. The network of rides enabled access to the wood with the total station and a series of radial points to be recorded. Among the terrain elevation samples, 140 were taken under the canopy while 104 were alongside rides, locating the prism on a pole of known height. For shrub canopy elevation, the prism was attached to an 8 m extendible pole. A total of 43 shrub canopy elevation samples were taken, 34 of which were along a 275m transect. For the tree canopy elevation, the total station was located at the top of a 15 m tower situated at the research centre of CEH Monks Wood. An 18m truck-mounted platform was used to provide access to upper canopies and to locate the prism. 25 of the 39 tree canopy elevation samples were located along a 275m transect that was easily accessible with the apparatus. All samples of tree and shrub canopies were collected at the edge of the wood. For all canopy samples, the reflecting prism was located at random on crown upper surfaces not necessarily representing crown apexes, thus measuring canopy elevation rather than tree elevation in a similar way to the LiDAR method. Further information on the acquisition of the reference datasets are detailed in Gaveau and Hill (2003).

4.2.5 Drymass density (49 trees)

An assessment of dry mass density in Monks Wood was made from coring samples of dominant tree species. The sampled trees were selected so that their DBH was roughly that of 25 ± 10 cm. Assuming unmanaged conditions and low productivity, this is the typical DBH for these trees species when aged between 70-80 years (the average tree age in Monks Wood) (Edwards and Christie 1981). A total of 49 trees were cored, from which tree rings were counted to estimate age. Dry mass density from these tree cores was estimated for all overstorey tree species (Table 4.3). The species averages with standard errors were used to construct a weighted mean and weighted standard deviation of means for the whole wood. The basal area of each species was used as weight (Table 4.3).

Table 4.3: Summary of 48 plots for calibration of the carbon model

Tree species	Ash	Maple	Oak	Others	Total [c.]
Tree count in all plots	838	239	138	1057 [46.5%]	2272
[Relative frequency, all trees considered] [a.]	[36.9%]	[10.5%]	[6.1%]		[100.0%]
Relative frequency, dominant species only [a.]	69 %	20%	11%	-	-
All tree species basal area (m^2 ha^{-1})	21.9	5.8	13.8	21.7	63.2
[Relative frequency, all trees considered] [a.]	[34.7%]	[9.2%]	[21.8%]	[34.3%]	[100.0%]
Relative frequency, dominant species only [a.]	52.9 %	13.9 % [e]	33.3 %	-	-
Tree density (g cm^{-3}) [b.]	0.70	0.61	0.68	-	0.68 [d.]
[Relative standard error]	[0.97%, *n*= 27]	[1.61%, *n*=10]	[1.70%, *n*=12]		[5.8% *n*=6] [e.]

a. *n*=48 plots

b. Trees of DBH = 25 cm ± 10 cm were sampled, corresponding roughly to trees between 70-80 years of age (Edwards and Christie 1981, refer to text).

c. Includes all trees and shrubs ≥ 7 cm DBH

d. Weighted average from birch, elm, aspen, oak, ash and maple (weight: basal area).

e. Value in bracket is the weighted standard deviation of species averages.

4.3 Modelling

4.3.1 Ground elevation (244 points)

Table 4.4, Figure 4.1 and Figure 4.2 present the summary statistics resulting from the comparison between the reference and the LiDAR elevation and height datasets (DTM and DCHM).

Table 4.4: Summary statistics of residuals in the DTM and the DCHM (Modified from Gaveau and Hill, 2003)

	a. DTM	b. DCHM	
		Shrubs	Trees
Range	-1.78 to +1.65	-2.50 to –0.05	-5.23 to + 0.11
Mean	+ 0.23	-1.02	-2.12
SE	2.9%	19.8%	7.1%
n=	244	43	39

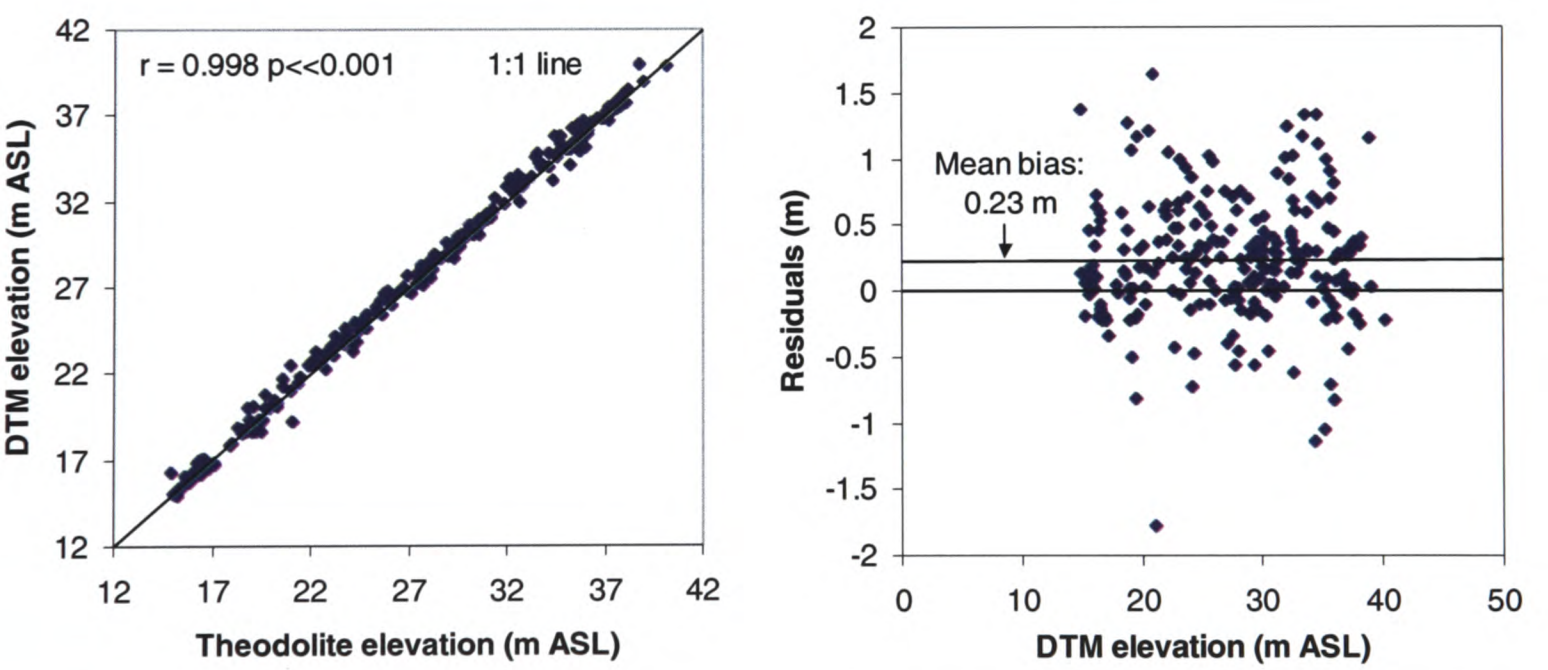


Figure 4.1:a: Digital terrain model (DTM) against reference elevation data (m above sea level). b: Digital terrain model (DTM) residuals (m)

Although Figure 4.1 a. shows a close agreement between the DTM and the reference elevation data, the DTM overestimates reference by an average of 0.23 metres (significantly different from 0, $p << 0.001$, two-tailed *t*-test) (Table 4.4 column a., Figure 4.1 b.). The difficulty of generating DTMs under dense canopy covers using LiDAR data has been widely recognised (Blair *et al.* 1999). Accurate DTM generation will be a function of sampling density, scanning angle, canopy density and canopy closure, and processing

methods (Gaveau and Hill 2003). Here, even if an adaptive morphological filter was applied to locate the local minima (from which the DTM was generated), the majority of last returns may have been reflected from surfaces above the ground, generating this overall overestimation of the reference elevation data. The DTM was thus calibrated by subtracting the systematic offset from pixel elevation values of the DTM.

4.3.2 Canopy height (82 points)

Table 4.4 b. presents statistics for the height residuals from the LiDAR DCHM. Canopy heights for the reference and the LiDAR canopy elevation were obtained by subtracting the calibrated DTM from both datasets (the latter yielding the DCHM). As shown in Figure 4.2, the DCHM consistently underestimates reference heights. Tree height underestimation using small footprint DRD LiDAR is not uncommon and is a function of several factors internal and external to the study site (Hyyppä *et al.* 2000, Lefsky *et al.* 2002, Gaveau and Hill 2003). Internal factors include the canopy structure (conical or spherical shapes) and the canopy density (plant surface area, perpendicular to illumination angle, per surface area). External factors include the configuration of the LiDAR system used as well as the sampling design. For example, high sampling density or large footprint sizes will increase the probability of sampling tree apexes. Other external factors include the strength and wavelength of the output signal, which will influence the strength of the returned signal; the threshold detection selected which defines how strong the return signal must be to trigger a recording; and the signal-to-noise ratio sensitivity (Hyyppä *et al.* 2000, Lefsky *et al.* 2002, Gaveau and Hill 2003). Here, internal factors are an important source of canopy height underestimation. As shown in Figure 4.2 and Table 4.4b, height underestimation increases as a function of canopy height. As Gaveau and Hill (2003) suggested, canopy density and structure variations across species, rather than height, is the main factor for height underestimation in Monks Wood. They noted that shrub species had a higher canopy density than trees. As such, the signal was less likely to penetrate deep into the shrub canopy before encountering sufficient matter to return a first significant signal (thus reducing height underestimation). Here, as no information on species is available per pixel in the DCHM, height is taken as a surrogate to differentiate trees and shrubs.

To calibrate the DCHM, alternatives to the use of standard linear regressions must be sought because both the reference and LiDAR datasets are measured with errors (Snedecor and Cochran 1980). Additionally, the variances of tree and shrub height residuals are heteroscedastic (statistical distributions with different variances, Figure 4.2). Both systematic and random errors appear to be a function of height and canopy density (the

larger the trees, the larger the mean and variance of residuals). Statistical analyses supported these observations as significant differences were found to exist between averages of tree and shrub canopy height residuals (t-test, $p \leq 0.001$) and between variances of tree and shrub height residuals (F-test, $p << 0.001$).

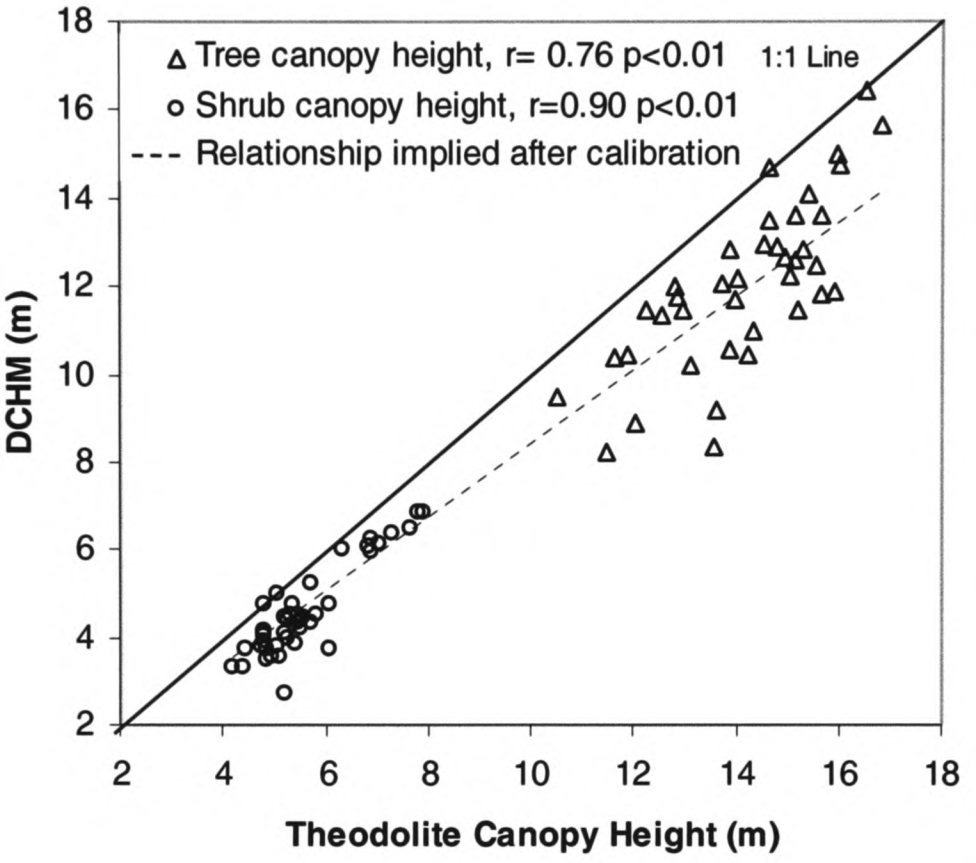


Figure 4.2: LiDAR against reference canopy height estimates (m)

Assuming that the variance of residuals is proportional to the theodolite canopy height (H_R) and that height is an acceptable surrogate for differentiating between the canopy densities of trees and shrubs, it is reasonable to use the ratios of means as the slope to the equation for calibrating the DCHM (Snedecor and Cochran 1980). The model below was used to calibrate all pixels in the DCHM (Equation 1, Figure 4.2).

Equation 1: Calibration of the Digital Canopy Height Model (DCHM)

$$H_{DCHM}' = bH_{DCHM}$$

Where:

$b = 1.19 = \sum H_R / \sum H_{DCHM}$

H_{DCHM}' = Calibrated pixel height

H_{DCHM} = Pixel height

H_R = Theodolite canopy height

After calibration, all 48 ground plots were located on the calibrated DCHM using the GPS coordinates available combined with the quantitative description of the location of the centre of each plot. From each centre coordinate, a circular plot of 20 meters diameter was overlaid on the DCHM.

4.3.3 Basis for a carbon model

Although canopy height variables are available from LIDAR, these are not the most commonly used predictors of above-ground biomass, volume or AGCC. Rather, tree diameter or stand basal area is most frequently utilised. However, height metrics have been used successfully as a surrogate for these variables when basal area or DBH were not available (Nelson *et al.* 1988a, Naesset 1997b, 2002). A form for the AGCC model using height metrics as a predictor was therefore developed from forestry yield tables. The starting point was a model predicting stemwood volumes from height derived from Sycamore-Ash-Birch (SAB) production tables (Edwards and Christie, 1981). These tables provide empirical growth data and models for plantation stands, relating stand variables such as dominant height (the average height of the 100 trees with largest DBH per hectare) to merchantable stemwood volume on a per hectare basis. Although yield tables were designed for plantations, they were selected here due to their wide availability and adaptability given UK environmental conditions and forest types.

For deciduous species, a limited number of yield tables were available: Oak; Sycamore-Ash-Birch (SAB); Beech; Hybrid poplars; and Southern Beech (Edwards and Christie 1981). The SAB tables were selected because ash is by far the most dominant species in Monks Wood. As shown in Table 4.3, ash contributes to more than 34% of the total basal area in the 48 plots and to nearly 37% of the population of all trees ≥7 cm DBH. Maple is also a common species at Monks Wood; nearly half of the total tree population in the 48 plots is composed of ash and maple. Since sycamore is an acceptable proxy for maple (Edwards and Christie 1981), the selection of the SAB yield tables appears appropriate. The equation (model) relating stemwood volume to a height variable was then modified by incorporating a conversion factor (total tree carbon per stem volume) to estimate AGCC.

The form of the equation selected thus uses a LiDAR height metric ($H_{\%}$) as predicting variable and is as follows:

Equation 2: Carbon model

$$AGCC = k\ a\ e^{b\ H_{\%}}$$

Where:

The parameter *k* converts stemwood volumes to total AGCC and is derived from empirical conversion factors available in the literature, (Dewar and Cannell 1992, Milne *et al.* 1998, Salway *et al.* 2001). Parameters *a* and *b* are site-specific and optimised against ground data (detailed below). Specifically, *a* represents the initial volume (m^3 ha^{-1}) found when $H_{\%}$ equals 0. This parameter enables to take into consideration the AGCC present in the ground vegetation and litter compartment when no height is "recorded" by the LiDAR; in Monks Wood, between 2.3 and 4.6 t ha^{-1} is found in ground vegetation and litter only (Patenaude *et al.* 2003). The *b* parameter can be considered as an indicator of the productivity of the site. Finally, $H_{\%}$ is derived from the LiDAR DCHM and is a variable surrogate to dominant height. Relying on a variable characteristic of a stand possesses the advantage of removing the need to identify individual trees from the LiDAR dataset. Estimates of total stemwood volumes and AGCC on a *per* hectare, rather than on a *per* tree basis are provided, given that an appropriate height metric characteristic of the stand is provided. Although dominant height is a suitable variable for characterising the height distribution of plantation stands, this variable would be inappropriate for a mixed deciduous woodlands such as Monks Wood as it may not reflect height distributions where trees are of mixed species and ages as it does for plantations. To select an appropriate height statistic ($H_{\%}$) representative of Monks Wood, height distributions for the 48 measured plots were plotted. A sub sample is presented in Figure 4.3.

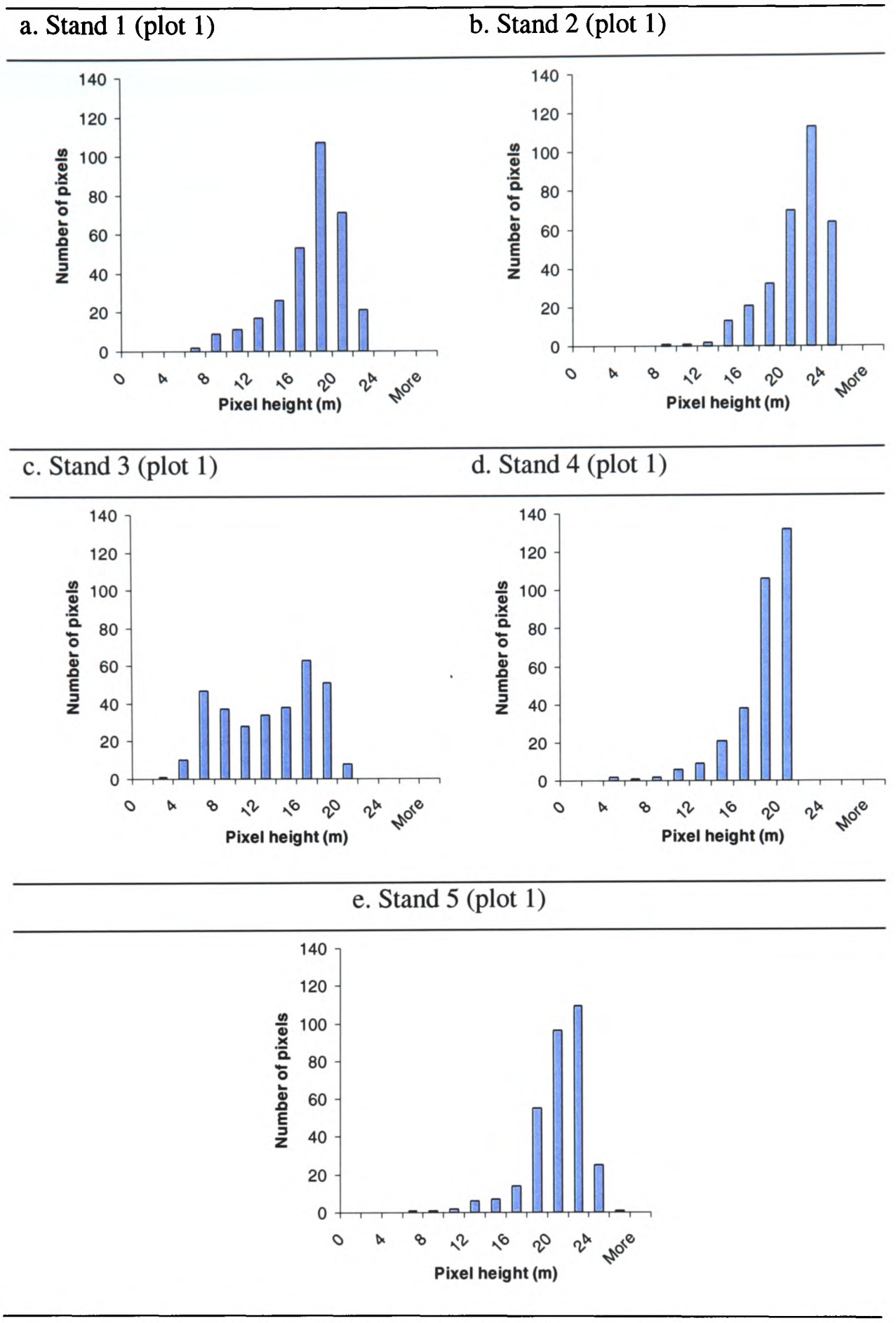


Figure 4.3: Height distribution of plots from the five stands

Of the 48 height distributions, most were skewed to the left and a few were bimodal. Thus, as the model presented in Equation 2 is exponential, the average height per plot would underestimate the weight of larger trees and shrubs on the AGCC of most plots. Likewise, the maximum height would disregard smaller trees; the AGCC in a plot with a majority of shrubs and one large tree would be significantly overestimated. Bimodal distributions render the mode an inappropriate statistic. Various percentiles of heights, selected to be above the median to seize the bulk of the distributions, were therefore chosen and tested as a best statistic descriptive of height distributions. This approach is not dissimilar to that

proposed by Naesset (1997a) and Magnussen and Boudewyn (1998) which used percentiles of LiDAR height estimates in coniferous plantations as estimators of average stand height.

Table 4.5: Optimised model parameters for Monks Wood

Parameters to optimised model			Notes
	a	19.186	At height 0, an initial volume of 19.186 m^3 ha^{-1} (equivalent to approximately 4 t ha^{-1} of carbon) is assumed. This is not unreasonable, as carbon content in ground vegetation and litter range between 2.3 and 4.6 t ha^{-1} in Monks wood (Patenaude *et al.* 2003).
	b	0.1256	
$k = dgh$	*d*	1.36	Biomass expansion factor for UK deciduous forests. Converts stemwood volume to total above-ground volume.[a.]
	g	0.68	Dry mass conversion factor. Converts volume to dry mass (Table 3).
	h	0.49	Carbon content conversion factor. Converts dry mass to carbon content for UK deciduous forests. [a.]

a. Conversion and biomass expansion factors in Dewar and Cannell (1992), Milne *et al.* (1998) and Salway *et al.* (2001).

The selection of the parameters *a* and *b* together with an appropriate height statistic ($H_{\%}$), was carried out by means of optimisation against ground data. The field-based estimates of AGCC were plotted against spatially corresponding height statistics from the DCHM (e.g. average height, 60th percentile, 80th percentile, maximum height) (Figure 4.4a).

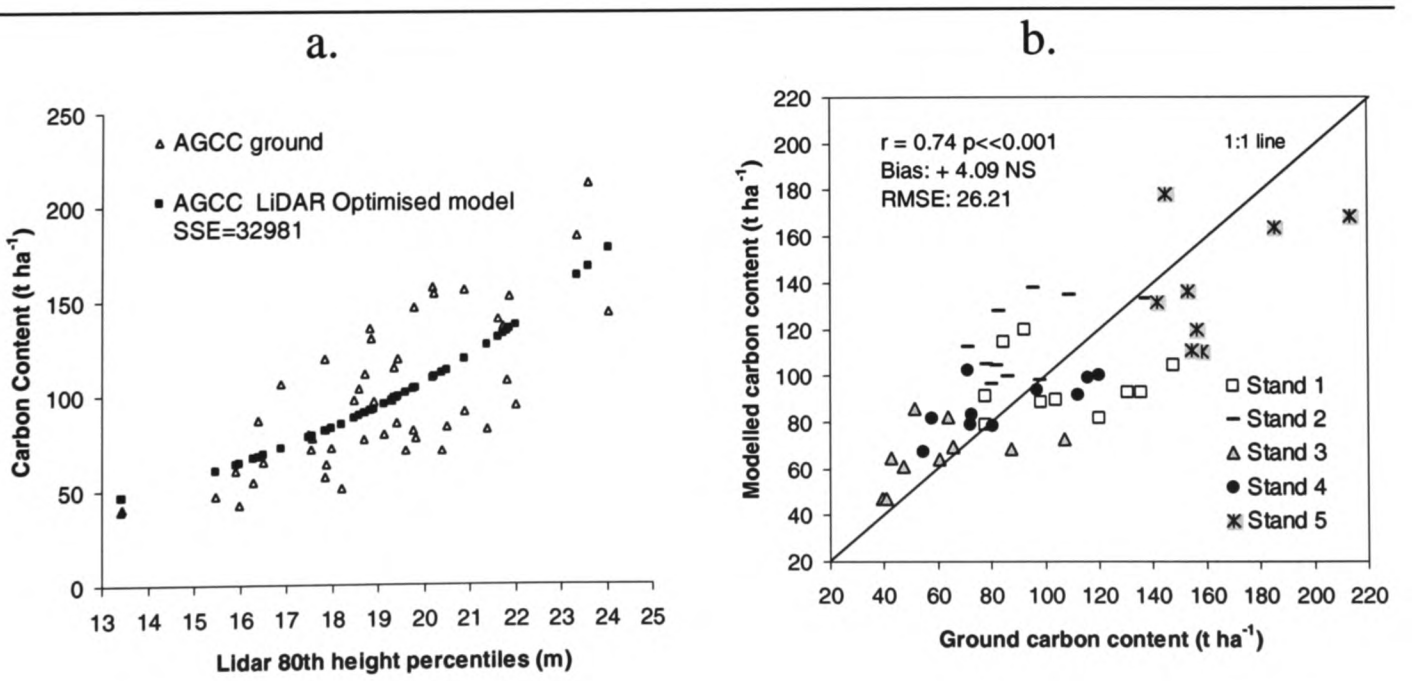


Figure 4.4: a: Field-based AGCC and AGCC from optimised model against the LiDAR 80th height percentiles (at the plot level) b: AGCC from optimised model against field-based estimates (at the plot level)

AGCC= Above-Ground Carbon Content; SSE= Sum of Square Errors.

For each statistic, *a* and *b* were varied to provide the best fit and lowest Sum of Square Error (SSE) between the modelled AGCC and the field-based estimates of AGCC. The best results were obtained with the 80th percentile and the parameters values presented in Table 4.6. SSEs are also shown. This statistic, conversely to the average or the maximum height, confers a larger weight to taller trees (which account for a larger portion of the AGCC) without disregarding the contribution of smaller trees. Coincidentally, the 80th percentile was also nearest to the mode for the majority of height distributions. In Figure 4.4 a., two datasets are plotted against the 80th percentile: firstly, the ground-based estimates of AGCC; secondly, the optimised AGCC obtained from the fine-tuned model (Table 4.5 and Table 4.6). Figure 4.4 b. shows the correspondence between the field-based AGCC and the modelled AGCC for all plots.

Table 4.6: Sum of square errors (SSE) between modelled and field-based AGCC

Parameters and SSE	Height statistics			
	Average	60th percentile	80th percentile	Max
a	38.308	24.620	19.186	15.349
b	0.1182	0.1231	0.1256	0.1322
SSE	35,798	33,765	32,981	34,757

Various statistics for fine-tuning the carbon model have been tested. The 80th percentile, which generated the lowest SSE, was selected.

4.3.4 Stand and woodland above-ground carbon content

Each of the five stands in the DCHM was divided into a grid of 20x20 m^2 cells (n>>10 per stand), the cell size corresponding to the dimensions of the plots used in ground-based sampling. For each grid cell, the 80th height percentile was extracted. This approach aims at capturing a maximum of variability within stands and within the whole woodland. The AGCC in tonnes per hectare for all grid cells was then averaged per stand. The same procedure was applied across the woodland to provide AG carbon density and total carbon content.

4.4 Results and discussion

Figure 4.4 b. shows the AGCC modelled from 80th percentiles plotted against field-based estimates of AGCC for all coincident plots. Overall, the agreement between the two approaches is good ($r=0.74$, $p<<0.001$). Although the modelled AGCC overestimated ground estimates by 4.09 t ha^{-1} on average, this bias is not significantly different from zero

(*t*-test, 0.01≥ p>0.001, *n*=48). The RMSE is small (26 t ha^{-1}) considering that these approaches are compared at the plot level, where the inter-plot variability is high.

The results at the stand and woodland level are presented in Figure 4.5, Figure 4.6 and in Table 4.7. At the stand level, the correspondence between the field-based estimates of AGCC scaled up in proportion to area and those derived using the 20x20m grid approach is good. The correlation is high (r=0.85) although significant only at 0.1≥p>0.05 due to the small number of stands considered (*n*=5). LiDAR stand estimates are within 14 % of the ground-recorded stand estimates, except for Stand 2, where LiDAR estimates are 33% larger than that from the ground. On average, the estimates from the grid approach are 3.54 t ha^{-1} lower than the ground estimates but this bias is not significantly different from zero (*t*-test, 0.05≥ p>0.01, *n*=5). This suggests that both methods are equally able to capture the AGCC and its spatial variation within each stand.

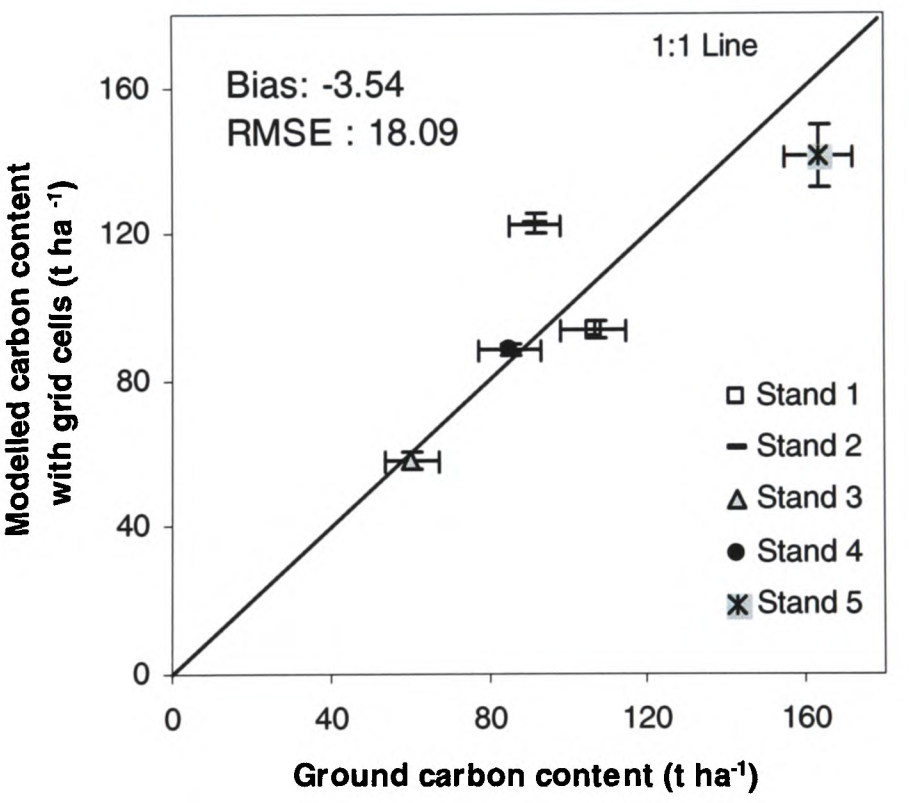


Figure 4.5: AGCC per stand using all grid cells (*n*>>10 per stand) against AGCC from upscaled ground-based plot data (8≤*n*≤10). Error bars are standard errors.

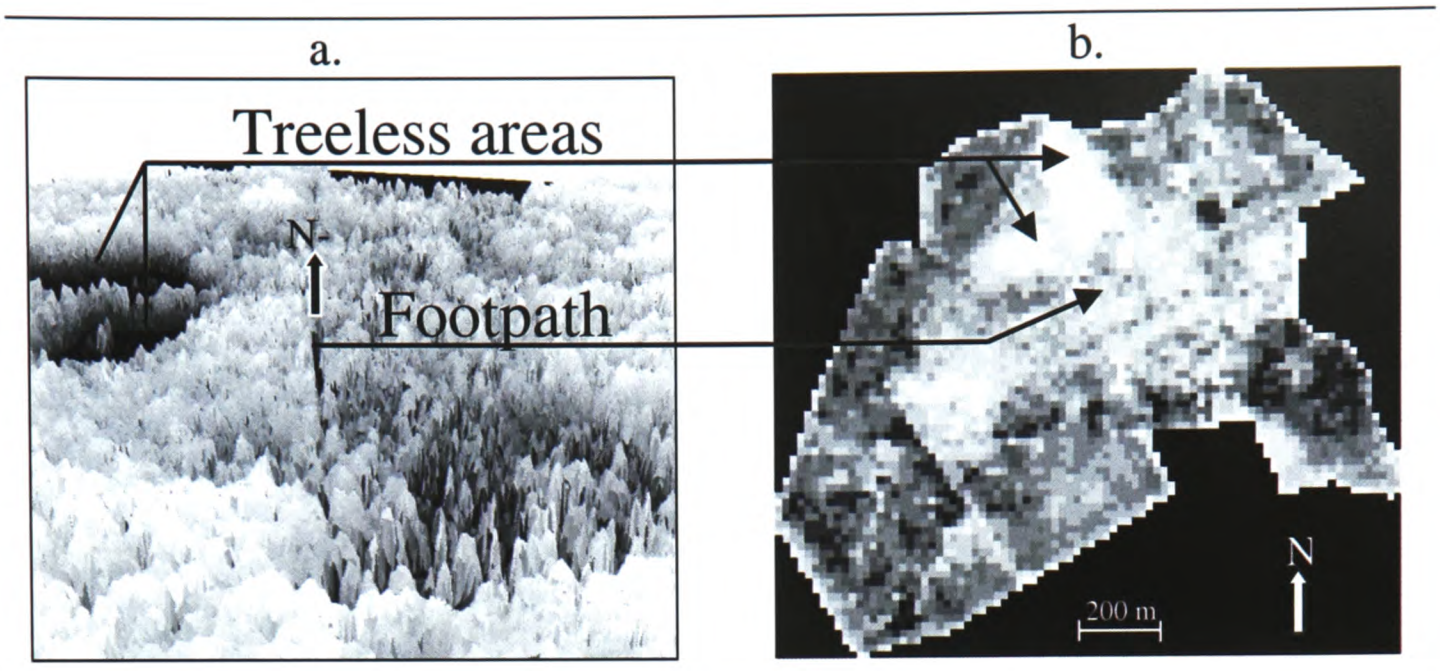


Figure 4.6: a: 3D view within the resulting DCHM. Gradients from black to white correspond to heights between 0 and 26 metres respectively. b: Final AGCC map of Monks Wood (t ha^{-1} per 20 x 20 m cells). Dark areas indicate high AGCC (max: 215 t ha^{-1}) and pale, low AGCC (min: 8 t ha^{-1}).

At the woodland level however, the AGCC estimates from the ground (n=48) and the grid approach (n=3638) contrast considerably (Table 4.7, columns a and b). The LiDAR grid estimate is lower than the ground-based estimates of total woodland AGCC by 23% (nearly 4000 tonnes). The differences between the two approaches at the plot and at the stand level are insignificant but are considerable at the woodland level. This implies that differences in estimates for the entire woodland do not arise from the accounting methods but rather, from the scaling approach used and the poor representation by the selected stands of the rest of woodland. To assess this, only the AGCC estimates from the 48 plots on the DCHM were considered to estimate the total woodland AGCC by using the same upscaling method as the ground-based approach i.e. for both approaches, n=5 stands of 8-10 plots each.

Table 4.7: Total above-ground carbon content estimate of Monks Wood from different approaches (see text)

	a. Field-based AGCC (Plot data only)	**b. LiDAR AGCC (All grid cells)**	**c. LiDAR AGCC (Plot data only)**
Total woodland carbon content (kt)	17.99	13.88	17.21

As shown in column a. and c. of Table 4.7, the resulting LiDAR estimate is of comparable magnitude to the field-based estimate (4.4% below the field-based value). Thus including all pixels grouped under 20x20m grids increases the accounting of the natural variability of AGCC within the woodland. Whereas variations within the stands are captured similarly by both approaches (as shown in Figure 4.5), the within-woodland heterogeneity appears to be

better captured by the LiDAR approach (Table 4.7). Treeless areas as well as path networks within the woodland are not accounted for in the ground sampling because these do not feature in the literature on the management of the woodland (path surface areas are merged to other management classes). The ground sampling approach relies on the assumption that the plots are representative of the stands, and the stands, of all woodland areas falling under the same management class. The high cost of fieldwork is usually prohibitive in producing detailed assessments of AGCC in structurally heterogeneous forests. Clearly, these treeless areas could be easily removed if their location were known using a GIS database. However, these are not always available and areas identified in a GIS database as forests may not appear as such in reality. LiDAR methods sample across the woodland rapidly and at high sampling density, thus acquiring data on variability.

The approach used is sensitive to the spatial scale of this analysis. Selecting the 80^{th} percentile per 20x20 m grid cell and calculating the AGCC for each grid cell from this percentile will not yield the same result as selecting the 80^{th} percentile of the woodland and calculating the AGCC of the woodland based on a single height estimate. If the carbon model were linear, the model would be independent of the selected scale because the contribution of heights is distributed proportionally. The exponential nature of the carbon model confers larger weights to larger 80^{th} percentile height values. An alternative approach to the use of percentiles would be to model height distributions across the stands, the woodland, or any area of interest. Weights for the AGCC estimates per height class would be provided according to the modelled height distribution. Such an approach would increase the accuracy of predictions in areas exhibiting non-Gaussian or bimodal height distributions. Additionally to the sensitivity of the approach, care should be taken in the use of exponential models. Although the model described here has an appropriate shape, it should only be applied to the range where it was fitted.

The results obtained here are comparable to those from similar studies making use of LiDAR to characterise above-ground biomass or volume in coniferous forest ecosystems. Unfortunately, very few studies have focussed on quantifying theses variables in temperate deciduous woodlands. Successful LiDAR estimates of forest variables have been achieved using WRD. The coefficient of determination between LiDAR derived variables and forest biomass or volume range between 0.78 to 0.96, in the studies by Nilsson (1996), Lefsky *et al.* (1997), Lefsky *et al.* (1999) and Means *et al.* (1999). Estimates using small footprint LiDAR have also yielded good results. Whereas only 0.53 of the ground biomass variance could be explained by metrics derived from LiDAR height measurements in mixed

hardwood forests (Nelson *et al.* 1988), the approach used by (Naesset 2002) explained more than 80% of the ground variations in volume for coniferous forests in Norway, and reached r^2=0.91 when the models were used for prediction purposes.

The literature on carbon accounting using LiDAR approaches is however limited. Using a helicopter mounted WRD, Drake *et al.* (2002) estimated the carbon content of various land covers in the Costa Rican landscape. At the plot level (0.05 to 0.25 ha), metrics derived from the LiDAR dataset explained between 89% and 93% of the variation in ground biomass estimates. These results have also demonstrated the non-saturating capabilities of WRD for carbon assessment across a variety of landscapes. Omasa *et al.* (2003) proposed a carbon accounting approach for all trees in Japanese coniferous forests, using a small footprint DRD. Carbon was estimated on a per tree basis. The approach yielded excellent results (r^2=0.93) but is inapt for large scale monitoring due to the intensive data requirement. It is clear that LiDARs have improved capabilities for monitoring 3-dimensional forests structure, biomass and carbon content. As long as there is no LiDAR on a satellite platform, it will be problematic to use LiDAR techniques for national scale carbon inventory and for improving our knowledge of the carbon cycle at broad scales. Until then, because WRD remain at a research stage and are still unavailable for commercial and operational use, most local to regional scale carbon accounting from LiDAR technology will need to use the easily accessible and low costs DRD.

Although this method provides a basis that may apply to similar forests elsewhere, further work is required on how implementation of the model may vary for different woodlands. Furthermore, for improving accuracy in above-ground carbon accounting from this approach, two difficulties remain to be tackled. Firstly, under dense canopies, the DTMs generated from LiDAR measurements tend to overestimate the actual ground elevation. If no ancillary data are available from which DTMs can be derived or adjusted, this overestimation can be minimised by dual flight campaign strategies. In temperate deciduous ecosystems, the DTM data collection could be planned during winter seasons after leaf fall, whilst DCHM data collection could be projected for summer periods, when the canopy density is at its highest. The second difficulty lies in the consistent underestimation of canopy heights as discussed in Section 4.3.2. The selection of an appropriate canopy height metric, accounting for some of the underestimation may help in alleviating this underestimation. However, because low canopy density is potentially the main factor for canopy height underestimation in temperate broadleaf woodland (Gaveau and Hill 2003),

further investigation is required to develop systematic monitoring of canopy density to relate this variable to LiDAR height underestimations.

Ultimately, as with all other remote sensing approaches, LiDAR is restricted to above-ground estimations of carbon content in forests. The soil carbon pool combined with the underground vegetation components, such as fine and coarse root systems, represent the largest carbon store in forest ecosystems. For these stores, ancillary data, field-based estimation and modelling techniques will still be necessary for comprehensive carbon accounting. Clearly, these need to be used synergistically for complete accounting, as neither remote sensing, nor ground-based approaches alone can fulfil either the national scale reporting requirements of the Kyoto Protocol or the scientific need to account for the missing carbon sink.

4.5 Conclusions

We have proposed a method for estimating AGCC in a temperate forest in the UK. Further work is nevertheless required to investigate the implementation of the model in different woodlands. Using this approach, no distinction between individual trees is required. Additionally, tree height is not a key variable here. Rather, the approach relies on the extraction of a canopy height statistic, such as percentiles, that is characteristic of the height distributions at the scale of the analysis. Furthermore, the approach makes use of widely available forestry yield table databases.

The results shown illustrate once more the need for combining remote sensing to ground surveying methods for carbon accounting. Whereas ground approaches allow for detailed but spatially limited AGCC quantification, remote sensing permits the scaling of these estimates to larger areas and the monitoring of areas not accounted for using ground-based approaches exclusively. Moreover, because the sensitivity of radar and passive optical approaches to biomass or AGCC decreases with increasing canopy structural heterogeneity and age, the potential of LiDAR techniques in such context should be stressed. Both politically and scientifically, there are unambiguous incentives for supporting research and development into DRD or WRD LiDAR missions for carbon accounting purposes.

Acknowledgements

We are grateful to Thomas Brown for his invaluable help in processing the LiDAR data. This project is funded by the British National Space Centre - Link Carbon Offset

Verification project, the Biffaward initiative and the Fonds Québécois de la Recherche sur la Nature et les Technologies.

Chapter 5

Bayesian calibration of 3-PG for Scots pine

Abstract

Process-based models needing extensive databases and complex parameterisation have been of limited use for practical forest management application. Although goodness-of-fit approaches have been used to optimise parameter values given available data, such techniques do not provide an uncertainty assessment for parameters and model outputs. In this paper, we present a Bayesian calibration of the 3-PG model for a Scot pine plantation in the UK. In using a Bayesian approach, the parameters and the data used in the calibration process are presented in the form of probability distributions, reflecting our degree of certainty about them. A total of 19 parameters, 14 above-ground biomass and 4 averaged leaf area index data points were selected for the calibration. As process-based models cannot be solved analytically, a Markov Chain Monte Carlo (MCMC) sampling method is used to approximate the full posterior probability distribution. Marginal distributions for individual parameters were of three types: near Gaussian, near uniform, and skewed or exponential. The parameter vector considered as the single "best" set was also presented in addition to parameters to which above-ground biomass and LAI outputs are most sensitive. Root biomass, foliage biomass (at an early age) and data pertaining to evapotranspiration and soil water balance are required to update these distributions.

5.1 Introduction.

Process-based models have been widely used in the fields of forest physiology and forest ecology, as they enable deeper insights into the drivers of forest production and growth and offer higher flexibility than conventional production tables (Landsberg and Waring 1997, Battaglia and Sands 1998). Owing to deterministic, mechanistic and/or stochastic algorithms simulating the processes affecting growth, this flexibility has enabled the exploration and quantification of environmental variables and underlying processes on growth. Such models have proven successful for forest ecosystem analysis across the globe and in contrasting environments (Running and Coughlan 1988, Vanclay 1989, Wang and Jarvis 1990, Cramer and Field 1999, White *et al.* 2000). However, in spite of the numerous models that exist, few have reached an operational status beyond that of the research realm and little is known about their reliability. Their practical value has been limited owing to

their complexity, their extensive data requirement and the need for appropriate parameterisation. Although optimisation approaches, which provide a maximum model fit to available data, have been used to counter this setback, they do not make it possible to quantify the uncertainty in the parameters and model outputs (Gertner *et al.* 1999, Green *et al.* 1999). Yet, the quantification of uncertainty associated with predictions is an important requirement for practical applications of models (Green *et al.* 2000). There is thus a clear need for a methodology quantifying model output and parameter uncertainty, while considering all the existing information, including that enclosed in the model itself.

By providing parameter estimates, along with measures of uncertainties, Bayesian calibration offers a solution (Gertner *et al.* 1999, Green *et al.* 1999, Green *et al.* 2000). The chief characteristic of this approach is that the parameters and the data used in the calibration process are presented in the form of probability distributions, reflecting our degree of certainty about them (Jansen 1999). As further information is gained, the distributions are updated. The Bayesian approach also considers the difference between prior information based on expert opinion from that based on data, a difference seldom made in uncertainty analyses (Green *et al.* 2000). By doing so, Bayesian calibration targets the much-needed platform for expressing parameter and output uncertainty in forest-growth modelling (Ghazoul and McAllister 2003, VanOijen *et al.* In press).

In this paper, a Bayesian approach was used to calibrate the 3-PG model (Physiological Processes Predicting Growth, Landsberg and Waring 1997, Sands and Landsberg 2002) for the production of a UK Scot pine plantation. 3-PG is built on a combination of process-based calculations, several key simplifying assumptions and few empirical relationships. The model predicts gross and net primary production as well as allocation to different pools. It has been widely and successfully applied worldwide and increasingly to new species (Landsberg and Waring 1997, Law *et al.* 2000, Waring 2000, Coops and Waring 2001, Coops *et al.* 2001, Sands and Landsberg 2002, Almeida *et al.* 2004, Stape *et al.* 2004). However, as clearly stated by Sands (2004, p.3): "In only a few cases have parameters characterising a species been rigorously determined, and even then this has been largely by a process of trial and error, e.g. for *E. globulus* by Sand and Landsberg (2002)".

In the UK, most forested lands are coniferous plantations. After Sitka spruce (*Picea sitchensis* Bong. Carr), Scots pine (*Pinus sylvestris* L.) is the second most abundant coniferous species in Britain and covers approximately 16% of the total surface area of

coniferous woodlands in Britain (Forestry Commission 2001). However, the parameterisation of 3-PG for this species requires data not commonly available nor routinely monitored. In this context, the aim of this paper is threefold: (i) to describe a Bayesian calibration to 3-PG for future applications of the approach (ii) to provide uncertainty estimates for parameters and model outputs given our current knowledge on the plantation studied and (iii) to explore whether a Bayesian calibration is adequate for the parameterisation of 3-PG for Scots pines in our study site.

5.2 Structure of the 3-PG model

The 3-PG model has monthly or annual time steps and entails five state variables –foliage, stem and root biomass, stocking density and available soil water – in conjunction with five submodels –biomass production, biomass allocation, soil water availability and evapotranspiration, mortality, and inventory variables. Of these, only the biomass production, biomass allocation and soil water balance submodels were implemented here. Mortality was prescribed in a 5 year thinning regime and no stand inventory variables were estimated. The required climatic data are monthly average values of solar radiation (MJ m^{-2} d^{-1}), atmospheric water pressure deficit (mbar), mean air temperature (°C), rainfall (mm $month^{-1}$) and frost days. Other input variables include site latitude, an estimate of soil fertility, maximum available soil water (mm per depth of rooting zone, in meters) and a general description of soil texture. 3-PG outputs considered in this study were leaf area index (LAI, projected) and above-ground biomass (subsequently referred to as ABG biomass, unless otherwise stated). Landsberg and Waring (1997) and Sands and Landsberg (2002) provide a comprehensive description of the model, with subsequent improvements since its creation, so only a brief description will be provided here

5.2.1 Biomass production

The biomass submodel converts solar radiation into dry matter. The interception of radiation is defined by Beer's law and canopy LAI. The amount of photosynthetically active radiation intercepted by a stand (ϕ_{pa}, mol MJ^{-1}) is then converted into carbohydrates by means of a canopy quantum efficiency coefficient (α_{cx}, mol mol^{-1}) and a conversion factor converting carbohydrates into dry matter. Further constraints on assimilation are then applied by dimensionless environmental factors varying between 0 and 1 (1 indicates optimal conditions). These factors, also referred to as modifiers in the text, are multiplicative and represent the influence of vapour pressure deficit (D) or soil moisture,

which ever is most limiting, stand age, mean air temperature (T), frost, and soil nutrition on photosynthetic assimilation (Sands 2004). Gross primary productivity (P_g, t ha^{-1} d^{-1}) is then converted to net primary productivity (P_n, t ha^{-1} d^{-1}) using a simple P_n / P_g ratio (Y).

5.2.2 Biomass allocation

P_n is then allocated to the different plant components (roots, foliage and stems including branches) at each time step. Allocation to roots is proportional to the harshness of the environment. It is influenced by site fertility, stand age and the most limiting between D or soil water, but does not fall below or exceed set values of minimum and maximum allocation to roots. The remaining P_n is shared between stems and foliage through a foliage-to-stem allocation ratio, given by an allometric relationship with mean diameter at breast height (Sands and Landsberg 2002, Sands 2004). DBH is itself obtained from an allometric relationship with stem biomass. Whereas P_n partitioning parameters must generally be estimated from fitting methods, those pertaining to the allometric relationship between stem biomass and diameter can be derived from forest mensuration (Sands and Landsberg 2002).

5.2.3 Soil water balance

Available soil water θ (mm) is governed by rainfall interception by the canopy (i_R), rainfall (R_P, mm month^{-1}) and evapotranspiration (E_T, mm month^{-1}). If the maximum available water at saturation is exceeded, the excess of water is lost as runoff.

Equation 3: Water balance

$$\theta = (1 - i_R)R_P - E_T$$

Rainfall interception increases with canopy LAI and is taken as a fraction of rainfall. E_T is calculated using the Penman Monteith equation controlled by the canopy conductance, solar radiation and D. Canopy conductance (g_C, m s^{-1}) increases with LAI but is bounded by the LAI value at which conductance is at a maximum (g_{Cx}, m s^{-1}). The relationship between g_C and LAI is further controlled by age and the most limiting factor controlling stomatal aperture, either vapor pressure deficit or soil moisture.

5.3 Methods

5.3.1 Study site and climatic data

Due to the aims of this research, a well studied site and typical of Scots pine plantation stands in the UK was required. The Thetford forest plantation located in East Anglia, U.K (52°30´ N, 0°30´ E) and covering over 100 ha was found to be ideal. The forest was created

by afforestation in the 1920s and 1930s and is composed mainly of mono-species, even-aged Scots Pine and Corsican Pine (*Pinus nigra* car. *maritima* (AIT.) Melv.) stands. Since the creation of the forests, Scots pine stands in the plantation have been extensively studied, providing data on tree height, growth patterns and biomass (Ovington 1957, Baker 1992, Luckman *et al.* 1997, Skinner and Luckman 2000), litterfall (Beadle *et al.* 1982), leaf area index (Ovington 1957, Beadle *et al.* 1982, Mencuccini and Grace 1996), stomatal and canopy conductances (Beadle *et al.* 1985a, Beadle *et al.* 1985b, Beadle *et al.* 1985c, Stewart 1988) and soil type and water holding capacity (Corbett 1973, Roberts 1976, Beadle *et al.* 1985a, Stewart 1988). Of all stands, Scots pines of yield class 10 were modelled here as this is the prevalent yield class occurring in Thetford. Yield classes indicate the productivity level of the stands (Edwards and Christie, 1981).

The soils of the plantation are sandy with deep alkaline chalky bedrock and drain freely throughout the forest (Corbett 1973, Mencuccini and Grace 1996). The area is generally flat and climatic variations within the area are probably insignificant (Ovington 1957). Long term average climatic conditions are summarised in Table 5.1. Minimum and maximum temperatures along with frosts days were derived from the Cambridge botanical garden meteorological station, (http://badc.nerc.ac.uk/home/index.html) while mean monthly precipitations and mean daily incident solar radiation were derived from the Climate Research Unit datasets (New *et al.* 2000). Although 3-PG permits the use of monthly climatic data, the use of averages covering several years is the normal procedure (Sands and Landsberg 2002, Esprey *et al.* 2004). Here, long term monthly averages were used as our interest lies in exploring the general behaviour of the model parameterised for Scots Pine, rather than in understanding the impact of specific climatic disturbances on growth.

Table 5.1: Climate database for Thetford

Monthly Climate data	Mean Tmax[a.] (°C)	Mean Tmin[a.] (°C)	D[c.] (mBar)	Rain[b.] (mm)	Solar rad[b.] (MJ $m^{-2}d^{-1}$)	Frost days[a.] (days)
January	6.47	1.08	1.5	55.0	2.52	10.7
Feb	7.29	0.97	1.8	42.4	4.53	11.2
March	10.18	2.13	2.7	51.9	8.26	7.9
April	13.13	3.95	3.5	48.0	13.10	3.3
may	16.86	6.70	4.7	55.0	16.58	0.8
June	20.08	9.73	5.7	55.0	18.43	0.0
July	22.31	11.83	6.5	54.0	16.64	0.0
Aug	22.15	11.58	6.5	58.0	14.42	0.0
Sep	19.17	9.64	5.1	61.1	10.00	0.0
Oct	14.99	6.66	3.6	61.1	5.80	1.5
Nov	10.07	3.51	2.2	69.0	2.86	5.7
Dec	12.61	2.04	3.8	61.1	1.96	9.1

[a.] 70 years average derived from the British Atmospheric Data Centre.

[b.] Rain and solar radiation derived from UEA climate research unit (New *et al.* 2000).

[c.] D=Vapour pressur deficit. Calculated from maximum and minimum monthly temperatures (Standard equation provided in 3-PG, Sands 2001).

5.3.2 Model initialisation

Initial biomass values were obtained from Ovington (1957) for the managed plantation stand (~14 years). Root, stem and foliage biomass were 10 t/ha, 16 t/ha and 7 t/ha respectively. Initial stocking of 4446 trees per hectare was obtained from the forest industry production tables (Edwards and Christie 1981).

The estimate of maximum available soil water is based on soil texture and soil water holding capacity. Storage capacity for sandy soils is approximately 150mm per metre of soil, and the permanent wilting point, 50 mm. In Thetford, as 95% of Scot Pine roots are located in the first meter of soil (Roberts 1976), we assumed that the maximum available water was approximately 100mm. Minimum available soil water was set at 0.

A thinning regime at 5-year intervals was prescribed, as this is the current practice in Thetford. The removed trees were assumed smaller than the average tree size; suppressed/standing tree volume ratios, assumed representative to that of biomass, were derived from the Forestry Commission production tables for Scots Pine of YC 10. These ratios varied as function of age and approached 1 near the end of the rotation.

All runs were made with 3-PGpjs, a Visual Basic implementation of 3-PG in Excel available at http://www.ffp.csiro.au/fap/3pg/download_details.htm.

5.3.3 Prescribed parameters

Sixteen out of 35 parameters, considered of low sensitivity by Esprey *et al.* (2004) and Sands (2004) or for which specific estimates were available, were kept constant in the calibration exercise. The parameters pertaining to the allometric relationship between stem mass and diameter at breast height, a_S and n_S, were derived from the data collected by Ovington (1957) in Thetford and the production table for YC 10 (Edwards and Christie 1981). The resulting relationship between DBH and woody biomass is shown in Figure 5.1. The sources for other constant parameters are given in Table 5.2.

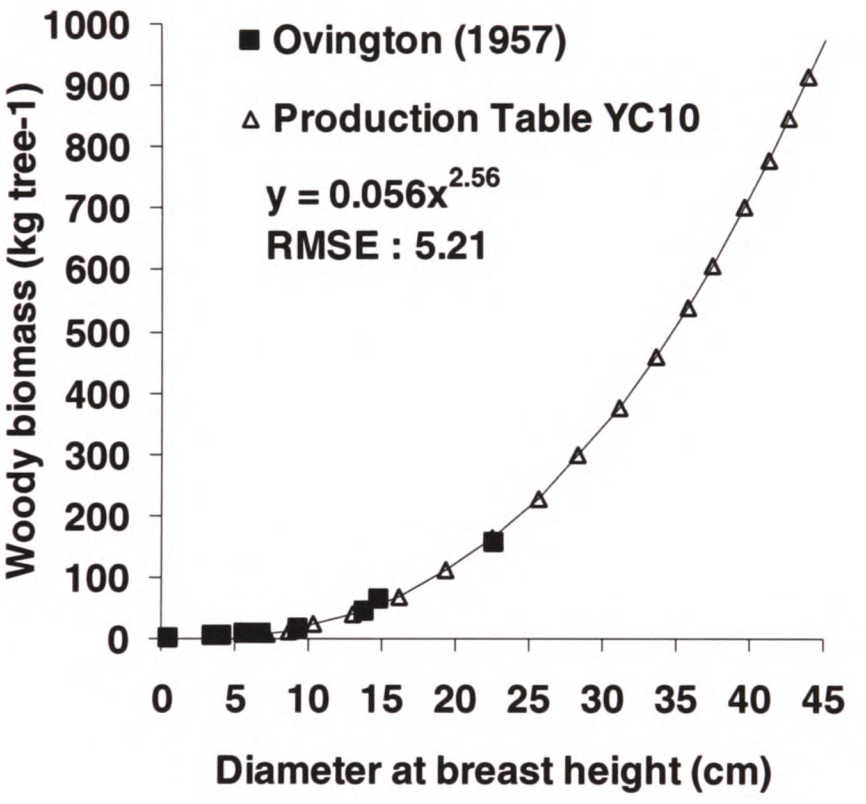


Figure 5.1: Total woody biomass (stem, branches and bark, kg per tree) versus diameter at breast height (cm) based on 10 Scot pine stand averages (derived from Ovington 1957) and the production tables (Edwards and Christie 1981)

The RMSE was calculated between the data from Ovington (1957) and the model derived from the Scots pine table of YC 10.

5.4 Bayesian calibration

Bayesian calibration was applied to the remaining 19 parameters. In Bayesian statistics, probability is interpreted as the degree of certainty for some quantity, conditional to available data and knowledge. As the selected 19 parameters are not precisely known, this uncertainty can be represented as a probability distribution over the parameters. Thus, if we define θ as a parameter vector for 3-PG, then $P(\theta)$ represents its probability distribution and

P(f(θ)) the uncertainty in model outputs (f(θ)) generated by the uncertainty in the parameters. In this context, Bayesian calibration is a method enabling P(θ) to be updated as new data come in. Given a dataset D, we can derive P(θ|D) from P(θ) by applying Bayes Theorem:

Equation 4: Bayes' Theorem

$$P(\theta|D) = P(\theta)\, P(D|\theta) / P(D)$$

In Bayesian terminology, P(θ|D) is the updated or posterior parameter distribution; P(θ) is the original distribution, referred to as the prior; P(D|θ) is the conditional probability of the data for a given parameterisation, called the likelihood; and P(D) is a normalization constant that may be referred to as the evidence.

5.4.1 The prior

The prior distribution is built from marginal distributions, which reflect our current knowledge of the parameters in the 19-dimensions parameter space (19 parameters are included in the vector). The distribution that best describes the available information about the parameter must be used. For example, one might use a normal, beta or *t*-distribution for the prior probability distribution to individual parameters. When limited information is available, Van Oijen *et al.* (In press) suggest the use of uniform or beta distributions, bounded by a biophysically or biologically reasonable maximum and minimum value for each parameter.

Details of the prior distributions are provided in Table 5.2. The boundaries to the prior were either obtained from direct observation on Scots Pine stands in Thetford (SP-T), or from the literature available on this species (SP-L). Otherwise, the values were obtained by analogy with other species, from set default values defined in 3-PG or from other species modelled in 3-PG (D) (Table 5.2)

Table 5.2: Definitions and units to the 35 3-PG parameters. The prescribed values and ranges for the prior are also given.

3-PG symbol: Description (units)	S Class[a]	Prescribed Parameters	Calibrated Parameters: ranges of values in the prior		Data Class	Source
			θ_{min}	θ_{max}		
a_S: Constant in stem mass *v* diam. relationship	M	0.056	-	-	SP-T	(Ovington 1957, Edwards & Christie 1981)
c_θ: Moisture ratio deficit which gives $f_\theta = 0.5$	H	0.7	-	-	D	Default for sandy soils
f_{N0}: Value of f_N when $FR = 0$	M	-	0.6	1	D	
FR: Fertility rating	?	-	0.5	1	SP-L	(Edwards & Christie 1981)
g_B: Canopy boundary layer conductance (m s^{-1})	L	0.2	-	-	D	
g_{Cx}: Maximum canopy conductance (m s^{-1})	H	-	0.025	0.030	SP-T	(Stewart 1988, Gash *et al.* 1989, Kelliher *et al.* 1995)
i_{Rx}: Maximum fraction of rainfall intercepted by canopy	M	0.15	-	-	D	
k: Extinction coefficient for PAR absorption by canopy	M	-	0.2	0.6		(Mencuccini & Grace, 1996)
k_F: Number of days production lost for each frost day (days)	L	1	-	-	D	
L_{Cx}: Canopy LAI for maximum canopy conductance (m^2 m^{-2})	L	-	2.5	4	SP-T	(Beadle *et al.* 1982, Beadle *et al.* 1985a, Beadle *et al.* 1985b, Beadle *et al.* 1985c, Granier *et al.* 1996)
L_{ix}: LAI for maximum rainfall interception (m^2 m^{-2})	L	5	-	-	SP-L	(Peter Savill, personal communication, 2003)
m_0: Value of m when $FR = 0$	?	0	-	-	D	
n_{age}: Power of relative age in f_{age}	L	4	-	-	D	
n_{fN}: Power of (1-*FR*) in f_N	L	1	-	-	D	
n_S: Power in stem mass *v* diam. relationship	H	2.56	-	-	SP-T	(Ovington 1957, Edwards & Christie 1981)
n_θ: Power of moisture ratio deficit in f_θ	L	9	-	-	D	Default for sandy soils
p_2: Ratio of foliage:stem partitioning at $B = 2$ (cm)	H	-	0.50	2.00	D	
p_{20}: Ratio of foliage:stem partitioning at $B = 20$ (cm)	H	-	0.10	0.50	D	
r_{age}: Relative age to give $f_{age} = 0.5$	L	-	0.50	0.95	D	

t_c: Age at full canopy cover (yr)	M	15	-	-	SP-L	(Peter Savill, personal communication, 2003)
T_{max}: Maximum temperature for growth (°C)	L	35	-	-	SP-L	(Peter Savill, personal communication, 2003)
T_{min}: Minimum temperature for growth (°C)	L	0	-	-	D	
T_{opt}: Optimum temperature for growth (°C)	M	-	10	25	SP-L	
t_x: Maximum stand age used to compute relative age (year)	L	-	60	160	D	
$t_{\gamma F}$: Age at which litterfall rate has median value (month)	L	24	-	-	D	
t_σ: Age at which specific leaf area = ½(σ_0+σ_1) (yr)	L	-	2	10	D	
Y: Ratio NPP/GPP	H	-	0.43	0.51	SP-L	(Waring & Running 1998)
α_{Cx}: Maximum canopy quantum efficiency (mol mol^{-1})	H	-	0.03	0.05	SP-L	(Stenberg *et al.* 1994, Wang *et al.* 2004)
γ_{F0}: Litterfall rate at t = 0 (month^{-1})	L	0.001	-	-	D	
γ_{F1}: Litterfall rate for mature stands (month^{-1})	H	-	0.02	0.035	SP-T	(Beadle *et al.* 1982, Cousens 1988)
γ_R: Average monthly root turnover rate (month^{-1})	L	-	0.008	0.015	SP-L	(Gill & Jackson 2000)
η_{Rn}: Minimum fraction of NPP to roots	M	-	0.10	0.30	SP-T	(Ovington 1957, Levy *et al.* 2004)
η_{Rx}: Maximum fraction of NPP to roots	M	-	0.30	0.80	SP-T	(Ovington 1957, Levy *et al.* 2004)
σ_0: Specific leaf area at stand age 0 (m^2 kg^{-1})	L	-	6	11	SP-L	(vanHees & Bartelink 1993)
σ_1: Specific leaf area for mature aged stands (m^2 kg^{-1})	H	-	3	4	SP-L	(vanHees & Bartelink 1993)

Sixteen parameters were given prescribed values and nineteen were used in the calibration. For the latter, ranges of values defining the maximum and minimum in the prior uniform distributions are given (see text for details).

[a.] Sensitivity class as defined by Sands (2004). L=Low, M=Medium, H=High.

[b.] SP-T: data on Scots pine derived from studies conducted in Thetford, SP-L: data on Scots pine obtained from the literature D: default values or data for other species used as surrogate.

5.4.2 The likelihood

Fourteen ABG biomass data points were derived from the forestry yield tables for Scots pine stands under an intermediate thinning strategy, planted at 2 meters spacing. A datum point was selected at each 5 to 10 years interval such that the entire rotation was captured (shown in Figure 5.4). Basic density and biomass expansion factors for Scots pine were used to convert stemwood volumes from the production tables, to total ABG biomass (Hamilton 1975, Edwards and Christie 1981, Levy *et al.* 2004). Additionally, four averaged projected LAI from 13 data points were used (Ovington 1957, Mencuccini and Grace 1996). Conversion of all sided LAI (LAI_t) and 0.5 LAI_t to projected LAI (LAI_p) was achieved as 0.5 LAI_t = 1.35 LAI_p (Flower-Ellis and Olsson 1993, Mencuccini and Grace 1996). No root data apart from the biomass values at initialisation were used in the calibration and no attempt was made to calibrate the water submodel.

To calculate the probability of the data given a specific model parameterisation, $P(D|\theta)$, information about measurement error must be available. No such detailed information was available as the data were derived from various sources. We therefore assumed that the errors were independent, Gaussian and that standard deviations (SD) of errors were equal to 5 t ha^{-1} for the ABG biomass and 0.05 for the LAI. $P(D|\theta)$ then follows from the comparison of each datum point D_i with the corresponding model output $f_i(\theta)$ as:

Equation 5: Data likelihood

$$P(D|\theta) = \prod_{i}^{n} \varphi(D_i - f_i(\theta); 0, SD_i)$$

where, φ symbolises a Gaussian function with 0 and SD_i as mean and standard deviation, and n=18, the number of points in the data sample (ABG biomass and LAI).

5.4.3 Approximating the posterior

The application of Bayes Theorem to process-based models has traditionally been hampered by two problems. Firstly, the models cannot be solved analytically, so a sampling method to explore the parameter space is required. Secondly, the models need to be run at every sampled point in parameter space (to calculate the likelihood), a highly time consuming and computer-intensive process. In recent years, Markov Chain Monte Carlo (MCMC) methods have been found useful to resolve this type of problem (Van Oijen In

press). Here, we used the MCMC Metropolis Hastings Random Walk, which has the two following steps:

1. After randomly choosing a first parameter vector, propose a new candidate for the next parameter vector in the chain from the parameter space as:

Equation 6: Metropolis-Hasting, candidate selection

$\theta' = \theta_t + \varepsilon$

Where θ' is the proposed candidate, θ_t is the current parameter vector and ε is a random vector enabling the exploration of the parameter space. ε is selected from a gaussian distribution with mean 0. Its standard deviation should be chosen to enable a wide exploration of the parameter space and to yield acceptance rates (of the rule described below) between 20 and 50%. We found that a standard deviation of 0.05 gave good results.

2. Run the model with the proposed candidate. The rule for accepting or rejecting the candidate has two components, namely:

(i). Calculate the ratio of probabilities β, which cancels out the need for estimating p(D):

Equation 7: Metropolis-Hasting , ratio of probability densities

$$\beta = \frac{p(\theta' | D)}{p(\theta_t | D)} = \frac{p(D | \theta') p(\theta')}{p(D | \theta_t) p(\theta_t)}$$

(ii). Generate a uniform random variable u ($0 \leq u \leq 1$). The new candidate θ' is accepted and becomes θ_{t+1} if $u \leq \beta$. If $\beta \geq 1$, the proposal is always accepted.

The acceptance criterion, based on the selection of a random variable, thus enables to accept marginal θ_i with lower probability than their predecessor in the chain. This procedure contrasts with many optimisation approaches by allowing downhill steps.

5.5 Results: Posterior distribution

5.5.1 Marginal posterior distributions of parameters

A sample from the posterior distribution consisting of approximately 32 000 parameter vectors was generated using the MCMC approach. Figure 5.2 shows examples of MCMC trace plots and marginal posterior distribution for the parameters approximating their true distributions. The distributions were classified as near uniform if the difference in frequency between classes (15) never exceeded 2000 (η_{Rx}, γ_R, f_{N0}, σ_0, σ_1, g_{Cx}, L_{Cx}). They were otherwise either classified as near-gaussian if at least 30% of the observations were located on either side of the mode (p_2, p_{20}, t_x, t_σ); or skewed, if none of the above conditions were met (η_{Rn}, γ_{F1}, T_{opt}, r_{age}, k, α_{Cx}, Y, FR). Summary statistics to the distributions are presented in Table 5.3.

Table 5.3: Statistics from the MCMC sample summarising the full posterior distribution over the 19-D parameter space.

$\theta(i)$	$\overline{\theta(i)}$	*SD*	θ_{MAPx}	2^{nd} θ_{MAP}	**Correlations between parameter |r| > 0.3**
f_{N0}	0.823	0.109	0.751	0.869	
FR	0.819	0.137	0.933	0.607	
g_{Cx}	0.027	0.001	0.027	0.025	η_{Rn}: 0.32
k	0.484	0.074	0.560	0.546	
L_{Cx}	3.308	0.405	3.094	2.980	
p_2	1.312	0.369	1.987	1.573	
p_{20}	0.384	0.062	0.335	0.341	γ_{F1}: 0.50
					σ_1:-0.34
r_{age}	0.766	0.110	0.563	0.796	T_x: -0.56
T_{opt}	14.95	3.37	18.39	13.08	
T_x	127.31	18.34	150.31	117.17	r_{Age}: -0.56
t_σ	5.437	1.929	4.998	2.797	
Y	0.476	0.021	0.443	0.444	
α_{Cx}	0.044	0.004	0.0487	0.049	η_{Rn}: 0.32
γ_{F1}	0.025	0.003	0.020	0.021	p_{20}: 0.50
γ_R	0.012	0.002	0.0115	0.012	
η_{Rn}	0.177	0.052	0.149	0.189	g_{Cx}: 0.32
					α_{Cx}: 0.32
η_{Rx}	0.529	0.139	0.713	0.709	
σ_0	8.34	1.38	9.26	7.10	
σ_1	3.516	0.273	3.075	3.293	p_{20}: -0.34

The mean and standard deviation to the marginal distributions of the parameters, the vector of highest a posteriori probability (θ_{MAPx}) and correlations between parameters are given.

Because the posterior distribution cannot be described analytically, the results are presented in the form of marginal distributions using descriptive statistics. As suggested by Van Oijen *et al.* (In press), in addition to means and standard deviations, we present the maximum *a*

posteriori (MAP) estimate of θ, considered as the single "best" parameter value estimated from the MCMC sample.

Equation 8: θ_{MAPx}

$$\theta_{MAPx} = \arg\max_{\theta} p(\theta \mid D)$$

Although this should not be interpreted as an optimised parameter vector, this nevertheless provides information as to what parameter vector has the highest probability density given the available data. The second best estimate (2^{nd} θ_{MAP}) is also presented in Table 5.3.

Additionally to these two θ_{MAP} indicators, a subsample of vectors, forming the 99.5 percentile of *highest a posteriori* (HAP) probability was selected (totalling 154 vectors). This enabled the investigation of whether a single best θ_{MAPx} (maximum in the 19-D parameter space) or rather several maxima or ridges in the 19-D parameter space were likely to exist. If a single best parameter vector existed, then parameters with high probability should lie in the vicinity of the 1^{st} θ_{MAPx} and the distance of each parameter from θ_{MAPx} should be correlated with its probability.

A similarity index was calculated as the normalised distance between each parameter vector (of probability above the 99.5% percentile) and θ_{MAPx}:

Equation 9 : Sum of normalised root squared errors

$$SRSE = \sum_{i=1}^{19} \frac{\sqrt{(\theta_{MAPxi} - \theta_{HAPi})^2}}{\theta_{MAPxi}}$$

where SRSE is the of the sum of normalised root squared errors, θ_{MAPx} the 1^{st} MAP and θ_{HAPi} a vector of HAP likelihood.

No relationship was found between the SRSE and the log of probabilities (r=0.03) (Figure 5.3). The two parameter vectors of highest probability (θ_{MAP}) are as dissimilar from one another as most HAP from the θ_{MAPx}, while two vectors of relatively lower probability are very similar to the θ_{MAPx}.

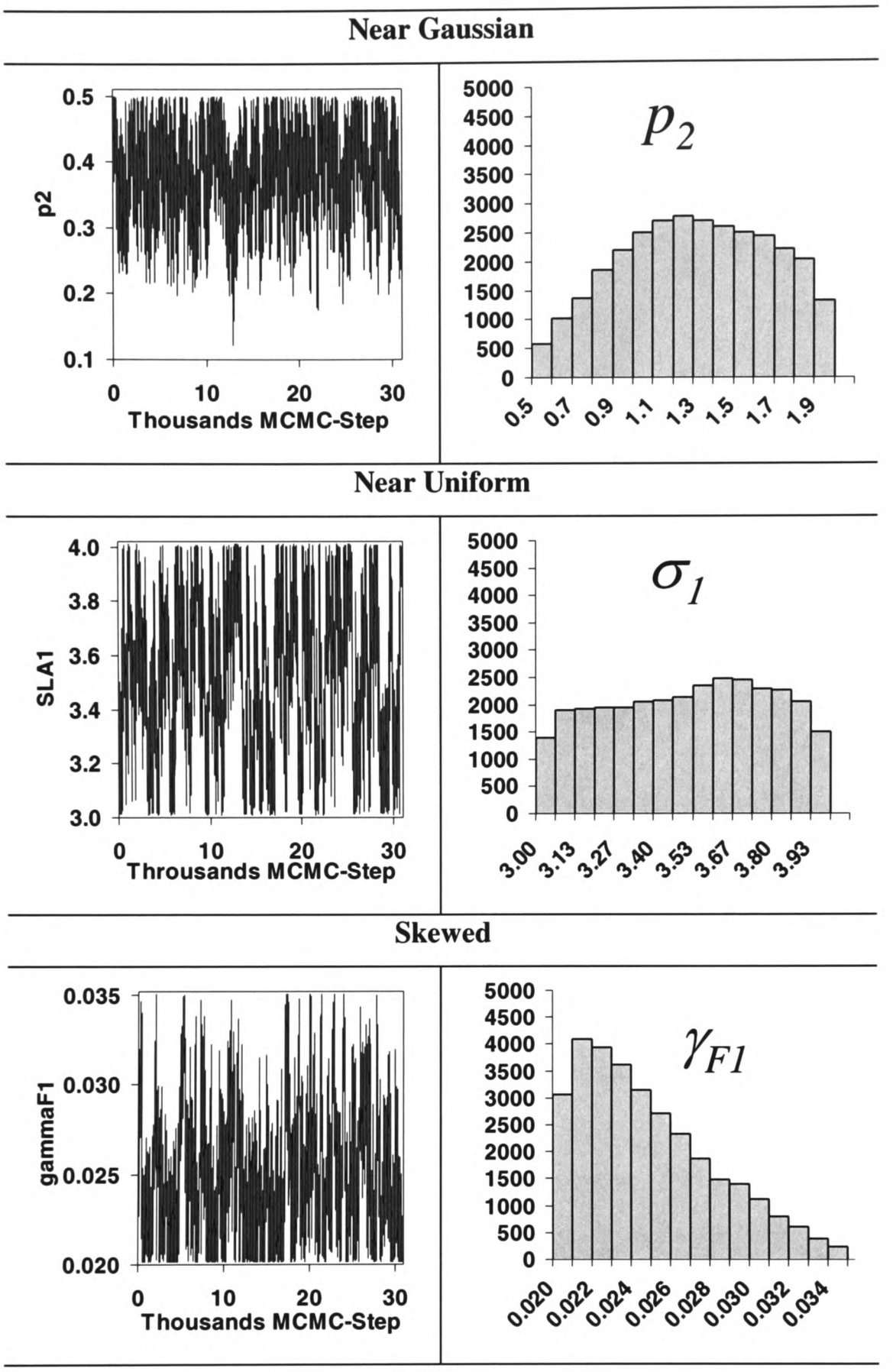


Figure 5.2: Examples of marginal posterior distributions resulting from the MCMC sampling

In addition to the distance from θ_{MAPx}, the width of the parameter ranges in the sub-sample relative to that of the prior was estimated, indicating whether or which HAP parameter values concentrate in a specific region. For p_2, p_{20}, T_{opt}, T_x, σ_1, k and α_{Cx} the range of values in the HAP sub sample was between 50-80% to that of the prior indicating that the uncertainty in these parameters has been reduced. However, for the majority of parameters, the range was similar to that given in the prior. These results, along with those presented in Figure 5.3 suggest that more than one maximum may be found in the 19-D parameter space. The most probable vectors do not have similar parameter values. This may result from large uncertainty remaining for some of the calibrated parameters.

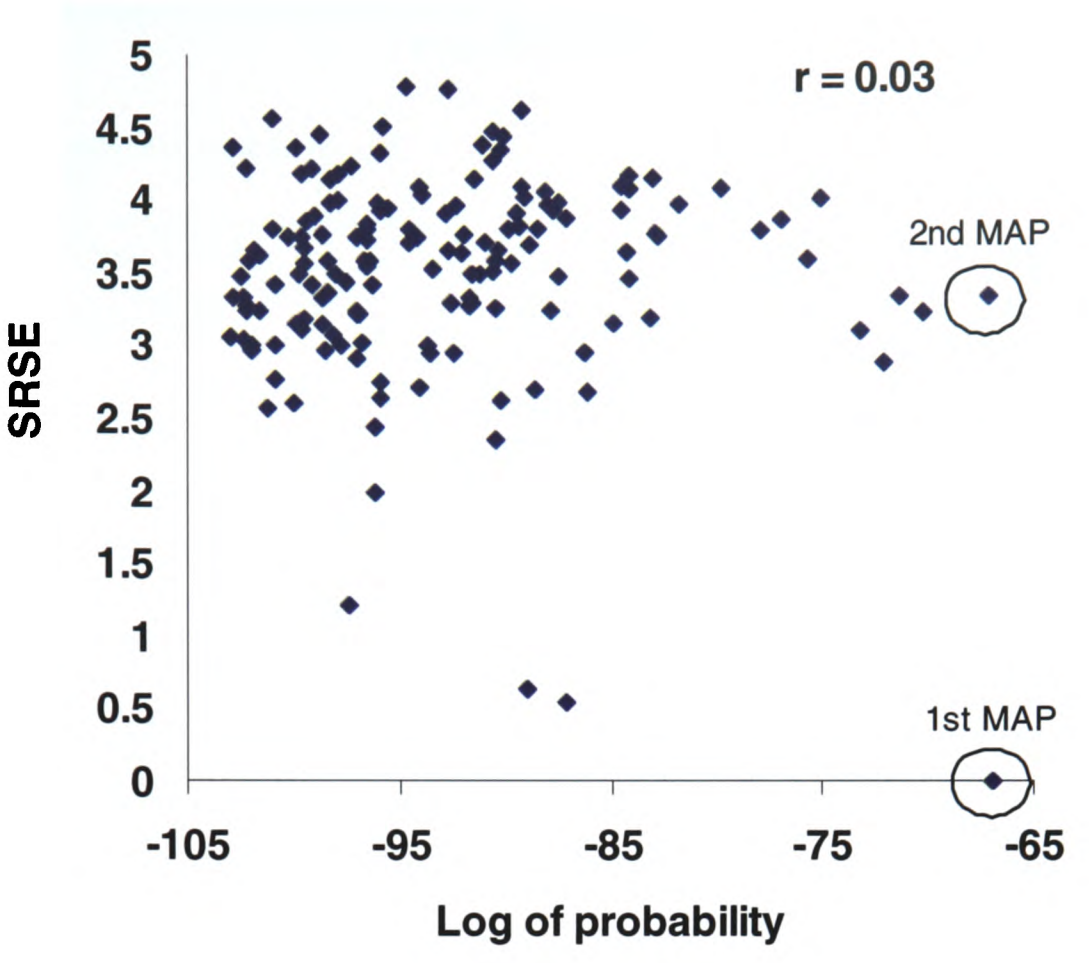
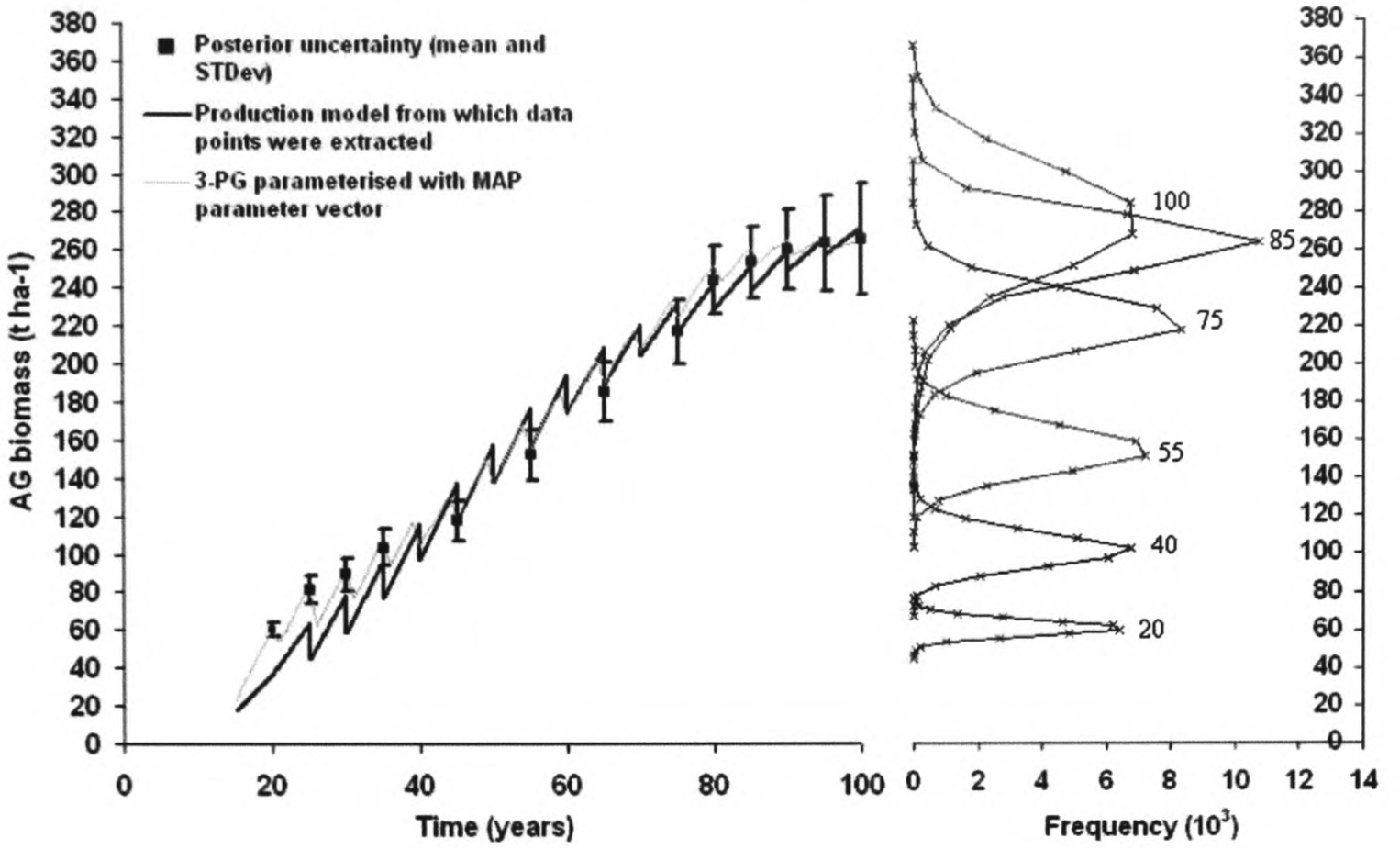


Figure 5.3: Similarity index (SRSE) between the θ_{MAPx} and the parameter vectors of highest probability

5.5.2 Marginal posterior distributions of outputs

For both ABG biomass and LAI, Figure 5.4 shows the dataset (Figure 5.4a. yield model of YC 10, Figure 5.4b. mean LAI), the posterior mean with uncertainty and 3-PG outputs from θ_{MAPx}. Smoothed histograms for selected years are also presented. For ABG biomass outputs, a general trend can be observed. As values increase, the width of the distribution, thus the uncertainty, increases. Times where the fit is good for both LAI and ABG biomass are mostly at the end of the rotation (high ABG biomass and low LAI). Average LAI values at young age are overestimated while being underestimated after canopy closure. The same pattern is observed for ABG biomass. While ABG biomass values are overestimated around initialisation, they are underestimated in the middle of the rotation.

a. Biomass



b. LAI

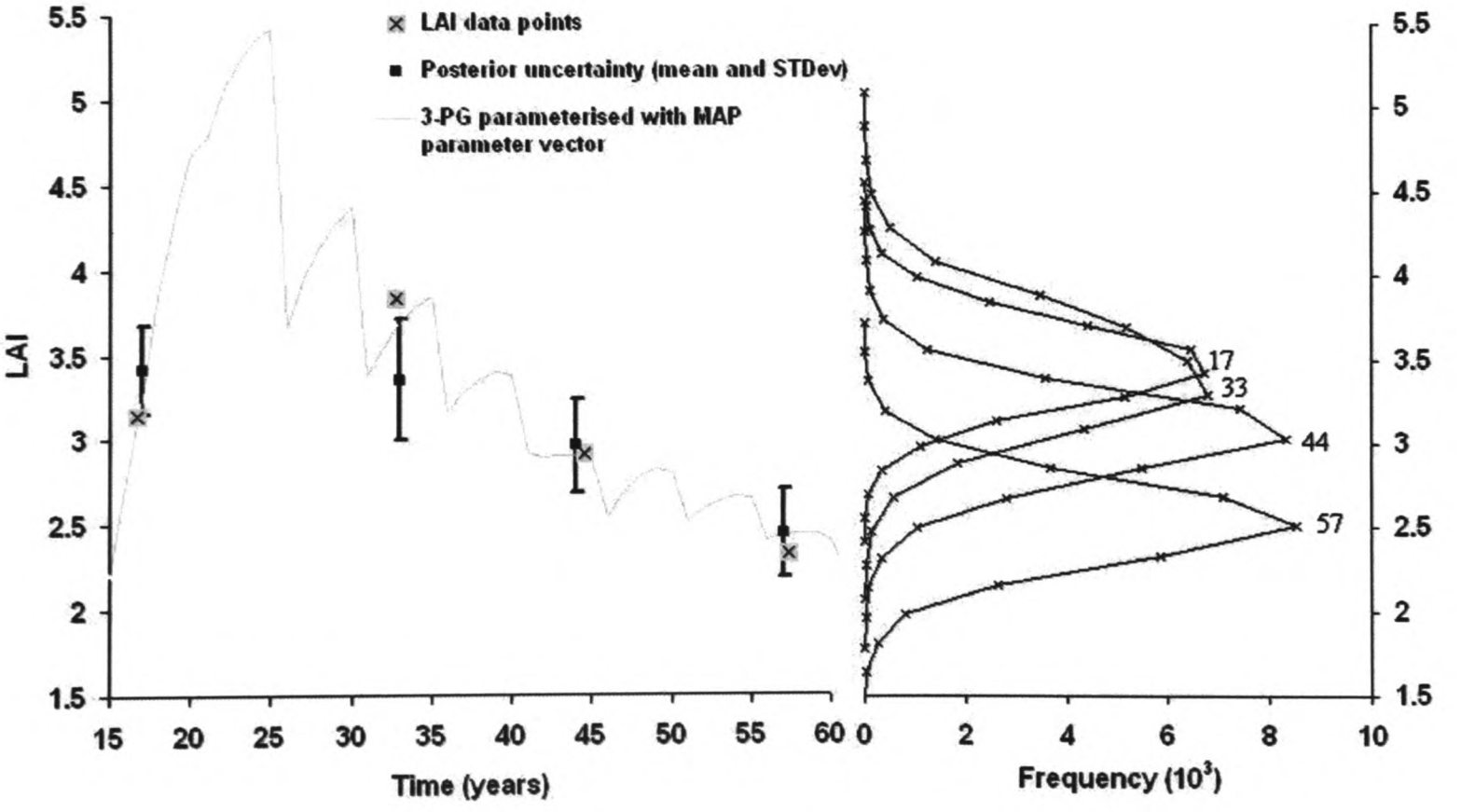


Figure 5.4: Mean and standard deviation (SD) of model outputs from the MCMC sample. Model outputs resulting from θ_{MAPx} are also shown in light grey

The smoothed histograms represent the marginal distributions of selected outputs (stand ages to the selected outputs are indicated at the right of the distribution). The saw-toothed pattern results from thinning events.

5.5.3 Analysis of uncertainty

The intercorrelation of a given model output with respect to a parameter has been estimated from the Bayesian analysis. Positive or negative partial correlation calculated between approximately 32 000 parameter and output vectors can indicate whether an increase in a parameter value results in an increase or decrease, respectively, in an output value (and *vice versa*).

Figure 5.5 shows a partial correlation fingerprint between parameters and outputs (ABG biomass and LAI). High negative correlations are indicated as dark blue and high positive correlations, as dark red. Light blue to light green regions indicate weak or no correlation. Seven out of 19 parameters are highly correlated with ABG biomass outputs and 4 out of 19 with LAI (at least one $|r| \geq 0.6$ during the rotation).

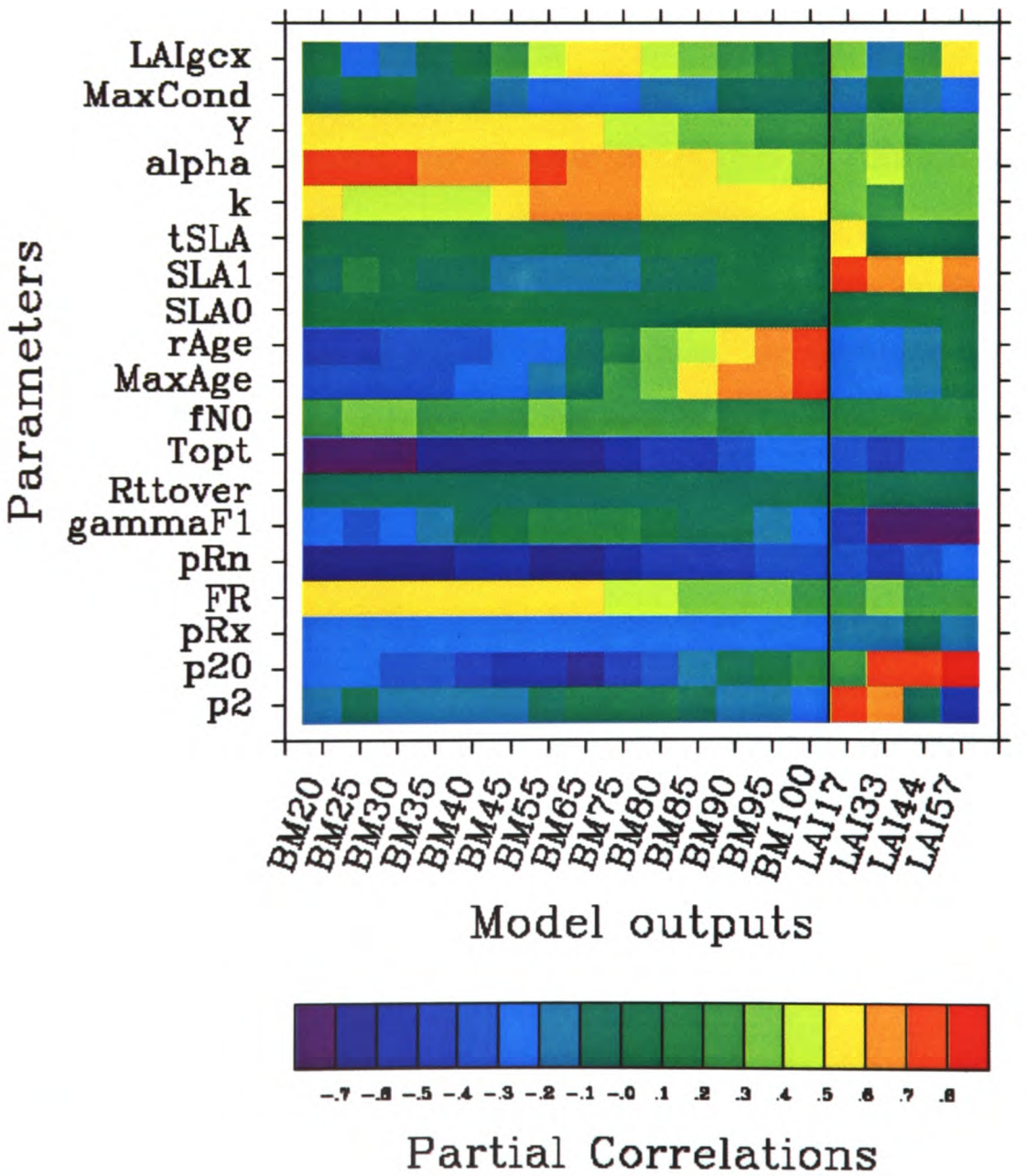


Figure 5.5: Partial correlations between parameters and model outputs. High positive and negative correlations are indicated as dark red and blue respectively

BM=biomass at the indicated stand age ; pRn=η_{Rn} ; pRx=η_{Rx} ; gammaF1=γ_{F1} ; tgammaF=$t_{\gamma F}$; Rttover=γ_R ; SLA0=σ_0 ; SLA1=σ_1 ; Max Age= t_x ; tSLA=t_σ ; alpha=α_{Cx} ; MaxCond=g_{Cx} ; LAIgcx=L_{Cx}

Parameters at least once highly correlated with ABG biomass or LAI outputs during the rotation are p_{20}, η_{Rn}, T_{opt}, t_x, r_{age}, k and α_{Cx} for ABG biomass and p_2, p_{20}, γ_{F1} and σ_1 for LAI ($|r| \geq 0.6$). Parameters of correlation $0.4 < |r| < 0.6$ are L_{Cx}, Y and FR. Parameters uncorrelated or with low correlations ($|r| \leq 0.4$) are η_{Rx}, γ_R, f_{N0}, σ_0, g_{Cx}, $t_{\gamma F}$. Further examination of Figure 5.5 can provide insights as to how specific parameters influence biomass or LAI outputs throughout the rotation. For instance, the litterfall rate (γ_{F1}) is weakly correlated with biomass outputs but highly correlated with LAI outputs. Likewise, the maximum canopy quantum efficiency (α_{Cx}) is decreasingly correlated with biomass outputs as the stand ages.

5.6 Discussion

Most commonly, 3-PG has been parameterised by adjusting the value of selected parameters for the model output to fit the data time series, without any indication of parameter and output uncertainty (Sands 2004). For example, White *et al.* (2000), Sands and Landsberg (2002), Stape *et al.* (2004) and Almeida *et al.* (2004) provide parameter sets for particular species and conditions, yet no error boundaries or confidence levels to the model predictions and parameters are given. Conversely, Esprey *et al.* (2004) provide an in depth analysis of 3-PG through a sensitivity and non-linearity analysis of selected parameters on stemwood volume and LAI. Such studies are highly informative on the influence of each parameter on outputs but do not fully capture the extent to which parameters are correlated with each other nor the uncertainty resulting from non-linear interactions. This is however achievable with the Bayesian calibration. To optimise benefits from a Bayesian calibration especially at the beginning of the investigation, one should make use of all the information available even if large uncertainty exists. Given relatively diffuse priors, the posteriors at first will be strongly influenced by the data. This influence will however decrease as the uncertainty in the prior decreases. Here, the literature sources mentioned below provided guidance for setting ranges of biophysical values in the priors (Table 5.3).

The results presented in this paper thus constitute the first attempt to quantify uncertainty simultaneously for parameters and model outputs in 3-PG, while also providing parameter estimates and a sensitivity analysis. Ideally, the full joint probability distribution over the 19-D parameter space should be presented but this is clearly impractical. As an alternative, statistics derived from the MCMC sample, which approximate the distribution, will be discussed.

5.6.1 Parameter marginal posterior distributions, θ_{MAPx}, and correlations between parameters

Marginal distributions of parameters provide both an indication of the most probable values of individual parameters and of the quality and usefulness of the data used in the calibration. A narrow-peaked, near-gaussian distribution implies that good data are available and that the uncertainty from the prior has been reduced. Four posterior distributions to the parameters were near-gaussian (p_2, p_{20}, t_x, t_σ). Near uniform distributions suggest that either compensation occurs between parameters such that the probability of all values are nearly equal (in such cases, the parameters might be correlated), that the data available are ineffective for the calibration of a specific parameter, or that the data uncertainty is too large. Conversely, skewed distributions may arise for various reasons. Firstly, the nature of the parameter itself, whose uncertainty has been reduced but whose distribution may be non-normal, may have given rise to a skewed or a beta distribution. Likewise, the non-linear and multivariate interactions in the model as well as the ranges set in the prior may strongly influence the marginal distribution of the parameters.

It is not possible to establish direct causal relationship from correlations alone between parameters. Nevertheless, correlations are indicative of interactions between parameters and can assist in understanding the model structure. For instance, compensation between parameters is a probable cause for covariation. Here, the four correlations for which $|r| \geq 0.3$ (Table 5.3) will be discussed. Firstly, the correlation between the relative age (r_{age}) and the maximum stand age (t_x) is an apparent example of compensation, as the parameters form a single ratio in the age modifier algorithm. As t_x increases, r_{age} increases and *vice versa*, suggesting that the ratio of these two parameters tends to fall within a narrow range. A similar compensation pattern is observed between the maximum canopy quantum efficiency (α_{Cx}) and the minimum fraction of P_n allocation to roots (η_{Rn}). Provided that other coefficients are kept constant, high values of α_{Cx} induce higher P_n. As ABG biomass and foliage are "constrained" by the available data, additional P_n must be allocated to roots. In a non-limited environment such as Thetford (see values for f_{N0} and FR, Table 5.3), η_{Rn} is the main driver of root allocation in 3-PG.

This interpretation also applies to the correlations between the litterfall rate for mature stands (γ_{F1}) and the p_{20} partitioning ratio between foliage and stem, as well as between the specific leaf area for mature stands (σ_1) and p_{20}. As LAI is constrained, an increase in allocation of P_n to leaves results in an increase in litterfall rate (and *vice versa*). Likewise,

the negative correlation between σ_l and p_{20} suggests that the higher the area of leaf per unit dry weight, the smaller the allocation to leaves. Although for a given LAI, a high specific leaf area and a low allocation of P_n to foliage equates to a low specific leaf area and a high allocation, these two statements are not equal in terms of photosynthetic capacity. What really drives photosynthesis is not LAI *per se* but rather the amount of leaf material carrying photosynthesis. Thus, the first statement yields lower photosynthetic potential than the second, as less biomass per leaf area is available for the process. In 3-PG growth is driven by LAI, thus one should aim to reduce the uncertainty of σ_l together with LAI, over that of p_{20}. Increasing the certainty of σ_l by field assessment may thereafter reduce the uncertainty of p_{20}.

The most probable individual parameter value in the marginal distribution and that in the θ_{MAPx} provide complementary information but may differ considerably, as parameters are not independent. While marginal distributions are informative of individual parameters, the θ_{MAPx} vector best characterises the joint probability distribution and provides a window into the multivariate interactions embedded in the model structure (VanOijen *et al.* In press). Below, we discuss the implications of some of the θ_{MAPx} parameter values for forest growth in Thetford and compare those with that found in the literature.

In 3-PG, the net primary production is proportional to the product of the maximum canopy quantum efficiency (α_{Cx}), the P_n / P_g ratio (Y), light interception and environmental constraints. The use of default or fitted values for Y and α_{Cx} respectively, is standard as these parameters are difficult to measure in the field. Estimates from other 3-PG studies nevertheless provide means for comparison. The value for α_{Cx} in θ_{MAPx} (0.049 mol mol^{-1}) is higher than values normally given for temperate coniferous species in 3-PG (approximately 0.04 mol mol^{-1}, e.g. Law *et al.* 2000) while Y is within the range normally cited (Waring and Running 1998) but lower than the default value provided in Sands (2004). Conversely, summer values of the light extinction coefficient of PAR trought the canopy (k) were estimated in Thetford for 8 Scots pine stands of various ages and ranged between 0.28 and 0.55, when k values for half LAI were converted to that for projected LAI (Mencuccini and Grace 1996). In θ_{MAPx}, k (0.56) is slightly higher than that measured in Thetford and may be compensating for the generally lower values of the maximum canopy quantum efficiency (α_{Cx}) and the P_n / P_g ratio (Y). Net primary production is further constrained by limiting conditions, represented by dimensionless environmental factors. The parameters in θ_{MAPx}

and the climatic database suggest that the most limiting factors in Thetford are soil water availability and air temperature.

Soil water availability is governed by the soil water balance submodel (Section 5.2.3). In our simulation with θ_{MAPx}, soil water availability reaches zero in average twice a year during productive months. When setting all other modifiers optimal, this implies a reduction in canopy quantum efficiency from 0.049 to 0.001. In the UK, monthly rainfall is relatively constant throughout the growing season. Additionally, the values for maximum fraction of rainfall intercepted by the canopy (i_{Rx}) and interception of rainfall by the canopy (L_{ix}) prescribed here have a minor effect on soil water availability. As guidance, we estimated that the monthly rainfall interception by the canopy (averaged over the rotation) is approximately 7%, calculated by taking the ratio between the average LAI over the rotation and L_{ix} and multiplied by i_{Rx} (details for soil water balance are given in Sands 2004). High evapotranspiration rates, governed in part by the maximum canopy conductance (g_{Cx}) and the LAI value at which g_{Cx} is maximal (L_{Cx}), are probably instigating desiccation and restraining growth. When potential evapotranspiration exceeds available water, stomatal closure inhibits photosynthesis and growth. In optimal conditions, g_{Cx} is reached as soon as the canopy LAI reaches L_{Cx}. In θ_{MAPx} while L_{Cx} (3.09) is slightly below the default value in 3-PG (Sands 2004), the maximum canopy conductance (g_{Cx}) in θ_{MAPx} is near 0.027 m s^{-1}, close to that estimated for Thetford (Stewart 1988, Gash 1989 and Kelliher *et al.* 1993) but high comparatively to the 0.020 estimate generally used for other species in 3-PG (Law *et al.* 2000, Coops *et al.* 2001, Waring *et al.* 2002, Sands 2004). Soil-atmosphere water exchanges in Thetford Scots pine stands may thus be considerable during the 17 to 40 age period where LAI > L_{Cx}, and especially during the long summer days found at high latitudes (Figure 5.4).

The optimal temperature for growth in θ_{MAPx} is 18° C, a value within the optimum temperature range for temperate species, estimated between 15-25°C (Waring and Running 1998, p. 67). The mean annual temperature in the UK is however much lower, approximating 10° C. The Scot pines stands considered here are thus seldom growing under optimal temperatures. Given the selected maximum and minimum temperature for growth, a monthly temperature of 5°C below or above that of the optimum reduces the quantum efficiency from 0.049 to 0.043 (other modifiers kept optimal). In the study by Esprey *et al.* (2004), stemwood volume and LAI were seen to have a high degree of non-linearity with respect to T_{opt}. In our study, we also found that these variables (ABG biomass and LAI) were highly sensitive to T_{opt} (Figure 5.5). We suggest that the temperature modifier

algorithm should be adapted if the model is to be applied to species growing outside of their optimal temperature range. Otherwise, the model outputs considered here become highly sensitive to, and probably highly non-linear with, T_{opt} (Figure 5.5, Esprey *et al.* 2004). Finally, other influences on biomass production, such as the fertility coefficient (FR) and the age declining modifier, are not significantly limiting growth. Values of FR and f_{N0} in θ_{MAPx} suggest that the site is relatively fertile (Table 5.3) and although the age related decline starts early in the rotation, its slope is very mild throughout. The influence of vapour pressure deficit (D) and frost days is also minor: there are less than 14% frost days per year and D never exceeds 6.5 mBar.

Net primary production is then allocated to the different plant components. Given the calibrated parameters in θ_{MAPx}, foliage biomass and the LAI response are principally governed by the ratios of foliage to stem partitioning (p_2 and p_{20}), as the non-linear effect of the specific leaf area and the litterfall rate functions apply at ages below that of initialisation, a result consistent with that found previously for Scots pines and other species (vanHees and Bartelink 1993, Sands and Landsberg 2002). The litterfall rate in θ_{MAPx} for mature stands is close to that measured in Thetford. Although large variations were observed between seasons and years, these averaged 0.020 kg per month (Beadle *et al.* 1982). This is not unreasonable, as Scots pine needles in temperate ecosystems live for an average of 3 to 4 years (Stenberg *et al.* 1994). As no root biomass data were used in the calibration, allocation to roots is determined by the surplus of P_n not allocated elsewhere, and available soil water. Values of minimum and maximum biomass allocation to roots (η_{Rn} and η_{Rx}) are very similar to that found in the literature. In a review of below-ground net primary productivity of pines, Ewel and Gholz (1991) found that the minimum allocation of total P_n to roots was 17%, while the maximum was 73%. Roots/total biomass ratios can also be indicative of the minimum fraction of P_n allocation. Levy *et al.* (2004) provide root:shoot biomass ratios for UK Scots pine forests. Conversion to root:total biomass ratios using simple arithmetic yielded a minimum root biomass of 14%, comparable to the result obtained here for η_{Rn}. Between η_{Rn} and η_{Rx}, η_{Rn} is the main determinant of root allocation in Thetford. Over a year, the influence of modifiers is generally minor and when soil water availability approaches zero, allocation to roots approaches η_{Rx} but then biomass production is reduced to a point where it is insignificant (as discussed above). The low value of η_{Rn} in θ_{MAPx} thus indicates a generally small residual P_n after allocation to foliage and stems. As for root turnover (γ_R) in θ_{MAPx}, it value is conservative. Any value is as probable as another and large uncertainty remains (Figure 5.5) since γ_R is uncorrelated with all biomass outputs

and the marginal distribution to the parameter is uniform. Data precisely on root turnover or biomass, although difficult to acquire, will be required for improving the calibration. In deed, the water uptake is not linked to root biomass in 3-PG such that an increase or decrease in root mortality has no impact on biomass production.

In summary, given our available data and θ_{MAPx} and the information contained in 3-PG, the Scot pines grown in Thetford have a generally lower P_n / P_g ratio than that used in 3-PG for other species elsewhere, a lower quantum efficiency, but a high radiation interception capacity. Thetford is a fertile site but not optimal for the biomass production of Scots pines, as the species is growing outside its optimal temperature range. Additionally, the combination of sandy soils, shallow rooting zone and the species' relatively high maximum canopy conductance are favourable conditions for soil desiccation. P_n is mainly allocated to the ABG components and allocation to roots is generally small. When limiting environmental conditions prevail and especially during droughts, root allocation may be high but biomass production is then considerably reduced.

5.6.2 Marginal posteriors distributions of outputs and analysis of uncertainty

The output uncertainties are reasonably low given that little data were available for the calibration (Figure 5.4). An increase with the mean is however observed for ABG biomass outputs. Such an increase with measurement values is not uncommon in biological studies. In modelling, it is often associated with the propagation of errors through non-linear multivariate interactions. Here, the relative error (SD/Mean) increases from 6% to 11%. Time dependent algorithms such as those prompted by the age decline and the age modifier may lead to increased variability at higher ABG biomass.

On the other hand, the uncertainty of the LAI is relatively constant throughout the rotation and does not increase with mean LAI. Of the four modelled LAI plotted in Figure 5.4, the highest LAI value found at age 17 has the lowest uncertainty while the highest uncertainty is observed at age 33. Consistent overestimation/underestimation of biomass and LAI values at the beginning/middle of the rotation respectively, could result from difficulties in meeting the data constraints arising from the model structure itself.

The sensitivity analysis presented in the form of a fingerprint graph (Figure 5.5) allows to identify which parameters influence which model outputs and how (the reverse is also true). In Table 5.4, the most influential parameters, obtained by locating correlations of $|r| \geq 0.6$ at

specific times during the rotation, are given (see Figure 5.5). Note that strong correlations do not necessarily imply that the impact of the parameter on the output is strong. These can provide guidance to reduce uncertainty in specific outputs at specific times in the rotation and help for future parameterisation of the model.

Table 5.4: Parameters for reduction in model output uncertainty

Stand Age	Biomass	Stand Age	LAI
[15-45[	Y, α_{Cx}, k, t_x, r_{age}, T_{opt}, η_{Rn}, FR	**17**	t_σ, σ_1, p_2
[45-75]	L_{Cx}, Y, α_{Cx}, k, T_{opt}, η_{Rn}, FR, p_{20}	**33 and 44**	σ_l, γ_{Fl}, p_2, p_{20}
]75-100]	α_{Cx}, k, t_x, r_{age}	**57**	L_{Cx}, σ_l, γ_{Fl}, p_2, p_{20}

The parameters highly correlated ($|r| \geq 0.6$) with outputs during specific stand age period are given

It is noteworthy to mention that most parameters highly correlated with outputs are those whose marginal posterior distribution is near Gaussian or skewed and whose range in the HAP sub-sample was between 80 to 50% that of the prior. This suggests that the available data have enabled to reduce their uncertainty. Parameters with no or low correlations with LAI or ABG biomass outputs are: the maximum allocation of P_n to roots (η_{Rx}), root turnover (γ_R), the value of f_N when the site is highly infertile (FR=0) (f_{N0}), the specific leaf area at stand age 0 (σ_0), and the maximum canopy conductance (g_{Cx}). Low correlations either indicate that these parameters are insensitive, but most likely point to a lack of data for the calibration. The fact that the marginal posterior distributions to these parameters are near uniform also supports this conclusion. Consequently, more data, especially on roots biomass, foliage biomass (at an early age) and data pertaining to the evapotranspiration and soil water balance soil model are required to update these marginal posterior distributions. Our preliminary study on Scots pine thus provides the basis for future calibration, as key ancillary data for uncertainty reduction have been identified. As more data will become available, the prior and posteriors will be updated.

5.7 Conclusion

While both optimisation and Bayesian approaches address the need to test whether a model can predict available data or not, in optimisation, parameter values are adjusted such that the model yields outputs closest to the data. Commonly used error minimisation approaches ignore uncertainty, a principal cause for mismanagement of natural resources including that of the once abundant fish stocks (Ghazoul and McAllister 2003). Additionally, approaches

such as the maximum-likelihood do not enable the full exploration of the parameter landscape. The resulting parameter vector may only be from a local maximum. Conversely, Bayesian calibration advocates the quantification of uncertainties to parameters, thereby yielding uncertainties in model outputs, over the derivation of an optimised set of parameter based on a goodness-of-fit approach (e.g. the maximum-likelihood approach).

This paper presented a preliminary but novel uncertainty assessment of 3-PG parameters and model outputs for UK Scots pine stands. Three main results were presented. Firstly, the outputs and parameters uncertainties were expressed as marginal probability distributions. Secondly, an analysis identifying the parameters to which LAI and ABG biomass outputs were most sensitive (and vice versa) was conducted, and finally, the exploration of a sub-sample of most probable parameter vectors was achieved. The sensitivity analysis with the uncertainty assessment identified 12 out of 19 parameters to which LAI and ABG biomass were most sensitive: L_{Cx}, t, p_2, p_{20}, η_{Rn}, γ_{F1}, t_x,, T_{opt}, r_{age}, σ_1, k, α_{Cx}, Y and FR. Parameters with no or low correlations were η_{Rx}, γ_R, f_{N0}, σ_0, g_{Cx}, $t_{\gamma F}$. For these, supplementary data on root, foliage and soil water availability would be required to update the marginal distributions. A discussion on the parameters values in the vector with highest probability has provided deeper insights into the functioning of 3-PG and about our study site, also identifying parameters to which priority should be given for uncertainty reduction. Finally, a similarity index was calculated between parameter vectors of highest probability and the parameter vector of maximum *a posteriori* probability which showed that more than one maximum in the 19-dimension parameter space may exist. Increasing the chain length of the MCMC sampling may enable further exploration of the 19-D landscape. This, along with including ancillary data on variables not currently compiled here may reduce uncertainties.

Acknowledgements

The authors would like to thank Richard Waring (Oregon State University), Georgios Xenakis and Maurizio Mencuccini (University of Edinburgh) and Peter Savill (University of Oxford) for sharing data and advices. Thanks are due to the British Atmospheric Data Centre for providing access to the Met Office Land Surface Observation Stations Data. This research was supported by the BNSC-Link Carbon Offset Verification project, the Biffaward initiative and the Fonds Québécois de la Recherche sur la Nature et les Technologies (FCAR).

Chapter 6

Bayesian calibration the 3-PG model for Corsican pine

The methodology presented in Chapter 5 prompted interest in calibrating 3-PG for other UK species. An important conclusion reached in that chapter was that the absence of root data in the calibration precluded the reduction of uncertainty for several parameters, particularly those pertaining to the allocation of net primary productivity (NPP) to roots and to root mortality. Likewise, acquiring data of varied nature was shown to be important for reducing the uncertainty of a wider range of parameters and outputs. Datasets available for Corsican pine stands in Thetford comprised data of different nature to that used in the calibration for Scots pine. The calibration was applied to this species. Although not widely distributed in the UK, Corsican pines still cover more than 30 thousand hectares of the UK land surface area (Forestry Commission, 2001). The Bayesian calibration conducted on two different species but located on the same study site also enabled the comparison between physiological differences, without the interference of contrasting climatic or environmental variables.

Chapter 6 differs from Chapter 5 in that different parameters and model inputs were included in the calibration process, as different datasets were available. In this chapter, the data sources included in the process are more wide-ranging and even include remote sensing estimates of LAI data points. Details of these differences are provided below. To avoid unnecessary duplication of information, the reader should refer to Appendix A for a detailed description of the 3-PG model, and to Chapter 5 for the Bayesian calibration methodology.

6.1 Methods

6.1.1 Study site, climatic data and available data

The calibration of the 3-PG model was conducted for Corsican pines stands (*Pinus nigra* car. *maritima* (AIT.) Melv.) of yield class 14 found in Thetford forest (Appendix A). The climatic dataset applied previously (Chapter 5, Table 5.1) was also adopted here.

The following datasets were principally used as data source for the calibration: the Maestro dataset, the GIS database, the SHAC dataset and the hyperspectral remote sensing images. The Maestro dataset consists of ground data collected as part of the remote sensing Maestro-1 Campaign conducted in 1989 (Baker 1992, Baker *et al.* 1994). Management practices applied to the stands on which data were collected, along with stand size were recorded. For the stands, forest structure parameters such as species composition, tree age, top height, stemwood volume and basal area (Baker and Mitchell 1989, Baker *et al.* 1994) were collected. Each sampled stand was allocated a Forestry Commission code, enabling its precise location on a GIS database (Forestry Commission, 2000). The GIS database, georectified to the British National Grid, is a spatially exhaustive catalogue comprising stand level information on species, yield class, planting year, planting density and stemwood volume. A third dataset was also used here, which consists of field measurements of DBH, top height, tree species, planting density and leaf area index. This dataset complements the maestro dataset, and was created as part of the SHAC remote sensing campaign conducted in 2000 (Skinner and Luckman, 2000). Finally, hyperspectral remote sensing data were available for the year 2000 and were used to estimate LAI for which few ground measurements were available. Figure 6.1 presents the GIS database for which the Corsican pine stands of yield class 14 are shown in green, overlaid to the Hyperspectral images for Thetford.

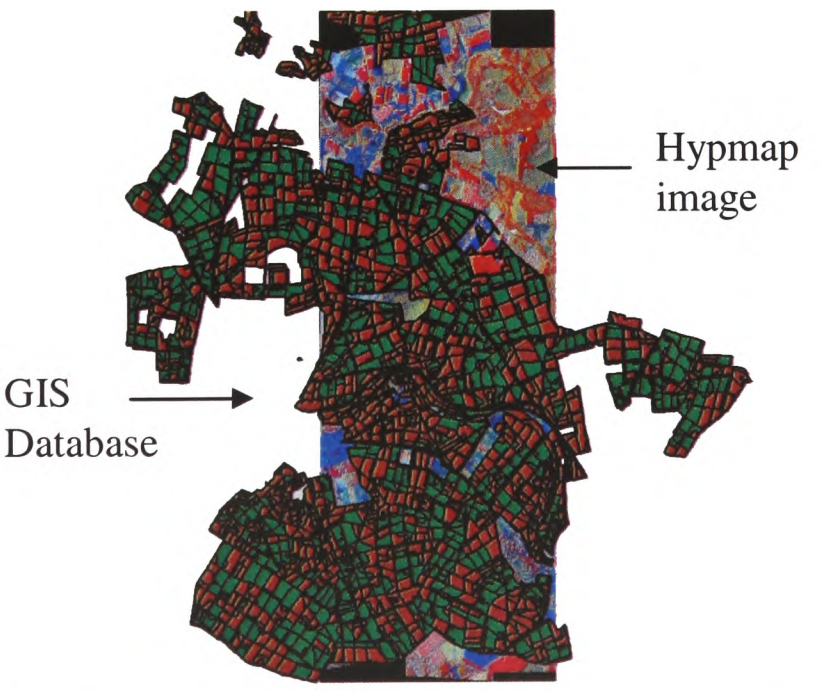


Figure 6.1: False color mosaicked hymap image with GIS overlay. The GIS overlay shows all the forest plantation stands where green areas indicate Corsican pine stands of yield class 14.

6.1.1.1 Remote sensing data

Hyperspectral images for Thetford were acquired using the SHAC airborne hyperspectral imaging spectrometer in June 2000. The instrument records data in 126 contiguous spectral bands, which together cover the spectral range between 436 nm-2486 μm. The spectral

resolution of each band is approximately 15 nm while the spatial resolution of the dataset is 4 m. The following processing was applied to the original images. Firstly, atmospheric correction was applied by the German Aerospace Center (DLR, Deutsche Forschungsanstalt für Luft und Raumfahrt) while georectification and geocorrection to British National Grid was conducted through SHAC by the Centre for Ecology and Hydrology, Monks Wood. Secondly, the three overlapping scenes available for Thetford were mosaicked together and normalised. Mosaicking is the process of joining georeferenced images together whereas normalisation minimises the effect of the sensor look angle and local topographic effects. These can be large across a scene especially if images were acquired from an airborne platform, as the average scene luminance may vary as the sensor looks both sides of the aircraft. Here, an equal area normalization algorithm has been applied which "shifts each (pixel) spectrum to the same overall average brightness" (Erdas Imagine, 2002, p.193). Finally, to remove noisy bands within the dataset, a signal to noise ratio analysis was conducted on all 126 bands. The signal to noise is defined as the ratio "mean to standard deviation" in a 3x3 moving window. Visual analysis of the resulting signal to noise ratios per band enabled the location and removal of noisy bands (Figure 6.2). A total of 9 bands were removed, many coinciding with atmospheric water absorption bands (Table 6.1).

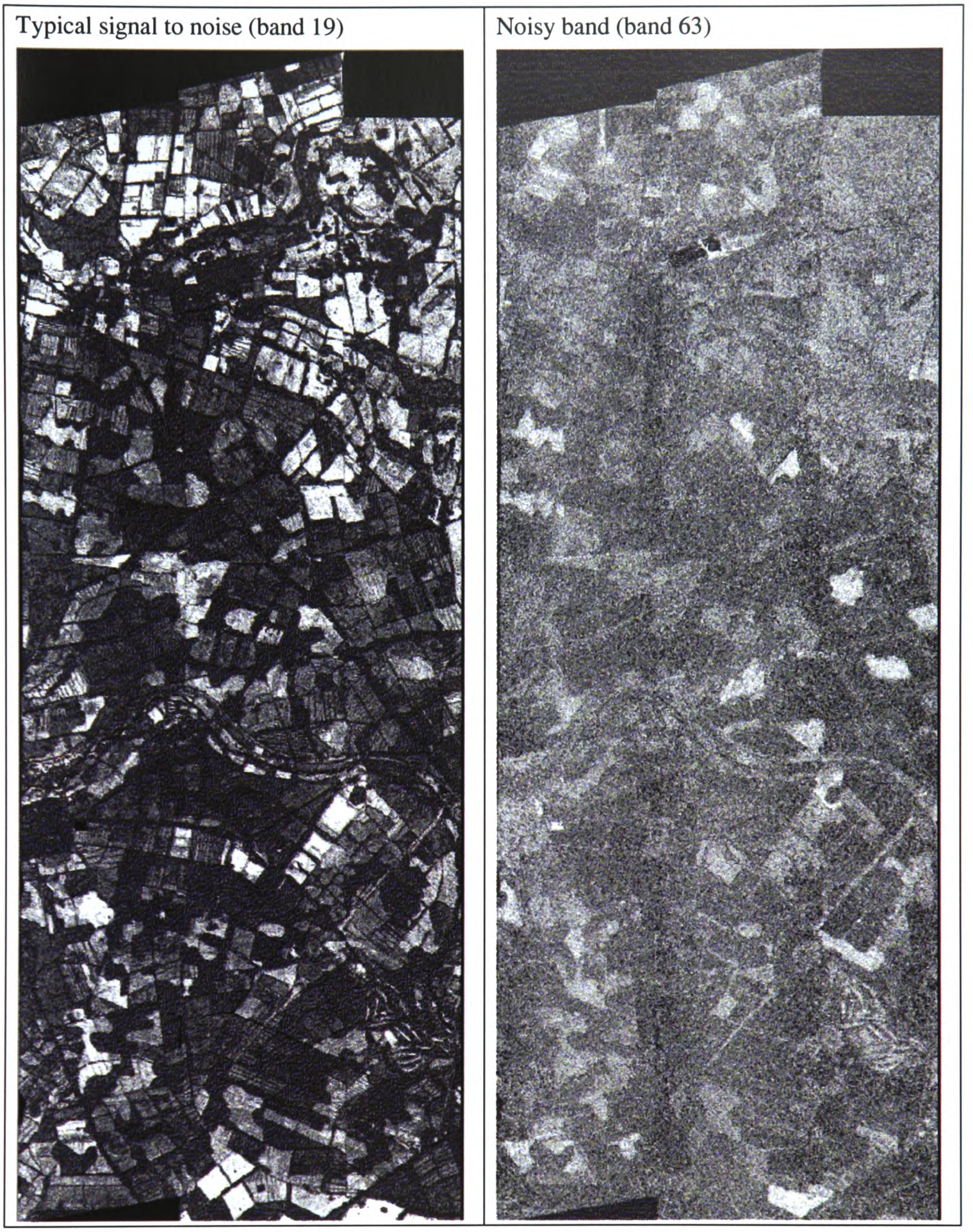


Figure 6.2: Visual contrast between (a.) normal and (b) noisy bands.

Table 6.1: Wavelength and spectral resolution of the Hyperspectral dataset. Strikethrough bands indicate those removed due to low signal to noise ratio.

Band	Value (nm)	Width (nm)	Band	Value (nm)	Width (nm)
~~**Band 1**~~	~~437~~	~~15~~	~~**Band 64**~~	~~1420.6~~	~~15.9~~
~~**Band 2**~~	~~448.9~~	~~11.2~~	~~**Band 65**~~	~~1434.4~~	~~16.4~~
Band 3	461.3	15.8	~~**Band 66**~~	~~1448.5~~	~~16.5~~
Band 4	477.3	15.5	~~**Band 67**~~	~~1462.6~~	~~16.1~~
Band 5	492.3	15.5	**Band 68**	1476.6	16.2
Band 6	507.4	15.8	**Band 69**	1490.3	16.5
Band 7	523.4	15.6	**Band 70**	1503.9	16.2
Band 8	538.8	15.9	**Band 71**	1517.2	16.2
Band 9	554.2	15.3	**Band 72**	1530.7	16.2
Band 10	569.5	15.4	**Band 73**	1544.1	16.6
Band 11	584.7	15.4	**Band 74**	1557.6	16.5
Band 12	600.1	15.5	**Band 75**	1570.6	16.1
Band 13	615.7	15.7	**Band 76**	1583.5	16.2
Band 14	631.3	15.6	**Band 77**	1596.5	16.6
Band 15	646.6	15.3	**Band 78**	1609.5	16.2
Band 16	661.7	15.1	**Band 79**	1622.3	15.9
Band 17	676.9	15.5	**Band 80**	1635.1	16.1
Band 18	692.4	15.8	**Band 81**	1647.8	16.1
Band 19	707.8	15.3	**Band 82**	1660.3	15.8
Band 20	722.9	15.3	**Band 83**	1672.7	15.5
Band 21	738.1	15.7	**Band 84**	1685.1	15.7
Band 22	753.4	15.3	**Band 85**	1697.5	15.6
Band 23	768.5	15.3	**Band 86**	1709.9	15.3
Band 24	783.5	15.3	**Band 87**	1722.1	14.9
Band 25	798.8	15.7	**Band 88**	1734.1	15.1
Band 26	814.1	15.5	**Band 89**	1746.5	15
Band 27	829.2	15.5	**Band 90**	1758.4	14.5
Band 28	844.4	15.8	**Band 91**	1770.3	14.2
Band 29	859.8	16.2	**Band 92**	1782.2	14.4
Band 30	875	15.9	**Band 93**	1794	14.4
Band 31	872.6	18.1	**Band 94**	1805.7	13.6
Band 32	890.3	20	~~**Band 95**~~	~~1951.6~~	~~20.9~~
Band 33	905.6	19	**Band 96**	1970.7	21.1
Band 34	922.2	18.8	**Band 97**	1989.5	21
Band 35	938	18.3	**Band 98**	2008.2	20.7
Band 36	953.6	18.5	**Band 99**	2027.1	20.9
Band 37	969.3	18.5	**Band 100**	2045.9	20.9
Band 38	984.8	18.7	**Band 101**	2064.5	20.7
Band 39	1000.9	18.7	**Band 102**	2082.7	20.4
Band 40	1016.5	18.8	**Band 103**	2100.8	20.2
Band 41	1032	18.9	**Band 104**	2118.7	20.3

Band 42	1047.5	18.8	**Band 105**	2136.7	20.4
Band 43	1063	18.3	**Band 106**	2154.7	20.3
Band 44	1078	18.6	**Band 107**	2172.2	19.6
Band 45	1093.1	18.5	**Band 108**	2189.2	19
Band 46	1108	18.3	**Band 109**	2206.6	20.7
Band 47	1122.9	18.7	**Band 110**	2224.8	18.8
Band 48	1137.6	18	**Band 111**	2241.7	19.2
Band 49	1152.2	18.1	**Band 112**	2259.4	19.4
Band 50	1166.7	17.9	**Band 113**	2276.6	18.2
Band 51	1181.4	18.3	**Band 114**	2293.5	18
Band 52	1196.1	18.1	**Band 115**	2310	17.8
Band 53	1210.3	17.4	**Band 116**	2326.3	17.8
Band 54	1224.5	17.5	**Band 117**	2342.8	17.9
Band 55	1238.7	17.9	**Band 118**	2359.7	18
Band 56	1253.2	17.7	**Band 119**	2375.8	17.7
Band 57	1267.3	17.3	**Band 120**	2391.8	17.4
Band 58	1281.4	17.1	**Band 121**	2407.6	17.3
Band 59	1295.4	17.3	**Band 122**	2423.6	16.5
Band 60	1309.4	18.1	**Band 123**	2439.3	16.3
Band 61	1323.6	16.5	**Band 124**	2455	16.8
Band 62	1336.8	16.9	**Band 125**	2470.5	17
~~**Band 63**~~	~~1406.4~~	~~17.2~~	~~**Band 126**~~	~~2485.9~~	~~16.5~~

All the Corsican pine stands of yield class 14 were then located on the processed hyperspectral image using the GIS database (Figure 6.1). The age of the stands provided in the GIS database made chronosequencing possible.

6.1.1.2 Prescribed parameters

A total of 14 parameters in 3-PG were prescribed at constant values in this analysis. Many of these parameters were considered to be non sensitive by Esprey *et al.* (2004). Otherwise, they were given a constant value following recommendation by the authors of 3-PG (e.g. soil water modifier) or because the parameters had no influence on the development of the stand (as the model is initialised at 15 years). The set parameters pertaining to the allometric relationship between stem mass and diameter at breast height, a_S and n_S, were derived from the Maestro dataset (Baker 1992, Baker *et al.* 1994) and the production table of YC14 (Edwards and Christie 1981). Figure 6.3 shows the resulting relationship between DBH and woody biomass.

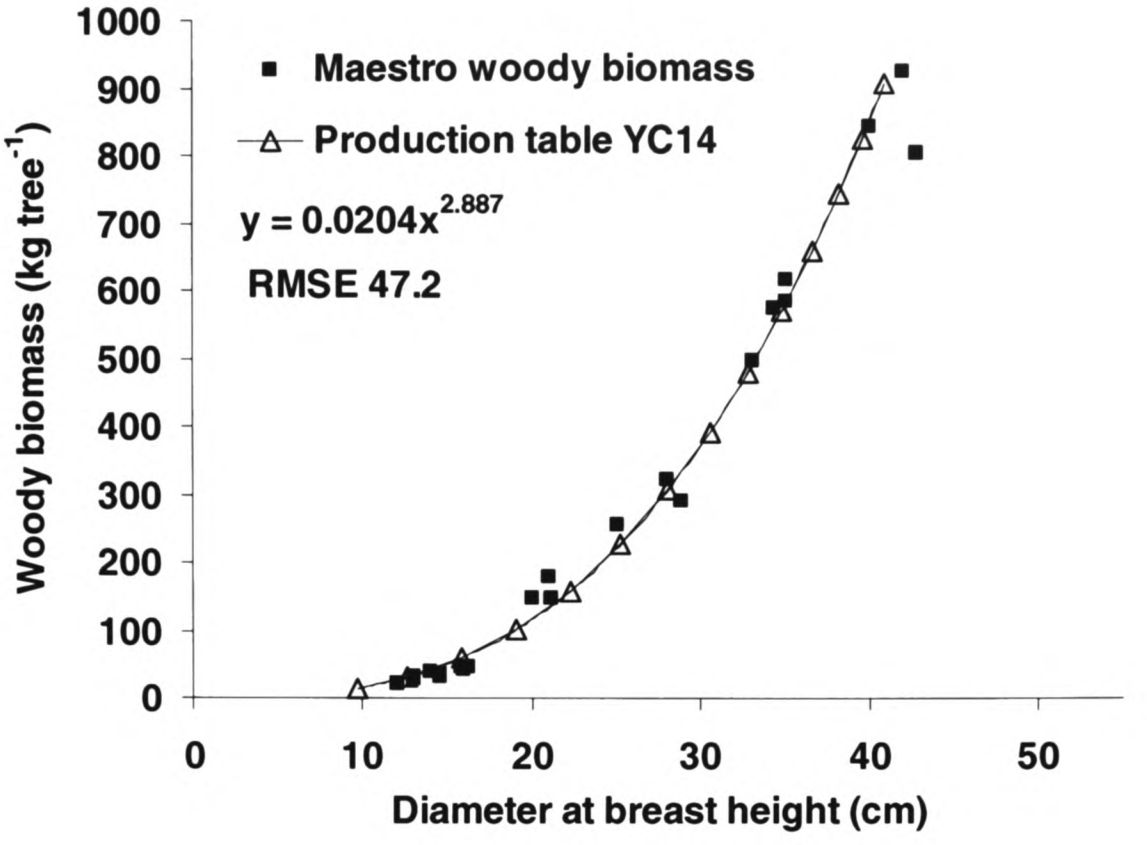


Figure 6.3: Relationship between woody biomass and DBH. The model shows a close agreement between the yield model (Corsican pine, YC 14) and the data measured in Thetford (Baker 1992, Baker et al. 1994).

6.1.1.3 Model initialisation

The model was initialised at tree age of 15 years using biomass data obtained from the Maestro dataset. Initialising the model at this age removes the need for extra parameterisation required by early growth processes (e.g. changes in specific leaf area). Root, stem and foliage biomass were 7.1 t/ha, 22 t/ha (including stem and branches) and 9.8 t/ha respectively. Initial stocking of 3955 trees per hectare was obtained from the production tables (Edwards and Christie 1981).

Minimum available soil water was set at 0 but the maximum available soil water was included in the calibration. In Chapter 5, the maximum available soil water was assumed to be 100mm, as the water storage capacity for sandy soils is approximately 150 mm per metre of soil, the permanent wilting point is 50 mm and 95% of the roots in Thetford are believed to be located in the first meter of soil (Roberts 1976). Even though such shallow rooting zone combined with highly permeable sandy soils and high summer evaporation rates represent prime conditions for desiccation (as assumed in Chapter 5), Stewart (1988) and Beadle *et al.* (1985) have shown that the permanent wilting point is seldom reached in Thetford forest. Estimates of maximum soil water deficit, taken during an exceptionally dry summer, reached 75-77 mm m^{-1}, an amount below that required for reaching the permanent wilting point. In the calibration presented in Chapter 5, the permanent wilting point is

reached at least 2 months a year, a result contrasting with the findings of Stewart (1988) and Beadle *et al.* (1985 a.). As uncertainty remains in estimating this parameter, it was included in the Bayesian calibration process (Table 6.2).

The prevailing intermediate thinning regime of 5-year intervals applied in Thetford was prescribed for all stands in the calibration. The suppressed/standing volume ratios were derived from the Forestry Commission production tables for Corsican pine of yield class 14 and approached 1 near the end of the rotation (see Section 5.3.2 for further details).

6.2 Bayesian calibration

6.2.1 The prior

The calibration was applied to the remaining 22 parameters in 3-PG, including the maximum available soil water and fertility rating. Our selection was guided by the results from Chapter 5 and the work from Esprey *et al.* (2004). The marginal prior distributions of the parameters were set uniform, bounded by a maximum and minimum value for each parameter. Details of these distributions are provided in Table 6.2. The boundaries to the prior were obtained from direct observation on Corsican pine stands in Thetford (CP-T), from literature on Corsican or other pine species (P-L), from surrogate species or 3-PG set default values (D) or finally as best guess estimates or fitting approaches (F).

Table 6.2: Definitions and units of the 3-PG parameters. The values for prescribed parameters are also given, as well as the prior ranges for the parameters included in the calibration.

3-PG symbol: Description (units)	**S Class**[a]	**Prescribed Parameter Values**	**Calibrated Parameters: ranges of values in the prior**		**Data Class**[b]	**Source**
			θ_{min}	θ_{max}		
a_S: Constant in stem mass *v* diam. relationship	M	0.02			CP-T	Baker 1992, Baker *et al.* 1994, Edwards and Christie 1981
c_θ: Moisture ratio deficit which gives $f_\theta = 0.5$	H	0.7			D	Default for sandy soils
f_{N0}: Value of f_N when $FR = 0$	M		0.6	1	F	
FR: Fertility rating	?		0.5	1	CP-T	Thetford GIS database (Forestry Commission, 2000)
g_B: Canopy boundary layer conductance (m s^{-1})	L	0.2			D	
g_{Cx}: Maximum canopy conductance (m s^{-1})	H		0.015	0.03	P-L	Kelliher *et al.* 1995
i_{Rx}: Maximum fraction of rainfall intercepted by canopy	M	0.15			D	
k: Extinction coefficient for PAR absorption by canopy	M		0.2	0.7	P-L	Stenberg *et al.* 1994, Mencuccini and Grace 1996
k_F: Number of days production lost for each frost day (days)	L	1			D	
L_{Cx}: Canopy LAI for maximum canopy conductance (m^2 m^{-2})	L		2	6	P-L	Kelliher *et al.* 1995, Mencuccini and Grace, 1996
L_{ix}: LAI for maximum rainfall interception (m^2 m^{-2})	L	0			D	
m_0: Value of *m* when $FR = 0$	?	0			D	
n_{age}: Power of relative age in f_{age}	L		2	15	F	
n_{fN}: Power of (1-*FR*) in f_N	L		1	10	F	
n_S: Power in stem mass *v* diam. relationship	H	2.88			CP-T	Baker 1992, Baker *et al.* (1994), Edwards and Christie 1981
n_θ: Power of moisture ratio deficit in f_θ	L	9			D	Default for sandy soils
p_2: Ratio of foliage:stem partitioning at $B = 2$ (cm)	H		0.5	2	P-L	Gower *et al.* 1994
p_{20}: Ratio of foliage:stem partitioning at $B = 20$ (cm)	H		0.1	0.5	P-L	Gower *et al.* 1994
r_{age}: Relative age to give $f_{age} = 0.5$	L	0.5			F	

t_c: Age at full canopy cover (yr)	M		0	20	CP-T	Peter Savill, pers. Communication, 2003
T_{max}: Maximum temperature for growth (°C)	L	40			P-L	Reviewed in Waring and Running, 1998
T_{min}: Minimum temperature for growth (°C)	L	0			P-L	Reviewed in Waring and Running, 1998
T_{opt}: Optimum temperature for growth (°C)	M		10	30		Reviewed in Waring and Running, 1998
t_x: Maximum stand age used to compute relative age (year)	L		60	300	F	Dependent on r_{age}
t_{yF}: Age at which litterfall rate has median value (month)	L	60			F	
t_σ: Age at which specific leaf area = ½(σ_0+σ_1) (yr)	L		2	30	F	
Y: Ratio NPP/GPP	H		0.43	0.51	P-L	Reviewed in Waring and Running, 1998
α_{Cx}: Maximum canopy quantum efficiency (mol mol^{-1})	H		0.03	0.06	P-L	Stenberg *et al.* 1994, Wang *et al.* 2004
θ_{sx}: Maximum soil available water (mm)			75	350	CP-T	Stewart 1988 and Beadle *et al.* 1985
γ_{F0}: Litterfall rate at t = 0 (month^{-1})	L	0.001			D	
γ_{F1}: Litterfall rate for mature stands (month^{-1})	H		0.015	0.035	P-L	Schoettle and Fahey 1994
γ_R: Average monthly root turnover rate (month^{-1})	L		0.006	0.015	P-L	Schoettle and Fahey 1994, Gill and Jackson 2000
η_{Rn}: Minimum fraction of NPP to roots	M		0.1	0.3	P-L	Dougherty *et al.* 1994, Levy *et al.* 2004
η_{Rx}: Maximum fraction of NPP to roots	M		0.3	0.8	P-L	Dougherty *et al.* 1994, Levy *et al.* 2004
σ_0: Specific leaf area at stand age 0 (m^2 kg^{-1})	L		6	11	P-L	Van Hees and Bartelink 1993,
σ_1: Specific leaf area for mature aged stands (m^2 kg^{-1})	H		2	6	P-L	Van Hees and Bartelink, 1993

Fourteen parameters were given prescribed parameter values and the remaining parameters were calibrated. For the latter, ranges of values defining the maximum and minimum in the prior uniform distributions are given (see text). θmin and θmax refer the mean and max value in the parameter vector.

a. Sensitivity class as defined by Sands (2004). L=Low, M=Medium, H=High.

b. The boundaries to the prior were obtained from direct observation on Corsican pine stands in Thetford (CP-T), from literature on Corsican or other pine species (P-L), from surrogate species or 3-PG set default values (D) or finally as best guess estimates or fitting approaches (F).

6.2.2 The likelihood

A total of 30 data points were used in the calibration exercise. These included total above-ground biomass (11), stem biomass including branches (3), foliage biomass (3), root biomass (5) and LAI (8).

6.2.2.1 Above-ground biomass

Above-ground biomass data were derived from the Maestro dataset (Baker 1992, Baker *et al.* 1994) and the forestry yield tables for Corsican stands of yield class 14, under an intermediate thinning strategy and planted at 2 meters spacing. As shown by Figure 6.4, where top height from yield tables is plotted against measured heights (Skinner 2002), the agreement between yield tables and the variable measured in Thetford is nearly 1:1. This suggests that in this circumstance, yield tables are an acceptable proxy to field measurements. Generic basic density for the conversion of volume to dry weight was obtained from Hamilton (1975). A biomass expansion factor, converting stemwood biomass to total above-ground biomass was derived from the Maestro dataset, in which both stemwood biomass and total above-ground biomass data are available. The average ratio across ages was used (i.e. 1.2).

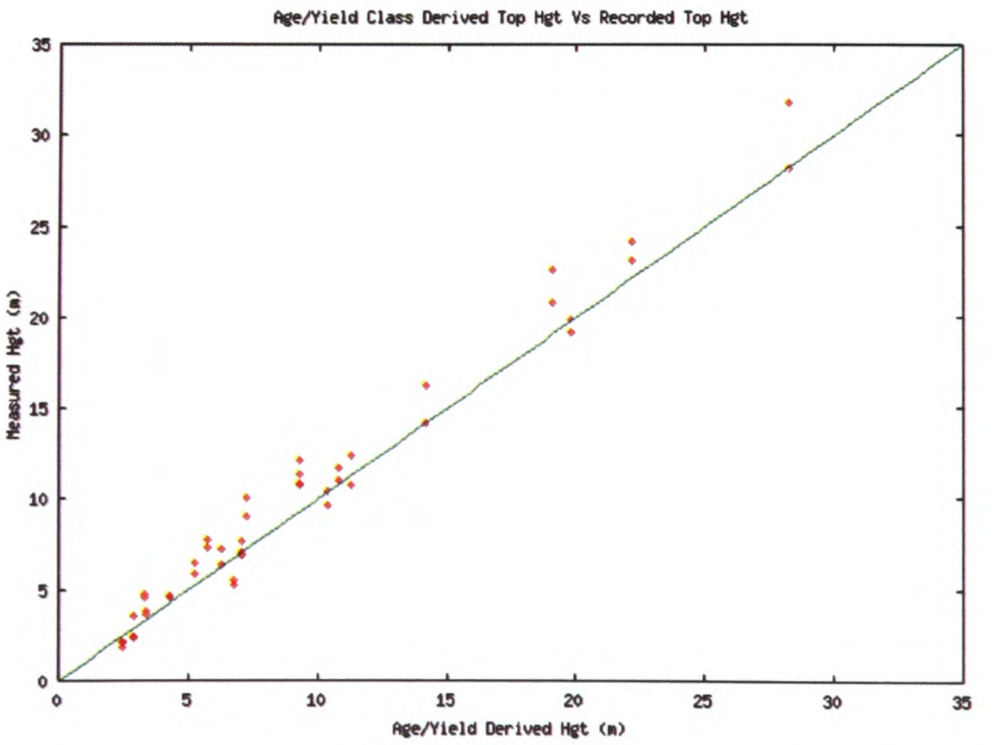


Figure 6.4: Measured against heights derived from yield tables (from Skinner, 2002)

6.2.2.2 Stem, foliage and root biomass

Stem and foliage biomass data points were derived from Baker (1992) and Baker *et al.* (1994). For root biomass, a ratio above to below-ground biomass data was derived from

Scot pine biomass data available in Ovington (1957). Root biomass was available for 6 stands above 15 yrs old. The ratio below to above-ground across ages (0.3) was assumed the same for Corsican pine as for Scots pine in Thetford. This ratio is consistent with the range of values provided by the IPCC for temperate coniferous forests (IPCC 2003). Using this ratio and the above-ground biomass dataset, 5 root biomass points were calculated. No attempt was made to calibrate the water submodel.

6.2.2.3 LAI

LAI data points were derived from the hyperspectral data. Leaf area index for pine plantations generally exhibit the following growth pattern (Vose *et al.* 1994, Menccuccini and Grace 1996, Waring and Running 1998, Figure 6.5).

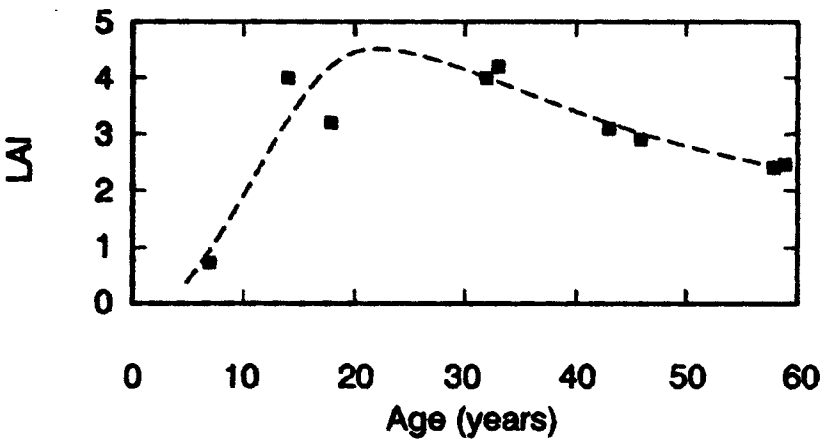


Figure 6.5: Example of leaf area index change with stand growth. Note the rapid increase in LAI followed by a slow decrease after canopy closure (from Waring and Running, 1998, data from Menccuccini and Grace, 1996).

This pattern can be expressed mathematically as:

Equation 10: Growth dynamic of leaf area index

$$LAI = ae^{-0.5\left(\frac{\ln(x/x_0)}{b}\right)^2}$$

Where a represents the maximum LAI value reached by a stand, x_0 the age at which this maximum is reached and b, a parameter controlling the tailing off of the LAI curve.

For Corsican pines in Thetford, the parameters in Equation 10 were derived from the hyperspectral dataset and a single ground-based measurement of LAI (Ovington, 1957).

The studies by Lee *et al.* (2004) and Pu and Gong (2004) show that for vegetation studies, the integration of a large amount of hyperspectral bands into statistical analyses, such as canonical correlation analysis and principal component analysis (PCA), produce better results than NIR and IR band vegetation indices. In these studies, LAI was proportional to the PCA result: as the LAI increased, so did the PCA value. Based on these results, PCA was used to estimate LAI growth patterns in Thetford Corsican pines stands. Other vegetation indices (e.g. NDVI, see Appendix A) were also estimated for comparison. While vegetation indices were designed to maximise the signature of vegetation, PCA optimises the information content of a dataset by reducing its dimensionality through the compaction of redundant information.

GIS attributes for all Corsican pine stands of yield class 14 were combined with hyperspectral indices (PCA and VI). Equation 10 was then solved in a two way procedure. Firstly, vegetation indexes estimated per stand (e.g. PCA, NDVI) were plotted against stand age. The parameters x_0 and b were then derived from the remote sensing data points by minimising the distance between the points and the model (Figure 6.6). These parameters pertain to the shape of the curve only, not the magnitude of LAI. To convert the indices to LAI values, the projected LAI datum derived from Ovington (1957) was used. The proportionality between the PCA and LAI found by Lee *et al.* (2004) and Pu and Gong (2004) was assumed here. Figure 6.6 and Table 6.3 present the resulting LAI curve and the parameters of Equation 10 from both PCA and NDVI. Note the greater variance of LAI derived by PCA to that by NDVI. The LAI derived from the PCA was selected semi-quantitatively, as it reflects best the LAI growth pattern shown in Figure 6.5.

Table 6.3: Parameters of Equation 10 as derived from PCA and NDVI

Parameters	**PCA**	**NDVI**
a	5.82	5.57
b	1.72	3.24
x0	16.85	16.40

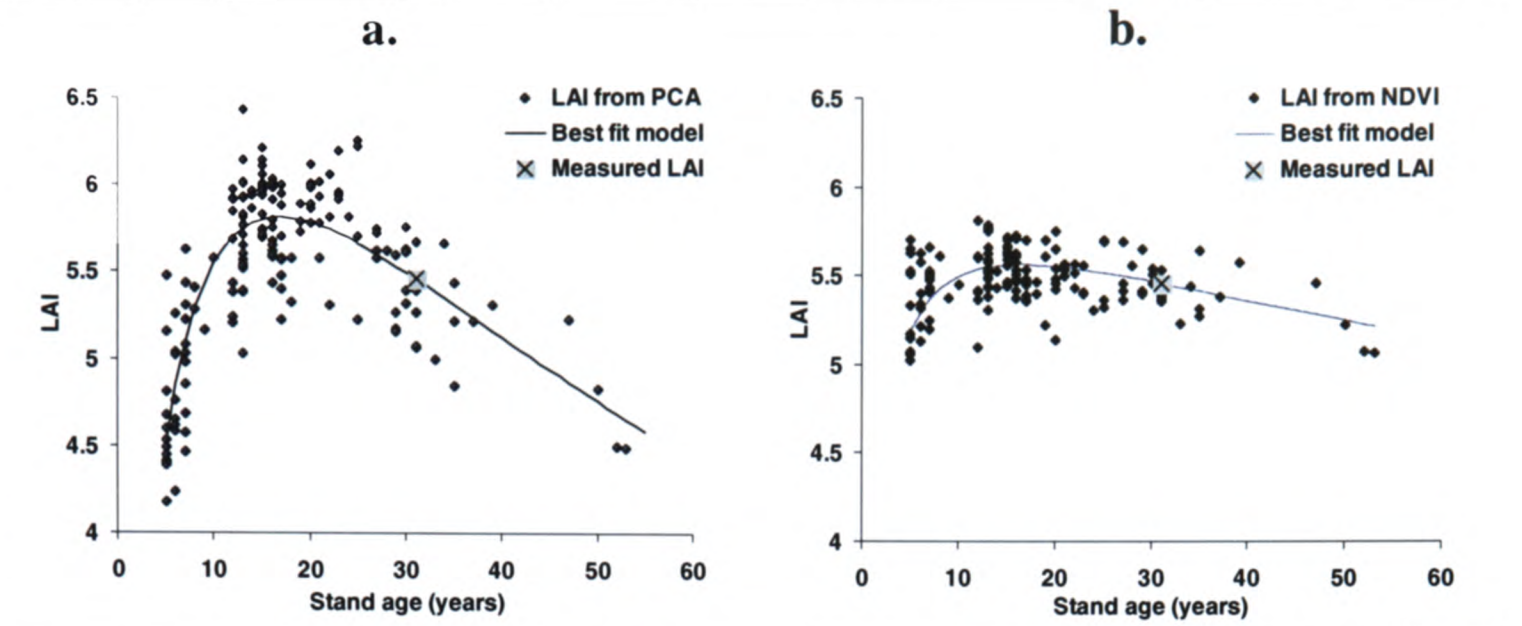


Figure 6.6: Variance of LAI derived from remote sensing indices: (a). PCA (b.) NDVI

Ultimately, a total of 8 data points were used in the calibration. Seven were derived from this curve at equal intervals, covering stand ages from 20 to 50 years. The LAI point measured by Ovington (1957) was also included.

As limited ground measurements of LAI were available, the LAI data points used in the calibration and derived from the hyperspectral data were given large uncertainties (standard deviation of 1). For all datasets namely below and above-ground components, the measurement errors were assumed Gaussian and independent. The standard deviation to the data points were estimated as 10 t ha^{-1} for above-ground, stem and root biomass, and 2 t ha^{-1} for foliage biomass. Standard deviations and data point values are shown in Figure 6.10 below.

6.3 Results: approximating the posterior distribution

6.3.1 Marginal posterior distributions of parameters and *a posteriori* probabilities

Finally, to estimate the posterior distribution, the Markov Chain Monte Carlo (MCMC) Metropolis Hastings Random Walk algorithm described in Section 5.4.3 was used and approximately 60 000 steps were executed. Figure 6.8 shows the MCMC trace plots and the resulting marginal posterior distributions for all the parameters. In Table 6.4, these distributions are categorised as near uniform, near Gaussian and skewed. Distributions whose difference in frequency between classes never exceeds 4000 (15 classes, 60,000 samples) were classified as near-uniform. Near Gaussian distributions do not meet the near uniform criteria and have at least 30% of observations on either side of the mode. The

remaining distributions are classified as skewed. Importantly, the near-normal and skewed distributions are peaked, indicating an in certainty for these parameters.

Table 6.4: Marginal distributions to the calibrated parameters

Marginal distribution	**Parameters**
Peaked and near normal	n_{fN}
Near uniform	θ_{sx}, L_{Cx}, g_{Cx}, Y, t_c, t_σ, σ_0, f_{N0}
Peaked and skewed	p_2, p_{20}, η_{Rn}, η_{Rx}, γ_R, γ_{Fl}, T_{opt}, t_x, σ_l, n_{age}, k, α_{Cx}, FR

Summary statistics of the posterior distribution including the maximum *a posteriori* parameter vector (θ_{MAP}) to these distributions are presented in Table 6.5. θ_{MAP} is the single parameter vector providing the maximum likelihood, given the data. In Figure 6.7, the prior and posterior distributions for T_{opt} are shown, which illustrates how much knowledge has been gained about this parameter through the calibration. Finally, correlations between the parameters are shown in Table 6.6.

Table 6.5: Statistics from the MCMC summarising the full posterior distribution over the 22-D parameter space.

$\theta(i)$	$\overline{\theta(i)}$	SD	θ_{MAPx}
f_{N0}	0.801	0.109	0.717
FR	0.770	0.147	0.691
g_{Cx}	0.023	0.004	0.024
k	0.508	0.120	0.400
L_{Cx}	4.001	1.094	4.473
n_{age}	7.632	3.767	6.774
n_{fN}	5.537	2.407	5.924
p_2	1.158	0.426	0.588
p_{20}	0.357	0.092	0.424
t_c	9.655	5.512	11.236
T_{opt}	17.720	4.676	12.852
t_x	191.777	49.288	147.009
t_σ	16.704	7.664	3.222
y	0.471	0.022	0.487
α_{Cx}	0.051	0.006	0.050
γ_{F1}	0.024	0.005	0.017
γ_R	0.010	0.002	0.006
η_{Rn}	0.221	0.048	0.242
η_{Rx}	0.594	0.133	0.617
θ_x	211.360	76.868	334.401
σ_0	8.579	1.402	7.757
σ_1	4.366	1.034	3.988

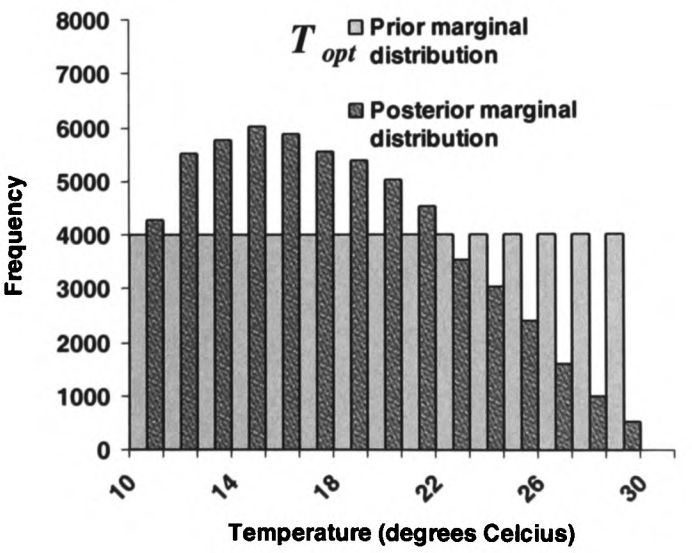
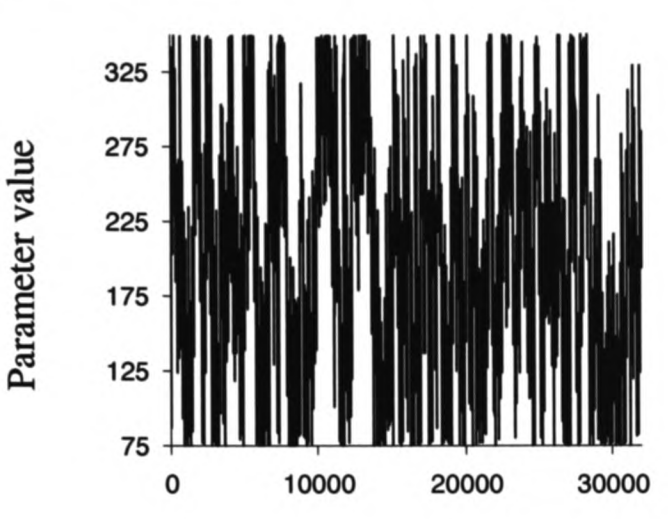
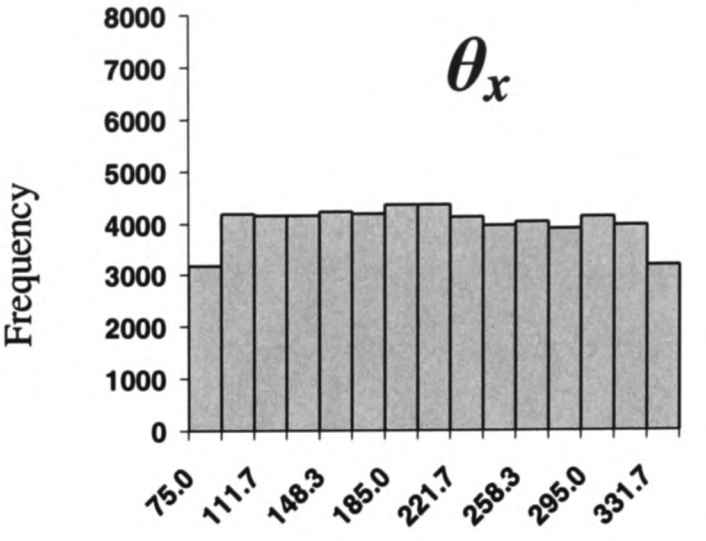
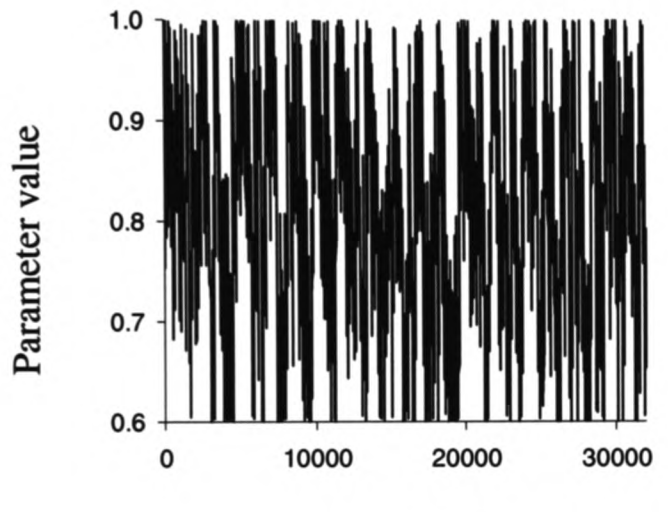
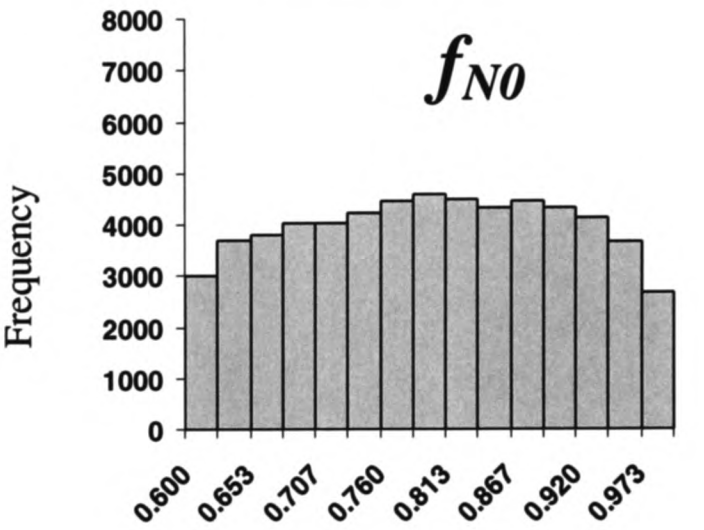


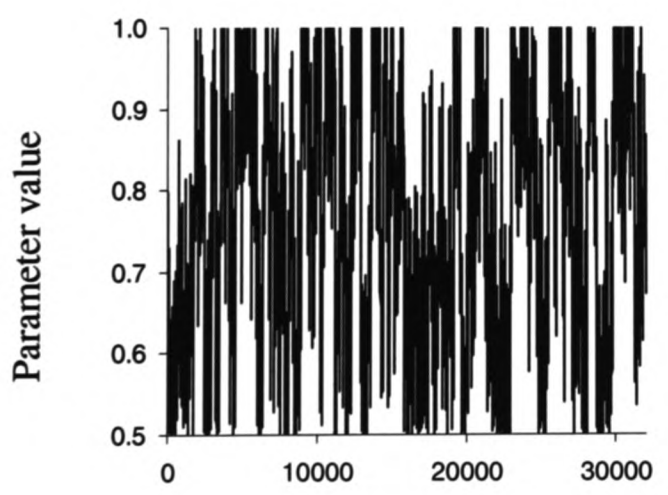
Figure 6.7: Uncertainty reduction arising from the Bayesian calibration

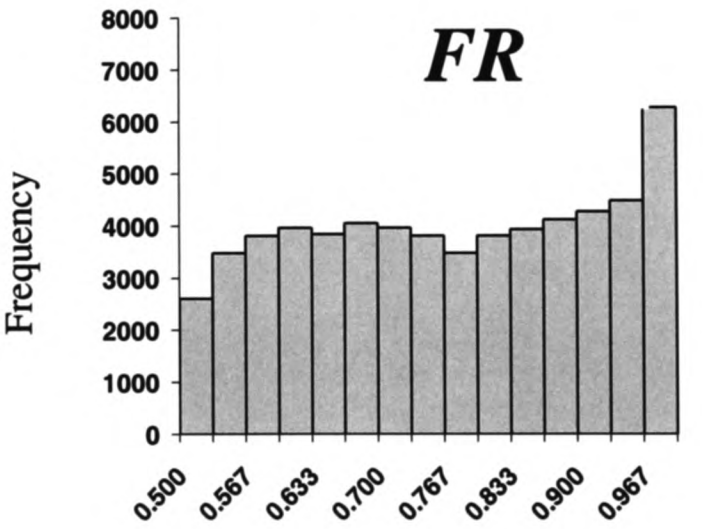

Parameter value
325
275
225
175
125
75
0
10000
20000
30000
MCMC steps

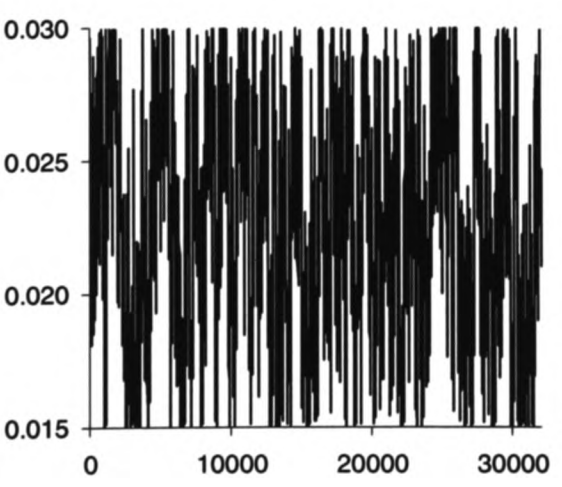

θ_x
Frequency
8000
7000
6000
5000
4000
3000
2000
1000
0
75.0
111.7
148.3
185.0
221.7
258.3
295.0
331.7
Parameter value

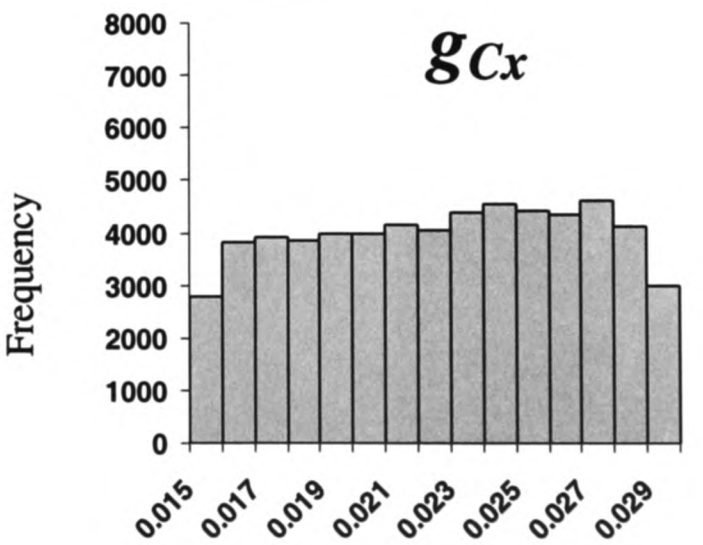

Parameter value
1.0
0.9
0.8
0.7
0.6
0
10000
20000
30000
MCMC steps

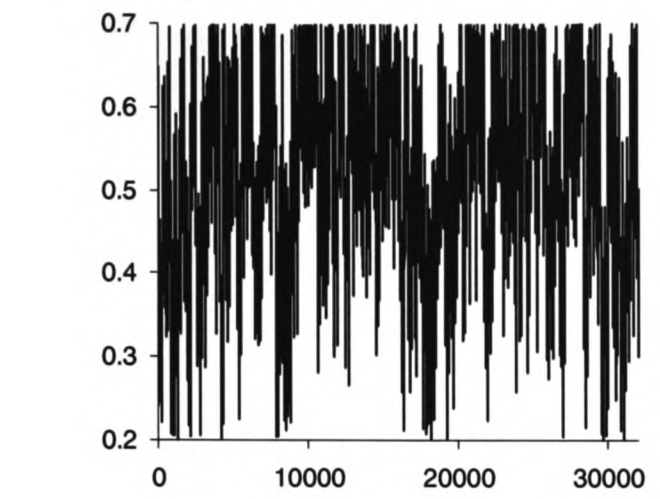

f_{N0}
Frequency
8000
7000
6000
5000
4000
3000
2000
1000
0
0.600
0.653
0.707
0.760
0.813
0.867
0.920
0.973
Parameter value

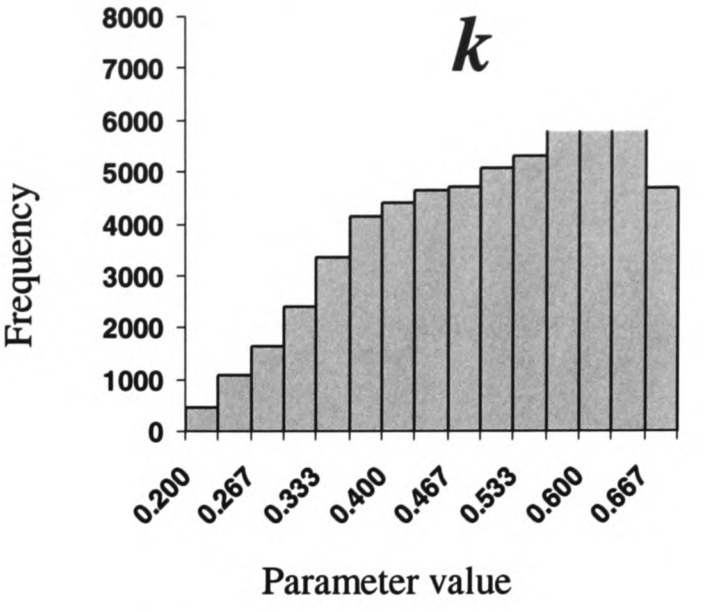

Parameter value
1.0
0.9
0.8
0.7
0.6
0.5
0
10000
20000
30000
MCMC steps

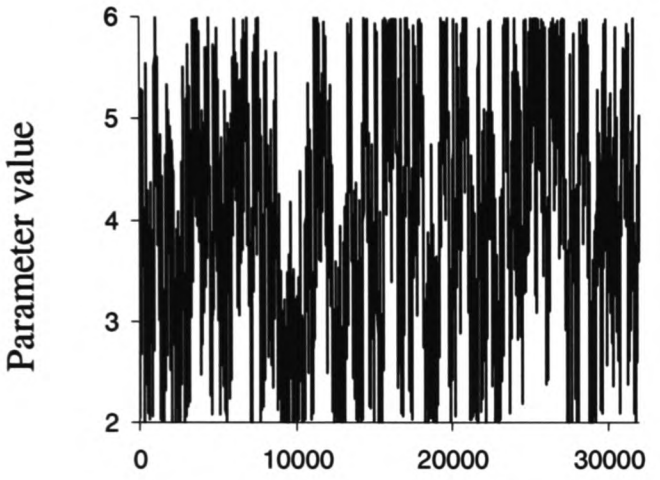

FR
Frequency
8000
7000
6000
5000
4000
3000
2000
1000
0
0.500
0.567
0.633
0.700
0.767
0.833
0.900
0.967
Parameter value

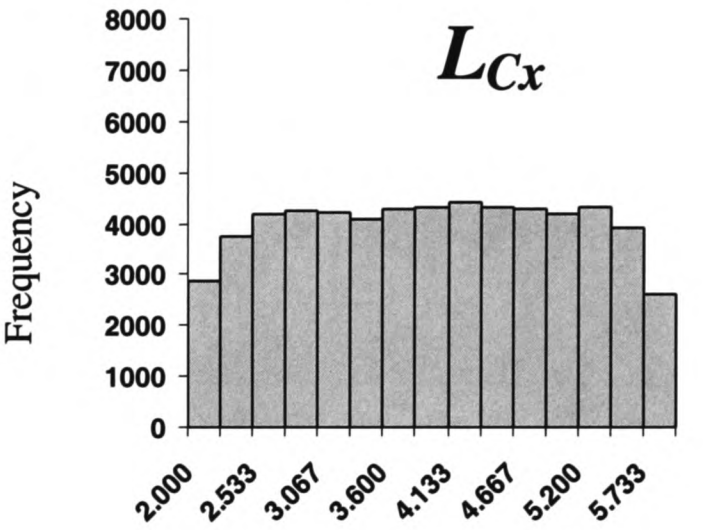

0.030
0.025
0.020
0.015
0
10000
20000
30000
MCMC steps

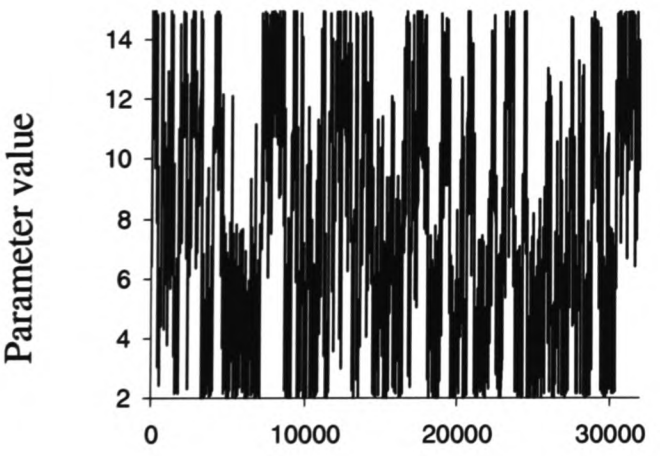

g_{Cx}
Frequency
8000
7000
6000
5000
4000
3000
2000
1000
0
0.015
0.017
0.019
0.021
0.023
0.025
0.027
0.029
Parameter value

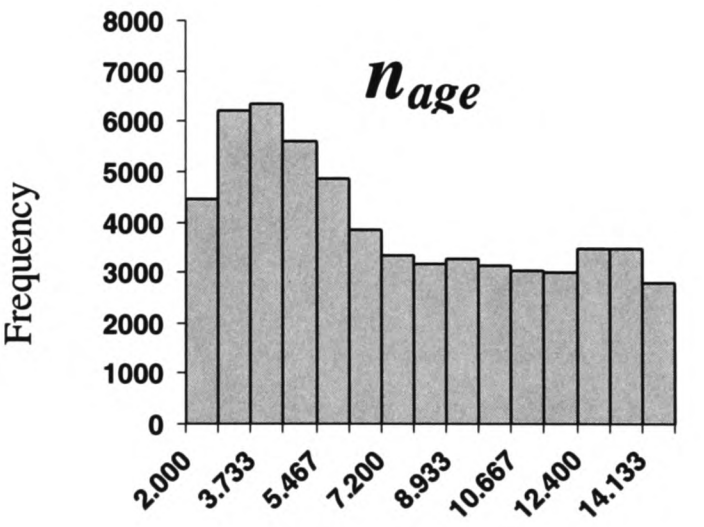

0.7
0.6
0.5
0.4
0.3
0.2
0
10000
20000
30000
MCMC steps

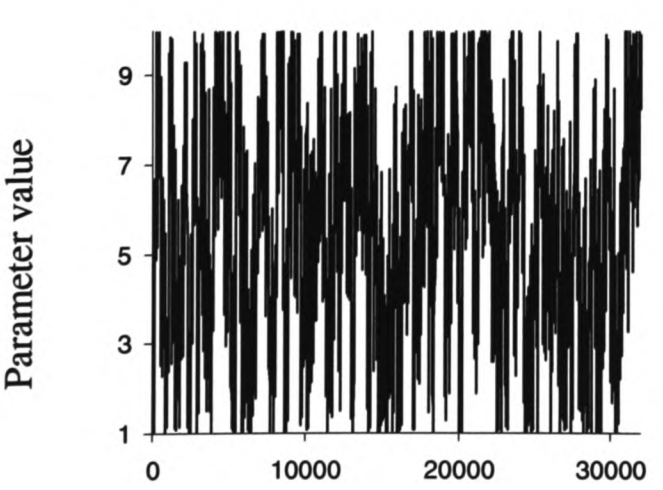

k
Frequency
8000
7000
6000
5000
4000
3000
2000
1000
0
0.200
0.267
0.333
0.400
0.467
0.533
0.600
0.667
Parameter value

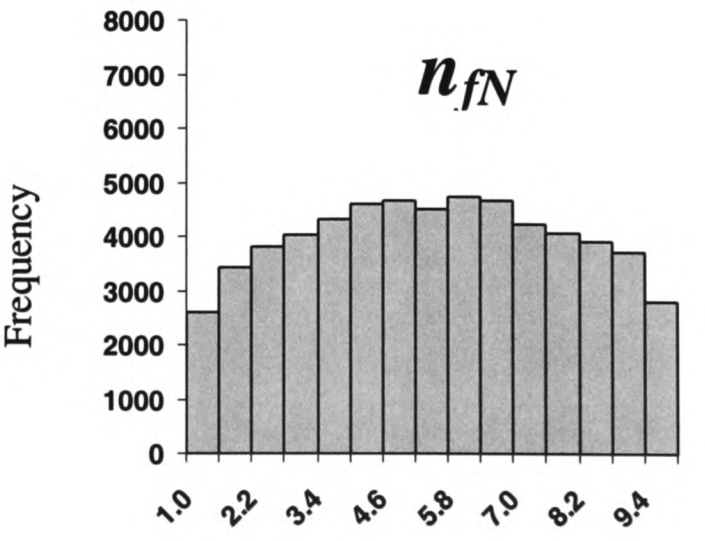

Parameter value
6
5
4
3
2
0
10000
20000
30000
MCMC steps

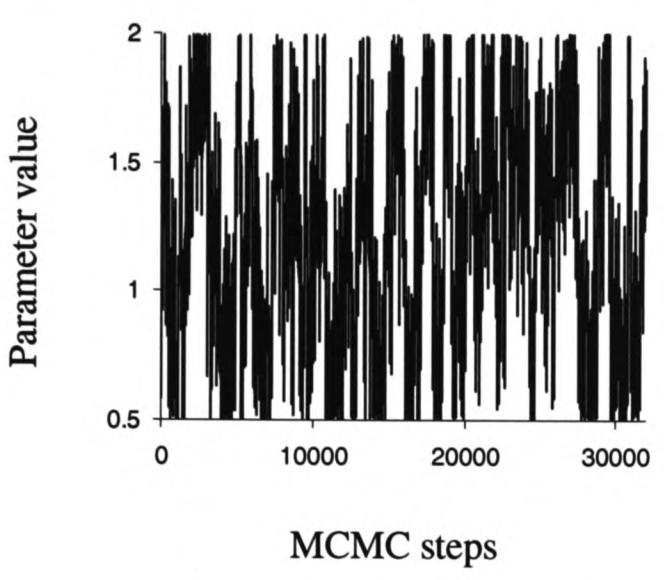

L_{Cx}
Frequency
8000
7000
6000
5000
4000
3000
2000
1000
0
2.000
2.533
3.067
3.600
4.133
4.667
5.200
5.733
Parameter value

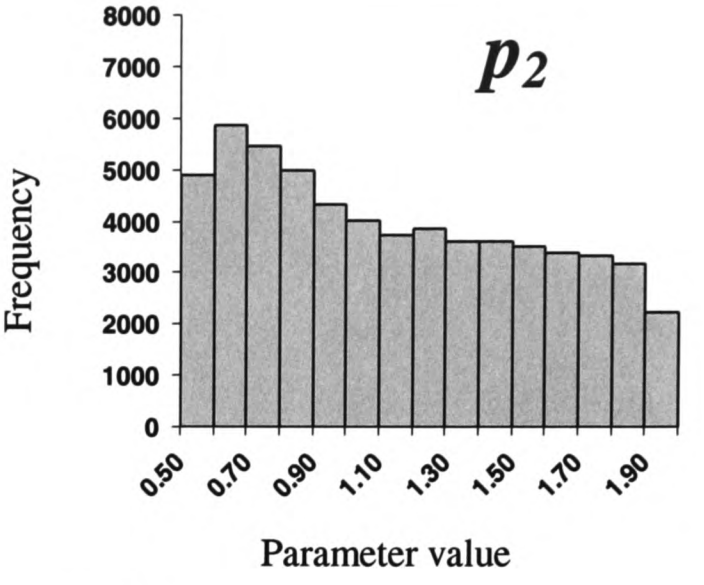

Parameter value
14
12
10
8
6
4
2
0
10000
20000
30000
MCMC steps

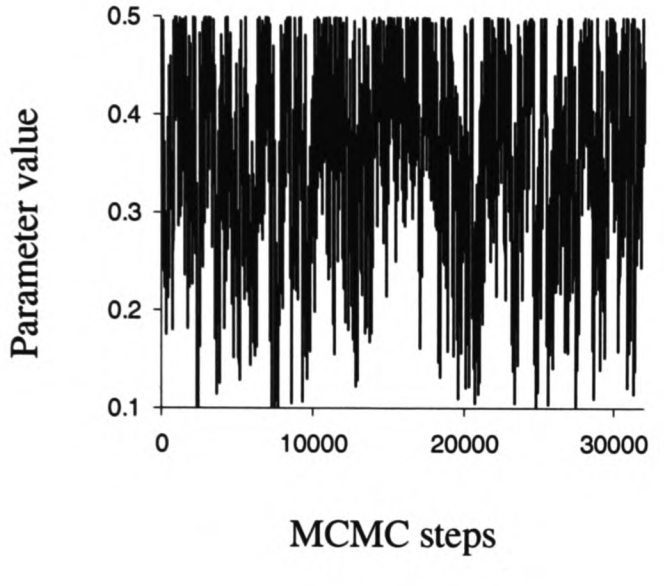

n_{age}
Frequency
8000
7000
6000
5000
4000
3000
2000
1000
0
2.000
3.733
5.467
7.200
8.933
10.667
12.400
14.133
Parameter value

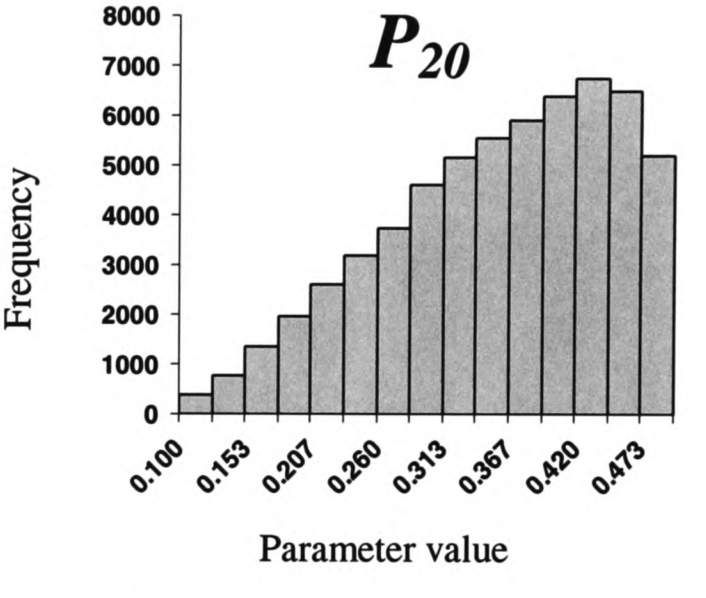

Parameter value
9
7
5
3
1
0
10000
20000
30000
MCMC steps

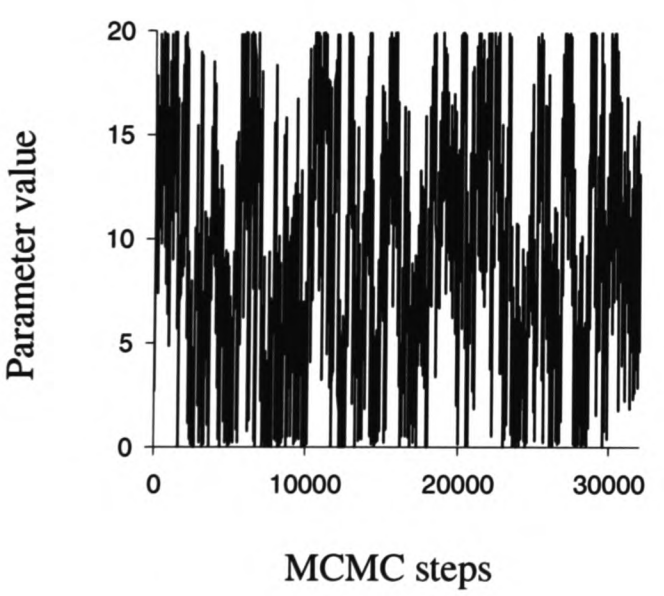

n_{fN}
Frequency
8000
7000
6000
5000
4000
3000
2000
1000
0
1.0
2.2
3.4
4.6
5.8
7.0
8.2
9.4
Parameter value

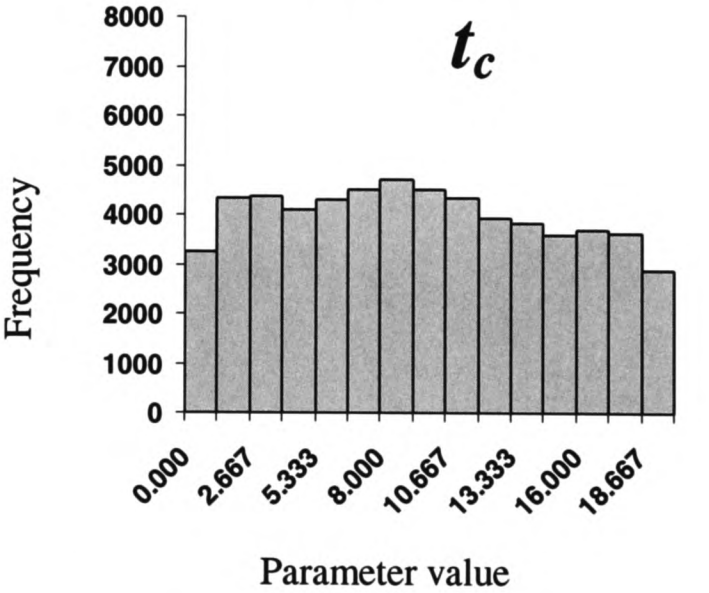

Parameter value
2
1.5
1
0.5
0
10000
20000
30000
MCMC steps

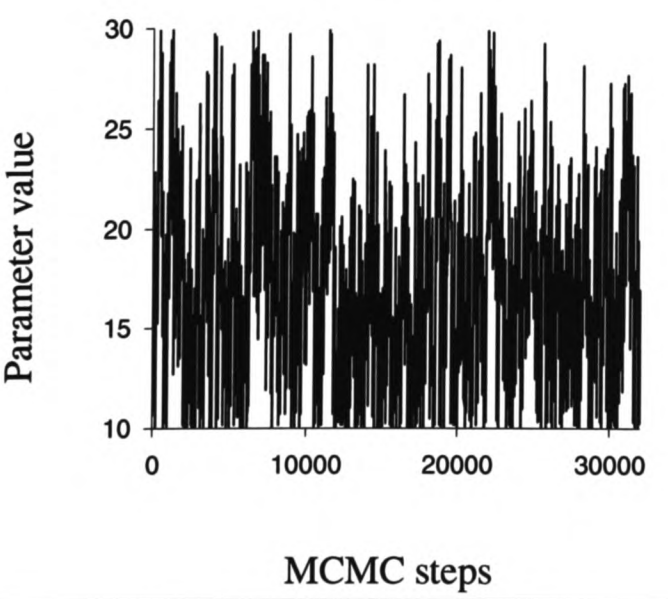

p_2
Frequency
8000
7000
6000
5000
4000
3000
2000
1000
0
0.50
0.70
0.90
1.10
1.30
1.50
1.70
1.90
Parameter value

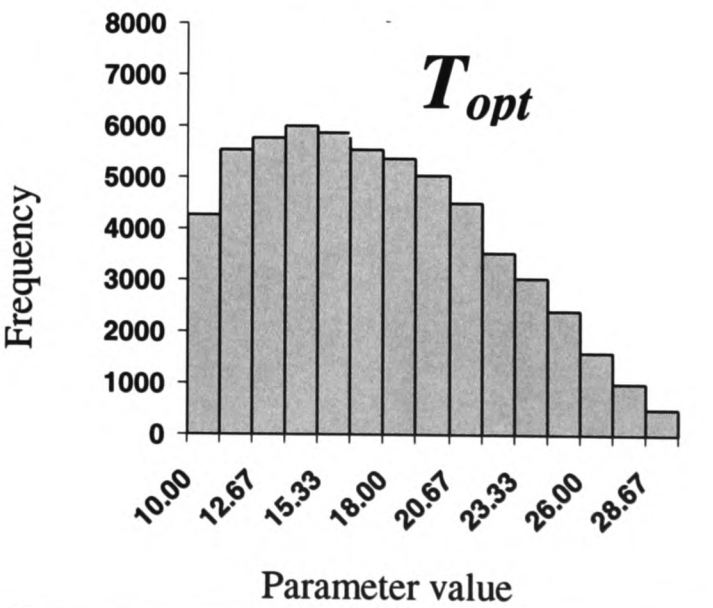

Parameter value
0.5
0.4
0.3
0.2
0.1
0
10000
20000
30000
MCMC steps

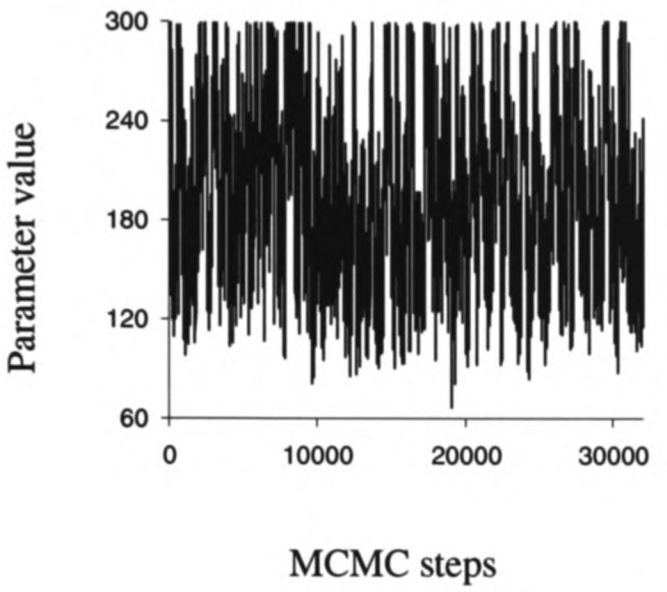

P_{20}
Frequency
8000
7000
6000
5000
4000
3000
2000
1000
0
0.100
0.153
0.207
0.260
0.313
0.367
0.420
0.473
Parameter value

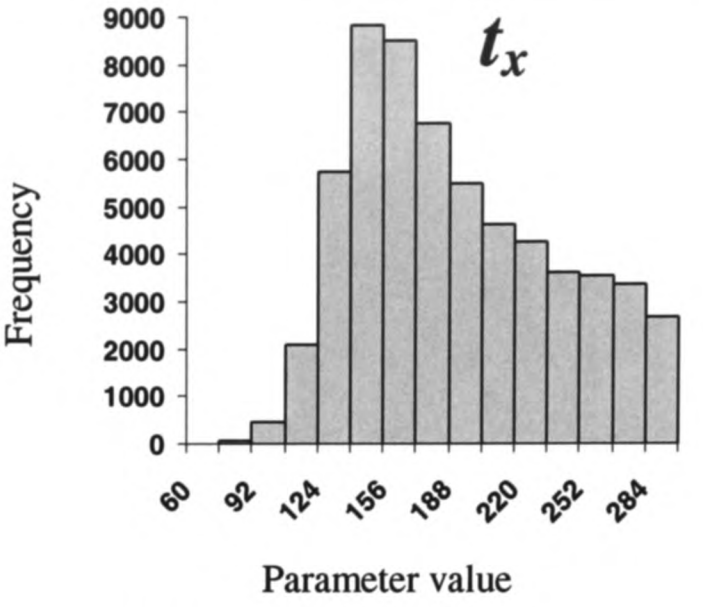

Parameter value
20
15
10
5
0
0
10000
20000
30000
MCMC steps

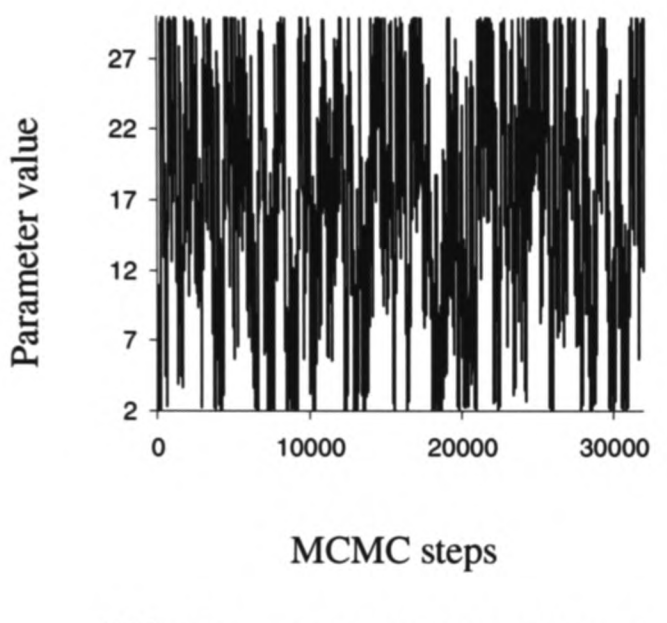

t_c
Frequency
8000
7000
6000
5000
4000
3000
2000
1000
0
0.000
2.667
5.333
8.000
10.667
13.333
16.000
18.667
Parameter value

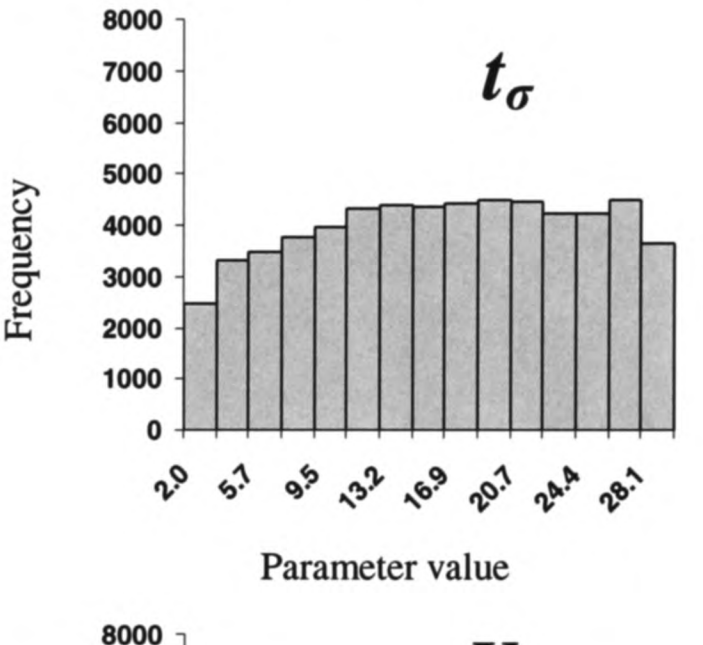

Parameter value
30
25
20
15
10
0
10000
20000
30000
MCMC steps

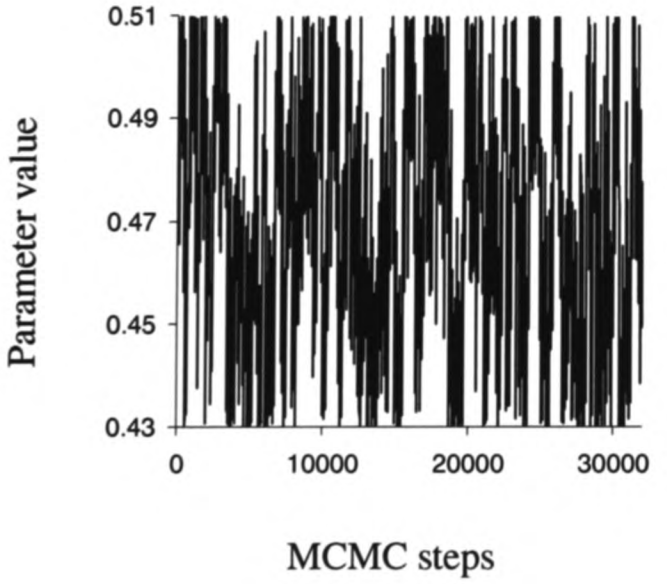

T_{opt}
Frequency
8000
7000
6000
5000
4000
3000
2000
1000
0
10.00
12.67
15.33
18.00
20.67
23.33
26.00
28.67
Parameter value

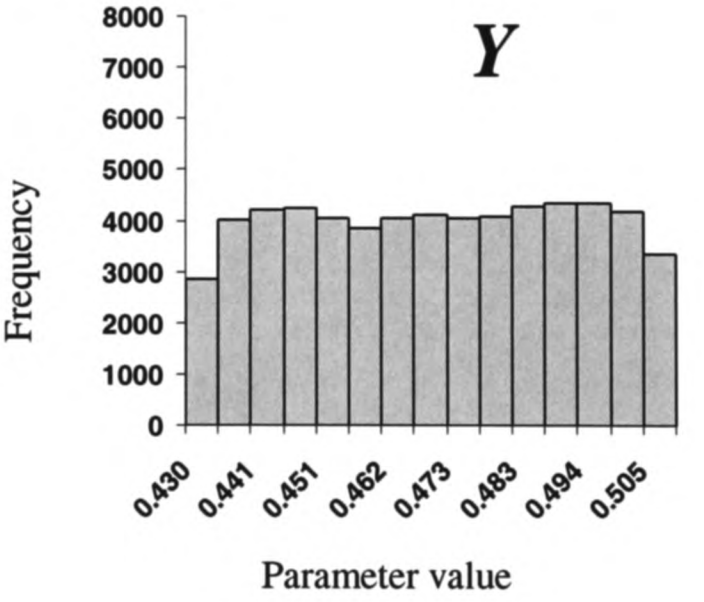

Parameter value
300
240
180
120
60
0
10000
20000
30000
MCMC steps

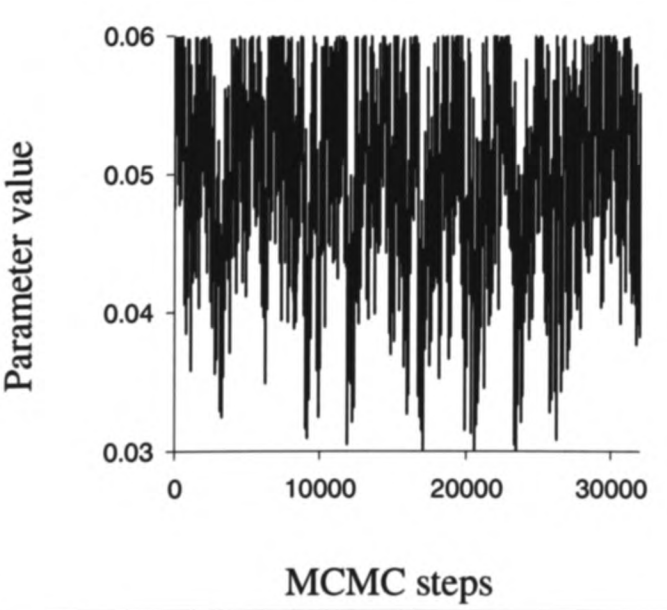

Frequency
9000
8000
7000
6000
5000
4000
3000
2000
1000
0
t_x
60
92
124
156
188
220
252
284
Parameter value

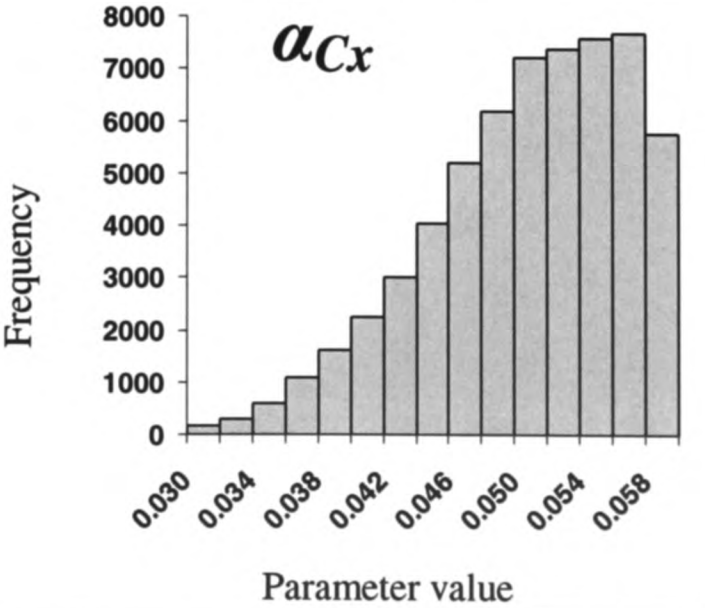

Parameter value
27
22
17
12
7
2
0
10000
20000
30000
MCMC steps

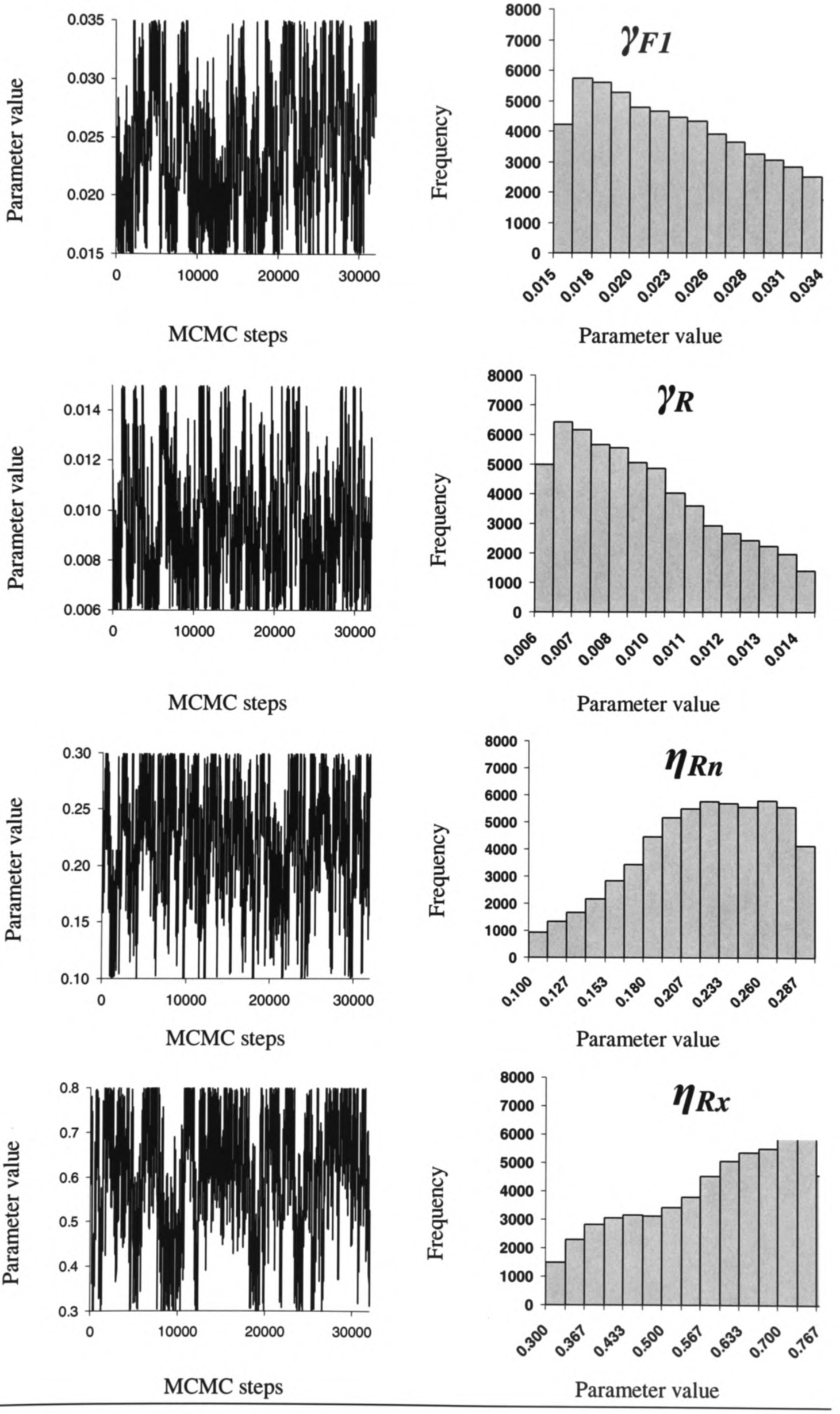

Frequency
8000
7000
6000
5000
4000
3000
2000
1000
0
t_σ
2.0
5.7
9.5
13.2
16.9
20.7
24.4
28.1
Parameter value


Parameter value
0.51
0.49
0.47
0.45
0.43
0
10000
20000
30000
MCMC steps


Frequency
8000
7000
6000
5000
4000
3000
2000
1000
0
Y
0.430
0.441
0.451
0.462
0.473
0.483
0.494
0.505
Parameter value


Parameter value
0.06
0.05
0.04
0.03
0
10000
20000
30000
MCMC steps


Frequency
8000
7000
6000
5000
4000
3000
2000
1000
0
α_{Cx}
0.030
0.034
0.038
0.042
0.046
0.050
0.054
0.058
Parameter value


Parameter value
0.035
0.030
0.025
0.020
0.015
0
10000
20000
30000
MCMC steps
Frequency
8000
7000
6000
5000
4000
3000
2000
1000
0
γ_{F1}
0.015
0.018
0.020
0.023
0.026
0.028
0.031
0.034
Parameter value
Parameter value
0.014
0.012
0.010
0.008
0.006
0
10000
20000
30000
MCMC steps
Frequency
γ_R
0.006
0.007
0.008
0.010
0.011
0.012
0.013
0.014
Parameter value
Parameter value
0.30
0.25
0.20
0.15
0.10
MCMC steps
η_{Rn}
0.100
0.127
0.153
0.180
0.207
0.233
0.260
0.287
Parameter value
Parameter value
0.8
0.7
0.6
0.5
0.4
0.3
MCMC steps
η_{Rx}
0.300
0.367
0.433
0.500
0.567
0.633
0.700
0.767
Parameter value

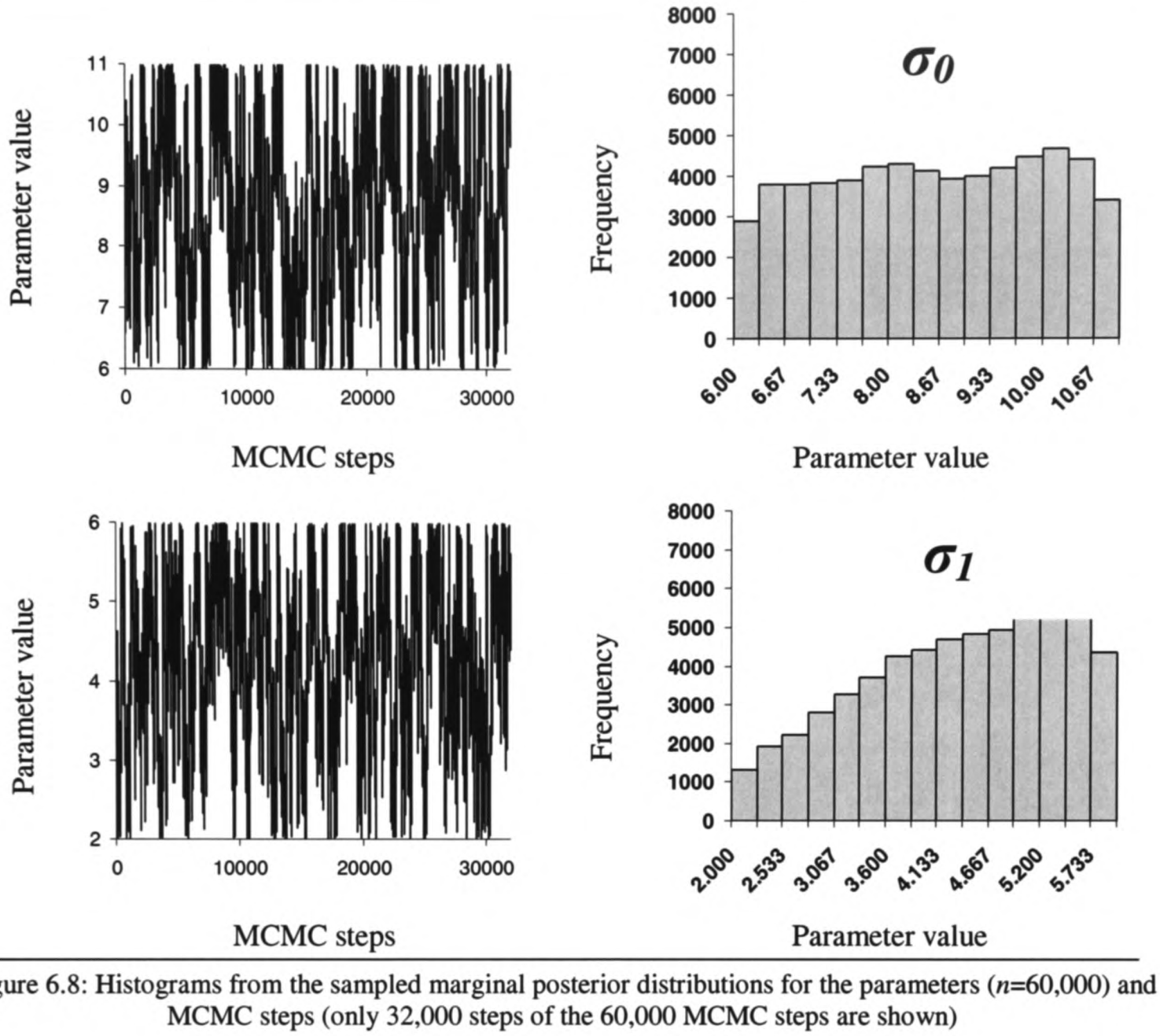


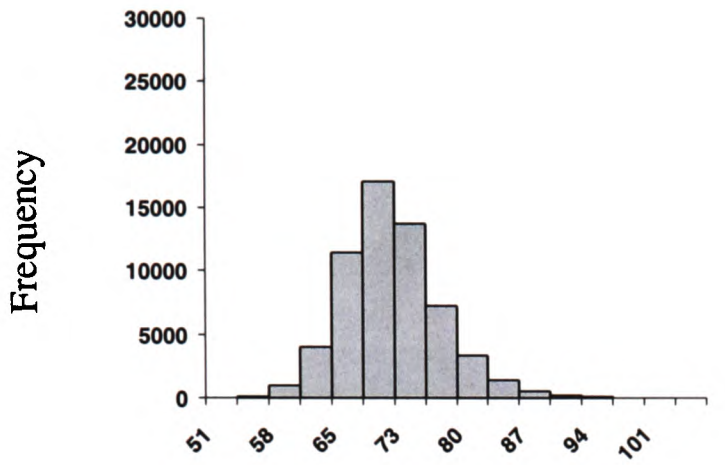
Figure 6.8: Histograms from the sampled marginal posterior distributions for the parameters (n=60,000) and MCMC steps (only 32,000 steps of the 60,000 MCMC steps are shown)

Table 6.6: Correlations between parameters. Correlations above 0.10 are indicated in bold and are underlined. The highest correlations are also highlighted.

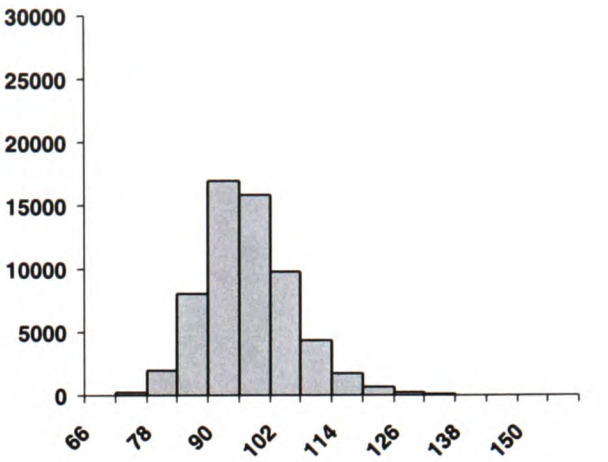
	p_2	p_{20}	η_{Rx}	FR	η_{Rn}	γ_{F1}	γ_R	T_{opt}	F_{N0}	n_{fN}	t_x	n_{age}	σ_0	σ_1	t_σ	k	t_c	α_{Cx}	y	g_{Cx}	L_{Cx}
p_2	1.00																				
p_{20}	-0.01	1.00																			
η_{Rx}	-0.02	0.01	1.00																		
FR	-0.06	-0.02	-0.06	1.00																	
η_{Rn}	-0.02	-0.05	<u>-0.12</u>	0.01	1.00																
γ_{F1}	<u>0.12</u>	0.02	-0.07	0.06	-0.01	1.00															
γ_R	-0.07	0.09	0.08	0.02	0.00	-0.02	1.00														
T_{opt}	-0.05	-0.02	-0.08	-0.05	<u>-0.15</u>	<u>-0.14</u>	0.00	1.00													
f_{N0}	-0.03	0.00	<u>-0.11</u>	0.01	-0.02	-0.03	0.01	0.04	1.00												
n_{fN}	-0.02	0.09	<u>-0.11</u>	-0.04	0.07	0.03	0.01	0.03	0.06	1.00											
t_x	0.04	-0.08	0.06	0.05	0.08	0.02	-0.03	0.02	0.02	-0.03	1.00										
n_{age}	0.02	-0.01	0.02	-0.05	-0.02	0.04	-0.07	0.06	-0.05	0.10	-0.04	1.00									
σ_0	0.06	-0.10	0.05	-0.01	-0.04	0.06	0.03	-0.03	0.00	-0.03	0.07	0.07	1.00								
σ_1	-0.05	-0.08	<u>-0.11</u>	-0.03	0.09	<u>0.14</u>	0.02	0.07	-0.02	0.03	-0.02	0.00	0.02	1.00							
t_σ	0.02	0.02	-0.02	0.00	0.01	<u>0.12</u>	-0.06	-0.03	0.05	-0.03	0.03	0.03	-0.01	-0.08	1.00						
k	0.01	-0.07	0.08	0.07	0.05	0.10	-0.04	0.08	-0.04	-0.01	<u>-0.15</u>	<u>-0.12</u>	-0.03	<u>-0.15</u>	0.04	1.00					
t_c	0.03	-0.03	0.05	-0.05	-0.07	-0.02	0.00	0.07	-0.05	<u>-0.11</u>	-0.07	-0.02	-0.01	-0.03	-0.05	0.00	1.00				
α_{Cx}	0.00	0.07	<u>0.16</u>	-0.04	<u>0.14</u>	-0.02	0.08	<u>0.36</u>	-0.04	-0.07	-0.09	-0.06	-0.03	-0.06	-0.04	<u>-0.15</u>	<u>0.13</u>	1.00			
y	0.01	0.02	0.03	-0.07	0.04	<u>-0.12</u>	0.00	0.08	0.00	-0.02	-0.05	0.02	-0.05	0.02	0.04	<u>-0.13</u>	-0.01	-0.09	1.00		
g_{Cx}	0.02	-0.02	-0.06	0.09	-0.02	-0.01	0.04	<u>-0.13</u>	0.00	0.03	0.00	-0.03	-0.01	-0.03	0.10	0.05	0.01	<u>0.18</u>	0.03	1.00	
L_{Cx}	-0.05	-0.04	0.04	0.03	-0.02	0.10	0.06	0.03	-0.05	-0.02	<u>-0.13</u>	-0.08	-0.01	-0.02	0.04	-0.08	-0.02	-0.06	0.02	0.05	1.00
θ_x	0.01	-0.03	-0.01	-0.02	0.04	-0.05	-0.03	0.01	0.01	-0.06	-0.10	-0.01	0.02	-0.05	0.04	0.06	0.03	0.00	0.00	-0.04	-0.04

6.3.2 Marginal posterior distributions of model outputs

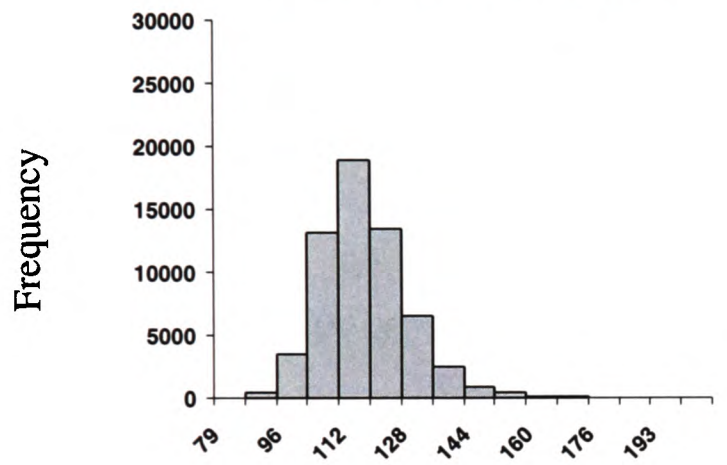
Figure 6.9 shows the histograms from the sampled posterior marginal distributions of the model outputs. In Figure 6.10, three datasets per graphs are shown. Firstly, the measured data or the data used in the calibration are shown in red. Standard deviations are also provided. Secondly, the average model outputs are shown as black rectangles (descriptive statistics to the marginal posterior distributions for the model outputs are provided in Table 6.7, which also summarise the histograms presented in Figure 6.9). Finally, the 3-PG outputs from θ_{MAP} are shown as the light grey line entitled best-fit. In Bayesian terms, best-fit should be understood as the model output generated from the parameter vector with highest a posterior likelihood.



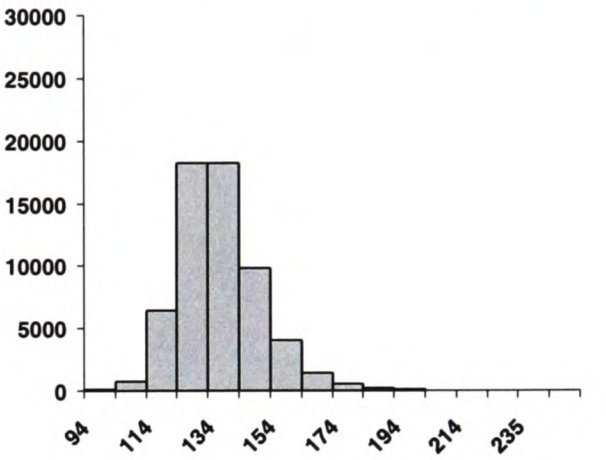
Above-ground biomass - 20 years



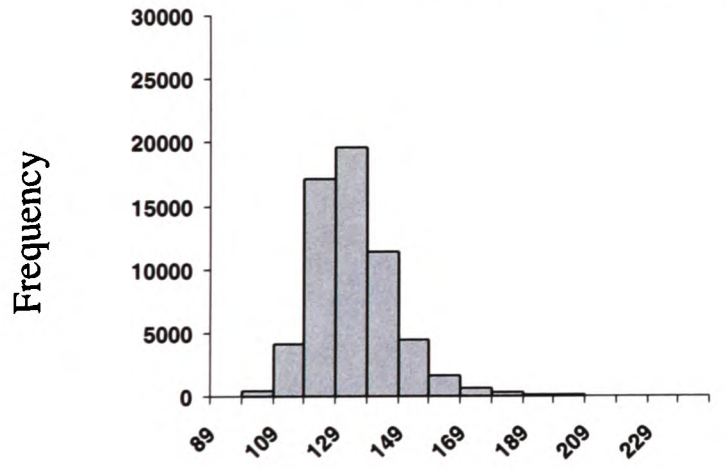
Above-ground biomass - 25 years



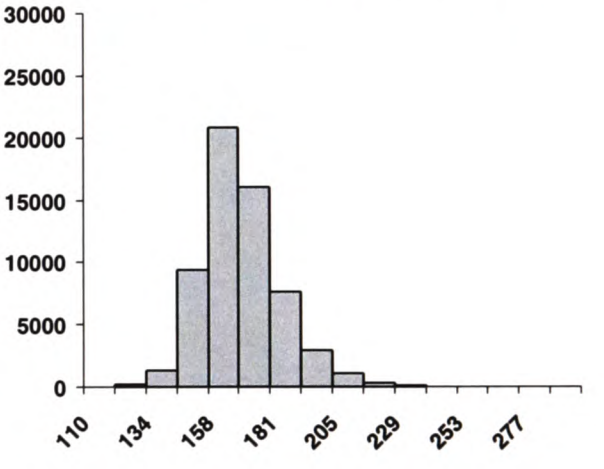
Above-ground biomass - 30 years



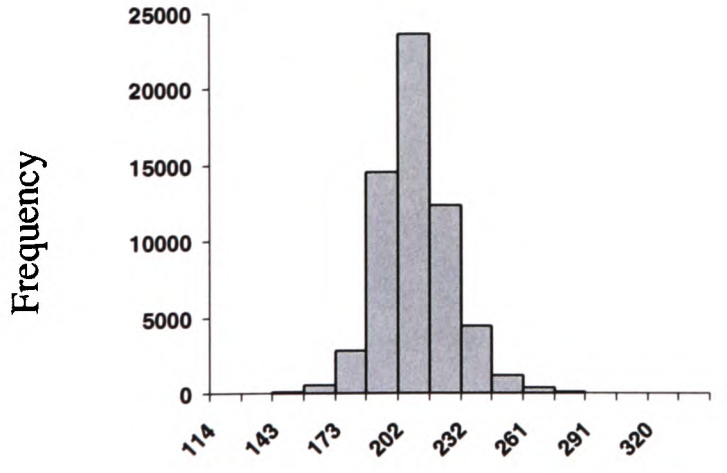
Above-ground biomass - 35 years



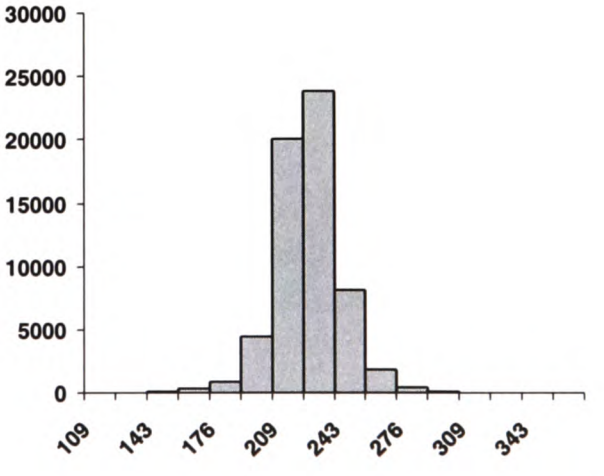
Above-ground biomass - 40 years



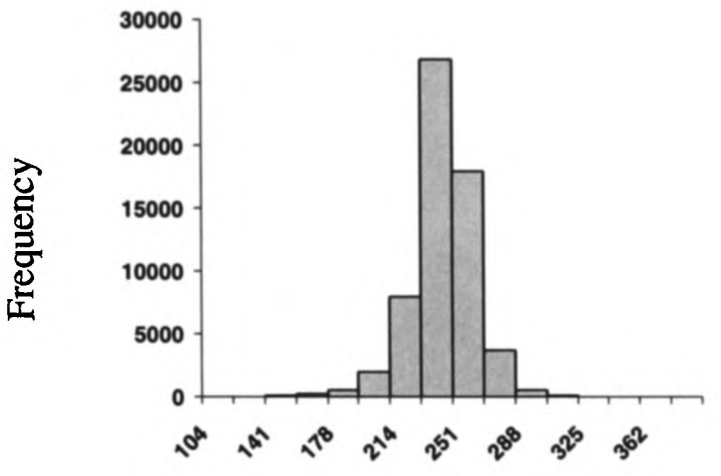
Above-ground biomass - 50 years



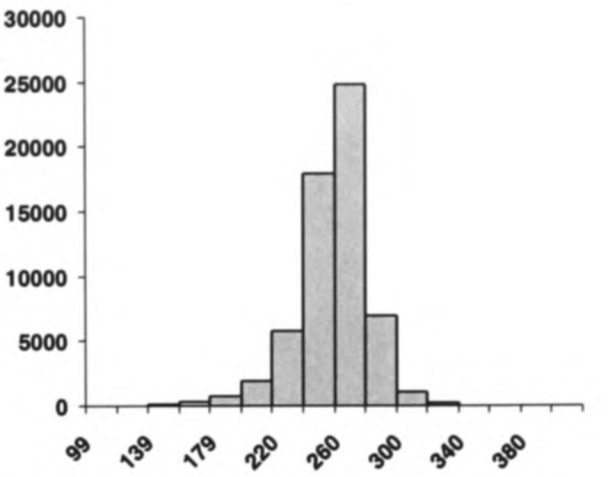
Above-ground biomass - 60 years



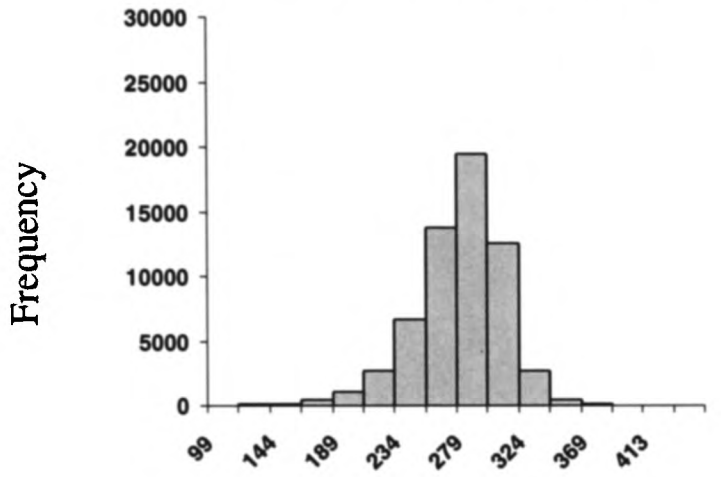
Above-ground biomass - 65 years



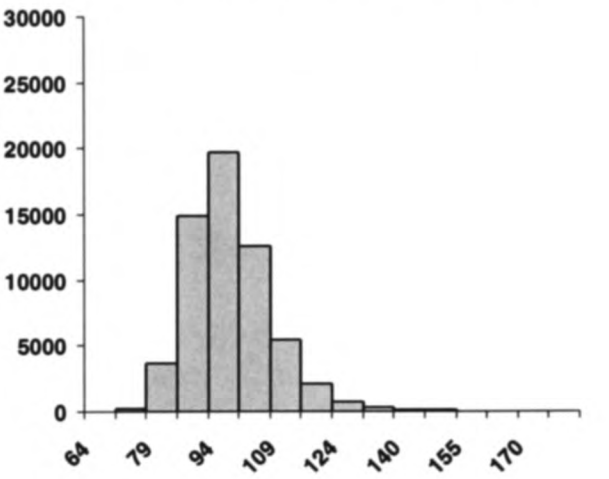
Above-ground biomass - 70 years



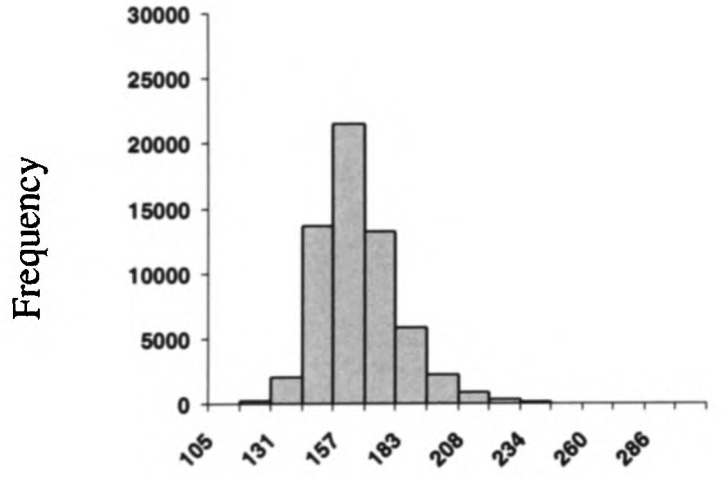
Above-ground biomass - 75 years



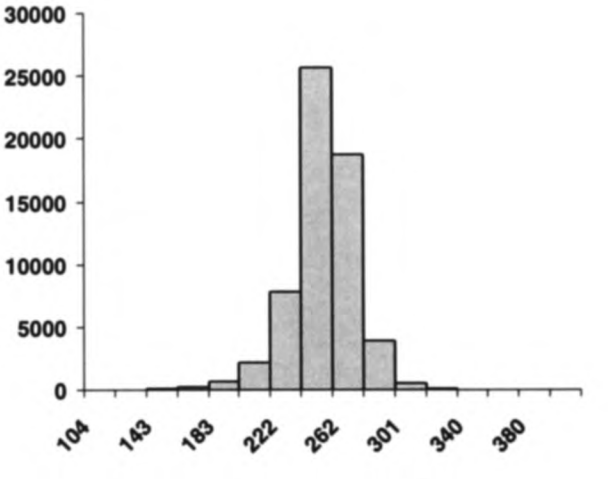
Above-ground biomass - 80 years



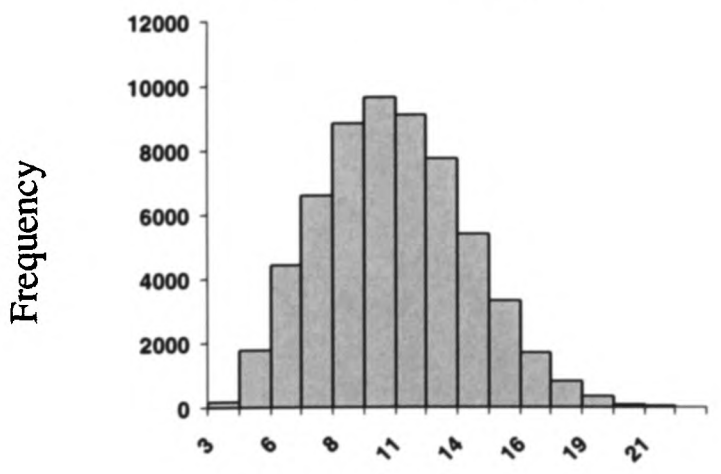
Stem biomass - 29 years



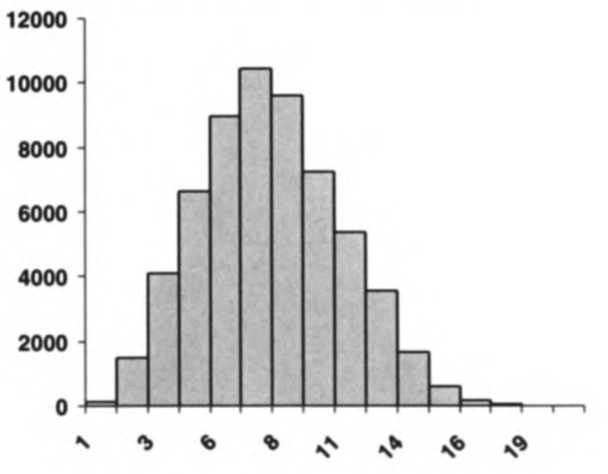
Stem biomass - 48 years



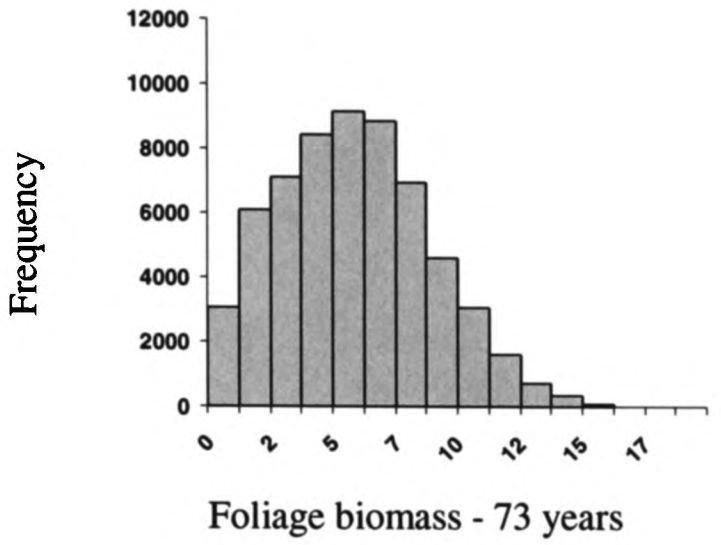
Stem biomass - 73 years



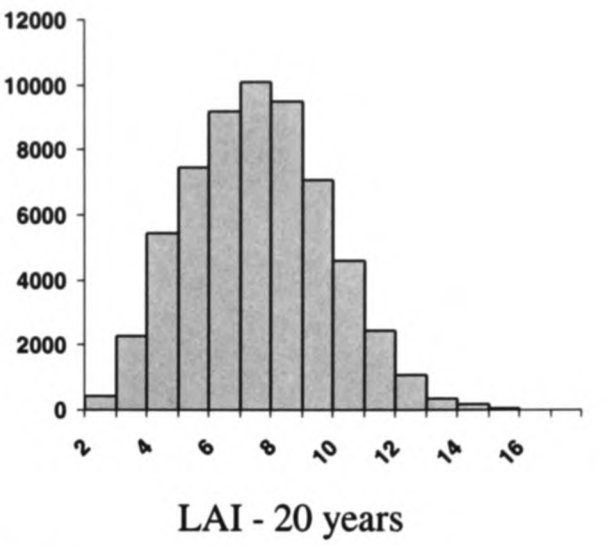
Foliage biomass - 29 years



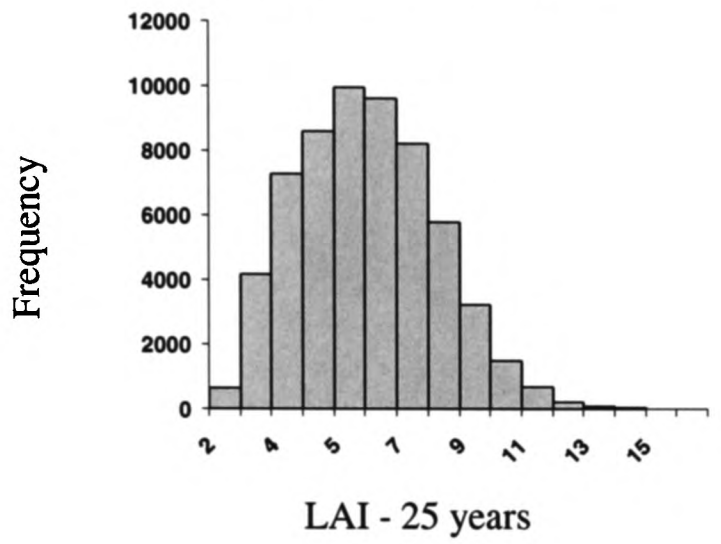
Foliage biomass - 48 years



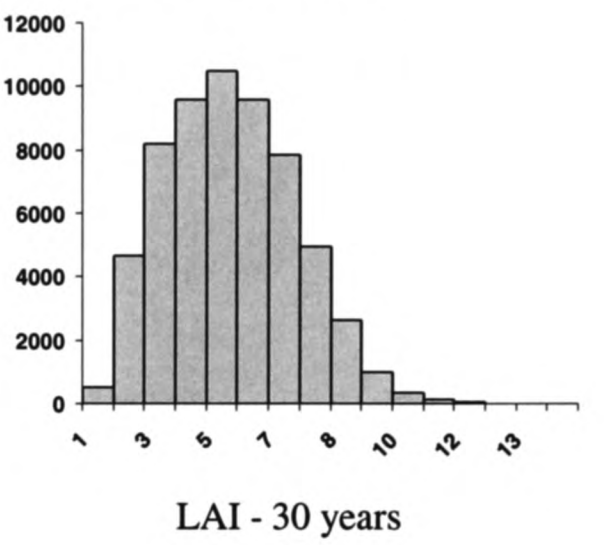
Foliage biomass - 73 years



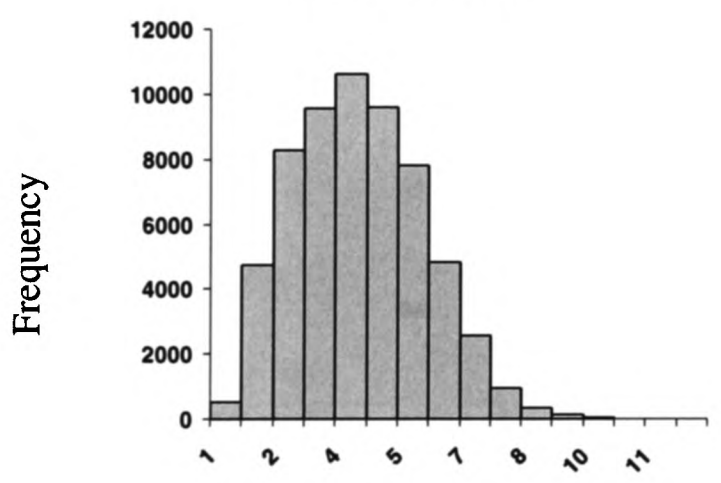
LAI - 20 years



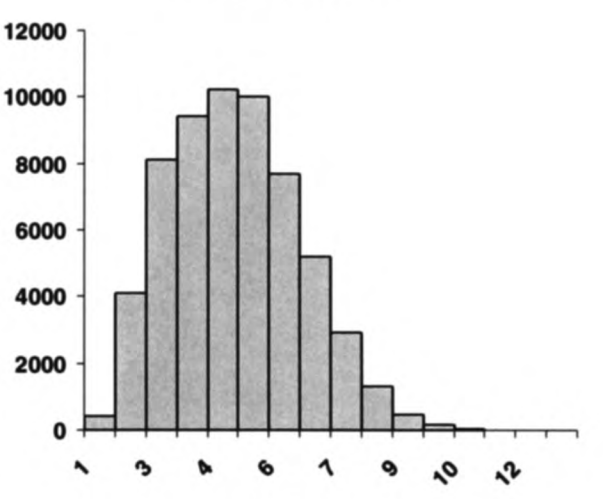
LAI - 25 years



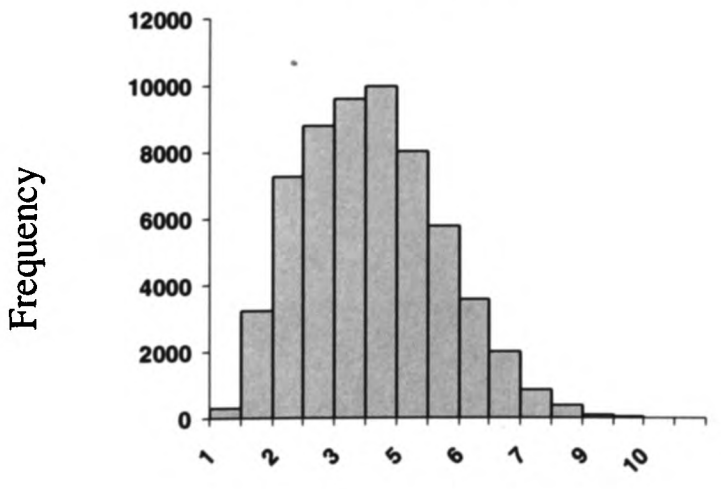
LAI - 30 years



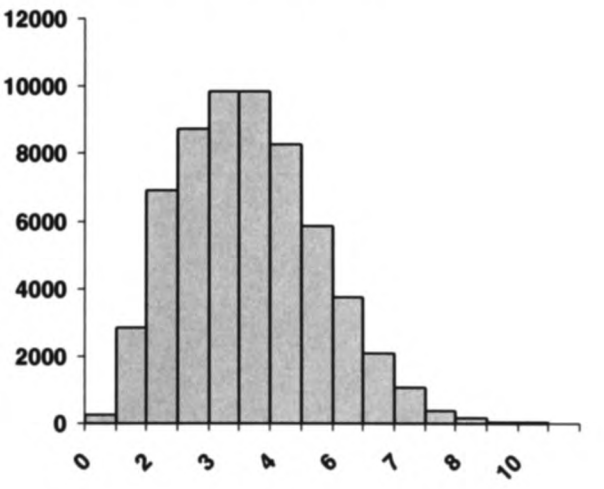
LAI - 31 years



LAI - 35 years



LAI - 40 years



LAI - 45 years

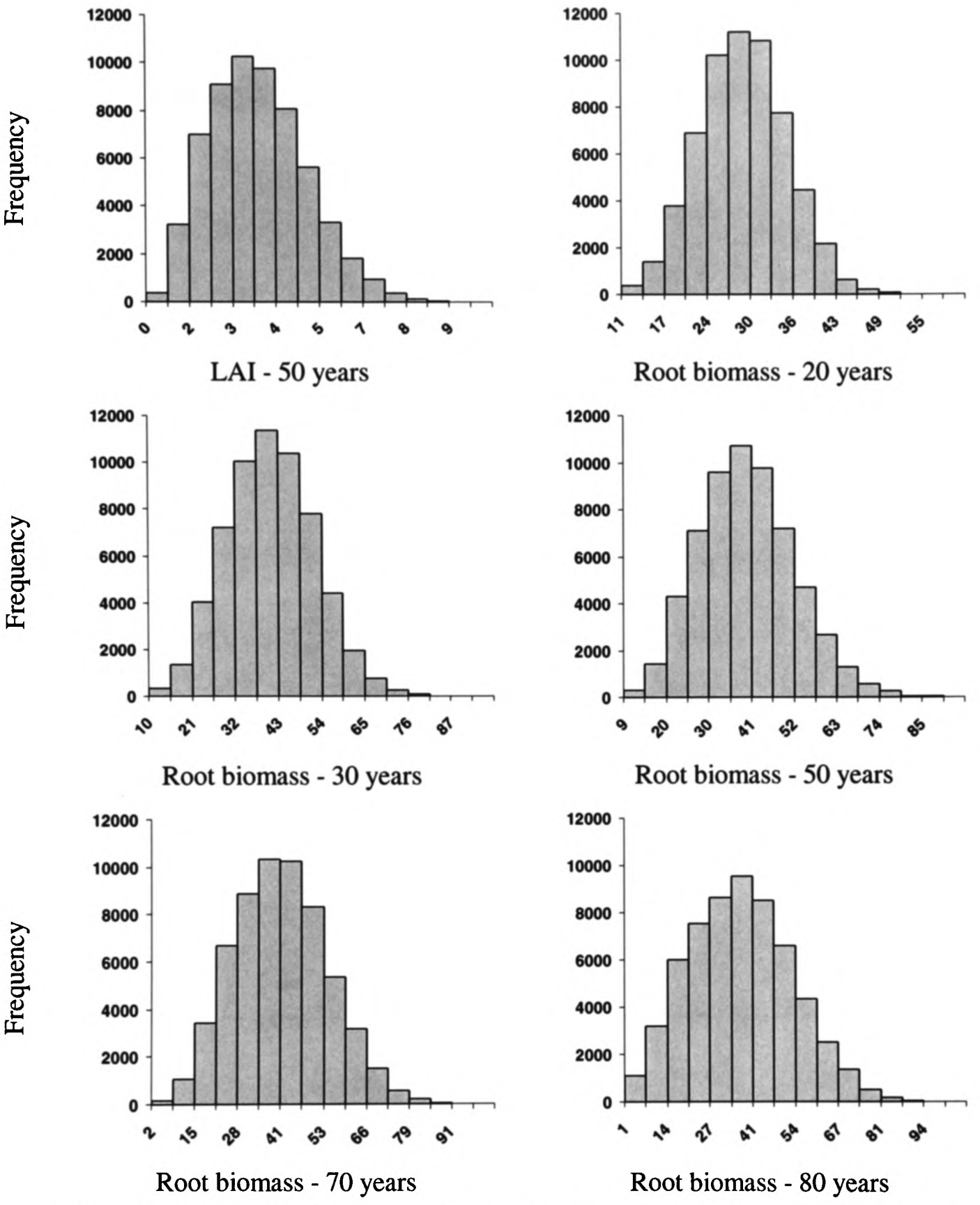
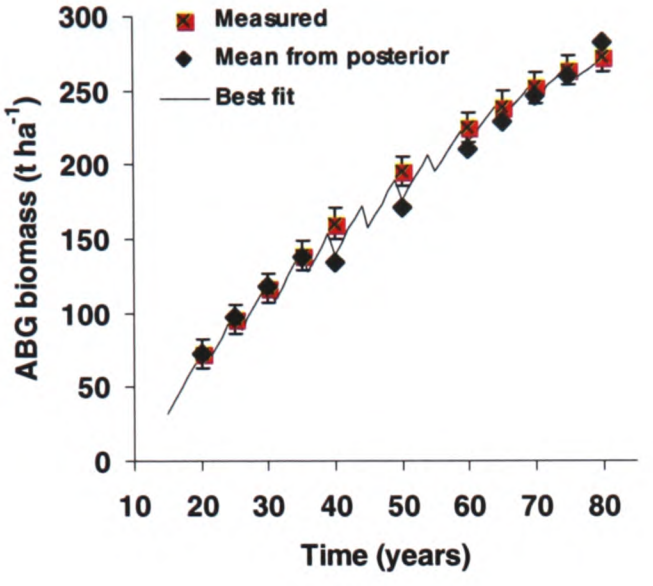
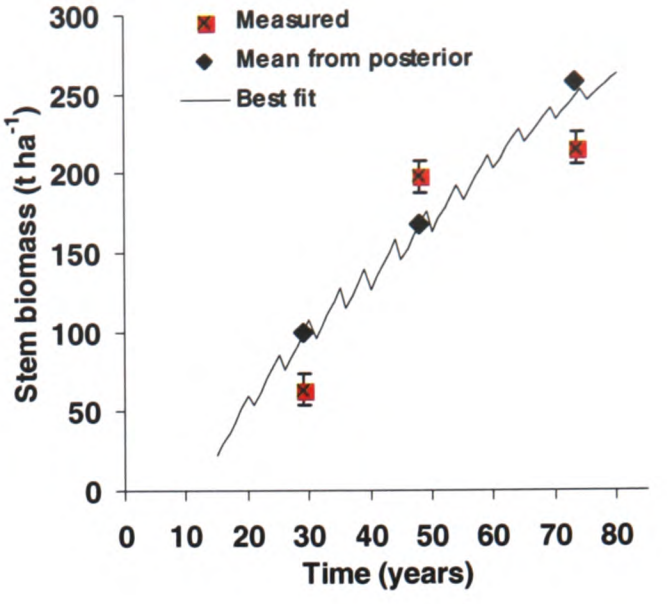


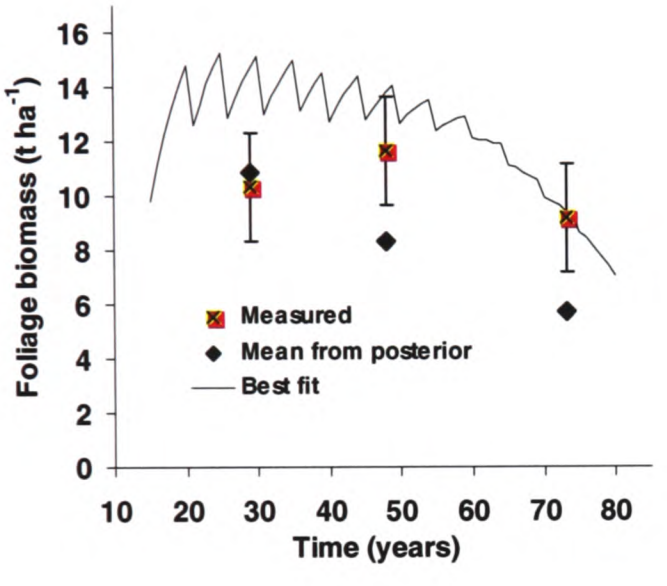
Figure 6.9: Histograms from the sampled marginal posterior distributions of the model outputs

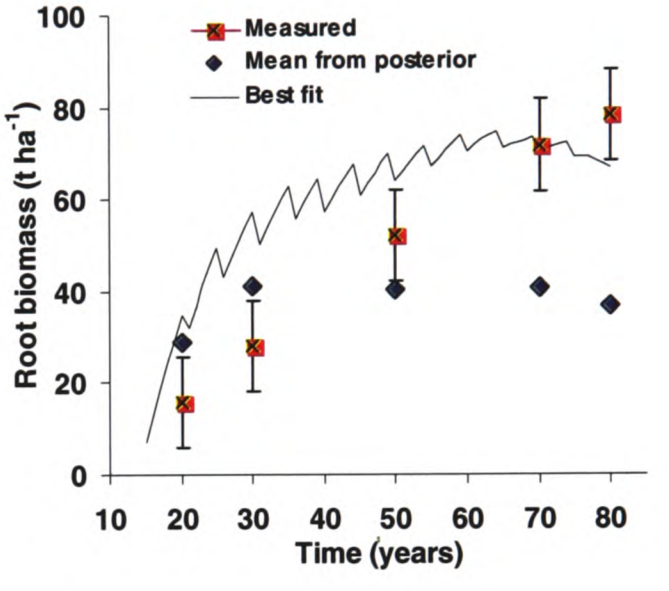
Table 6.7: Descriptive statistics from the 60 000 MCMC models outputs sampling

	Stand age	Mean	SD	Min	Max
Above-ground biomass	20	72.3	5.5	51.0	105.0
	25	97.7	8.9	65.6	156.1
	30	118.5	11.5	79.4	200.7
	35	137.8	13.6	93.6	244.7
	40	134.5	13.2	89.1	238.6
	50	170.6	15.6	109.6	289.4
	60	210.5	16.7	113.6	334.8
	65	229.0	17.1	109.4	359.5
	70	246.0	18.7	104.0	380.0
	75	259.4	22.8	99.3	399.9
	80	281.3	31.0	99.3	435.8
Stem biomass	29	99.6	10.3	63.8	177.6
	48	167.4	16.6	104.9	299.0
	73	256.1	20.6	104.0	399.6
Foliage biomass	29	10.9	3.1	3.0	22.8
	48	8.4	2.9	0.8	19.9
	73	5.7	3.0	0.0	18.4
Root biomass	20	28.9	6.4	10.9	58.3
	30	41.2	11.0	10.4	92.0
	50	40.1	11.9	8.9	89.9
	70	40.6	13.8	2.3	97.8
	80	36.9	16.0	0.6	100.9
LAI	20	7.6	2.2	2.1	17.0
	25	6.5	2.1	1.7	15.8
	30	5.4	1.8	1.3	14.3
	31	4.5	1.5	1.0	12.0
	35	4.8	1.6	1.0	12.6
	40	4.2	1.5	0.7	10.9
	45	3.9	1.4	0.5	10.2
	50	3.6	1.4	0.3	9.9









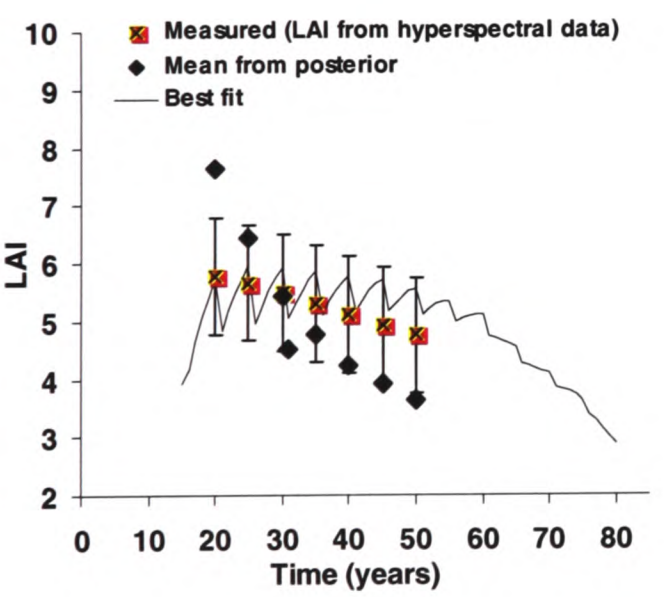


Figure 6.10: Graphic summary of results from the MCMC sampling (average model outputs from the marginal posterior, black rectangles, and best fit, grey line) in comparison with available data. The grey line and the dark rectangle points were calibrated using the red data points.

6.3.3 Analysis of uncertainty

Figure 6.11 shows a fingerprint graph of partial correlation coefficients between parameters and outputs. Dark blue and red areas indicate high negative and positive correlations, respectively. Light green indicates a weak or non existent correlation. Correlations of $|r| > 0.6$ between parameters and model outputs are summarised in Table 6.8.

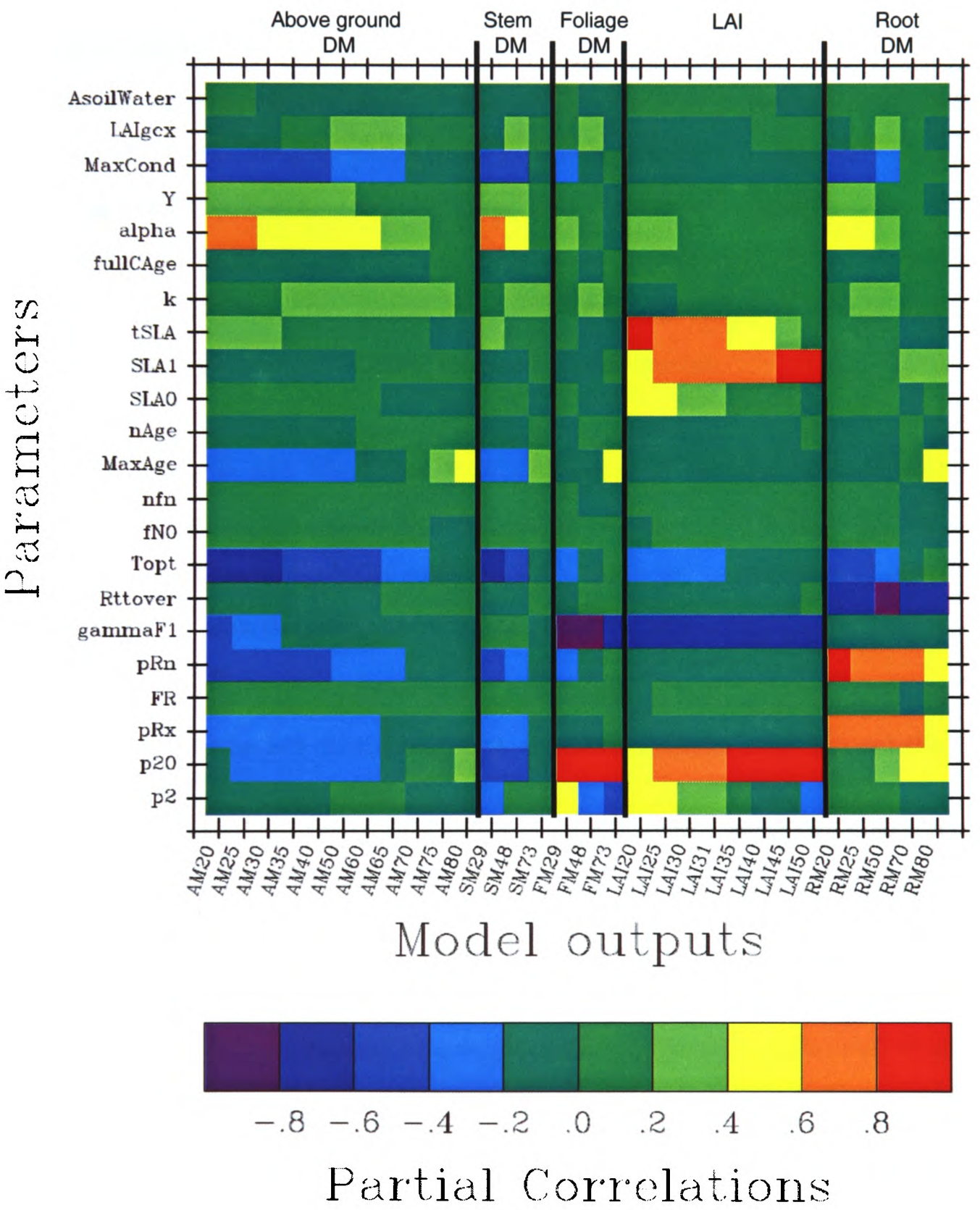


Figure 6.11: "Fingerprint" of partial correlation between 3-PG parameters and model outputs (n=60,000).

Table 6.8: Partial correlations of |r| > 0.6 between parameters and model outputs

	Positive	Negative
Above-ground biomass	α_{Cx}	T_{opt}
Stem biomass	α_{Cx}	T_{opt}
Foliage biomass	p_{20} p_2	γ_{F1}
LAI	t_σ σ_1 p_{20}	γ_{F1}
Root biomass	η_{Rn} η_{Rx}	γ_R

6.4 Discussion

The discussion to this chapter extends from that of Chapter 5. In addition to considering the knowledge gained about Corsican pine stands in Thetford from the Bayesian calibration, a comparison between the results from Scots pines to those for Corsican pine provide a window through which differences between species can be identified. This comparison also provides useful insights into the functioning of 3-PG and helps in identifying critical parameters for which more information is required across species.

The uncertainty analysis has also been extended here. A detailed examination of the uncertainties arising from the model structure itself is made, providing insights into the behaviour of uncertainties through the rotation. This led to the exploration of how the data used in the calibration have helped in reducing the uncertainties of the model outputs.

6.4.1 Marginal posterior distributions of parameters and correlations between parameters

After the calibration exercise, the uncertainty for 14 out of 22 calibrated parameters has been reduced (Figure 6.8). Eight posterior distributions for the parameters remained near uniform. The parameters for which little has been gained from the calibration, pertain either to the water submodel (θ_{sx}, L_{Cx}, g_{Cx}) or to canopy development processes (t_c, t_σ, σ_0). For the calibration of the parameters pertaining to the water submodel, either measurements on the parameters themselves will be required, or data on soil water availability. To reduce the uncertainty of t_c, t_σ, σ_0, simulations initialised at a younger stand age will be necessary, along with corresponding leaf biomass data. The inclusion of data on root and foliage biomass in this calibration has helped in reducing the uncertainty of several parameters. In effect, compared to the calibration for Scots pine (Chapter 5), the uncertainty of the maximum allocation of NPP to roots (η_{Rx}), root turnover (γ_R) as well as of the specific leaf area at maturity (σ_1) has been reduced from the integration of ancillary data on root and foliage biomasses.

Correlations between parameters are shown in Table 6.6. Twenty three correlations are, in absolute terms, above 0.10. No correlations were found above |r|=0.36. The two strongest correlations were between α_{Cx} and T_{opt} (r=0.36) and between α_{Cx} and g_{Cx} (r=0.18). Provided that environmental conditions are not constraining growth, an increase in α_{Cx} is directly proportional to an increase in NPP and to subsequent allocation of biomass to the plant components. In the calibration exercise, biomass production is constrained by the data. Thus, as α_{Cx} increases, environmental constraints must restrict growth. The correlation between α_{Cx} and T_{opt} suggests that among environmental modifiers, T_{opt} is a critical parameter exerting control on NPP. As discussed in Chapter 5, above-ground biomass model outputs were found to be highly sensitive to this parameter, in particular since the average temperature in the UK is approximately 10°C annually, and 15°C over the growing season (May-September, Table 5.1). High values of optimum temperature imply that temperatures at which optimum growth occurs arise infrequently, thereby exerting a strong constraint on NPP.

The second highest correlation is observed between α_{Cx} and the canopy conductance (g_{Cx}). The canopy conductance determines the ability of tree tissues to transport soil water to the canopy, controls potential evapotranspiration and thereby determines water availability. In 3-PG, everything else being equal, an increase in g_{Cx} will yield an increase in potential evapotranspiration and given the right climatic conditions, a decrease in soil water availability. Thus indirectly, g_{Cx} controls soil water availability. This suggests that the positive effect of increasing α_{Cx} on NPP can be limited by a simultaneous increase in g_{Cx}.

6.4.2 Marginal posterior distributions for the parameters: comparison with Scots pines

A comparison between the posterior distributions of Scots and Corsican pine parameters can assist in appreciating fundamental physiological differences between these species. The following Table 6.9 compares parameters for which the uncertainty has been reduced in both calibrations.

Table 6.9: Statistics from the marginal posterior distributions of Corsican and Scots pine parameters. Only the parameters for which uncertainty has been reduced for both species are shown (i.e. parameters whose distribution are not near-uniform).

$\theta(i)$	Centre of modal class	
	Corsican Pine	**Scots Pine**
Growth modifiers		
FR	0.98	0.98
T_{opt}	14.6	12.5
Canopy structure and mortality		
γ_{F1}	0.017	0.022
σ_1	5.6	3.6
t_x	148	123
Biomass allocation		
p_2	0.65	1.25
p_{20}	0.43	0.38
Light interception and production		
k	0.62	0.56
α_{Cx}	0.057	0.048

Corsican and Scots pine trees are known to grow well even on unproductive sandy soils. The results presented in Table 6.9 support this observation, as for both species, Thetford appears suitably fertile (FR=0.98; 1= optimal fertility). In this table, the results show that for both tree species, the uncertainty concerning the optimum temperature for growth has been reduced (Figure 6.7 and Figure 5.2, histograms of the parameters per species). Differences are nevertheless observed between the modal class values. The mode for Corsican is higher than for Scots pine. One would expect such a result, as Corsican pines, prevalent in the Mediterranean region, are native to Corsica where hot days occur four times more frequently than in lowland Britain (Kerr 2000). Although in its native geographical region, Corsican trees grow at altitudes between 900 to 1500 metres where the climate resembles that of lowland Britain (Brown 1960), optimum temperature for growth of Corsican trees is almost certainly higher than that for Scots pine, whose geographical coverage extends to Scandinavia.

Corsican pines are also known for their higher productivity on sandy soils compared with Scots pines (Greig 1987, Jinks and Kerr 1999). As for both species, the site is considered equally fertile, this increased productivity is embodied in 3-PG via the canopy quantum efficiency, which after the calibration, appeared considerably higher for Corsican pines. Another important observed difference between these species is in their canopy

development and light interception ability. While Corsican pines preserve their conical shape at maturity, the pyramidal feature characteristic of most coniferous trees is not observed in Scots pines. Scots pine canopies develop into numerous forms, but most commonly into broad spreading, round or flat top shapes. This has an important influence on the light interception ability of the canopy and may explain why the extinction coefficient of PAR absorption is lower for Scots pines than for Corsican pines. The other leaf and canopy development parameters, σ_1 and p_2, p_{20}, suggest that Scots pines allocate more NPP to foliage at an early ages, but that at maturity, the specific leaf area (σ_1) is less than for Corsican pines.

Finally, a comparison between the maximum age for growth suggests that Corsican pines live longer than Scots pines. The maximum age for Scots pines is believed to approximate 250 to 300 years. Brown (1960) found that many Corsican pine stands occurring in Corsica were between 150-200 years old, suggesting that trees are likely to reach ages above this level. Nevertheless, the longevity of Corsican pines in the UK has not been assessed, as the species was only introduced in the late 18th century and since, Corsican pines stands have been mainly managed on short 55-65 years rotations (Kerr 2000).

6.4.3 Marginal posterior distribution of outputs: identification of key parameters and analysis of model structure

Figure 6.11 shows the fingerprint of partial correlations between parameters and outputs. The results shown in Figure 6.11 were summarised in Table 6.8. This table identifies the model outputs to target in order to reduce the uncertainty of a given parameter. Likewise, the opposite is also true. If one is interested in reducing the uncertainty to specific model outputs, one may use this fingerprint graph to target specific parameters. Interestingly, most parameters identified in Table 6.4 were also identified in Chapter 5 for Scots pines.

In Figure 6.10 the data used for the calibration, the mean model outputs, and the model output using the θ_{MAP} parameter vector are shown. Although this Figure illustrates how close the average model outputs and the best fit are from the data, this does not show whether the close fit is due to the information embodied in the data, or in the structure of the model itself. To address this, the MCMC sampling process has been executed again by setting unrealistically wide standard deviation values to fictitious data points in the calibration. By doing so, the data become uninformative and the model output uncertainties predominantly result from the model structure as a very weak prior was used, namely a joint uniform probability distribution with wide parameter ranges. This is nearly equivalent to

removing all the data from the calibration (thereafter referred to as the no-data MCMC). In deed, even though the posterior distribution to the parameters is proportional to the prior parameter distribution times the data likelihood, if both the prior and likelihood are uninformative, the resulting posterior will be near-uniform.

The results are presented in Figure 6.12, Figure 6.13, and Figure 6.14. In Figure 6.12, the mean model output from the "no data" MCMC against stand age is shown which can be compared to that when data were included. This shows how the model behaves, without rigorous calibration. In Figure 6.13, the standard deviations of the model outputs resulting from the calibration with and without real data are plotted against stand age. This illustrates how the uncertainties of the model outputs have been reduced by the real datasets. In particular, it can be observed that for the above-ground biomass component, an important uncertainty reduction has been achieved. This is expected, as although data for root and foliage biomass as well as for LAI were included in the calibration, confidence in these measurements was lower than that for the stem and above-ground biomass.

In Figure 6.14, the uncertainty (standard deviation) is plotted against the mean output value when data and no data were included in the calibration. Together, Figure 6.13, and Figure 6.14 show how uncertainty behaves as a function of stand age or mean model output. For above-ground biomass, the uncertainty increases as function of both stand age and mean output value. For LAI, the uncertainty decreases with stand age, but increases with the mean output value. An increase of uncertainty with mean value is often observed in biological sciences (Sokal and Rohlf 1995) and was expected here. However, for roots, while an increase in uncertainties is observed through the rotation, this pattern is not observed with the mean. This suggests that low root biomass values at the beginning of the rotation have smaller uncertainties than the equivalent root biomass values at the end of the rotation.

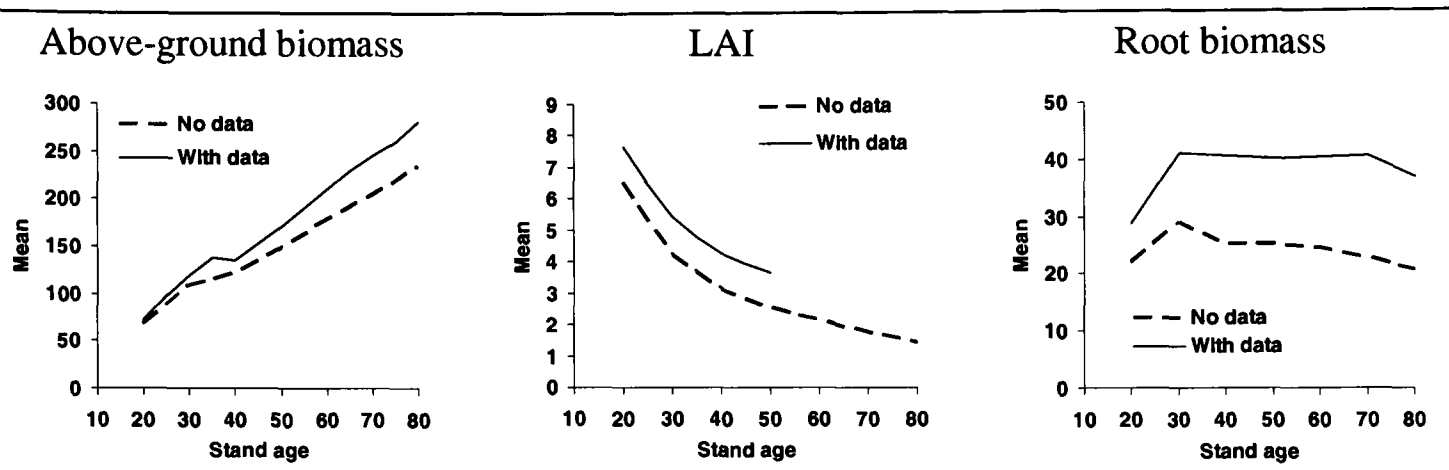


Figure 6.12: Mean model outputs from sampled marginal posterior distributions (n=60,000). In the "No data" series, data with unrealistically high standard deviations were used in the calibration. In doing so, the data become uninformative and the uncertainties of the model outputs result predominantly from the model structure. The "With data" shows the mean model output from the calibration exercise with the real data for Thetford

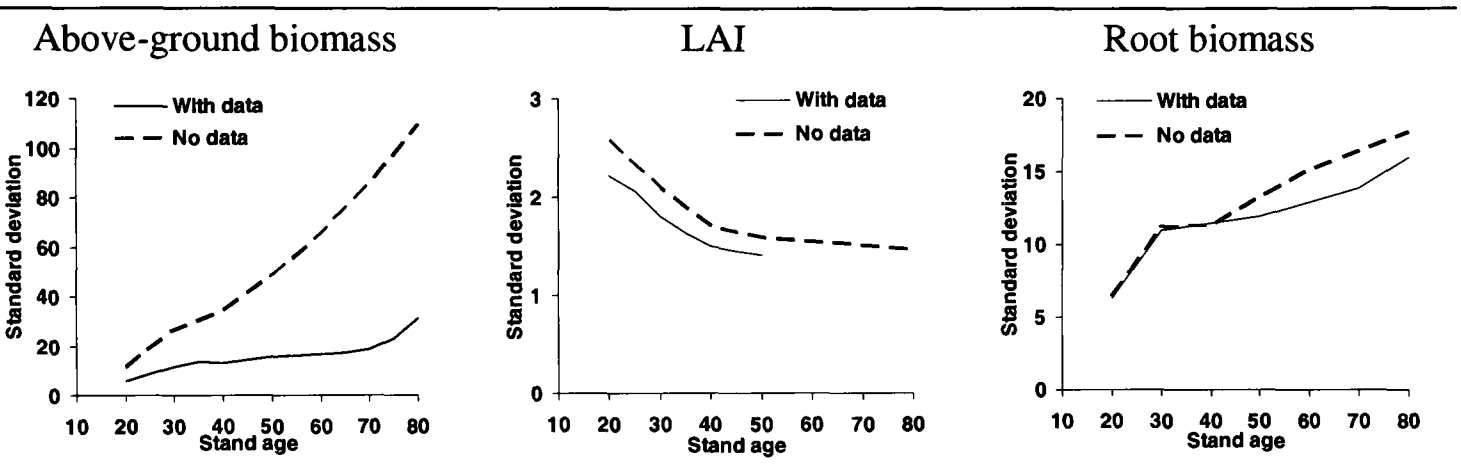


Figure 6.13: Reduction of model output uncertainty from the available data. The "No data" series indicate that the data used in the calibration were given unrealistically high standard deviations. In doing so, the data become uninformative and the uncertainties of the model outputs result predominantly from the model structure. The "With data" shows the model output uncertainties from the calibration exercise with the real data for Thetford (data shown in Figure 6.10).

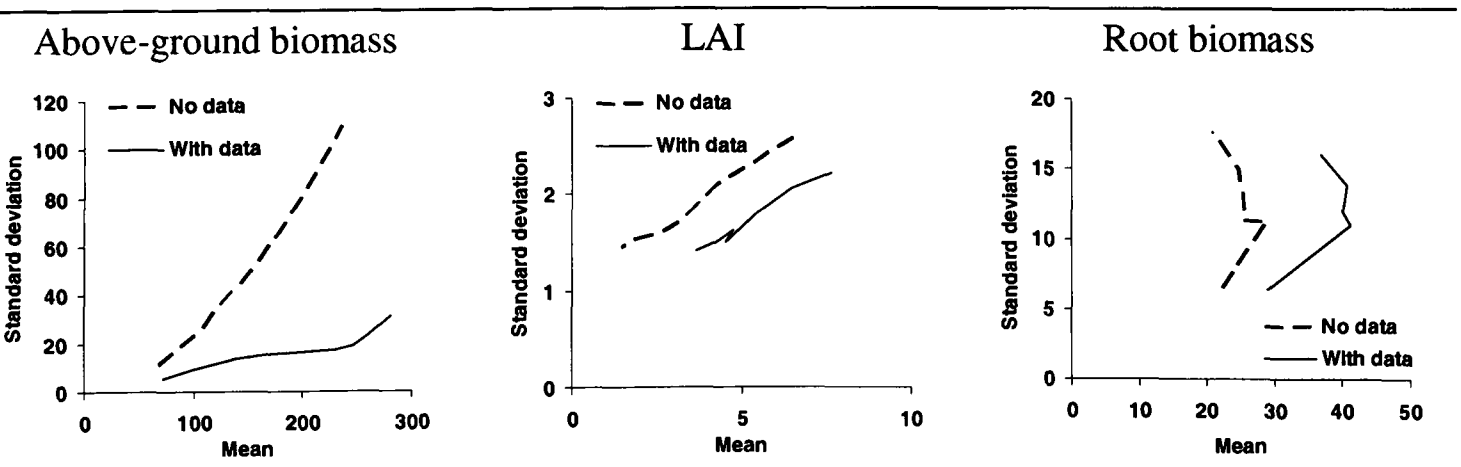


Figure 6.14: Model output uncertainty as function of mean model output (from the 60,000 MCMC sample). In this MCMC sampling exercise, data with unrealistically high standard deviations were used in the calibration. In doing so, the data become uninformative and the model output uncertainty result predominantly from the model structure. The "With data" shows the standard deviation of model outputs from the calibration exercise with the real data for Thetford

An important observation drawn from this analysis is that by simulating forest growth with ranges of parameter values realistically assigned but without informative data, one can suggest that the mean model outputs from these simulations represent "a typical behaviour or dynamic" of the model. Naturally and in average, the model will tend to produce certain results, unless specific parameters are given. By looking at the results, one can assess if the model dynamics are realistic. As shown in Figure 6.12 and given these conditions, 3-PG simulates above-ground growth in an almost linear fashion. Interestingly, root allocation increases early in the rotation and decreases thereafter (the small kink in the simulation is believed to be an artefact of the thinning regime applied). This is contradictory to the ecological results which show that in average, NPP allocation to root is proportional to the allocation to the above-ground components: as trees grow, roots grow (e.g. Levy *et al.* 2004, IPCC 2003, Lehtonen *et al.* 2004), although variations occur as function of environmental conditions. The exponential curve representing LAI along the rotation is also unexpected, as it is distant from the pattern shown in Figure 6.5.

The second observation drawn from this analysis is that the structure of the model predominantly determines the dynamics of the forest growth and the data included in the calibration only affect the magnitude of allocation. In the Bayesian calibration conducted here, even when real data are used, the underlying influence of the model structure is evident. The growth patterns described above are also observed on the results shown in Figure 6.12, Figure 6.13, and Figure 6.14.

6.5 Conclusion

This chapter explored the potential of Bayesian calibration to reduce the uncertainty concerning Corsican pine parameters. The analysis of correlations between parameters from the MCMC suggests that the growth of Corsican pine in Thetford is mostly limited by soil water availability and temperature. This result is consistent with that found for Scots pines in Thetford. A second analysis was conducted which consisted in comparing the statistics from the marginal posterior distributions of Scots and Corsican pine parameters. This enabled the identification of important physiological differences between the species. An analysis of the marginal posterior distributions for the model outputs was also conducted and comprised two main components. Firstly, an uncertainty analysis was achieved with uninformative data, such that the resulting model output uncertainty arose predominantly from the model structure itself. The comparison between the results from this fictitious simulation and that using the real data showed how the integration of data helps in reducing the uncertainty of the model outputs. Additionally, this provided useful insights into the

functioning of 3-PG. The underlying influence of the model structure could be clearly observed on the simulations produced with real data.

Finally, the partial correlation analysis between the model outputs and parameters provided a preliminary identification of model outputs to target in order to reduce the uncertainty of a given parameter (and vice versa). This chapter, along with Chapter 5, provides the first uncertainty analysis ever conducted for 3-PG.

Chapter 7

Thesis summary and conclusions

7.1 Introduction

This thesis reviewed, tested and developed methods relevant to support the Kyoto Protocol. This chapter therefore discusses the aims achieved and presents a synthesis of the main results, principal limitations, and key conclusions to each chapter. Three global aims were defined in the introduction:

1. To design and investigate methodologies to help the UK build verification strategies of its forest carbon stocks and changes. The methods presented belong to the verification categories 3-4-5 (Table 1.3) suggested by the IPCC.
2. To investigate the potential for uniting methods and data sources within a process-based model framework
3. To find and assess an appropriate statistical approach on a process-based model, enabling the consideration of all data sources

Sub-objectives relevant to the selected methodologies were also defined. Accordingly, the discussion will be subdivided into objectives, methods and relevant sub-objectives.

7.2 Estimating the carbon content of selected forest ecosystems (objective 1)

This objective was addressed by Chapters 2, 3, 4, 5 and 6. Although in Chapters 5 and 6, biomass instead of carbon estimates were made, the relationship between these variables is direct. The Chapters are not presented here in a sequential manner but in the approximate sequence of the sub-objectives addressed.

7.2.1 Field-based measurements

7.2.1.1 Estimating the carbon content of a semi-natural, deciduous woodland: implication for estimates at national scale (sub-objective i and ii)

Chapter 3, comprising of a paper published in the journal *Forestry*, provided the first exhaustive field-based assessment of the carbon content held in a UK semi-natural woodland. The research was designed such that five stands, contrasting in terms of species composition and structure, were surveyed. In addition to being representative of the stands

found within the woodland, the selection of these stands should help in assessing the carbon content of UK woodlands falling under similar management regimes; for this purpose, a detailed description of the soils, management and the structure of each of the stand as well as the carbon content estimates was provided.

Within each stand, between 8 to 10 plots were randomly located and the total carbon content within each plot, assessed. The carbon content in seven forest components was estimated, grouped under overstorey, understorey, foliage, deadwood, ground vegetation and litter, roots and soils. The results across the stands and plots were, in increasing pool size: 2 t ha^{-1} for dead wood, 3 t ha^{-1} each for foliage and ground vegetation and litter, 18 t ha^{-1} for the understorey, 28 t ha^{-1} for roots, 78 t ha^{-1} for overstorey and finally, 335 t ha^{-1} for soils. Soils contain by far the largest pool, followed by overstorey. The vegetation pool (dead and alive) contains nearly a third as much carbon as soils. Notably, understorey represents an important carbon pool, which equates to 23% that held in the overstorey. The carbon content of the stands, which were under different management regimes, ranged from 346 t ha^{-1} to 616 t ha^{-1}. As each stand was representative of a management class found in the woodland, a scaled up estimate to the woodland level was made. In total, the woodland was estimated to hold approximately 79 kt of carbon and 23 kt, if soils are excluded.

The results of this study have important implications for the national estimates of carbon held in forests. In the UK, it was previously estimated that, although broadleaved woodlands cover only approximately 4.1% of the total rural surface area, they contained nearly 50% of all the carbon held in vegetation. In this study, it was shown that the importance of these carbon stores could be much greater. The figures for the UK were calculated on the basis that broadleaved woodlands hold, on average, 61.9 t ha^{-1} compared with 21 t ha^{-1} for coniferous forests. On average, stands in Monks Wood hold 47% more carbon than the value estimated in Cannell and Milne (1995). For the UK, the assumption that all broadleaved woodlands are commercial plantations is made. This excludes the significant contribution of understorey trees and shrubs, deadwood, or ground vegetation and litter, which in semi-natural woodlands may be non-negligeable. In Monks Wood, these represent nearly 30% of the total carbon content estimated in the vegetation component.

In the UK, the conversion factor used for providing estimates to the UNFCCC which converts stemwood volumes to total vegetation carbon content (in all relevant pools) is 0.38 t m^{-3}. This factor is based on commercial broadleaved woodlands where the stemwood volume holds a high proportion of the total vegetation carbon content. In Monks Wood

when averaged over the 5 stands, this conversion equates to 0.57 t m^{-3}. The UK estimate of the carbon content held in deciduous woodlands is therefore probably underestimating the importance of semi-natural woodlands. However, further information on the proportions of natural and commercial broadleaved woodlands is required to assess the importance of this result on the national estimate of carbon held in UK forests. Such results are of prime importance for building strategies and policies aiming at increasing the contribution of semi-natural woodlands to carbon storage.

Main limitations of field-based measurements in support of the Protocol

- Due to the logistics of data collection, only limited field-based measurements are practicable at national scales. Appropriate statistical sampling methods are required for spatial extrapolation beyond the surveyed plots.
- The data collection is time consuming and can be cost inefficient for national inventory purposes or for the monitoring of areas difficult to access.
- If no destructive measurements are allowed, models and data derived elsewhere are required. Quantifying the uncertainty of the estimates and estimating their accuracy can be difficult.

Conclusions A

- **Field-based measurements are the most exhaustive approach available to quantify carbon stocks.**
- **Representative sampling of diverse forest types (not only plantations) is required to produce an accurate national inventory.**
- **Large variability is observed between the carbon content of different forest components and forest types (e.g. stands). This variability can only be properly estimated through ground observations.**
- **Although exhaustive field-based assessments are difficult to achieve at national scales, sufficient field-based sampling should nevertheless be integrated as an essential component of a full inventory.**

7.2.2 Remote sensing

Chapter 2 specifically addressed an important gap in the literature, and provided a quantitative appraisal of remote sensing methods, with emphasis on their operational status. This was achieved by examining a real case study, exemplifying how these approaches may be applied in a specific national context. To do so, a literature review on each main approach was conducted from which conclusions were drawn.

This chapter was published in *Environmental Science and Policy* and provides the most comprehensive discussion on the subject currently available in the literature. Although the *Intergovernmental Panel on Climate Change (IPCC) Good practice guidance for land-use, land-use change and forestry* (IPCC 2003) addresses briefly the potential of remote sensing techniques to meet specific Kyoto requirements, the nature of the manuscript and the extent of material covered implied that only brief guidance could be provided.

7.2.2.1 Reviewing remote sensing approaches for assessing forest to non forest land cover change (sub-objective iii)

Assessing remote sensing approaches for forest to non forest land cover discrimination is of prime importance, as all afforestation, reforestation and deforestation activities since 1990 must be reported. Under the Protocol, the activities are specifically defined as directly human-induced. Whereas such inference cannot be made from remote sensing alone, these techniques nevertheless enable the observation of land cover change. By identifying where a land cover change has occurred, areas for which ancillary data are required to infer a human-induced land-use change can be identified. In Chapter 2, it was shown that although in the UK, afforestation and reforestation activities have been consistently recorded since the 1920s, large discrepancies exist between estimates of deforestation rates (Levy and Milne, 2004). Thus emphasis was given to the monitoring of deforestation activities.

A principal result from this review was that both optical and radar approaches were suitable for land cover change assessments. Optical techniques have been in operation for several decades and the experience gained over the years has led to the development of various classification algorithms as well as techniques that minimise the influence of external factors on the signal of interest. The capabilities of optical remote sensing for forest to non forest discrimination and for broader land cover mapping is now widely recognised and in the UK, several land cover maps and forest inventory have already been derived from optical datasets. These include the UK inventory of woodland and trees (Forestry Commssion 2001) and the UK land cover maps (1990 and 1998, Fuller *et al.* 1994, 2002). The accuracy of these maps ranged between 67% to 94%. This synthesis also showed that forest to non forest classification have been successfully achieved from radar approaches, especially when multifrequency (longer wavenlengths), multi-polarimetric Synthetic Aperture Radar methodologies were used. The accuracies in land cover classification were generally above 80% at level-I. At this level, discrimination between forests and non forest land covers is made while differentiation between deciduous and coniferous forests is

achieved at level-II. Classifications achieved at level-II, although of lower accuracies than at level-I, were nevertheless typically above 60%. Albeit discrimination at level-I is sufficient to infer a forest to non-forest land cover change, classification at level-II can provide ancillary information about the loss of carbon suffered from deforestation, as the carbon content of deciduous forests can be considerably different from that in coniferous forests.

Finally, a remote sensing technique recently applied to forestry, the Light Detection And Ranging (LiDAR), could possibly be used for the systematic, georeferenced and stratified detection of land cover change, provided that instrumentation and techniques suitable for forest monitoring become available from satellite platforms. Although not an imaging system, LiDAR enables the quantification of ground surface elevation and heights of surfaces above it. This capability may help in identifying areas where considerable change has occurred and for which further ancillary data are required to infer that deforestation has occured. However, until a LiDAR system becomes available from satellite platforms, this approach remains untested.

7.2.2.2 Quantifying forest above-ground carbon content from remote sensing: current and future trends (sub objective iii, v, and vi):

This synthesis also reviewed operational and near-operational remote sensing techniques to quantify above-ground carbon content in forests and argued that optical approaches, although suitable contextually, are not apt for biomass quantification at national scales. Optical wavelengths are not directly sensitive to biomass, and the results across ecosystems and forest types are inconsistent (e.g. Brockhaus and Khorram 1992; Trotter *et al.* 1997; Holmgren and Thuresson 1998; Wulder 1998; Fazakas *et al.* 1999). Instead, the strength of optical data for this purpose most likely rests in retrieving forest stand variables that strongly influence growth, such as fPAR and the leaf area index (LAI) (e.g. Lucas and Curran 1999). An example of how such variables may be retrieved from optical data is provided in Chapter 6.

Unlike optical approaches, radar wavelengths are directly sensitive to biomass. The results of this study, bringing together the work conducted by Imhoff (1995), Luckman *et al* (1997, 1998), Fransson and Israelsson (1999), Franson *et al.* (2000), and Skinner (2002) amongst others, show that although the potential of radar is limited where forest biomass is high, nearly 52% of UK forest biomass could be monitored using SAR C or L-Band (Table 2.6). Indeed, to quantify stand variables closely related to forest carbon content (e.g. biomass or

woodvolume), radar was most successful in relatively young, homogeneous coniferous forests. Most UK forests comprise of young growing coniferous stands which are those that contribute most significantly to carbon uptake. Additionally, of the remaining 48% of forests which cannot be assessed due to the saturation of the signal, many are in a mature state and are unlikely to significantly contribute to carbon fluxes.

Although radar approaches may be suitable to quantify part of the UK forest carbon stocks, the total surface area potentially monitored using this technique is likely to decrease, unless a solution to the saturation setback is found: the average UK forests are ageing and in so doing, the overall UK average in forest biomass is increasing. Likewise, in areas such as Scotland, the applicability of radar approaches may be limited where the influence of topography is considerable. Considering these limitations, LiDAR approaches, although not yet operational for the monitoring at such scales, are possibly most promising: LiDAR signals are directly sensitive to biomass and do not saturate. The accuracy in retrieving variables closely related to the biomass and carbon content (e.g. stemwood volumes or tree heights) was generally high (e.g. Lefsky *et al.* 1997, Naesset, 1997b; Lefsky *et al.*, 1999a; Means *et al.* 2000; Naesset, 2002; Persson *et al.* 2002). At the start of this project, nothing had been published on the capability of LiDAR approaches to estimate carbon content in deciduous woodlands.

7.2.2.3 *Estimating the costs to acquire remote sensing datasets (sub-objective iv):*

Chapter 2 also provided estimates of costs for using these approaches under the Protocol (data acquisition only, no processing). Ultimately, the decision to rely on a specific approach will depend on its cost efficiency as well as on its accuracy. Approximately 28,000 km^2 of the UK are forested areas. The most expensive approaches for the complete monitoring of UK forests are airborne radar (£7,000,000) and LiDAR approaches (£8,400,000) (as no satellite carrying suitable sensors were available at the time of the study) followed by ground surveys (£3,500,000). The cost for acquiring satellite optical data or satellite and shuttle-borne radar data is a less than £3,000. The potential for merging low-cost, low resolution imagery with spatially resolved techniques (e.g. airborne LiDAR) should be further investigated.

Main limitations of these approaches in support of the Protocol

- Several external environmental factors, inherently heterogeneous at national scales affect the remote sensing signals (e.g. atmospheric attenuation and environmental

contamination). Complex processing is required to minimise the influence of these factors on the signal of interest.

- Intrinsic factors pertaining to the sensors and to current analytical methods limit their applicability for biomass monitoring (e.g. the saturation of the signal at high biomass; spectral, spectral, radiometric or temporal resolutions).
- The limited availability or unavailability of satellite sensors adapted for this purpose.
- To detect change and growth of vegetation, the response from the combined estimates (e.g. difference between $Time_2$ and $Time_1$) must be greater than the combined noise in the datasets.

Conclusions B

- **Remote sensing is a unique approach enabling the rapid and repeatable observation of forests at national scales.**
- **For discriminating between forests to non-forests land covers, both radar and optical approaches have been successful. Further ancillary data are required for an assessment of land-use change to be made.**
- **For the quantification of biomass in young and homogeneous coniferous woodlands, approaches based on radar (SAR) backscatter have been successful. These forests contribute most to the atmospheric carbon uptake by UK forests.**
- **Ultimately, LiDAR approaches do not suffer from a saturation of the signal and may provide the only viable remote sensing tool available for this purpose.**
- **The potential for fusion of approaches, combining low-resolution, low cost images with the increased resolution of others, should be investigated further.**

7.2.2.4 Quantifying the above-ground carbon content of deciduous woodlands from LiDAR (sub-objective vi and vii)

As a result of the review provided in Chapter 2, where LiDAR was identified as the most promising forthcoming remote sensing technique for quantifying carbon content in temperate forest ecosystems, a LiDAR-based method for carbon content quantification was developed and presented in Chapter 4. The methodology and results, published in *Remote Sensing of Environment*, provided one of the first attempts to produce estimates from this approach. The novel methodology was designed to rely on LiDAR derived canopy height metrics.

The methodology was designed for a deciduous, semi-natural woodland as methodologies and data available for UK semi-natural woodland are limited: most researches have been conducted in forest plantations, intrinsically far more homogeneous than natural woodlands. The quantification of carbon in such ecosystems was designed to address two challenges. Firstly, the aim was to increase our knowledge about the carbon content of semi-natural woodlands, and secondly, if successful, the exercise would yield a framework for the quantification of carbon in such ecosystems.

The proposed approach relies on the extraction of a canopy height metric from LiDAR, considered representative of the distribution of canopy heights found in an area of concern. The height metrics are extracted at equal intervals from a digital canopy height model (DCHM) produced from the LiDAR point measurements of canopy elevation. Above-ground carbon content is thereafter estimated from a model derived from forestry yield tables, and calibrated using the available field-based data.

The approach used was shown to be highly correlated with ground-based estimates of carbon content at the plot level ($r=0.74$, $p<<0.001$, $n=48$) and at the stand level ($r=0.85$, $0.1 \leq p < 0.05$ due to the small number of stands, $n=5$). In general, LiDAR estimates were 3.54 t ha^{-1} lower than the ground estimates, but this bias was found to be non significant, suggesting that both approaches were equally suitable for capturing the above-ground carbon content and its spatial variation between plots and stands.

The upscaled field-based above-ground carbon content estimates for the woodland were then compared with LiDAR-based estimates covering the entire woodland. When the LiDAR-based above-ground carbon content estimates were upscaled to the woodland level, using the ground-based upscaling approach ($n=48$ plots), the results between the two approaches were of similar magnitude. However, when the entire woodland was divided into 20x20 m^2 grid cells and the above-ground carbon content estimated for each cell using the LiDAR approach, the estimate for the woodland was nearly 23% lower then its ground counterpart. Thorough comparison between the LiDAR map and field-based upscaling methodologies revealed that the management data used by the field-based approach did not include the tree-less path network across the woodland leading to higher field-based estimates of carbon content. This suggests that the spatially explicit LiDAR method captured better the natural variability within the woodland.

Main limitations of the LiDAR-based approach in support of the Protocol

- LiDAR canopy heights tend to underestimate field-based height measurements. Although methods have been derived to counteract this setback (e.g. the use of quantiles), further research is required on understanding the causes for underestimation.
- The consideration of other variables (such as basal area or diameter at breast height) as independent variable into the carbon model, may increase the capability of the LiDAR approach to explain the variance in the ground-based carbon content.
- The carbon model is exponential, and should only be applied to the data range where it was fitted.
- Further work is required on how the implementation of the model may vary for different woodlands.

Conclusions C

- **LiDAR does not suffer from a signal saturation setback common to other remote sensing approaches.**
- **By covering larger areas than field-based approaches, LiDAR approaches are better at capturing the natural variability of extensive forest areas.**
- **Tree height is an acceptable proxy variable to quantify carbon content, provided that a suitable quantile, representative of the area under investigation, is selected.**
- **Currently unavailable from satellite, there is a need for launching a space-borne LiDAR sensor, specifically designed for terrestrial carbon stock monitoring.**

7.2.3 Process-based modelling (objective 2 and 3)

7.2.3.1 Above-ground biomass quantification, integration of datasets and uncertainty analysis (objective 1, 2 and 3, sub-objectives viii and ix)

Chapter 5 and 6 investigated the potential for integrating data sources within a process-based modelling framework. In contrast with the approaches discussed in Chapters 2, 3 and 4, process-based model provide estimates of the below-ground carbon content without the need for destructive sampling. Additionally, estimates of changes in forest growth and carbon storage can be made, as a result of varying environmental conditions without the need for extensive data collection. Much uncertainty however arises in the use of process-based model, especially at national scales, from the lack of information available on model parameter values. Although extensive datasets on model outputs have been collected (e.g. tree heights, DBH, stemwood biomass etc.), little is known about parameter values for specific case studies. As a matter of fact, parameters may vary widely between ecosystem

types, species, or even genotypes not withstanding differences arising from external environmental variability.

Likewise, the integration of several datasets within a process-based model framework (e.g. parameters, model inputs) implies complex non-linear interactions of uncertainties. A variety of datasets are likely to be integrated for the estimation and verification of national scales forest carbon stocks. For an exhaustive quantification of uncertainty, all the data included in the procedure should be treated probabilistically. To do so, in Chapter 5 and 6, a Bayesian calibration was applied for the quantification of model output and parameter uncertainty, which takes into consideration the uncertainty contained in the measured data, and the knowledge available for producing estimates. This work thereby contributes to the nascent body of literature interested in uncertainty quantification in model parameters and outputs, while considering all prior knowledge (Sivia, 1996, Bernardo and Smith 1994, Jansen and Hagenaars 2004). Bayesian calibration is the only exhaustive statistical approach available for the quantification of uncertainties from a system as a whole.

The 3-PG model was selected for this exercise. This model was originally designed to address both scientific and practical needs and has been successfully applied to simulate forest production worldwide (e.g. Landsberg and Waring 1997, Coops 1999, Waring 2000, Landsberg *et al.* 2003). However, 3-PG remained to be tested for many coniferous species in the UK thus the simulations were conducted for Thetford forest stands, whose management and species composition are characteristic of many coniferous ecosystems found in the UK.

Chapter 5 was submitted to *Ecological Modelling*. Together, Chapters 5 and 6 provide the first full uncertainty assessment of the 3-PG model. The overall contribution of these chapters however, lie beyond the uncertainty analysis and are manifold. Firstly, through the Bayesian calibration, knowledge about the Scots and Corsican pine 3-PG parameters was gained. The uncertainty to more than half of the parameters included in the Scots and Corsican pine calibrations was reduced (peaked marginal distributions). Partial correlations between parameters and outputs enabled the identification of key parameters whose uncertainty reduction could lead to a reduction in specific model outputs (and vice versa). A comparison between the modal class of the marginal posterior distribution of Scots and Corsican pine parameters identified critical physiological differences betweent the species.

Secondly, in Chapter 6, an analysis of the model behaviour was made. This was achieved by including uninformative data and weak priors (uniform distributions) in the calibration. Results from the Markov Chain Monte Carlo analysis generated patterns of model outputs as well as model output uncertainties, which arose predominantly from the structure of the model. The conclusions drawn from these analyses were highly relevant for future improvement of the model. In particular, although the growth pattern of above-ground biomass was reasonable, the growth patterns of LAI and roots was not consistent with the theoretical patterns of these variables. Proportionality between below and above-ground biomass is generally assumed in forest ecosystems which was not observed (e.g. Figure 6.12). Likewise, the general LAI growth pattern shown in Figure 6.5 (rapid LAI increase until canopy closure, and mild decrease thereafter) is inadequately modelled by 3-PG.

The uncertainty analysis of the model behaviour also assisted in exploring how the data used in the calibration have been informative for reducing model output uncertainty. Given the data available, uncertainty has been reduced for above-ground biomass, but little has been gained from the inclusion of root and foliage data. This suggested that either (i) more data (and of increased accuracy) on these variables, (ii) improved knowledge about the related parameters, or (iii) improvements on 3-PG structure, are required to best describe the data. It appeared from the uncertainty analysis conducted in Chapter 6 that the dynamics of the model are set by the structure of the model much more than by the data. This was shown in Figure 6.12, Figure 6.13, and Figure 6.14 where the model outputs resulting from the calibration with and without data show the same growth dynamics.

Main limitations of process-based models (3-PG) in support of the Protocol

- Parameterisation of the models for specific forest types is required.
- Model intercomparison is necessary for selecting the most appropriate and accurate model given specific national circumstances or ecosystem types.
- The complex non-linear interactions embedded in the model structure render difficult the targeting of specific parameters or algorithms to improve the model dynamics.
- For 3-PG, future research will be required to identify the origins of the root and LAI dynamics for future improvement.

Conclusions D

- **Process-based models enable the quantification of carbon content in pools difficult to quantify otherwise.**
- **The reliability of process-based models must be tested against ground data and other process-based models**

Main limitations of Bayesian calibration in support of the Protocol

- Treating everything in a probabilitic manner within a process-based framework is highly time consuming and computer demanding.
- Defining *a priori* probability distributions for the parameters and variables included in the calibration may be a difficult task. There are no specific guidelines as to whether a normal or beta distribution should be used, or if a uniform distribution is used, how the minimum and maximum boundaries should be assigned.
- The presentation of the results is complex, and requires a good understanding of uncertainty analyses. This may prove difficult if such results are to be presented to policy makers.

Conclusions E

- **Bayesian calibration is a statistical approach that quantifies the uncertainty of a system as a whole.**
- **The statistical approach recognises that knowledge is a flow in continuous process. As knowledge is gained, the parameter distributions are updated.**
- **Bayesian calibration provides estimates of the precision of the model.**
- **Model intercomparison is required to assess the relative accuracy of models.**

7.3 Thesis conclusion

Future emphasis will need to be given to the framework for uniting methods, expertise, data, and systems to conduct truly integrative work, as the logistics of meeting the LULUCF reporting requirements are highly intricate. Whereas the reporting guidelines of emissions arising from sectors other than the LULUCF are covered within a single document (e.g. the energy, industrial or waste sectors, IPCC 2000), reporting guidelines for LULUCF estimates alone are outlined in a collection of lengthy documents (e.g. IPCC 2005, 2006).

In the UK, net emissions from LULUCF contribute less than 1% of the total emissions of CO_2 (data for 1999, Table 1.1). Yet, comparatively to other sectors, the production of LULUCF estimates is among the most costly of all. Sadly, efforts currently spent on reporting LULUCF activities are likely to be made at the expense of addressing the real drivers of climate change.

If LULUCF activities remain a reporting requirement under the next commitment periods, than the reporting complexity and costs should become proportional to the contribution of these activities in terms of GHG emissions. In the UK, educated guess by national and international experts should suffice for the provison of GHG fluxes arising from Article 3.3 and 3.4 activities. Efforts and resources could then be better spent on the development of proficient policies and measures to increase energy efficiency and the nationwide production of renewable energy.

References

Aber, J. D. and Federer, C. A. (1992). A generalized, lumped-parameter model for photosynthesis, evapotranspiration and net primary production in temperate and boreal forest ecosystems. *Oecologia*, **92**: 463-474.

Ahern, F.J., Erdle, T., Maclean, D.A., Kneppeck, I.D. (1991). A quantitative relationship between forest growth-rates and Thematic Mapper reflectance measurements. *International Journal of Remote Sensing*, **12**:387-400.

Ajtay, G.L., Ketner P., Duvigneaud P. (1979). Terrestrial primary production and phytomass. In: Bolin B, Degens E.T., Kempe S., Ketner P. (eds). *The global carbon cycle*. Wiley, Chichester, pp.129-181.

Albrektson, A. (1988). Needle litterfall in stands of Pinus sylvestris L. in Sweden, in relation to site quality, stand age and latitude. *Scandinavian Journal of Forest Research*, **3**: 333-342.

Aldred, A. H. and Bonner, M. (1985). Application of airborne lasers to forest surveys., Petawawa National Forestry Centre, Canadian Forestry Service. 62p.

Almeida, A.C., Landsberg, J.J., Sands, P.J. (2004). Parameterisation of 3-PG model for fast-growing Eucalyptus grandis plantations. *Forest Ecology and Management*, **193**:179-195.

Anderson, J.R., Hardy, E.E., Roach, J.T., Witmer, R.E. (1976). A land use and land cover classification system for use with remote sensor data. *Geological survey paper 964*, United States Geological Survey, Washington, D.C.

Avery, G. S. (1933). Structure and development of the tobacco leaf. *American Journal of Botany*, **20**: 595-592.

Axelsson, P.E. (1999). Processing of laser scanner data - algorithms and applications. *ISPRS Journal of Photogrammetry and Remote Sensing*, **54**:138-147.

Baker, J.R. (1992). The UK element of the Maestro-1 SAR campaign. *International Journal of Remote Sensing*, **13**:1593-1608.

Baker, J. R., P. L. Mitchell, Cordney, R.A., Groom, G. B., Settle, J. J. and Stileman, M. R. (1994). Relationships between physical characteristics and polarimetric radar backscatter for corsican pine stands in Thetford forest, Uk. *International Journal of Remote Sensing*, **15**(14): 2827-2849.

Baskerville, G.L. (1966). Dry matter production in immature Balsam fur stands: roots lesser vegetation and total stand. *Forest Science*, **12** (1): 49-53.

Baltsavias, E. P. (1999). Airborne laser scanning: existing systems and firms and other resources. *Isprs Journal of Photogrammetry and Remote Sensing*, **54**(2-3): 164-198.

Balzter, H. (2001). Forest mapping and monitoring with interferometric synthetic aperture radar (InSAR). *Progress in Physical Geography*, **25**:159-177.

Balzter, H., Skinner, L., Luckman, A.Brooke, R. (2003). Estimation of tree growth in a conifer plantation over 19 years from multi-satellite L-band SAR. *Remote Sensing of Environment*, **84**(2): 184-191.

Barr, C.J., Bunce, R.G.H., Clarke, R.T., Fuller, R.M., Furse, R. T., Gillepsie, M.K., Groom, G.B., Hallam, C.J., Hornung, M., Howard, D.C. and Ness, M.J. (1993). *Countryside survey 1990, main report*. Department of the Environment, London, 174 p.

Battaglia, M., Sands, P.J. (1998). Process-based forest productivity models and their application in forest management. *Forest Ecology and Management*, **102**:13-32.

Bate, R., (1998). *Global Warming. The continuing debate*. Cambridge, The European Science and Environment Forum (ESEF), Cambridge. 231p.

Baulies, X. and Pons, X. (1995). Approach to forestry inventory and mapping by means of multispectral airborne data. *International Journal of Remote Sensing*, **16**:61-80.

Bayer, T., Winter, R., Schreier, G. (1991). Terrain influences in SAR backscatter and attempts to their correction. *IEEE Transactions on Geoscience and Remote Sensing*, **29**:451-462.

Beadle, C.L., Jarvis, P.G., Talbot, H., Neilson, R.E. (1985a). stomatal conductance and photosynthesis in a mature Scots pine forest .2. Dependence on environmental variables of single shoots. *Journal of Applied Ecology*, **22**:573-586.

Beadle, C.L., Neilson, R.E., Talbot, H., Jarvis, P.G. (1985b). stomatal conductance and photosynthesis in a mature Scots pine forest .1. Diurnal, seasonal and spatial variation in shoots. *Journal of Applied Ecology*, **22**:557-571.

Beadle, C.L., Talbot, H., Neilson, R.E., Jarvis, P.G. (1985c). stomatal conductance and photosynthesis in a mature Scots pine forest .3. Variation in canopy conductance and canopy photosynthesis. *Journal of Applied Ecology*, **22**:587-595.

Beadle, C.L., Talbot, H., Jarvis, P.G. (1982). Canopy structure and leaf-area index in a mature Scots pine forest. *Forestry*, **55**:105-123.

Bengtsson, L. and Enell, M. (1986). Chapter 21: Chemical analysis. In *The handbook of Holocene palaeoecology and palaeohydrology*, Berglund, B.E. (ed.). Chichester, John Wiley and Sons Ltd., pp. 423-448.

Bernardo, J. M. and Smith, A. F. M. (1994). *Bayesian theory*. Chichester, John Wiley & Sons Ltd. 586p.

Bird, A.C., Taylor, J.C., Brewer, T.R. (2000). Mapping national park landscape from ground, air and space. *International Journal of Remote Sensing*, **21**:2719-2736.

Birdsley, R.A. (1990). Potential changes in carbon storage through conversion of lands to plantation forests. In *North American conference on forestry response to climate change*. May 15-17, Washington D.C., 446 p.

Blair, J.B., Rabine, D.L., Hofton, M.A. (1999). The laser vegetation imaging sensor: a medium-altitude, digitisation-only, airborne laser altimeter for mapping vegetation and topography. *ISPRS Journal of Photogrammetry and Remote Sensing*, **54**:115-122.

Bolin, B., Sukumar, R., Ciais, P., Cramer, W., Jarvis, P.G., Kheshgi, H., Nobre, C.A., Semenov, S. and Steffen, W. (2000). Global perspective. In: R.T. Watson, Noble, I.R.Bolin, B., Ravindranath, N.H., Verardo, J., Dokken, D.J. (eds), IPCC special report on land use, land-use change, and forestry. Cambridge, Cambridge University Press. 377p.

Bousquet, P., Peylin, P., Ciais, P., Le Quere, C., Friedlingstein, P., Tans, P.P. (2000). Regional changes in carbon dioxide fluxes of land and oceans since 1980. *Science*, **290**:1342-1346.

Brady, N.C. (1990). *The nature and properties of soil* (10th edition). Macmillan, New York, 960 p.

Brandtberg, T., Warner, T.A., Landenberger, R.E, McGraw, J.B. (2003). Detection and analysis of individual leaf-off tree crowns in small footprint, high sampling density Lidar data from the eastern deciduous forest in North America. *Remote Sensing of Environment*, **85** (3): 290-303.

Briggs, B. (2001). Quantification of carbon in a British semi-natural woodland. Undergraduate thesis. *Department of plant Sciences*, University of Oxford, Oxford.

Briggs G.E., Kidd F, West C. (1920). A quantitative analysis of plant growth. II. *Annals of Applied Biology* **7**: 202–223.

Brockhaus, J.A., Khorram, S. (1992). A comparison of Spot and Landsat-TM data for use in conducting inventories of forest resources. *International Journal of Remote Sensing*, **13**:3035-3043.

Brown, J.M.B. (1960). The Corsican pine in its native island, Part 2. *Empire Forestry Review*, **39**: 422-436.

Cannell, M.G.R. (1982). *World forest biomass and primary production data.* London, Academic Press, 391 p.

Cannell, M.G.R., Dewar, R.C. (1995). The carbon sink provided by plantation forests and their products in Britain. *Forestry*, **68**:35-48.

Cannell, M.G.R., Milne, R. (1995). Carbon pools and sequestration in forest ecosystems in Britain. *Forestry*, **68**:361-377.

Cannell, M.G.R., Milne, R., Hargreaves, K.J., Brown, T.A.W., Cruikshank, M.M., Bradley, R.I., Spencer, T., Hope, D., Billett, M.F., Adger, W.N., Subak, S. (1999). National inventories of terrestrial carbon sources and sinks: the UK experience. *Climatic Change*, **42**:505-530.

Cannell, M.G.R. (1999). Growing trees to sequester carbon in the UK: answers to some common questions. *Forestry*, **72** (3): 237-247.

Ciais, P. (1999). Holocene climate - Restless carbon pools. *Nature*, **398**(6723): 111-112.

Cloude, S.R., Papathanassiou, K.P. (1998). Polarimetric SAR interferometry *IEEE Transactions on Geoscience and Remote Sensing*, **36** (5): 1551-1565.

Coleman, K., Jenkinson, D.S. (1996). Roth-C-26.3- A model for turnover of carbon in soil. In: Powlson D.S., Smith P., Smith J.U. (eds). *Evaluation of soil organic matter*

models using existing, long term datasets, Vol. 38. Springer-Verlag, Heidelberg, p 237-246.

Coops, N. C. (1999). Improvement in predicting stand growth of pinus radiata (D. Don) across landscapes using NOAA AVHRR and Landsat MSS Imagery combined with a forest growth model (3-PGS). *Photogrammetric Engineering and Remote Sensing*, **65**(10): 1149-1156.

Coops, N.C., Waring, R.H. (2001). The use of multiscale remote sensing imagery to derive regional estimates of forest growth capacity using 3-PGS. *Remote Sensing of Environment*, **75** (3): 324-334.

Coops, N.C., Waring, R.H., Landsberg, J.J. (1998). Assessing forest productivity in Australia and New Zealand using a physiologically-based model driven with averaged monthly weather data and satellite-derived estimates of canopy photosynthetic capacity. *Forest Ecology and Management*, **104**:113-127.

Coops, N.C., Waring, R.H., Landsberg, J.J. (2001). Estimation of potential forest productivity across the Oregon transect using satellite data and monthly weather records. *International Journal of Remote Sensing*, **22**:3797-3812.

Corbett, W.M. (1973). Breckland forest soils: special survey no.7, Rothamsted Experimental Station, Harpenden, Herts. 120p.

Cousens, J.E. (1988). Report of a 12-year study of litter fall and productivity in a stand of mature Scots pine. *Forestry*, **61**:255-266.

Cramer, W., and Field, C.B. (eds). (1999). The Potsdam NPP model intercomparison, *Global Change Biology*, Vol 5. Blackwell Science, Oxford.

Crampton, A. (1996). Monks wood NNR : an insight into the stand structure and dynamics of an ash-oak woodland. *Department of plant sciences*, University of Oxford. 34p.

Crockford, K.J. (1987). *An evaluation of British woodlands for fuelwood and timber production*. Ph. D. thesis, *Department of Plant Sciences*, University of Oxford. 219 p.

Crowley, T. J. and North, G. R. (1988). Abrupt climate change and extinction events in earth history. *Science*, **240**(4855): 996-1002.

Cruz, F.W., Burns, S.J., Karmann, I., Sharp, W.D., Vuille, M., Cardoso, A.O., Ferrari, J.A., Dias, P.L.S. and Viana, O. (2005). Insolation-driven changes in atmospheric circulation over the past 116,000 years in subtropical Brazil. *Nature*, **434** (7029): 63-66.

Dansgaard, W., Clausen, H.B., Gundestrup, N., Hammer, C.U., Johnsen, S.F., Kristinsdottir, P.M. and Reeh, N. (1982). A new greenland deep ice core. *Science*, **218** (4579): 1273-1277.

Dansgaard, W., Johnsen, S.J., Clausen, H.B., Dahl-Jensen, D., Gundestrup, N.S., Hammer, C.U., Hvidberg, C.S., Steffensen, J.P., Sveinbjornsdottir, A.E., Jouzel, J. and Bond, G. (1993). Evidence for general instability of past climate from a 250-Kyr ice-core record. *Nature*, **364**(6434): 218-220.

Dansgaard, W., White, J.W.C. and Johnsen, S.J. (1989). The abrupt termination of the Younger Dryas climate event. *Nature*, **339**(6225): 532-534.

Danson, F. M. and Curran, P. J. (1993). Factors affecting the remotely sensed response of coniferous forest plantations. *Remote Sensing of Environment*, **43**(1): 55-65.

DEFRA (2001). The UK's Third National Communication under the United Nations Framework Convention on Climate Change. London, DEFRA Publications. 120 p.

Dewar, R. C. (1991). Analytical model of carbon storage in the trees, soils, and wood products of managed forests. *Tree Physiology*, **8**: 239-258.

Dewar, R.C., Cannell, M.G.R. (1992). Carbon sequestration in the trees, products and soils of forest plantations: an analysis using UK examples. *Tree Physiology*, **11**:49-71.

Dobson, M.C., Ulaby, F.T., Letoan, T., Beaudoin, A., Kasischke, E.S., Christensen, N. (1992). Dependence of radar backscatter on coniferous forest biomass. *IEEE Transactions on Geoscience and Remote Sensing*, **30**:412-415.

Dobson, M.C., Ulaby, F.T., Pierce, L.E. (1995a). Land-cover classification and estimation of terrain attributes using synthetic-aperture radar. *Remote Sensing of Environment*, **51**:199-214.

Dobson, M.C., Ulaby, F.T., Pierce, L.E., Sharik, T.L., Bergen, K.M., Kellndorfer, J., Kendra, J.R., Li, E., Lin, Y.C., Nashashibi A., Sarabandi K., Siqueira P. (1995b). Estimation of forest biophysical characteristics in northern Michigan with Sir-C/X-SAR. *IEEE Transactions on Geoscience and Remote Sensing*, **33**:877-895.

Dougherty, P. M., Whitehead, D., Vose, J. M. (1994). Environmental influences on the phenology of pine. *Ecological Bulletins*, **43**: 64-75.

Drake, J.B., Dubayah, R.O., Clark, D.B., Knox, R.G., Blair, J.B., Hofton, M.A., Chazdon, R.L., Weishampel, J.F., Prince, S.D. (2002). Estimation of tropical forest structural characteristics using large-footprint LiDAR. *Remote Sensing of Environment*, **79**:305-319.

Edwards, P.N., Christie, J.M . (1981). Yield models for forest management, *Forestry Commission booklet* no. 48. London, HMSO. 274 p.

Ellison, A.M. (1996). An introduction to Bayesian inference for ecological research and environmental decision-making. *Ecological Application*, **6**: 1036–1046.

Enquist, B.J. and Niklas, K., J. (2001). Invariant scaling across tree-dominated communities. *Nature*, **410**: 655-660.

Erdas Imagine. (2002). *Erdas Fieldguide*. Leica Geosystems GIS and Mapping Division. Atlanta, Georgia. 386p.

Esprey, L.J., Sands, P.J., Smith,C.W. (2004). Understanding 3-PG using a sensitivity analysis. *Forest Ecology and Management*, **193**:235-250.

Evans, G. C. (1972). *The quantitative analysis of plant growth*. Oxford, Blackwell Scientific Publications. 734p.

Ewel, K.C., Gholz, H.L. (1991). A simulation-model of the role of belowground dynamics in a Florida pine plantation. *Forest Science*, **37**:397-438

Falloon, P., Smith, P., Szabo, J., Pasztor, L. (2002). Comparison of approaches for estimating carbon sequestration at the regional scale. *Soil Use and Management*, **18**:164-174.

Fazakas, Z., Nilsson, M., Olsson, H. (1999). Regional forest biomass and wood volume estimation using satellite data and ancillary data. *Agricultural and Forest Meteorology*, **98-99**:417-425.

Fehse, J., Hofstede, R., Aguirre, N., Paladines, C., Kooijman, A. and Sevink, J. (2002). High altitude tropical secondary forests: a competitive carbon sink? *Forest Ecology and Management*, **163**(1-3): 9-25.

Finer, L. (1996). Variation in the amount and quality of litterfall in a Pinus sylvestris L stand growing on a bog. *Forest Ecology and Management*, **80**(1-3): 1-11.

Flood, M., Gutelius, B. (1997). Commercial implications of topographic terrain mapping using scanning airborne laser radar. *Photogrammetric Engineering and Remote Sensing*, **63**:327-29, 363-66.

Flower-Ellis, J.G.K., Olsson, L. (1993). Estimation of volume, total and projected area of Scots pine needles from their regression on lenght. *Studia Forestalia Suecica*, **190**:1-19.

Forest Research. (2001). Woodfuel Resource: study into the potentially available woodfuel resource of Great Britain http://www.woodfuelresource.org.uk/, UK.

Forestry Commission. (2000). GIS database, Forestry Commission. Thetford.

Forestry Commission. (2001). National inventory of woodlands and trees. Report No. http://www.forestry.gov.uk/forestry/HCOU-54PG9U, Edinburgh, Forest Research, Forestry Commission.

Forestry Commission. (2002a). Forestry facts and figures 2002: a summary of statistics about woodland and forestry in Great Britain. http://www.forestry.gov.uk/website/pdf.nsf/pdf/fff2002.pdf/$FILE/fff2002.pdf Forestry Commission, Edinburgh, UK.

Forestry Commission. (2002b). Forestry statistics 2002, a compendium of statistics about woodland, forestry and primary wood processing in the United Kingdom. http://www.forestry.gov.uk/website/pdf.nsf/pdf/forestrystatistics2002.pdf/$FILE/forestrystatistics2002.pdf, Forestry Commission, Edinburgh, UK.

Franklin, J., Logan, T.L., Woodcock, C.E., Strahler, A.H. (1986). Coniferous forest classification and inventory using Landsat and digital terrain data. *IEEE Transactions on Geoscience and Remote Sensing*, **24**:139-149.

Fransson, J.E.S., Israelsson, H. (1999). Estimation of stem volume in boreal forests using ERS-1 C- and JERS-1 L-band SAR data. *International Journal of Remote Sensing*, **20**:123-137.

Fransson, J.E.S., Walter, F., Ulander, L.M.H. (2000). Estimation of forest parameters using CARABAS-II VHFSAR data. *IEEE Transactions on Geoscience and Remote Sensing*, **38**:720-727.

Fuller, R.M., Groom, G.B., Jones, A.R. (1994). The land-cover map of Great-Britain - an automated classification of Landsat Thematic Mapper data. *Photogrammetric Engineering and Remote Sensing*, **60**:553-562.

Fuller, R.M., Smith, G.M., Devereux, B.J. (2003). The characterization and measurement of land cover change through remote sensing: problems in operational applications? *International Journal of Applied Earth Observation and Geoinformation*, **4**:243-253.

Fuller, R.M., Smith, G.M., Sanderson, J.M., Hill, R.A., Thomson A.G. (2002). The UK Land Cover Map 2000: construction of a parcel-based vector map from satellite images. *Cartographic Journal*, **39**:15-25.

Garmin Corporation. (1997). GPS 12XL personal navigator: Owners manual and reference. GARMIN (Europe) Ltd., Hampshire, UK. 58p.

Gash, J.H.C., Shuttleworth, W.J., Lloyd, C.R., Andre, J.C., Goutorbe, J.P., Gelpe, J. (1989). Micrometeorological Measurements in Les-Landes Forest During Hapex-Mobilhy. *Agricultural and Forest Meteorology*, **46**:131-147.

Gaveau D.L.A., Hill R.A. (2003). Quantifying canopy height underestimation by laser pulse penetration in small-footprint airborne laser scanning data. *Canadian Journal of Remote Sensing*, **29**:650-657.

Gertner, G.Z., Fang, S.F., Skovsgaard, J.P. (1999). A Bayesian approach for estimating the parameters of a forest process model based on long-term growth data. *Ecological Modelling*, **119**:249-265.

Ghazoul, J., McAllister, M. (2003). Communicating complexity and uncertainty in decision making contexts: Bayesian approaches to forest research. *International Forestry Review*, **5**:9-19.

Gholz, H.L., Nakane, K., Shimoda, H. (1997). *The use of remote sensing in the modeling of forest productivity*. Dordrecht, Netherlands. Kluwer Academic Publishers. 323p.

Gill, R.A., Jackson, R.B. (2000). Global patterns of root turnover for terrestrial ecosystems. *New Phytologist*, **147**:13-31.

Gobron, N., Pinty, B., Verstraete, M.M., Widlowski, J.L. (2000). Advanced vegetation indices optimized for up-coming sensors: design, performance and applications. *IEEE Transactions on Geoscience and Remote Sensing*, **38**:2489-2505.

Goel, N. S. and Norman, J. M. (1992). Biospheric models, measurments and remote sensing of vegetation. *ISPRS Journal of Photogrammetry and Remote Sensing*, **47**: 163-188.

Goetz, A. F. H., Vane, G. Solomon, J. E., Rock, B. N. (1985). *Imaging Spectrometry for Earth Remote-Sensing*, *Science* **228**(4704): 1147-1153.

Goetz, S. J. and Prince, S. D. (1996). Remote sensing of net primary production in boreal forest stands, *Agricultural and Forest Meteorology*, **78**: 149-179.

Gong, P., Pu, R. L. Biging, G. S., Larrieu, M. R. (2003). Estimation of forest leaf area index using vegetation indices derived from Hyperion hyperspectral data. *Ieee Transactions on Geoscience and Remote Sensing*, **41**(6): 1355-1362.

Gower, S. T., Gholz, H. L., Kaneyuki, N., Clark, B. V. (1994). Production and carbon allocation patterns of pine forests. *Ecological Bulletins*, **43**: 115-135.

Granier, A., Biron, P., Breda, N., Pontailler, J.Y., Saugier, B. (1996). Transpiration of trees and forest stands: Short and longterm monitoring using sapflow methods. *Global Change Biology*, **2**:265-274.

Grace, J., Lewis, P. and Quaife, T. (2004). Estimating land cover specific Carbon fluxes from Flux Tower measurements and Earth Observation data. In: R. Milne and D.C. Mobbs (eds), *UK Emissions by Sources and Removals by Sinks due to Land Use, Land Use Change and Forestry Activities*. Edinburgh, DEFRA Contract CEPG 1/GA01054CEH No. C02275.

Green, E.J., MacFarlane, D.W., Valentine, H.T. (2000). Bayesian synthesis for quantifying uncertainty in predictions from process models. *Tree Physiology*, **20**:415-419.

Green, E.J., MacFarlane, D.W., Valentine, H.T., Strawderman, W.E. (1999). Assessing uncertainty in a stand growth model by Bayesian synthesis. *Forest Science*, **45**:528-538.

Greig, B.J.W. (1987). History of *Peridermium* stem rust of scots pine in Thetford forest, East Anglia. *Forestry*, **60**: 193-202.

Guyot, G., Guyon, D., Riom, J. (1989). Factors affecting the spectral response of forest canopies: a review. *Geocarto International*, **4**:3–18.

Hamilton, G.J. (1975) *Forest mensuration handbook. Forestry Commission Booklet*, No. **39**. London ,H.S.M.O. 274 p.

Hamilton, G.J., and Christie, J.M.. (1971). Forest Management Tables (Metric). Forestry Commission Booklet: **34**. London, England.

Hill R.A., Hinsley S.A., Bellamy P.E., Baltzer H. (2003). Ecological applications of airborne laser scanner data: woodland bird habitat modelling. *Scandlaser conference proceedings, Umeå, Sweden*. 78-87 p.

Hinsley, S.A., Hill, R.A., Gaveau, D.L.A., Bellamy, P.E. (2002). Quantifying woodland structure and habitat quality for birds using airborne laser scanning. *Functional Ecology*, **16**:851-857.

Hodge, C.A.H., Seale, R.S. and Burton, R.G.O. (1973). Geology and soils. In *Monks Wood, a nature reserve record.* Steele, R.C. and Welch, R.C. (eds.). The Nature Conservancy. Huntingdon. 4-16 p.

Hoekman, D.H., Quinones, M.J. (2000). Land cover type and biomass classification using AirSAR data for evaluation of monitoring scenarios in the Colombian Amazon. *IEEE Transactions on Geoscience and Remote Sensing*, **38**:685-696.

Holmgren, P., Thuresson, T. (1998). Satellite remote sensing for forestry planning - A review. *Scandinavian Journal of Forest Research*, **13**:90-110.

Houghton, J. (2004). *Global warming the complete briefing Global Warming -The Complete Briefing* (3rd edition) John T. Houghton (ed). Cambridge, Cambridge University Press. 351p.

Houghton, J.T., Ding, Y., Griggs, D.J., Noguer, M., van der Linden, P.J., Xiaosu, D., Maskell, K., Johnson, C.A. (eds). (2001). *Climate Change 2001: The Scientific Basis. Contribution of Working Group I to the Third Assessment Report of the Intergovernmental Panel on Climate Change*. Cambridge, Cambridge University Press. 944 p.

Houghton, R.A. and Skole, D., L. (1990). Carbon. In: B.L. Turner (eds), *The Earth as transformed by human action : global and regional changes in the biosphere over the past 300 years*. Cambridge, Cambridge University Press with Clark University. 393-408 p.

Howard, P. J. A., Loveland, P. J., Bradley, R. I., Dry, F.T., Howard, D.M., Howard, D.C. (1995). The carbon distribution of soil and its geographical distribution in Great Britain. *Soil Use and Management*, **11**: 9-15.

Huete, A.R. (1988). A Soil-Adjusted Vegetation Index (SAVI). *Remote Sensing of Environment*, **25**:295-309.

Hyyppä J., Hyyppä H., Inkinen M., Schardt M., Ziegler M. (2000). Forest inventory based on laser scanning and aerial photography. *Laser Radar Technology and Applications*, **V**:106-118.

Hyyppä, J., Kelle, O., Lehikoinen, M., Inkinen, M. A (2001). segmentation-based method to retrieve stem volume estimates from 3-D tree height models produced by laser scanners. *IEEE Transactions on Geoscience and Remote Sensing*, **39** (5): 969-975.

Imhoff, M.L. (1995). Radar Backscatter and Biomass Saturation - Ramifications for Global Biomass Inventory. *IEEE Transactions on Geoscience and Remote Sensing*, **33**:511-518.

IPCC. (1997a). *IPCC Revised 1996 guidelines for national greenhouse gas inventories, Volume 1, Greenhouse Gas Inventory Reporting Instructions*, IPCC WGI Technical Support Unit, Hadley Centre, Meteorological Office, Bracknell, UK.

IPCC.(1997b). *IPCC Revised 1996 guidelines for national greenhouse gas inventories, Volume 2, Greenhouse Gas Inventory Workbook*, IPCC WGI Technical Support Unit, Hadley Centre, Meteorological Office, Bracknell, UK.

IPCC. (1997c). *IPCC Revised 1996 guidelines for national greenhouse gas inventories, Volume 3, Greenhouse Gas Inventory Reference Manual*, IPCC WGI Technical Support Unit, Hadley Centre, Meteorological Office, Bracknell, UK.

IPCC. (2000). *Good practice and uncertainty management in national greenhouse gas inventories*. IPCC Technical Support Unit, IGES, Kanagawa, Japan.

IPCC. (2003). *IPCC Good Practice Guidance for Land Use, Land-Use Change and Forestry*, http://www.ipccnggip.iges.or.jp/public/gpglulucf/gpglulucf_contents.htm Institute for Global Environmental Strategies, Japan.

Jansen, M.J.W. (1999). Data use and Bayesian statistics for model calibration. In: Stein A., Penning de Vries F.W.T. (eds). *Data and models in action*. Kluwer, Dordrecht, p 69-80.

Jansen, M.J.W. and Hagenaars, T.J. (2004). Calibration in a Bayesian modelling framework. In: M.A.J.S. van Boekel, A. Stein and A.H.C. van Bruggen (eds), *Bayesian statistics and quality modelling in the agro-food production chain*. Kluwer, Dordrecht. 47-55 p.

Jinks, R. L. and Kerr, G. (1999). Establishment and early growth of different plant types of Corsican pine (Pinus nigra var. maritima) on four sites in Thetford Forest. *Forestry*, **72**(4): 293-304.

Jordan, C.F. (1969). Derivation of leaf-area index from quality of light on the forest floor. *Ecology*, **50**:663-666.

Jordan, C. F. (1971). Productivity of a tropical forest and its relation to a world pattern of energy storage. *Journal of Ecology*, **59**: 127-142.

Kasischke, E.S., Melack, J.M., Dobson, M.C. (1997). The use of imaging radars for ecological applications - A review. *Remote Sensing of Environment*, **59**:141-156.

Keeling, C.D. and Whorf, T.P. (1999). Atmospheric CO2 records from sites in the SIO air sampling network. In: T.A. Boden (eds), *Trends: a compendium of data on global change*. Carbon Dioxide Information Analysis Centre. Oak Ridge, Oak Ridge National Laboratory. 984 p.

Kelliher, F.M., Leuning, R., Raupach, M.R., Schulze, E.D. (1995). Maximum Conductances for Evaporation from Global Vegetation Types. *Agricultural and Forest Meteorology*, **73**:1-16.

Kelliher, F.M., Leuning, R., Schulze, E.D. (1993). Evaporation and Canopy Characteristics of Coniferous Forests and Grasslands. *Oecologia*. **95**:153-163.

Kerr, G. (2000). Natural regeneration of Corsican pine (Pinus nigra subsp laricio) in Great Britain. *Forestry*, **73**(5): 479-488.

Kilian, J., Haala, N., Englich, M. (1996). Capture and evaluation of airborne laser scanner data. *International Archives of Photogrammetry and Remote Sensing*, **53**:193-203.

Krabill, W. B., Collings, J. G., Swift, R.N., Butler, M.L. (1980). Airborne laser topographic mapping results from Initial Joint NASA/U.S. Army Corps of Engineers Experiment, Wallops Flight Centre.

Kraenzel, M., Castillo, A., Moore, T. and Potvin, C. (2003). Carbon storage of harvest-age teak (Tectona grandis) plantations, Panama. *Forest Ecology and Management*, **173**(1-3): 213-225.

Kumar, M. and Monteith, J. L. (1982). Remote sensing of plant growth. In *Plants and the Daylight Spectrum*, H. Smith (ed). London, Academic Press. 133-144 p.

Landsberg, J.J., Waring, R.H. (1997). A generalised model of forest productivity using simplified concepts of radiation-use efficiency, carbon balance and partitioning. *Forest Ecology and Management*, **95**:209-228.

Landsberg, J. J., Waring, R. H., Coops, N. C. (2003). Performance of the forest productivity model 3-PG applied to a wide range of forest types. *Forest Ecology and Management* **172**: 199-214.

Law, B.E., Waring, R.H., Anthoni, P.M., Aber, J.D. (2000). Measurements of gross and net ecosystem productivity and water vapour exchange of a *Pinus ponderosa* ecosystem, and an evaluation of two generalized models. *Global Change Biology*, **6**:155-168.

Lee, J.S., Cloude, S.R., Papathanassiou, K.P., Grunes, M.R., Woodhouse, I.H. (2003). Speckle filtering and coherence estimation of polarimetric SAR interferometry data for forest applications. *IEEE Transactions on Geoscience and Remote Sensing*, **41** (10): 2254-2263.

Lee, K. S., Cohen, W. B., Kennedy, R. E., Maiersperger, T. K., Gower, S. T. (2004). Hyperspectral versus multispectral data for estimating leaf area index in four different biomes. *Remote Sensing of Environment*, **91**(3-4): 508-520.

Lefsky, M.A., Cohen, W.B., Acker, S.A., Parker, G.G., Spies T.A., Harding D. (1999a). LiDAR remote sensing of the canopy structure and biophysical properties of Douglas-fir western hemlock forests. *Remote Sensing of Environm*ent, **70**:339-361.

Lefsky, M.A., Harding, D., Cohen, W.B., Parker, G., Shugart, H.H. (1999b). Surface LiDAR remote sensing of basal area and biomass in deciduous forests of eastern Maryland, USA. *Remote Sensing of Environment*, **67**:83-98.

Lefsky, M.A., Cohen, W.B., Acker, S.A., Spies, T.A., Parker, G.G., Harding, D. (1997). LiDAR remote sensing of forest canopy structure and related biochemical parameters at the H.J. Andrews experimental forest, Oregon, USA. In: Greer J.D. (ed) *Natural resources management using remote sensing and GIS*. ASPRS, Washington, D.C., p 79-91.

Lefsky, M.A., Cohen, W.B., Parker, G.G., Harding, D.J. (2002). LiDAR remote sensing for ecosystem studies. *Bioscience*, **52**:19-30.

Lehtonen, A., Makipaa, R., Heikkinen, J.Sievanen, R., Liski, J. (2004). Biomass expansion factors (BEFs) for Scots pine, Norway spruce and birch according to stand age for boreal forests. *Forest Ecology and Management*, **188**(1-3): 211-224.

Levy, P., Milne, R. (2004). Estimation of GB deforestation rates. *Forestry*, **77**:9-16.

Levy, P.E., Hale, S.E., Nicol,l B.C. (2004). Biomass expansion factors and root: shoot ratios for coniferous tree species in Great Britain. *Forestry*, **77**(5): 421-430.

Lillesand, T.M and Kiefer, R.W. (2000). *Remote Sensing and Image Interpretation*. The 4th Edition. New York, John Willey and Sons. 724 p.

Lim, K., Treitz, P., Wulder, M., St-Onge, B., Flood, M. (2003). LiDAR remote sensing of forest structure. *Progress in Physical Geography*, **27**:88-106.

Locke, G.M.L. (1987). *Census of woodlands and trees 1979-82. Forestry Commission,* Bulletin **63**. London H.S.M.O.

Luckman, A., Baker, J., Kuplich, T.M., Yanasse, C.D.F., Frery, A.C. (1997). A study of the relationship between radar backscatter and regenerating tropical forest biomass for spaceborne SAR instruments. *Remote Sensing of Environment*, **60**:1-13.

Luckman, A., Baker, J., Honzak, M., Lucas ,R. (1998). Tropical forest biomass density estimation using JERS-1 SAR: Seasonal variation, confidence limits, and application to image mosaics. *Remote Sensing of Environment*, **63**:126-139.

Lucas, N. S. and Curran, P. J. (1999). Forest ecosystem simulation: the role of remote sensing. *Progress in Physical Geography*, **23**(3): 391-423.

Magnussen, S., Boudewyn, P. (1998). Derivations of stand heights from airborne laser scanner data with canopy-based quantile estimators. *Canadian Journal of Forest Research-Revue canadienne de recherche forestière*, **28**:1016-1031.

Magnussen, S., Eggermont, P., LaRiccia, V.N. (1999). Recovering tree heights from airborne laser scanner data. *Forest Science*, **45**:407-422.

Malhi, Y., Baker, T. R., Phillips, O. L., Almeida, S.,Alvarez, E., Arroyo, L., Chave, J., Czimczik, C. I., Di Fiore, A., Higuchi, N., Killeen, T. J., Laurance, S. G., Laurance, W. F., Lewis, S. L., Montoya, L. M. M., Monteagudo, A., Neill, D. A., Vargas, P. N., Patino, S., Pitman, N. C. A., Quesada, C. A., Salomao, R., Silva, J. N. M., Lezama, A. T., Martinez, R. V., Terborgh, J., Vinceti, B. Lloyd, J. (2004). The above-ground coarse wood productivity of 104 Neotropical forest plots. *Global Change Biology*, **10**(5): 563-591.

Malhi, Y., Baldocchi, D.D. and Jarvis, P.G. (1999). The carbon balance of tropical, temperate and boreal forests. *Plant Cell and Environment*, **22**(6): 715-740.

Martrat, B., Grimalt, J.O., Lopez-Martinez, C., Cacho, I., Sierro, F.J., Flores, J.A., Zahn, R., Canals, M., Curtis, J.H. and Hodell, D.A. (2004). Abrupt temperature changes in the Western Mediterranean over the past 250,000 years. *Science*, **306**(5702): 1762-1765.

Matthews, G. A.R. (1993). The Carbon Content of Trees. *Forestry Commission Technical Paper,* no. **4**. Forestry Commission, HSMO, London, 22 p.

Matthews, R. W. and Broadmeadow, M. S. J. (2003). UK emissions by sources and removals by sinks due to land use, land use change and forestry activities: section 10 survey methods for Kyoto Protocol monitoring and verification of UK forest carbon stocks. DEFRA Contract EPG1/1/160, CEH No. C01504, http://www.nbu.ac.uk/ukcarbon/, Edinburgh, Department for the Environment, Food and Rural Affairs, Global Atmosphere Division.

McCarthy, J. J., Canziani, O. F., Leary, N.A., Dokken, D. J. and White, K.S. (eds). (2001). *Climate change 2001: Impacts, adaptation and vulnerability.* Cambridge, Cambridge University Press. 1032p.

McMurtrie, R. E., Rook, D. A., and Kelliher, F.M. (1990). Modelling the yield of *Pinus radiata* on a site limited by water and nitrogen. *Forest Ecology and Management*, **30**: 381-413.

McMurtrie, R. E., Leuning, R., Thompson, W. A., and Wheeler, A. M. (1992). A model of canopy photosynthesis and water use incorporating a mechanistic formulation of leaf CO2 exchange. *Forest Ecology and Management*, **52**: 261-278.

Means, J.E., Acker, S.A., Fitt, B.J., Renslow, M., Emerson, L., Hendrix, C.J. (2000). Predicting forest stand characteristics with airborne scanning LiDAR. *Photogrammetric Engineering and Remote Sensing*, **66**:1367-1371.

Means, J.E., Acker, S.A., Harding, D.J., Blair, J.B., Lefsky, M.A., Cohen, W.B., Harmon, M.E., McKee, W.A. (1999). Use of large-footprint scanning airborne LiDAR to estimate forest stand characteristics in the western Cascades of Oregon. *Remote Sensing of Environment*, **67**:298-308.

Mencuccini, M., Grace, J. (1996). Hydraulic conductance, light interception and needle nutrient concentration in Scots pine stands and their relations with net primary productivity. *Tree Physiology*, **16**:459-468.

Milne, R. (1992). The carbon content of vegetation and its geographical distribution in Great Britain. In *Carbon sequestration by vegetation in the UK*. Interim report to the Department of the Environment, Contract No. PECD 7/12/79, Midlothian, 107 p.

Milne, R. and Brown, T.A. (1997). Carbon in vegetation and soils of Great Britain. *Journal of Environmental Management*, **49**:413-433.

Milne, R., Brown, A.W. and Murray, T.D. (1998). The effect of geographical variation of planting rate on the uptake of carbon by new forests of Great Britain. *Forestry*, **71**:297-309.

Milne, R. and Brown, T.A. (2000). Mapping of carbon pools in the vegetation and soils of Great Britain. In *Vegetation mapping: from patch to planet*. R. Alexander and A.C. Millington (eds.). Chichester, John Wiley & Sons Ltd. 330 p.

Milne, R., Brown, T.A. (2003). *UK emissions by sources and removals by sinks due to land use, land use change and forestry activities: Section 6, mapping carbon fluxes for British afforestation and land use change*. DEFRA Contract EPG1/1/160, CEH No. C01504, http://www.nbu.ac.uk/ukcarbon/, Edinburgh, Department for the Environment, Food and Rural Affairs, Global Atmosphere Division.

Milne, R., Tomlinson, R.W., Murray, T.D. (2003). *UK emissions by sources and removals by sinks due to land use, land use change and forestry activities: Section 2, Land Use Change and Forestry, the 2001 greenhouse gas inventory and projections to 2020*. DEFRA Contract EPG1/1/160, CEH No. C01504, http://www.nbu.ac.uk/ukcarbon/, Department for the Environment, Food and Rural Affairs, Global Atmosphere Division, Edinburgh.

Myneni, R. B. and Williams, D. L. (1994). On the relationship between FPAR and NDVI. *Remote Sensing of Environment*, **49**: 200-211.

Myneni, R. B., Hall, F. G., Sellers, P. J., & Marshak, A. L. (1995). The interpretation of spectral vegetation indexes. *IEEE Transactions on Geoscience and Remote Sensing*, **33**(2), 481-486.

Naesset, E. (1997a). Determination of mean tree height of forest stands using airborne laser scanner data. *ISPRS Journal of Photogrammetry and Remote Sensing*, **52**:49-56.

Naesset, E. (1997b). Estimating timber volume of forest stands using airborne laser scanner data. *Remote Sensing of Environment*, **61**:246-253.

Naesset, E. (2002). Predicting forest stand characteristics with airborne scanning laser using a practical two-stage procedure and field data. *Remote Sensing of Environment*, **80**:88-99.

Naesset, E., Okland, T. (2002). Estimating tree height and tree crown properties using airborne scanning laser in a boreal nature reserve. *Remote Sensing of Environment*, **79**:105-115.

Nelson, R., Krabill W., Tonelli, J. (1988a). Estimating forest biomass and volume using airborne laser data. *Remote Sensing of Environment*, **24**:247-267.

Nelson, R., Swift, R., Krabill, W. (1988b). Using airborne lasers to estimate forest canopy and stand characteristics. *Journal of Forestry*, **86**:31-38.

Nelson, R., Jimenez, J., Schnell, C.E., Hartshorn, G.S., Gregoire, T.G., Oderwald, R. (2000). Canopy height models and airborne lasers to estimate forest biomass: two problems. *International Journal of Remote Sensing*, **21**:2153-2162.

Nelson, R., Valenti, M.A., Short, A., Keller, C. (2003) A multiple resource inventory of Delaware using airborne laser data. *Bioscience*, **53**:981-992.

New, M., Hulme, M. and Jones, P. (2000). Representing twentieth-centurey space-time climate variability. Part II: Development of 1901-96 monthly grids of terrestrial surface climate. *Journal of Climate*, **13**(13):2217-2238.

Nilsson, M. (1996). Estimation of tree heights and stand volume using an airborne LiDAR system. *Remote Sensing of Environment*, **56**:1-7.

Norby, R. J., Wullschleger, S. D., Gunderson, C. A., Johnson, D. W., Ceulemans, R. (1999). Tree responses to rising CO2 in field experiments: implications for the future forest. *Plant Cell and Environment*, **22**(6): 683-714.

Northern Ireland Department of Agriculture .(2002). Forestry facts and figures 2001/02. http://www.dardni.gov.uk/frames/forest06.htm

Nuesch, D.R., Kasischke, E.S. (1989). Imaging radar fundamentals. In: *Applications of Remote Sensing to Agrometeorology*, F, Toselli (ed). Dordrecht, The Netherlands, Kluwer Academic Publishers, , p 157-180.

Omasa, K., Qiu, G.Y., Watanuki, K., Yoshimi, K., Akiyama, Y. (2003). Accurate estimation of forest carbon stocks by 3-D remote sensing of individual trees. *Environmental Science* and *Technology*, **37**:1198-1201.

Ovington, J.D. (1957). Dry-matter production by *Pinus sylvestris* L. *Annals of Botany*, **XXI**:288-314.

Pairman, D., Belliss, S.E., McNeill, S.J. (1997). Terrain influences on SAR backscatter around Mt Taranaki, New Zealand. *IEEE Transactions on Geoscience and Remote Sensing*, **35**:924-932.

Patenaude G.L., Briggs, B.D.J., Milne, R., Rowland, C.S., Dawson, T.P., Pryor, S.N. (2003). The carbon pool in a British semi-natural woodland. *Forestry*, **76**:109-119.

Patenaude, G., Hill, R.A., Milne, R., Gaveau, D.L.A., Briggs, B.B.J., Dawson, T.P. (2004). Quantifying forest above ground carbon content using LiDAR remote sensing. *Remote Sensing of Environment*, **93**: 368-380.

Persson, A., Holmgren, J., Soderman, U. (2002). Detecting and measuring individual trees using an airborne laser scanner. *Photogrammetric Engineering And Remote Sensing*, **68** (9): 925-932.

Pfister, C., Luterbacher, J., Schwarz-Zanetti, G., Wegmann, M. (1998). Winter air temperature variations in Centreal Europe during the Early and High Midle Ages (A.D. 750-1300). *Holocene*, **8** (5): 535-552.

Pierce, L.E., Ulaby, F.T., Sarabandi, K., Dobson, M.C. (1994). Knowledge-based classification of polarimetric SAR images. *IEEE Transactions on Geoscience and Remote Sensing*, **32**:1081-1086.

Porcello, L.J., Massey, N.G., Innes R.B., Marks, J.M. (1976). Speckle reduction in synthetic radars. *Journal of the Optical Society of America*, **66**:1305-1311.

Prentice, I.C., Farquhar, G.D., Fasham, M.J.R., Goulden, M.L., Heimann, M., Jaramillo, V.J., Keshgi, H.S., Le Quere, C., Shcoles, R.J. and Wallace, D.W.R. (2001). The carbon cycle and atmospheric carbon dioxide. In: Climate Change 2001: *The Scientific Basis*. Contribution of Working Group I to the Third Assessment Report of the Intergovernmental Panel on Climate Change, J.T. Houghton et al. (eds). Cambridge, Cambridge University Press. 183-237 pp.

Prince, S. D. and Goward, S. N. (1995).Global Primary production: a remote sensing approach. *Journal of Biogeography*, **22**: 815-835.

Pu, R. L., Gong, P., Biging, G. S., Larrieu, M. R (2003). Extraction of red edge optical parameters from Hyperion data for estimation of forest leaf area index. *Ieee Transactions on Geoscience and Remote Sensing*, **41**(4): 916-921.

Pu, R.L. and Gong, P. (2004). Wavelet transform applied to EO-1 hyperspectral data for forest LAI and crown closure mapping. *Remote Sensing of Environment*, **91**(2): 212-224.

Ranson, K.J., Saatchi, S., Sun, G.Q. (1995). Boreal Forest Ecosystem Characterization with Sir-C/X Sar. *IEEE Transactions on Geoscience and Remote Sensing*, **33**:867-876.

Ranson, K.J., Sun, G.Q. (1994). Mapping biomass of a northern forest using multifrequency SAR data. *IEEE Transactions on Geoscience and Remote Sensing*, **32**:388-396.

Rayner, P.J., Enting, I.G., Francey, R.J., Langenfelds, R. (1999). Reconstructing the recent carbon cycle from atmospheric CO_2, delta C-13 and O-2/N-2 observations. *Tellus Series B-Chemical and Physical* Meteorology, **51**:213-232.

Reginal, I.S, Tarazona, T. and Calvo, R. aboveground biomass in a Beech forest and a Scots pine plantation in the sierra de la Demanda area of northern Spain. *Annales des Sciences Forestières*, **54**:261-269.

Ripple W.J., Wang S., Isaacson D.L., Paine D.P. (1991). A preliminary comparison of Landsat Thematic Mapper and Spot-1 HRV multispectral data for estimating coniferous forest volume. *International Journal of Remote Sensing*, **12**:1971-1977.

Roberts, J.M. (1976). A study of root distribution and growth in a Pinus sylvestris L. (scots pine) plantation in East Anglia. *Plant and Soil*, **44**:607-621.

Rosenqvist, A., Milne, A., Lucas, R., Imhoff, M., Dobson, C. (2003). A review of remote sensing technology in support of the Kyoto Protocol. *Environmental Science & Policy*, **6**:441-455.

Rouse, J.W., Haas, R.H., Deering, D.W., Schell, J.A., Harlan, J.C. (1974). *Monitoring the vernal advancement of retrogradation of natural vegetation*, Type III, Final Report, NASA/GSFC, Greenbelt, MD.

Rowell, D. L. (1994). *Soil science methods and applications*. Edinburgh, Prentice Hall. 350p.

Running, S.W., Coughlan, J.C. (1988). A general model of forest ecosystem processes for regional applications I. Hydrological balance canopy gas exchange and primary production processes. *Ecological Modelling*, **42**:125-154.

Running, S.W., Gower, S.T. (1991). Forest-BGC, a general-model of forest ecosystem processes for regional applications .2. Dynamic carbon allocation and nitrogen budgets. *Tree Physiology*, **9**:147-160.

Ruppert, G.S., Wimmer, A., Beichel, R., Ziegel, M. (2000). Adaptive multiresolution algorithm for high precision forest floor DTM generation. In: Kamerman U.N., Singh T.P., Werner C., Molebny V.V. (eds). *Laser radar technology and applications V.* Proceedings of SPIE. 97-105 pp.

Salajanu, D., Olson, C.E. (2001). The significance of spatial resolution - Identifying forest cover from satellite data. *Journal of Forestry*, **99**:32-38.

Salway, A.G., Murrells, T.P., Milne, R. and Ellis, S. (2001). *UK Greenhouse Gas Inventory. 1990 to 1999 Annual Report for submission under Framework Convention on Climate Change*. National Environmental Technology Centre. AEA Technology Centre, Oxon.

Sands, P.J. (2004). Adaptation of 3-PG to novel species : guidelines for data collection and parameter assignment. *Technical Report. No. 141*, CSIRO, CRC Sustainable Production Forestry, Hobart.

Sands, P.J., Landsberg, J.J. (2002). Parameterisation of 3-PG for plantation grown Eucalyptus globulus. *Forest Ecology and Management*, **163**:273-292.

Satchell, J.E. (1971). Feasibility study. In *Productivity of forest ecosystems: proceedings of the Brussels symposium organised by the UNESCO and the International Biological Programme.* 27-31 October 1969, Brussels. UNESCO, Paris, pp 619-630.

Satoo, T. & Madgwick, H.A.I. (1982). *Forest Biomass*. Martinus Nijhoff/Dr W. Junk Publishers, 155p.

Saxe, H., Ellsworth, D.S. and Heath, J., (1998). Tree and forest functioning in an enriched CO2 atmosphere. *New Phytologist*, **139**(3): 395-436.

Schimel, D., Melillo, J., Tian, H.Q., McGuire, A.D., Kicklighter, D., Kittel, T., Rosenbloom, N., Running, S., Thornton, P., Ojima, D., Parton, W., Kelly, R., Sykes,

M., Neilson, R. and Rizzo, B. (2000). Contribution of increasing CO2 and climate to carbon storage by ecosystems in the United States. *Science*, **287**(5460): 2004-2006.

Schlesinger, W.H., 1997. Biogeochemistry : an analysis of global change. San Diego ; London, Academic Press. 588 p.

Schoettle, A. W. and Fahey, T. J. (1994). Foliage and fine root longevity of pines. *Ecological Bulletins* **43**: 136-153.

Sellers, P. J. (1985). Canopy reflectance, photosynthesis and transpiration. *International Journal of Remote Sensing*, **6**(8): 1335-1372.

Sellers, P. J. (1987). Canopy reflectance, photosynthesis and transpiration. II. the role of biophysics in the linearity of their interdependance. *Remote Sensing of Environment*, **21**: 143-183.

Sellers, P. J. (1989). Vegetation-canopy spectral reflectance and biophysical properties. *Theory and Applications of Optical Remote Sensing*. G. Asrar. New York, Wiley and Sons.

Shaw, D. T., Malthus, T. J., Kupiec, J. A. (1998). High-spectral resolution data for monitoring Scots pine (Pinus sylvestris L.) regeneration. *International Journal of Remote Sensing*, **19**(13): 2601-2608.

Sivia, D. S. (1996). *Data analysis: a Bayesian tutorial*. New York, Oxford University Press. 189p.

Skinner, L. (2002). *Estimating forest parameters from Synthetic Aperture Radar: A case study of Thetford forest*. Ph.D. thesis, *Department of Geography*, University of Wales.

Skinner, L., Luckman, A. (2000). Thetford forest ground data collection campaign in support of the SHAC SAR aquisition, June 2000, University of Wales Swansea, Swansea, Unpublished report. 34p.

Smith, P. (2001). Verifying Sinks under the Kyoto Protocol. http://www.vertic.org/assets/breifingpaper01-03.doc, VERTIC Briefing Paper 01/03. Last accessed, 06 April 2004.

Snedecor, G.W., Cochran, W.G. (1980). *Statistical methods*. Ames, The Iowa State University Press. 507 p.

Sozanska, M., Smith, P., Milne, R., Brown, T.A. (2002). UK emissions by sources and removals by sinks due to land use, land use change and forestry activities: Section 5: linking soil and vegetation carbon dynamic models. DEFRA Contract EPG1/1/160, CEH No. C01504, http://www.nbu.ac.uk/ukcarbon/, Edinburgh, Department for the Environment, Food and Rural Affairs, Global Atmosphere Division.

Spanner, M., Johnson, L., Miller, J., McCreight, R., Freemantle, J., Runyon, J., Gong, P. (1994). Remote-sensing of seasonal leaf-area index across the Oregon transect. *Ecological Applications*, **4**:258-271.

Stape, J.L., Ryan, M.G., Binkley, D. (2004). Testing the utility of the 3-PG model for growth of Eucalyptus grandis X urophylla with natural and manipulated supplies of water and nutrients. *Forest Ecology and Management*, **193**:219-234.

Steele, R.C., Welch, R.C. (eds). (1973). *Monks Wood: A nature reserve record.* Cambridge, The Nature Conservancy. 337p.

Stenberg, P., Kuuluvainen, T., Kellomaki, S., Grace, J.C., Jokela, E.C., Gholz, H.L. (1994). Crown structure, light interception and productivity of pine trees and stands. *Ecological Bulletins*, **43**:20-34.

Stewart, J.B. (1988). Modeling Surface Conductance of Pine Forest. *Agricultural and Forest Meteorology*, **43**:19-35.

Swift, M.J., Healey, I.N., Hibberd, J.K., Sykes, J.M., Bampoe, V. and Nesbitt, M.E. 1976 The decomposition of branch-wood in the canopy and floor of a mixed deciduous woodland. *Oecologia*, **26**, 139-149.

Thenkabail, P. S., Enclona, E. A., Ashton, M. S.,Van der Meer, B. (2004).Accuracy assessments of hyperspectral waveband performance for vegetation analysis applications. *Remote Sensing of Environment*, **91**(3-4): 354-376.

Thomasson, A.J. (1971). *Soils of the Melton Mowbray district.* Soil Survey of Great Britain, Harpenden. 118 p.

Treitz, P.M., Howarth, P.J. (1999). Hyperspectral remote sensing for estimating biophysical parameters of forest ecosystems. *Progress in Physical Geography*, **23**:359-390.

Trotter, C.M., Dymond, J.R., Goulding, C.J. (1997). Estimation of timber volume in a coniferous plantation forest using Landsat TM. *International Journal of Remote Sensing*, **18**:2209-2223.

Tucker, C.J. (1979). Red and photographic infrared linear combinations for monitoring vegetation. *Remote Sensing of Environment* 8:127-150.

UNFCCC. (1992). United Nations Framework Convention on Climate Change. http://unfccc.int/

UNFCCC.(1997). Kyoto Protocol to the United Nation Framework Convention on Climate Change. http://unfccc.int/

UNFCCC. (2001). The Marrakesh Accords. FCCC/CP/2001/13/Add.1, http://unfccc.int/, United Nations.

Ustin, S.L., Trabucco, A. (2000). Using hyperspectral data to assess forest structure. *Journal of Forestry*, **98**:47-49.

van Hees, A.F.M., Bartelink, H.H. (1993). Needle Area Relationships of Scots Pine in the Netherlands. *Forest Ecology and Management*, **58**:19-31.

Van Oijen, M., Rougier, J., Smith, R. (In press). Bayesian calibration of process-based models: bridging the gap between models and data. *Tree Physiology*.

Vanclay, J.K. (1989). A growth model for North Queensland rainforests. *Forest Ecology and Management* 27:245-271.

Vanzyl, J.J. (1993). The effect of topography on radar scattering from vegetated areas. *IEEE Transactions on Geoscience and Remote Sensing*, **31**:153-160.

Verstraete, M.M., Pinty, B. (1996). Designing optimal spectral indexes for remote sensing applications. *IEEE Transactions on Geoscience and Remote Sensing*, **34**:1254-1264.

Vitousek, P. M. and Howarth, R. W. (1991). Nitrogen Limitation on Land and in the Sea - How Can It Occur. *Biogeochemistry*, **13**(2): 87-115.

Vitousek, P. M., Walker, L. R., Whiteaker, L. D., Matson, P. A. (1993). Nutrient Limitations to Plant-Growth During Primary Succession in Hawaii-Volcanos-National-Park. *Biogeochemistry* **23**(3): 197-215.

Vogt, K. 1991 Carbon budgets of temperate forest ecosystems. *Tree Physiology*, **9**, 69-86.

Vose, J. M., Dougherty, P. M., Long, J. N., Smith, F. W., Gholz, H. L., Curran, P. J. (1994). Factors influencing the amount and distribution of leaf area of pine stands. *Ecological Bulletins* **43**: 102-114.

Wang, K.Y., Kellomaki, S., Zha, T.S., Peltola, H. (2004). Component carbon fluxes and their contribution to ecosystem carbon exchange in a pine forest: an assessment based on eddy covariance measurements and an integrated model. *Tree Physiology*, **24**:19-34.

Wang, Y.P., Jarvis, P.G. (1990). Description and Validation of an Array Model - Maestro. *Agricultural and Forest Meteorology*, **51**:257-280.

Waring, R.H. (2000). A process model analysis of environmental limitations on the growth of Sitka spruce plantations in Great Britain. *Forestry*, **73**:65-79.

Waring, R.H., Running S.W. (eds). (1998) *Forest ecosystems : analysis at multiple scales*, 2nd Ed. Academic Press, London 270 p.

Watson, R.T., Noble, I.R., Bolin, B., Ravindranath, N.H., Verardo, J., Dokken, D.J. (eds). (2000) *IPCC special report on land use, land-use change, and forestry*, Cambridge, Cambridge University Press, 377 p.

Wayman, J.P., Wynne, R.H., Scrivanl, J.A., Reams, G.A. (2001). Landsat TM-based forest area estimation using iterative guided spectral class rejection. *Photogrammetric Engineering and Remote Sensing* 67:1155-1166.

Wehr A., Lohr, U. (1999). Airborne laser scanning - An introduction and overview. *ISPRS Journal of Photogrammetry and Remote Sensing*, 54:68-82.

Woodcock, C. E. and Strahler, A. H. (1987). The Factor of Scale in Remote-Sensing. *Remote Sensing of Environment*, **21**(3): 311-332.

Appendix A

Additional information for the selected methods

This appendix introduces the approaches and provides a brief description of the study sites where the research has been conducted. The publication style of the Chapters does not allow for an extended introduction on methods. Some fundamental notions are therefore provided on:

(i) Empirical forestry methods

(ii) Remote sensing techniques

(iii)Process-based models

(iv)Bayesian statistics

It should be noted that this chapter does not aim at reproducing the literature review and the critical discussion of the approaches provided elsewhere.

8.1 Empirical forestry methods

This section, mainly relevant to Chapter 3, introduces field-based methods for the quantification of forests carbon content.

8.1.1 Carbon content of trees

Destructive measurements have been used to estimate the full carbon or biomass content of individual trees to derive species-specific regression relationships between tree volume, biomass or carbon content, to easily quantifiable variables such as diameter at breast height (DBH) (Ovington 1957, Crockford 1987, Kraenzel *et al.* 2003). Upscaling to stand level is possible, provided that *a priori* knowledge of the species density and composition is known and that measurements of the independent variables used in the models are available. For that purpose, standard forestry measurement conventions for both trees and understorey shrubs are detailed in Hamilton (1975) or Satoo and Madgwick (1982).

Such approaches have been used widely in the UK and elsewhere (e.g., Baskerville 1966, Satchell 1971, Kraenzel *et al.* 2003). However, difficulties arise when no destructive measurements are possible or allowed. Then, an estimate must be made based on published models derived from data collected elsewhere (e.g. Malhi *et al.* 2004). Extensive databases

exist for this purpose (e.g. Ovington 1957; Cannell 1982) but the errors inherent in utilising this method are difficult to quantify.

8.1.2 Carbon content in other pools

Estimating the carbon content of ground vegetation, litter or deadwood often involves cutting down vegetation to the soil level and collecting all leaf and woody debris within a specified area (Satchell 1971, Ajtay *et al.* 1979, Albrekson 1988, Cousens 1988, Vogt 1991, Finer 1996). For these components, carbon content is believed to approximate 45% of dry weight (Ajtay *et al.* 1979, Vogt 1991). Litter traps are also used for the assessment of foliage dry weight and litterfall rates (Cousens 1988, Finer 1996). Large variability in litterfall and ground vegetation arises as a function of canopy cover, tree density, mortality rates, species, phenology and management practices but the relative importance of this carbon pool in forests, compared to that in woody stems, is small.

In contrast, below-ground carbon pools are considerable. In a study conducted in Meathop Wood, UK, 72 trees and 30 hazels were excavated (cited in Cannell, 1982). The root dry weight resulting from this study was 59.7% of total above-ground wood dry weight. Estimating below-ground carbon content from root system excavation is intrinsically more difficult than above-ground carbon content estimation. When no destructive measurements are possible, estimates based on data collected elsewhere on similar forest types to that of interest, or on data averaged over specific climatic zones and ecosystems have been used. Otherwise, when no regressions are available, provisional root biomass estimates based on species-specific root to shoot biomass ratios or biomass expansion factors available in the literature can be made (Lehtonen *et al.* 2004, Levy *et al.* 2004, IPCC 2003). This yields large uncertainties in root biomass estimates, as this pool varies considerably as function of genotypes and environmental constraints (e.g. Gower *et al.* 1994, Schoettle and Fahey 1994).

Soil carbon content is a considerable carbon pool, especially in forest ecosystems (Bolin *et al.* 2000). Additionally, this pool is highly variable spatially, partly due to land-use and vegetation cover (Dewar and Cannell 1992, Howard *et al.* 1995, Milne and Brown 1997, Milne and Brown 2000). Spatially extensive sampling is required for accurate representation. A first step in estimating soil carbon involves soil sampling by coring to a pre-determined soil depth and volume. Carbon content is estimated by the oxidation of soil organic carbon with acid dichromate solutions (Rowell 1994). However, where facilities do

not permit such analyses, techniques of loss on ignition, the process of burning off the organic matter from oven-dry soils, are applied (e.g. Bengtsson and Enell 1986, Rowell 1994, Jones *et al.* 2000).

Field-based estimations are often debatably referred to as ground truth. Although this terminology is misleading (as one could argue that all estimates are representations of reality), destructive measurements of plant components, extraction of roots systems and soil sampling probably provides the closest representation of reality at the scale of the analysis (e.g. tree to plot scale). However, such analyses are impractical for producing complete regional to national scale estimates. For these, alternative methods must be sought.

8.2 Alternative methods

Chapter 4, 5 and 6 to the thesis make continuous reference to yield tables and yield models. A description of these datasets is thus provided below. Carbon accouting models, based on these tables, are introduced in section 8.2.2. These models are used by the UK to provide national estimates of forest carbon stock changes to the UNFCCC (Milne *et al.* 2003).

8.2.1 Yield tables

For forest plantations, yield tables and yield models have been designed in the UK and elsewhere to quantify and forecast tree growth, given prevailing environmental conditions and management practices, thereby considerably reducing the need for ground data collection (Hamilton 1975, Edwards and Christie 1981). The UK tables were originally published in 1966 by the UK Forestry Commission and were since converted to the metric system (Hamilton and Christie 1971). These were originally compiled from extensive field-based forest surveys, and subsequently summarised into empirical yield tables. From these, relationships between forest variables such as Diameter at Breast Height (DBH), basal area, age, top height and stemwood volumes can be derived (Edwards and Christie 1981, see glossary for definitions). These models rely on the assumption that the general pattern of growth is typical of all even-aged stands but differences of growth occur within the same species on different sites: some stands will grow faster than others (Figure 8.1). Additionally, growth patterns of even-aged, monospecific stands vary as a result of management practices (e.g. thinning or varying planting density). Consequently, the complete range of growth variables per species (e.g. stem wood volume, DBH) has been divided into separate yield classes (YC). These yield classes implicitly account for the influence of environmental conditions and predict the maximum growth rate in $m^3\ ha^{-1}\ yr^{-1}$.

A yield class of 14 suggests that the maximum growth rate that a stand can achieve is 14 m^3 ha^{-1} yr^{-1} (Edwards and Christie 1981). The higher the yield class, the higher the productivity and growth rate. Supplementary tables to account for different management regimes are also provided.

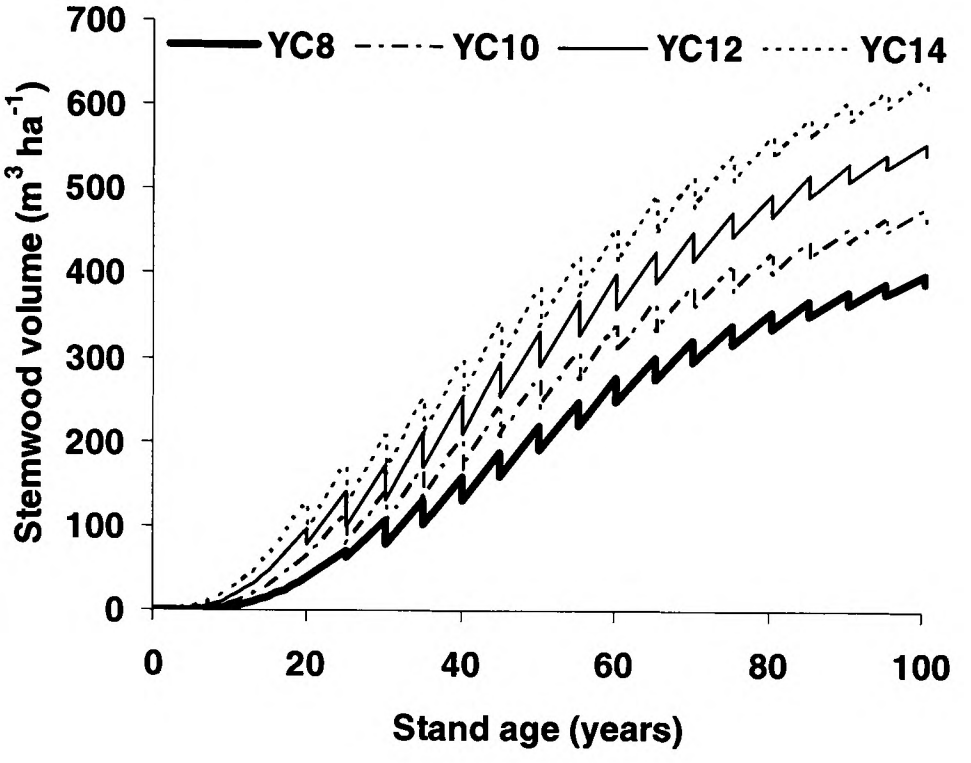


Figure 8.1: *Pinus sylvestris* L. yield model for stemwood volume production per hectare as function of stand age. The saw-toothed pattern shows the intermediate thinning regime applied. Yield Classes (YC) 8, 10,12 and 14 are shown (see text for details).

8.2.2 Carbon accounting models

Several models have been derived from yield tables. These include C-flow (Dewar 1991), CO2-fix (http://www2.efi.fi/projects/casfor/models.htm), as well as other commercial models such as the ECO2 model (EcoSecurities Ltd.[10], unavailable publicly) and the SGS-COV model (SGS Ltd.[11], unavailable publicly). Some of these models, also referred to as carbon accounting models, are currently used as a basis for estimating carbon stocks and changes in forests to provide estimates to the UNFCCC (e.g. Dewar and Cannell 1982, Milne 1992, Milne and Brown 1997, Cannell *et al.* 1999, Milne and Brown 2000; Matthews and Broadmeadow 2003). A complete carbon accounting model requires a minimum amount of input data (e.g. tree spacing, planting year, tree species and thinning practices) and should take into consideration the following pools: growing trees, litter pool, soil organic matter and derived products (including short-lived products such as paper and fuel wood, and long-lived merchandise, Dewar 1991).

[10] Ecosecurities Ltd. is an environmental finance company, specialising in advising on strategy regarding global warming issues.
[11] SGS Ltd. is the world's leading inspection, verification, testing and certification company.

The principal limitation of carbon accounting models and production tables is that although they are adequate for estimating the carbon content of relatively homogeneous plantation stands, they may not be suitable for UK semi-natural woodlands, which are often heterogeneous in terms of species composition and structure and are submitted to minimal anthropogenic management. Whereas for even-aged and monospecific stands, a good relationship exists between forest variables at the stand level, this may not be the case for heterogeneous natural woodlands. Additionally, the information required for carbon accounting models may not be available at national scales (e.g. forest type). This information can however be retrieved from satellite based remote sensing, which enable the classification of forests into deciduous and coniferous types.

8.3 Remote sensing

This section provides complementary information to the technical descriptions of LiDAR[12] provided in Chapters 2 and 4, and hyperspectral remote sensing techniques discussed in Chapters 2 and 6.

8.3.1 Overview

Remote sensing is the process of recording information about features from a device not in direct contact with the object. Recording devices, carried on airplanes or satellites, provide unique opportunities to acquire earth surface information, repetitively, and over large areas. Additionally, unlike cartography, digital and analogue images are not mediated until processing and analyses are applied, thereby providing the closest visual depiction of reality one can achieve at such scales. Field-based data collections are still required to evaluate the accuracy of the processing and interpretation.

In this thesis, techniques for understanding and inventorying forest ecosystems are discussed. In particular, approaches recording data measured in the visible, near infrared (NIR), middle infrared (MIR) as well as in the microwave portion of the electromagnetic spectrum are considered (Figure 8.2). The visible, NIR, and MIR combined are subsequently referred to as the optical range, which depend on solar illumination.

[12] Also referred to as Laser Altimetry, Airborne Laser Terrain Mapping (ALTM) or Airborne Laser Scanning (ALS)

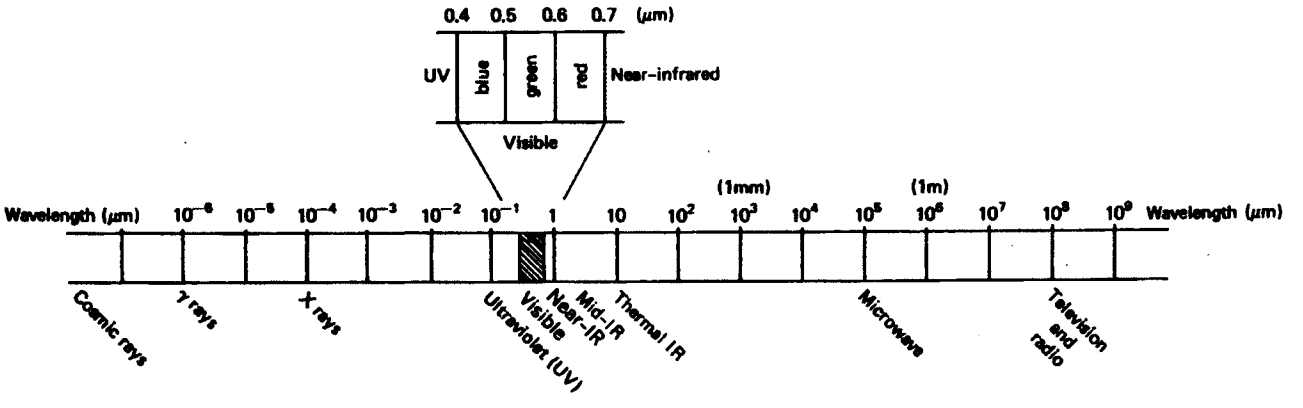


Figure 8.2: Wavelengths of the electromagnetic spectrum (from Lillesand and Kiefer, 2000)

Table 8.1 describes comparatively the main advantages and disadvantages of digital optical, radar and Light Detection And Ranging (LiDAR) remote sensing techniques for monitoring forest features. The table also emphasises the differences between passive and active sensors. Whereas passive systems record naturally occurring radiation, active systems generate their own source of electromagnetic radiation. Passive techniques recording in the optical wavelengths are referred to as optical systems; active systems recording in the visible and NIR range, to LiDAR; and finally, active systems recording in the microwave portion of the electromagnetic spectrum, to radar (Figure 8.2).

Table 8.1: Broad advantages and disadvantages of remote sensing approaches. Only the approaches discussed in this thesis are presented

Description	Main advantages	Main disadvantages
Optical: Passive system λ = ~ 0.4 to 2.5 µm	- Several airborne and satellite sensors available - Several spatial and temporal resolutions - Many operational techniques - Can be relatively cheap - Extensively studied - Available from satellite platforms -Uniqueness of vegetation spectral signature -20-30 years of archives	- Strongly affected by atmospheric attenuation, topography - 2-dimensional views of canopy surfaces (limited for forest structure and biomass estimation) -Saturation of signal as foliage density increases
Radar: Active system λ = ~1 cm to 10 m (for VHF)	- Active system, independent of sunlight - Not impeded by clouds or light precipitation - Directly sensitive to forest structure - Potential for improvement of newly designed approaches (e.g. interferometry) - Different bands sensitive to different forest components	- Complex interpretation of the returned signal - Affected by speckle, soil moisture content and topography. - Not yet operational - Most useful bands for monitoring biomass not available from satellite - Saturation of signal at high biomass
LiDAR: Active system λ = ~ 0.9 to 1.064 µm	- Active system, independent of sunlight - High resolution - Easily and quickly processed - Interaction between signal and surveyed matter simple to interpret -High vertical and horizontal accuracy - Directly sensitive to forest structure and biomass -Operational	- Not an imaging system: interpolation between point samples is required - Unavailable from satellite platform thus localised coverage only - Expensive for large scale surveys - Affected by atmospheric attenuation, topography

Additional to the advantages and disadvantages of each technique, specific sensor resolutions need to be considered prior to selecting an approach for forestry applications. These are discussed in Chapter 2.

In the sections below, LiDAR and hyperspectral remote sensing methods, which are directly used and tested in this thesis for the purpose of forest monitoring, are described.

8.3.2 LiDAR

The potential of LiDAR for forestry application was first demonstrated in the early 1980s (Krabill *et al.* 1980, Arp *et al.* 1982, Aldred and Bonner 1985). The technology has since seen a rapid development. Whereas in 1996, there existed only one company providing commercial LiDAR systems, today a plethora of companies are now exist, as well as a variety of methodologies for the monitoring of forests (see Baltsavias 1999 and www.airbornelasermapping.com for a review of systems and companies).

A complete LiDAR system entails the following components (Baltsavias 1999):

1. A laser range finder (including all relevant electronic components i.e. laser, transmitting and receiving optics, signal detector, a precise time counter)
2. Computer and operating system for the online data acquisition
3. Scanner
4. Differential global positioning system (DGPS) including both ground reference station and onboard GPS
5. An inertial navigation unit (INS)
6. Platform (most commonly airborne)

The functioning of the system is as follow (Figure 8.3). A near infrared laser pulse is emitted from a platform towards targets on the ground, and the returned signal is recorded. Elevation information of targets on the ground is calculated by estimating the elapsed time for the signal to travel from the detector to the feature and back, supplying accurate point sample elevation data for the ground surface and/or objects on it.

The INS and DGPS provide accurate information on the heading, roll and pitch of the aircraft for determining the orientation and flight path. Using this information, the precise position of the aircraft can be estimated and each LiDAR point measurement is georeferenced. The laser produces thousands of light pulses per second at a specified frequency. A rotating mirror inside the transmitter causes the laser pulses to sweep through an angle, scanning a line on the ground perpendicular to the direction of flight. This generates a saw tooth pattern along the ground path (Figure 8.3).

For forestry applications, the first and last significant signals are most commonly recorded, which after processing, correspond to canopy and ground surface elevation, respectively. A significant return implies that the signal is strong enough to trigger a recording (Figure 8.3). The difference between elevations derived from these returns provides height information.

The methodology for interpolation between sample points for thematic mapping and for deriving canopy heights is described in Chapter 4.

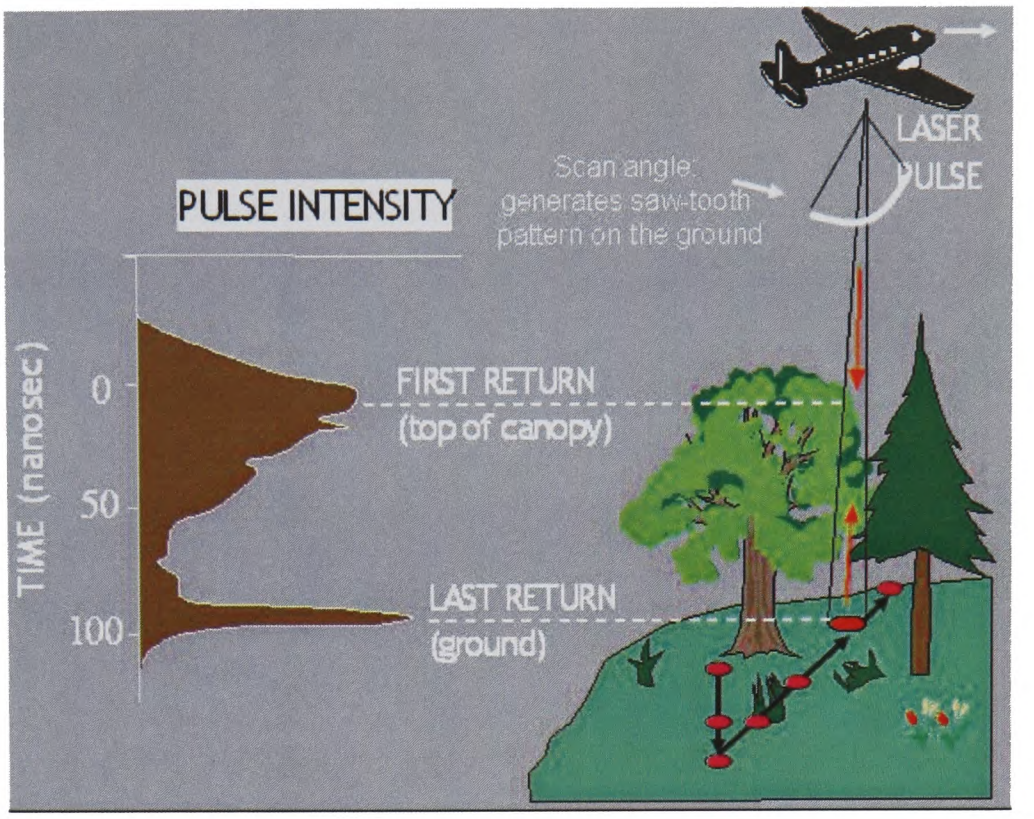


Figure 8.3: Operation of a Lidar system (Modified from Hill *et al.* 2002)

In this research, data collected with an Airbone Laser Terrain Mapper Optech 1210 were used. Specifications to this sensor, along with that of other commercially available devices, are described in Table 8.2.

Table 8.2: Specifications to selected airborne LiDAR systems. The ALTM 1210 system was used in this study (adapted from Baltsavias, 1999)

System	λ (μm)	Scan angle θ (°)	Flying height *h* (min/max) (m)	Laser footprint (m)	Point density (points/m^2)	No. of echoes per pulse/ minimum vertical object separation	Intensity recording	Pulse width (ns)	Company/ references
ALTM 1020	1.047	0-40	330-1000 (2000 optional)	0.3 at 1000m *h*	Na	1st and/or last	Optional	10	Optech (Canada)
ALTM 1025	1.047	0-40	100-1000	0.3 at 1000m *h*	0.5-200	1st and last	Optional	8	Optech (Canada)
ALTM 1210	1.047	0-40	400-1200 (2000 optional)	0.3 at 1000m *h*	20-50	1st and last or 4/1.5-2m	No	8	Optech (Canada)
TopEye	1.064	0-40	200-1000	0.5, 1, 2 at 500 m *h*	1/16-1	1st or last	Yes	7	Saab survey System (Sweden)
Topo Sys I	1.540	14	60-1000	0.3 at 600 m *h*	5-25	1st or last	No		Toposys (Germany)
Topo Sys II			60-1600		3-25	1st and last	Yes		
ALTMS	1.064	0-30	450-1500	0.9 at 900 m *h*	variable	4/0.75 m	No	7	TerraPoint (Built by HARC with NASA support)

8.3.3 Hyperspectral

8.3.3.1 Monitoring of vegetation

Akin to other passive optical approaches, hyperspectral data are not directly sensitive to forests biomass. Conversely to radar wavelengths, which are directly sensitive to the forest structure as the wavelengths penetrate the forest canopy, optical sensors only "see" and capture reflectance data from the surface perpendicular to the look direction of the sensor. In forest ecosystems, this surface is often dominated by canopy leaves.

Fortunately, advances in the field of terrestrial ecology have produced an important simplifying variable quantifying canopy leaf density per unit ground area. The leaf area index (LAI, m^2 m^{-2}), made its appearance after Briggs *et al.* (1920) and Avery (1933) showed how plant productivity was closely related to leaf surface area. LAI defines the surface area where canopy processes such as leaf litterfall, photosynthesis, respiration, evapotranspiration and other gaseous emissions take place, including net carbon absorption (e.g. Evans 1972). This variable has become an essential component to many forest ecosystem models concerned with estimating forest productivity and biomass change (Cramer *et al.* 1999, Coops *et al.* 1998, Running and Coughlan 1988). In this thesis, LAI is specifically defined as the projected leaf surface area per unit ground area, unless otherwise stated (further details in Chapter 5 and 6). Projected leaf surface area has been used to quantify the surface area of non-horizontal or non-flat leaves.[13] Remote sensing, using satellite or aircraft-mounted sensors, provides significant advantages over field-based approaches for monitoring canopy variables including leaf area index. Canopy dynamics can change rapidly because of seasonality, especially in the case of herbaceous, deciduous, or short-season vegetation types. Such rapid changes are difficult to assess from field-based methods alone (Waring and Running, 1998).

Spectral optical bands commonly used to monitor forest ecosystem and LAI range from the visible (0.4-0.7 μm), near infrared (0.7-1.4 μm) and middle infrared (1.4-2.5 μm) (Lillesand

[13] Some have defined LAI as the total leaf surface area per unit ground surface area, half of the total leaf surface area per unit ground surface area or the projected leaf surface area per unit ground surface (see for instance Ovington 1957, Mencuccini and Grace 1997). If the leaves are oriented randomly on the tree, then the conversion factor between total LAI and projected LAI is approximately 0.25 (e.g. Barclay and Goodman, 2000).The absence of a standard or consistent LAI definition has lead to important confusions (Chen *et al.* 1997). For instance, Breuer *et al* (2004) provide a review of LAI values across temperate forest ecosystems for input into ecosystem models. In reviewing the original papers from which the LAI values were extracted, it was clear that no distinction between total, projected or 0.5 LAI had been made made by these authors. Projected leaf surface area has been used to quantify the surface area of non-horizontal or non-flat leaves.

and Kiefer, 2000). In these bands, vegetation exhibits a unique spectral signature as illustrated in Figure 8.4. The strong infrared reflectance is due primarily to internal cell structure, the strong red absorption and green reflectance, to leaf chlorophyll pigmentation and finally, leaf water content influences the signature in the MIR range. Vegetation indices as well as assumptions underlying indices designed to maximise this signature and factors affecting the spectral response of forest canopies are presented in Chapter 2 and below.

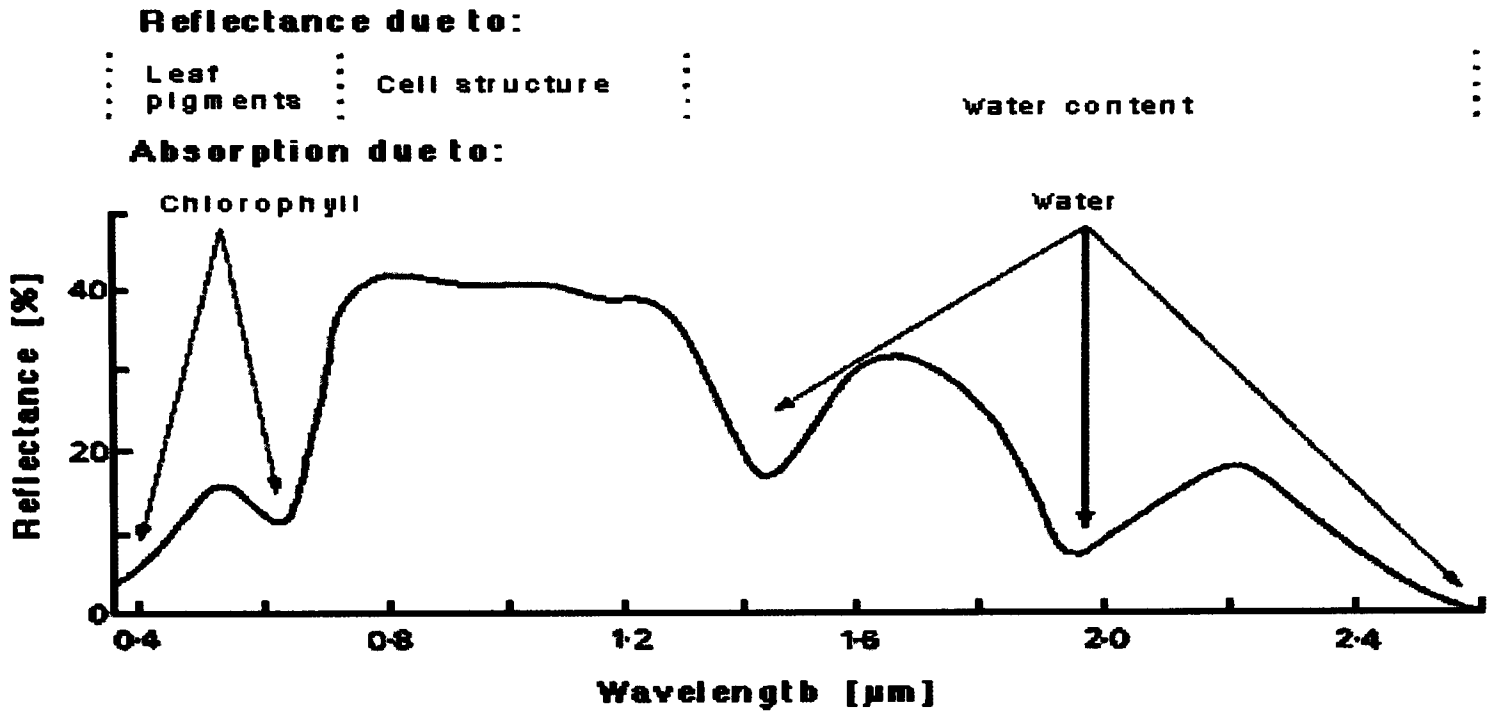


Figure 8.4: Typical reflectance and absorption characteristics of green vegetation (adapted from Swain and Davis, 1978).

Several relationships between vegetation indices and LAI have already been derived (e.g. Lucas and Curran 1999, Gholz *et al.* 1997, Sellers 1989, Jordan 1971, Jordan 1969). These relationships rely on the following assumption: as leaf area increases, the vegetation reflectance in the NIR spectral region increases, whereas it decreases in the visible (Goel and Norman 1992). These relations have provided useful tools for the linkage of satellite imagery to biomass productivity (Cramer *et al.* 1999) and have been tested at different scales, with various sensors and in a number of contrasting study sites including agricultural crops and forested areas (e.g. Danson and Curran 1993, Myneni *et al.* 1995, Goetz and Prince 1996).

8.3.3.2 Functioning

Hyperspectral remote sensing made its emergence nearly 20 years ago (Goetz *et al.* 1985). Since then, the capability of hyperspectral sensors to resolve specific absorption or

reflection features over very narrow bands has led to the development of approaches for the identification and differentiation of plant materials (Figure 8.5). This ability is only matched by laboratory or field spectroradiometers. By analogy, hyperspectral sensors are also referred to as imaging spectrometer.

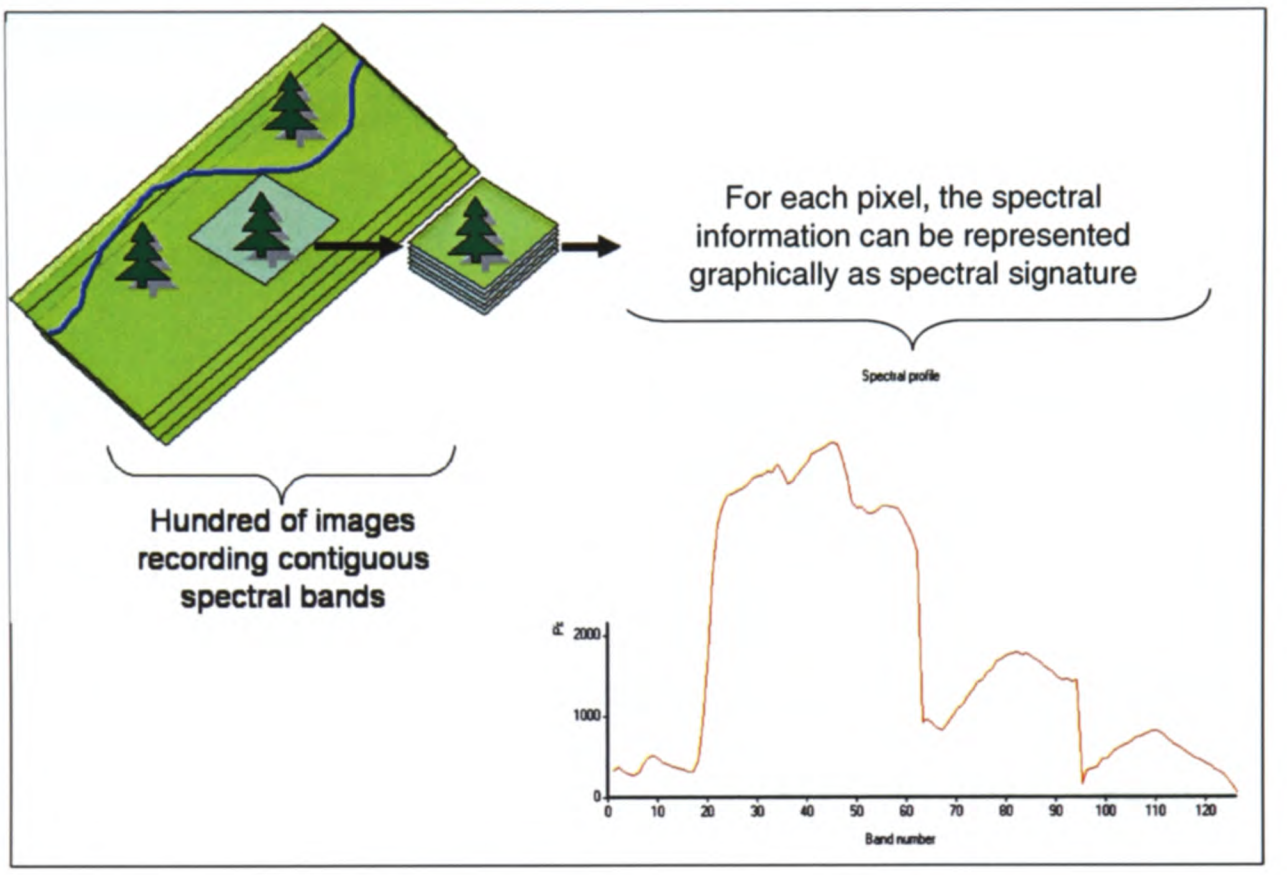


Figure 8.5: Hyperspectral remote sensing. Pixel values refer to the intensity of the reflectance.

In the past 3 decades, multispectral satellite-borne remote sensing instruments, such as the Landsat Thematic Mapper (TM) and the Advanced Very High Resolution Radiometer (AVHRR), have been used for the monitoring of forests. However, the use of multispectral comparatively to hyperspectral data results in a critical loss of information for the monitoring of forests. The information content of narrow bands offered by the new generation of hyperspectral remote sensors has been valuable for determining biophysical characteristics of vegetation (e.g. Gong *et al.* 2003, Thenkabail *et al.* 2004, Lee *et al.* 2004).

Nevertheless, the volume of data collected by hyperspectral compared to multispectral sensors, given equal surface areas and spatial resolutions, is considerably larger. This poses great challenges for data processing and interpretation. Consequently, research for optimal and redundant wavebands for specific forestry applications (e.g. Thenkabail *et al.* 2004, Martin *et al.* 1998), the use of vegetation indices (Gong *et al.* 2003, Pu *et al.* 2003), or of first order-derivatives indices (Pu *et al.* 2003, Shaw *et al*, 1998), have been made as means

for compacting information. However, these approaches make use of only a few bands out of the entire spectrum available. Statistical approaches condensing all the information contained in the datasets maximise the benefits from hyperspectral imaging. The studies by Lee *et al.* (2004) and Pu and Gong (2004) show that such analyses are indeed more successful in mapping LAI than conventional approaches. In the study by Lee *et al.* (2004), canonical correlation analysis conducted on hyperspectral bands was shown to be better than the ubiquitous Normal Differential Vegetation Index (Appendix A) in monitoring vegetation cover. Likewise, Pu and Gong (2004) showed that principal component analysis was more effective than individual band selection approaches for mapping forest LAI.

Remote sensing offers the ability to cover large areas for the assessment of carbon content in forests and for producing estimates at national scales. However, its potential is limited for the production of exhaustive forest carbon content estimates as its monitoring capabilities are limited to above-ground observation. For a complete assessment of above and below-ground forest biomass and change, the coupling of remote sensing to ecosystem models is recommended (Battaglia and Sands 1998).

8.4 Ecosystem modelling

Conversely to field data collection and remote sensing approaches, which are principally empirically based (driven by data collection), process-based models fundamentally rely on biological theory (Green *et al.* 2000). More specifically, they are mathematical representation of forest ecosystems, relying on our understanding of processes governing growth. The models mimic natural dynamics that operate at various scales, mostly in a deterministic fashion, such that model outputs are determined by model inputs. This helps in identifying key environmental variables influencing productivity.

In comparison with the remote sensing approaches described above, the use of process-based models for carbon stocks and change estimations has the following advantages :

(i) Identifies the principal processes governing growth

(ii) Quantifies the influence of environmental variables independently, thereby laying out the principal drivers or limitations on growth

(iii) Factors out anthropogenic influences on growth such as that arising from management or from CO_2 and nitrogen fertilisation

(iv) Simulates the carbon allocation between carbon pools, including above and below-ground components

An exhaustive description of the dynamics of forest ecosystem is provided in Waring and Running (1998). Table 8.3 summarises the processes which control growth and ecosystem productivity. In particular, the fundamental assumptions underlying process-based models is that firstly, while growth is governed by solar radiation, environmental constraints limit production and secondly, a certain amount of the biomass produced through photosynthesis (Gross Primary Production, GPP) is lost through respiration processes. The net result is referred to as the Net Primary Production (NPP).

Table 8.3: Component processes of a comprehensive ecosystem biochemical model (from Waring and Running, 1998)

Energy balance	
Short wave radiation balance (incoming-outgoing); Sensible heat flux; Soil heat flux	Long wave radiation balance (incoming-outgoing); Latent heat flux
Water balance	
Precipitation partitioning (snow versus rain); Litter and **canopy interception** and storage; Soil surface infiltration; **Soil water content**	Subrooting zone outflow; Hill slope hydrologic routing; **Evaporation;Transpiration**
Carbon balance	
Photosynthesis, gross primary production; Maintenance respiration; Growth respiration; Photosynthate storage; **Net primary production**; Net ecosystem production	**Carbon allocation (Leaves, stem branches roots,** defensive compound, reproduction); **Phenological timing (Canopy growth/senescence; Litter fall of leaves; Turnover of stems and roots)**; Decomposition
Elemental balance	
Sources (atmosphere, rock weathering, biological fixation); Soil solution transformation; Immobilization, nitrification, denitrification ; Mineralization; Root uptake.	Tissue storage ; Internal recycling ; Volatilisation ; Leaching; Export through harvesting and erosion

The integration of all these processes within a single process-based model is impracticable due to the different spatial and temporal scales at which these processes take place. In reality, models are thematic representations of reality and the selection of processes which are considered is driven by the purpose for which the model was created. Thus, models differ largely in their prioritisation and translation of reality into mathematical

conceptualisation, as well as in the spatial and temporal scales that are considered. The 3-PG model selected in this thesis includes the processes indicated in bold in Table 8.3.

8.4.1 The 3-PG model

Several process-based models designed principally for research on ecosystem productivity are available. Well known ones include Forest-BGC (Running and Coughlan, 1988) and BIOMASS (McMurtrie *et al.* 1992, McMurtrie *et al.* 1990). The model selected in this study, the *Physiological Processes Predicting Growth* model (3-PG, Landsberg and Waring 1997, Sands and Landsberg 2002) constrasts with these models as it was designed equally for research purposes and as a forestry practical tool (Landsberg and Waring 1997, Coops *et al.* 1998). The main components of the model are shown in Figure 8.6.

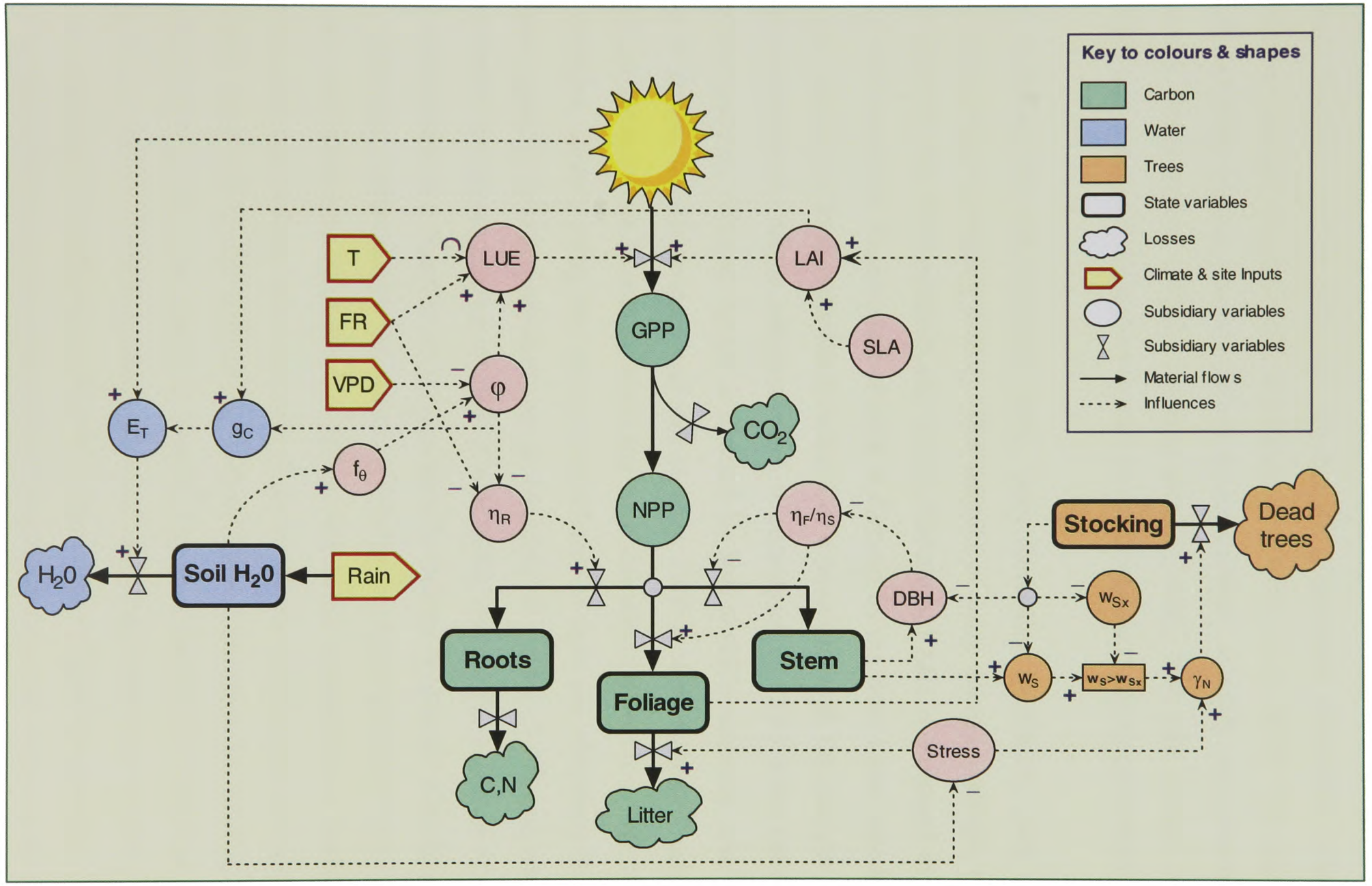


Figure 8.6: 3-PG structure (From Sands 2000, Adaptation of 3-PG to novel species). Further details on variables and parameters are provided in Chapters 5 and 6.

8.4.1.1 3-PG functioning

The model relies both on empirical and mechanistic processes to predict forest stand development on a monthly basis. 3-PG is built upon a few key-simplifying concepts, requires monthly weather data and site-specific parameters obtainable either from the literature or through standard field measurements (White *et al.* 2000). The main inputs are climate variables (vapour pressure deficit, air temperature, monthly precipitations and solar radiation). Other inputs include stocking density, stem, root and foliage biomass and available soil water at initialisation as well as site latitude and soil characteristics.

State variables are soil available water, stem (including branches), roots and foliage biomasses and tree stocking density. The amount of solar energy available to plants for photosynthesis (the *P*hotosynthetically *A*ctive *R*adiation, PAR) is estimated as 50% of the global solar radiation. Interception of PAR is dictated by the Beer's law, which determines how the intensity of solar radiation is reduced as it passes through the canopy. The amount of photosynthetically active radiation which is intercepted (APAR) is not necessarily used for photosynthesis. Utilised APAR is dictated by soil water availability, tree age, vapour pressure deficit, air temperature and soil fertility. GPP is then estimated using a canopy quantum efficiency coefficient, symbolizing the efficiency of plants to convert light energy into biomass. Models using this concept are referred to light use efficiency (LUE) models as these quantify primary productivity as function of APAR. 3-PG assumes that NPP approximates a constant fraction of GPP (0.47± 0.04). Allocation of carbon to the different plant components is a function of species-specific factors or generic allometric equations. Roots allocation is dictated by soil water availability or vapour pressure deficit (which ever lowest), and stand age. Allocation to foliage and stems depends on a partitioning ratio between stem and foliage, itself function of an allometric relationship between stem mass and DBH. Root and foliage mortality is dictated by root turnover and litterfall rates, while stem mortality can either be applied as thinning regime or be density dependent. If mortality is applied as part of the management practices, thinning events are included as inputs at specific times during the rotation. Otherwise, the density dependent mortality can be used, based on the self-thinning rule and current stocking density: the mean single tree biomass never exceed a maximum permissible tree stem biomass.

Soil water availability is function of precipitation and evapotranspiration. Evapotranspiration is calculated from the Penman-Monteith equation for which an estimate

of canopy conductance is required. Canopy conductance varies as function of age, vapour pressure deficit or soil available water, which ever smallest.

Outputs include monthly predictions of GPP and NPP, as well as of state variables. NPP is a closely related to the net amount of carbon stored in plants. An additional submodel not presented in Figure 8.6 enables the quantification of stand variables from the three biomass pools and stem number. These variables include stem volume (without branches), DBH, basal area and stem height. Additional parameterisation and species-specific allometric relationships are however required to implement this submodel.

8.4.1.2 3-PG applications worldwide

Both 3-PG and 3-PGS, a model derived from 3-PG that uses remote sensing for estimating APAR, have been applied to forest environments worldwide (Landsberg and Waring 1997, Coops 1999, Waring 2000, Landsberg *et al.* 2003). The model was first tested in two plantation sites in Australia and New-Zealand. The correspondence between the measured and predicted stem growth was excellent at both sites (Landsberg and Waring 1997). White *et al.* (2000) also used 3-PG to predict biomass change of vegetation forest and scrubs in New-Zealand. After calibration of key parameters for New-Zealand vegetation types and conditions, the model was tested at the plot, regional and national level. The correspondence between measured and predicted biomass was excellent at the plot level (r^2=0.98 $p<0.01$ not biased). The correspondence between predicted values at the regional and national level with those found in the literature was also good (r^2=0.82 and r^2 = 0.77 respectively, $p<0.01$). In the latter case, 3-PG estimates were lower than values found in the literature. The authors argued that the overrepresentation of mature forests was likely to account for the higher estimates found in the literature. Landsberg *et al.* (2003) describe the calibration procedure to model growth of different vegetation types. Using African, Australian, and Northern European case studies, the model was calibrated for each ecosystem type and tested by simulating growth on forests independent to those used for calibration. The experiment was designed to evaluate the response of the model to various treatments (fertility, irrigation, spacing) applied to the forests. Results were correlated highly with ground estimates of variables such as volume (generally above $r^2>0.9$). The 3-PG model has also been used to diagnose climatic limitations on the growth of 12 Sitka spruce plantations in the UK (Waring 2000).

In 3-PGS, remotely sensed data were used to infer spatial and temporal variability in the fraction of radiation intercepted by the canopy (fPAR) (Coops *et al.* 1998). This variable has been related empirically and theoretically to spectral reflectance and vegetation indices (Kumar and Monteith 1982, Sellers 1985, 1987, Myneni and Williams 1994). Despite various limitations of the relationship (e.g. influence of understorey and soil reflectance, effect of canopy shadowing), vegetation indices seem to provide good approximation of fPAR values (Prince and Goward 1995). Additionally, unlike with predicting LAI, relationships between vegetation indices and fPAR do not generally saturate, hence the advantage of using of this parameter to characterise growth processes. Using this approach, Coops *et al.* (1998) estimated above-ground NPP for eight forests located in New Zealand and Australia aged between 20 and 40 years. Considering the coarse spatial resolution of the AVHRR dataset used (8x8 km), the resulting relationship between field data and the model prediction was generally good (overall error of ±20%). Likewise, Coops (1999) investigated the potential of this model linked to AVHRR and higher resolution Landsat MSS imagery to predict stand growth in an Australian forest plantation. The linear relationship between predicted and measured wood production was good (r^2=0.84).

8.4.1.3 Main limitations to process based models

Several limitations to most process-based models have however precluded their use outside the research community. This includes 3-PG, which was originally designed to also address the needs of forest practitioners. Even though the models are deterministic, in that no random components are considered in the simulation, the model results are subject to error and should be treated probabilistically. Process-based models, comprising numerous highly non-linear algorithms, are not solvable analytically. In this context, the quantification of uncertainty to model output is technically complex and involves intricate sampling approaches. These uncertainties arise from the fact that our comprehension the processes governing growth and interaction between these processes is still far from complete (.e.g Mencuccini and Grace, 1996; Enquist and Niklas, 2001). In particular, the uncertainty to model outputs is dependent on the uncertainty to model parameters. The data available on parameters are however often inadequate or simply inexistent. When available, the data are either insufficient to infer probability distribution or inadequate: the generalisation of parameter values across species and study sites is not always possible as parameters may vary widely between genotypes and environments (Gertner *et al.* 1999). As a result, "*in only a few cases have parameters characterising a species been rigorously determined, and*

even then this has been largely by a process of trial and error" (Sands 2002, p.3). The next section presents a statistical approach which attempts to address these limitations.

8.5 Bayesian calibration

"Doubt is not a pleasant condition, but certainty is absurd" Voltaire (1694 - 1778)

This citation clearly illustrates the importance of recognizing uncertainty in our estimates. In this section, an alternative approach to the conventional statistical paradigm is presented to calibrate model parameters and quantify uncertainty. Bayesian statistic (Bayes 1763 and Laplace 1812) is an alternative paradigm to the conventional statistics (frequentist approach). This appendix is not meant as an epistemological discussion between paradigms but rather, as an introduction to the selected approach. For an extensive review of the subject, one should refer to Sivia (1996) or Bernardo and Smith (1994).

The application of Bayesian statistics to process-based models achieves two goals simultaneously:

1. Calibration of parameters
2. Quantification of uncertainties to the model outputs and parameters

This can be understood by looking at the different components of Bayes' theorem:

Equation 11: Bayes' Theorem

$$P(\theta|D) = P(\theta)\, P(D|\theta) / P(D)$$

The prior probability, $P(\theta)$, has been interpreted in three different ways (Ellisson 1996, p.1040):

> *"(1) a frequency distribution whose parameters reflect analysis and synthesis of existing data; (2) an "objective" statement of what is rational to believe about [the values of the parameters before new data come in]; or (3) a subjective measure of what the investigator actually believes".*

In this thesis, the definitions (1) and (2) are adopted. The second component of the numerator, $P(D|\theta)$, is referred to as the likelihood and refers to the probability of the data, given a specific model parameterisation. It takes into consideration the measurements error in the data. The third component of the theorem, the denominator P(D), is called the evidence and is a normalisation constant. As P(D) is constant, the Bayesian theorem can be

read: the probability of the parameter or parameters, given available data, is proportional to the prior times the likelihood. Finally, $P(\theta|D)$ is the resulting probability density function proportional to the likelihood times the prior, which reflects posterior knowledge about the parameter(s), updated given available data. The resulting posterior distribution is best understood by examining Figure 8.7.

Let us imagine that our model has a single parameter θ, and $P(\theta)$, is the probability density function reflecting our prior knowledge about this parameter. The parameter probability distribution is given by the prior distribution shown in Figure 8.7. Data are also available for which measurement error is Gaussian and distributed as shown in the same figure (the likelihood). Then, given this prior and likelihood, the resulting posterior distribution is illustrated by the continuous line.

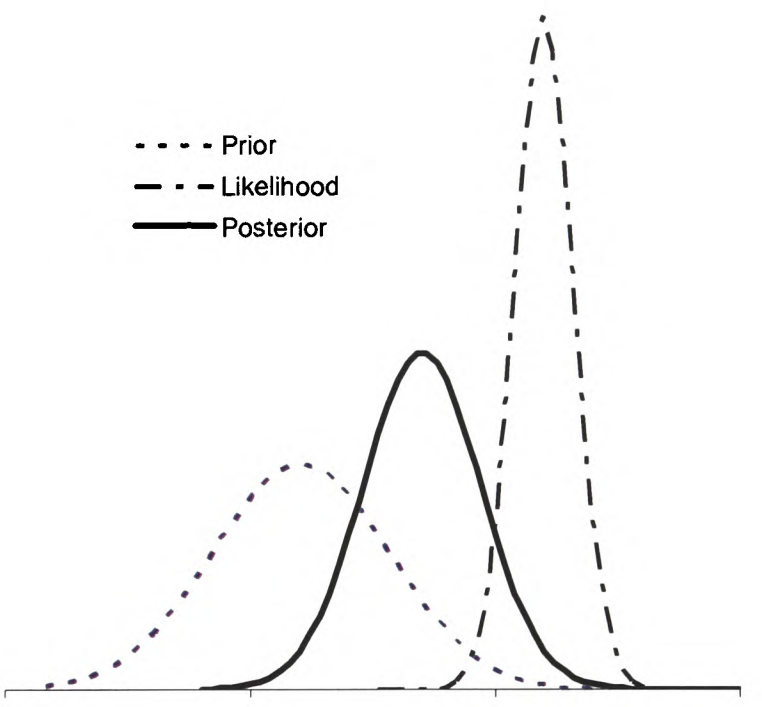


Figure 8.7: A simplified example of Bayesian inference

Therefore, the likelihood function becomes the determining factor by which posterior expectations are inferred from prior knowledge. Since the Bayesian calibration is an iterative process, the posterior distribution resulting from a first experiment can become the prior distribution for the next experiment: as data and knowledge are gained along the way, the posterior distribution is updated and the influence of the data on the posterior distribution, relative to that of the prior, increases.

A common criticism of the Bayesian approach is that the selection of the prior is believed subjective (point 3). Conventional statisticians argue that unlike the Bayesian paradigm,

statistics should be in accordance with the scientific method, completely devoid of subjective influences, and should let the data speak for themselves (Ellisson 1996). However, as rightly argued by Ellisson (1996) frequentist approaches themselves are not devoid from subjective influences, as subjectivity is involved in the selection of hypotheses, if only in the use of prior knowledge for setting up and designing research experiments.

Bayesian inference and calibration have developed rapidly over the last 50 years but have been slow in reaching the fields of environmental sciences. This is partly due to the fact that methods for estimating Bayesian posterior probabilities often require the integration of functions only solvable through numerical integration. This is highly time consuming and computer-demanding. In Chapters 5 and 6, a Markov Chain Monte Carlo analysis is used to randomly sample from the posterior distribution resulting from the analysis. Further details of this technique is provided in the relevant chapters.

8.6 Study sites

The research presented in this study was conducted in two forest sites (Figure 8.8): a semi-natural woodlands, composed of uneven-aged, mixed deciduous species (Monks Wood National Nature Reserve, Cambridgeshire, UK) and a coniferous plantation composed principally of mono-species, even-aged stands (Thetford forest plantation, Norfolk, UK). Both forest types are believed to contribute significantly but distinctively to the UK carbon pool and sink. UK deciduous woodlands are considerable carbon stocks while growing coniferous forests sink carbon dioxide rapidly from the atmosphere (Cannell and Milne, 1995). For both sites, extensive datasets and management information was available (for Monks Wood, see for instance Steele and Welch, 1973, Crampton 1996, Briggs 2001; for Thetford, see for example Ovington 1957, Baker 1992, Baker and Luckman 1999, Jinks and Kerr 1999, Skinner 2002, Balzter *et al.* 2003).

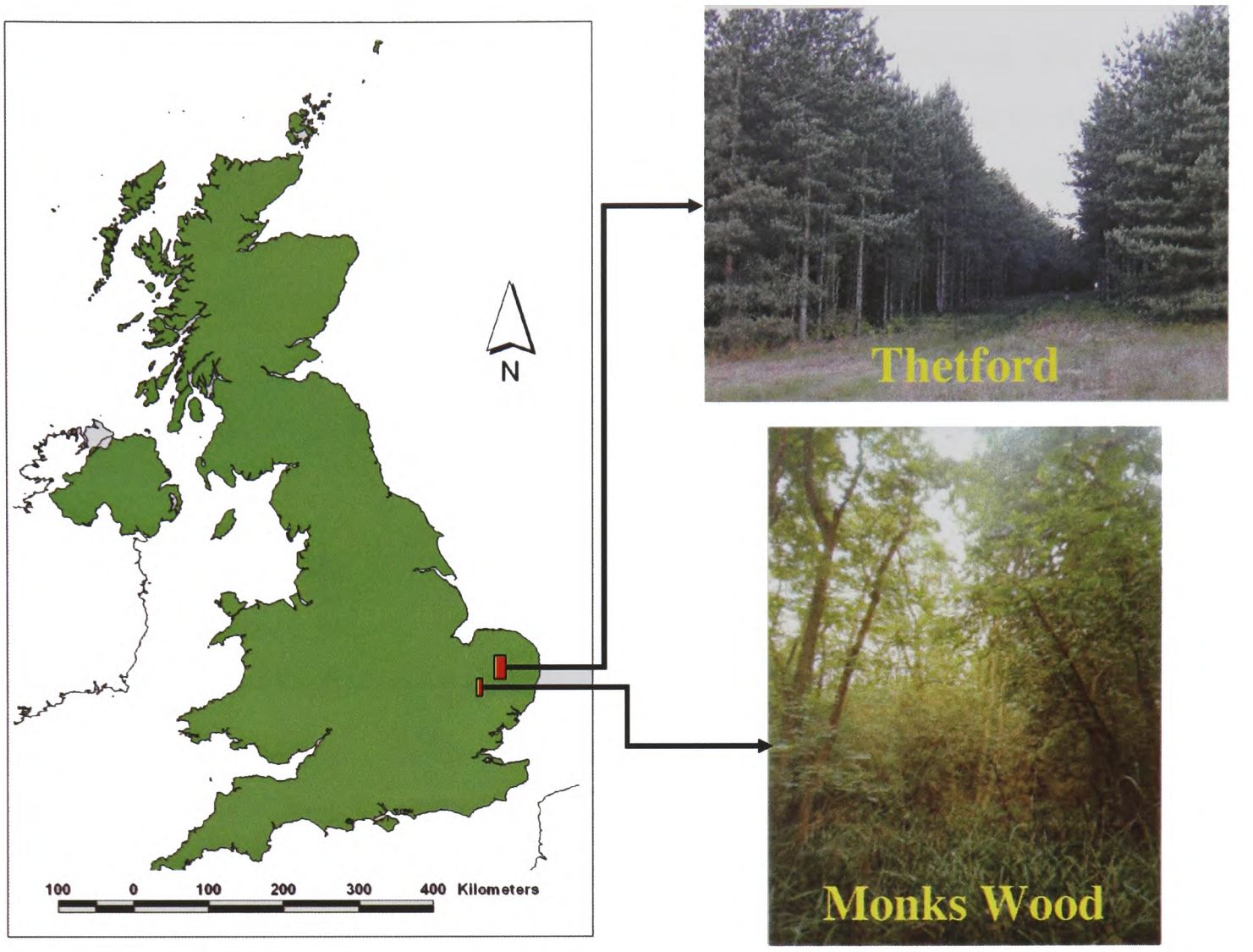


Figure 8.8 Location of Monks wood and Thetford forest study sites in the UK. The map was derived from the Environmental System Research Institute database (ESRI Inc.). The location of the woodlands is approximate (Photos: Courtesy of Brian Briggs and Laine Skinner, 2002).

8.6.1 Monks Wood

Monks Wood, located in Cambridgeshire, was purchased in 1953 for the establishment of a National Nature Reserve (NNR) (Massey 1994). The forest, an approximately 2x2 km^2 mixed deciduous woodland, is composed mainly of 5 dominant tree species: ash (*Fraxinus excelsior* L.), elm (*Ulmus carpinifolia* Gleditsh), field maple (*Acer campestre* Linn.), oak (*Quercus robur* L.) and aspen (*Populus tremula* Linn.). Dominant shrub species include hawthorn (*Crataegus monogyna* Jacq.), hazel (*Corylus avellana* Linn.), blackthorn (*Prunus spinosa* Linn.), dogwood (*Cornus sanguinea* Linn.), and wild privet (*Ligustrum vulgare* Linn) (Steele and Welch, 1973). Since 1950s, the management strategy of the forest has been principally one of non-intervention, which allowed for natural change to occur (Briggs 2001, Crampton 1996).

Semi-natural deciduous forests are intrinsically far more irregular than homogeneous coniferous plantations. The diversity of species and ages as well as the various canopy layers ranging from ground vegetation, shrubs and saplings understorey and overstorey trees compose an arbitrary arrangement of elements. In Monks Wood, some stands contain a large proportion of relatively small woody stems whereas others have a higher proportion of larger stems. Measuring the carbon content of such forest is therefore complex and challenging. However, Monks wood is representative of the larger (27-157 ha) fragments of woodland which remain in the intensive arable farmland of eastern England and thus represents a good sample of the type of temperate forests found in this region.

8.6.2 Thetford forest

Thetford forest is located in East Anglia at a distance of approximately 45 km South-West of Norwich, UK (see Figure 8.8). The main forest covers an area of approximately 20x30 km^2 (Skinner and Luckman, 2000). The woodland is a managed Forestry Commission plantation and is primarily made up of even-aged mono-species stands of Scots Pine (*Pinus sylvestris* L.) and Corsican Pine (*Pinus nigra* var. *maritima* (AIT.) Melv.). The forest was created earlier this century (1920-30) by afforestation of low-grade agricultural land and heathland and a second crop was planted in 1980 (Baker 1992, Baker *et al.* 1994). The plantation has a long management history, minimal topographic variation and has been widely monitored by remote sensing techniques. Plantations are generally more uniform in age, spacing, and species composition than natural deciduous woodlands. Thetford forest thus provides a study site of reduced complexity where single species and even-aged stands provide excellent sites for constraining variables and removing the difficulties arising from the heterogeneity of biophysical variables of natural forests. The wide ranging datasets available and their extensive temporal coverage justify the choice of this area for the purpose of this study.

8.7 Examples of common band ratios used for the remote sensing of vegetation using multispectral scanners

INDEXES	FORMULAS
Simple Subtractions	NIR-R
Simple Division	NIR/R
Complex Division	NIR/ (R + other wavelengths)
Normalised Difference Vegetation Index (NDVI)	(NIR-R)/ (NIR+R)
Complex Normalised Difference Vegetation Index	$\sqrt{O.5+[(NIR-R)/(NIR+R)]}$

R: red wave band, IR: Near Infrared waveband

8.8 Factors affecting the spectral response of forest canopies

(adapted from Treitz and Howarth 1999)

External Factors	Description
Size of viewed area	Variability of the spectral response of a forest canopy will depend on the size of the instantaneous field of view.
Sun elevation	Solar radiation penetrates more deeply into a canopy at steep angles; bi-directional reflectance increases in the visible and decreases in the near infrared with the increasing sun elevation, particularly with dense forest canopies; leaf transmittance is low in the visible but up to 50% in the near infrared.
Zenith view angle	Natural surfaces do not perform as Lambertian reflectors; spectral radiance of surfaces varies as function of view, zenith and orientation angles; bi-directional reflectance for continuous canopy is wavelength dependant.
Cloud cover	Clouds modify the irradiance level for a given sun elevation and significantly change the proportion of direct and diffuse radiation reaching the earth`s surface.
Atmospheric aerosols	Modify the optical path between satellites and the earth surface, wavelength dependant, more pronounced at shorter wavelengths.
Wind speed	Affects the geometry of the forest canopy.
Internal Factors	
Orientation of tree rows (plantation)	Light penetration varies as function of row direction (a function of plantation); these structural aspects of plantations are thought to be more directly correlated with spectral response than canopy cover.
Soil optical properties	Background spectra may confound changes in the spectral response of the overstoreyvegetation; optical properties of soil chow an increase in reflectance from the visible to middle infrared.
Canopy geometry (closure, density)	The most significant factor acting on the optical properties of forest canopies (controls the fractions of overstorey and understorey visible to the sensor).
Terrain (slope angle and aspect)	Terrain elements account for appreciable variations in response in all wavelength bands; slope and aspect can produce a wide range of pixel values within one cover class; this effect is linked to solar elevation at azimuth.
Height, vigor and composition of species	Density, height and vigor of vegetation and percent of composition of species affect the spectral response of forest canopies; these effects directly impact forest change assessment and classification.

Appendix B

Location of plots and stands in Monks Wood and propagation of uncertainties

9.1 Stand location in Monks Wood

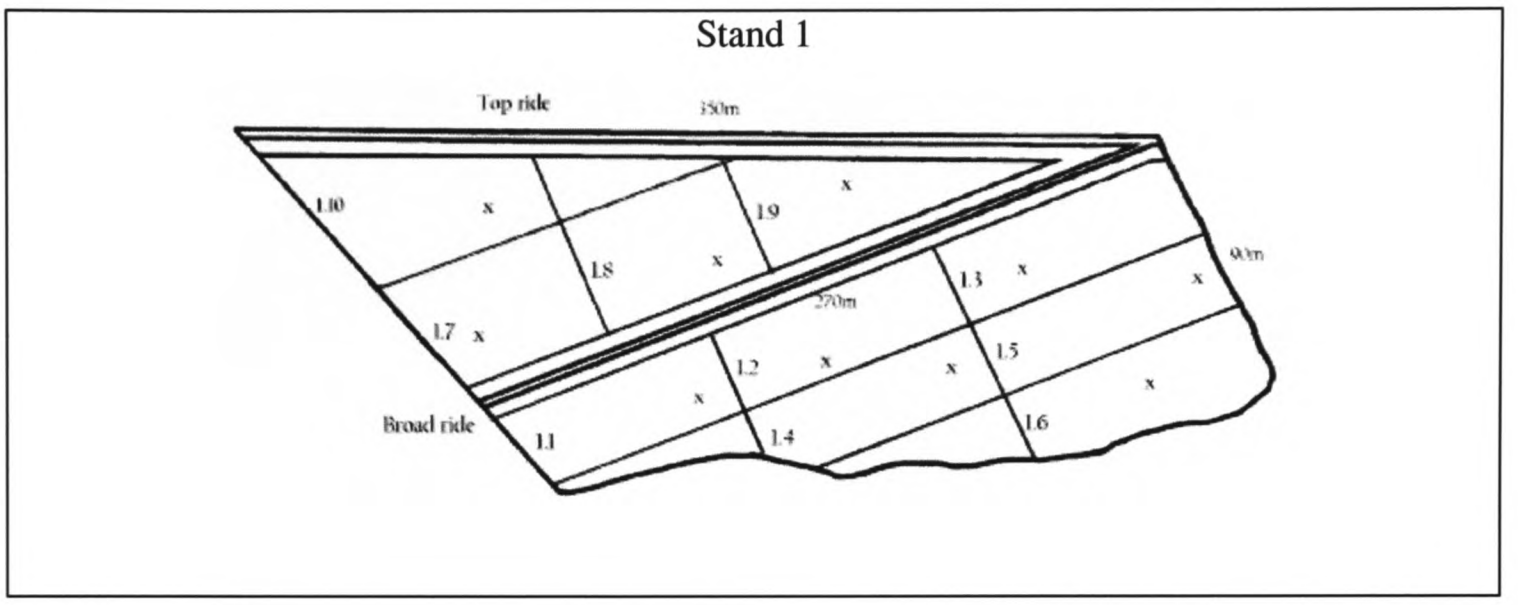
The following appendix provides additional information related to the ground data collection in Monks Wood.



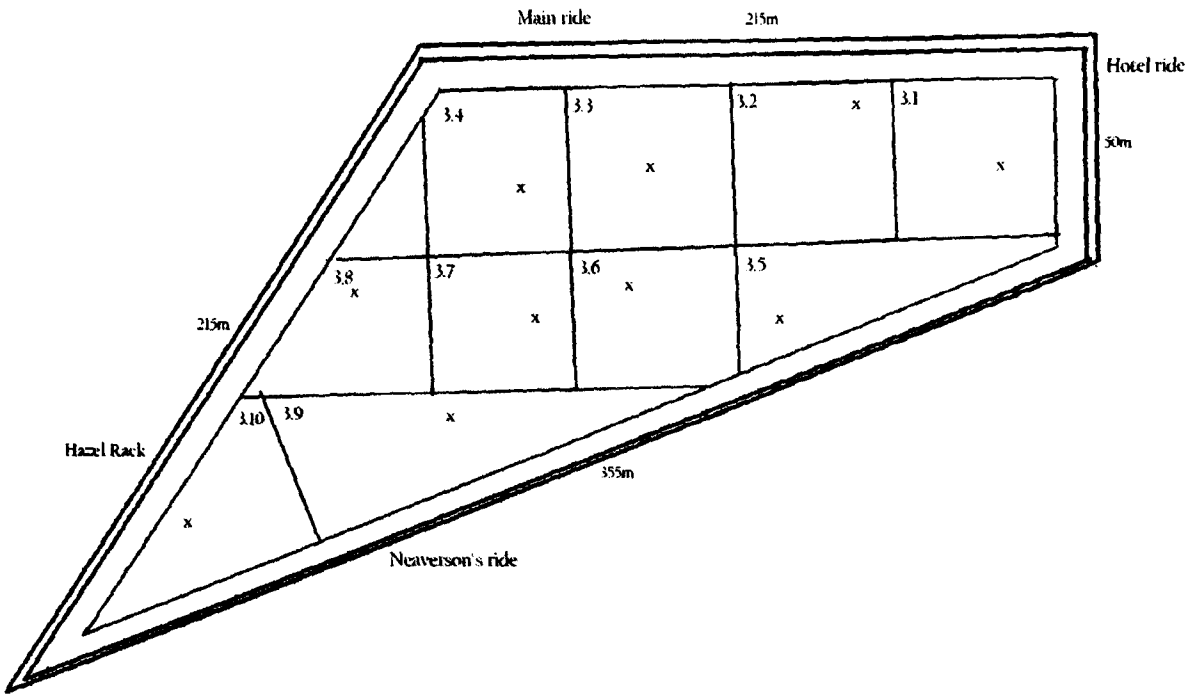
Figure 9.1: Location of each stand within the woodland (photos are a courtesy of Brian Briggs)

9.2 Plot location in Monks Wood

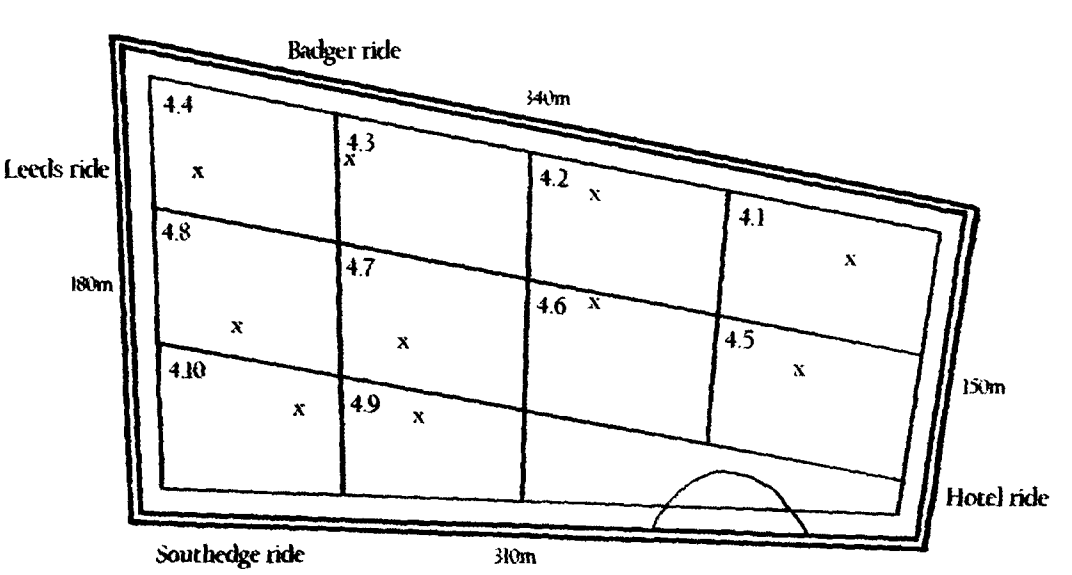
The following figure shows the location of the centre of each plot within each stand (Briggs 2000).



Stand 3



Stand 4



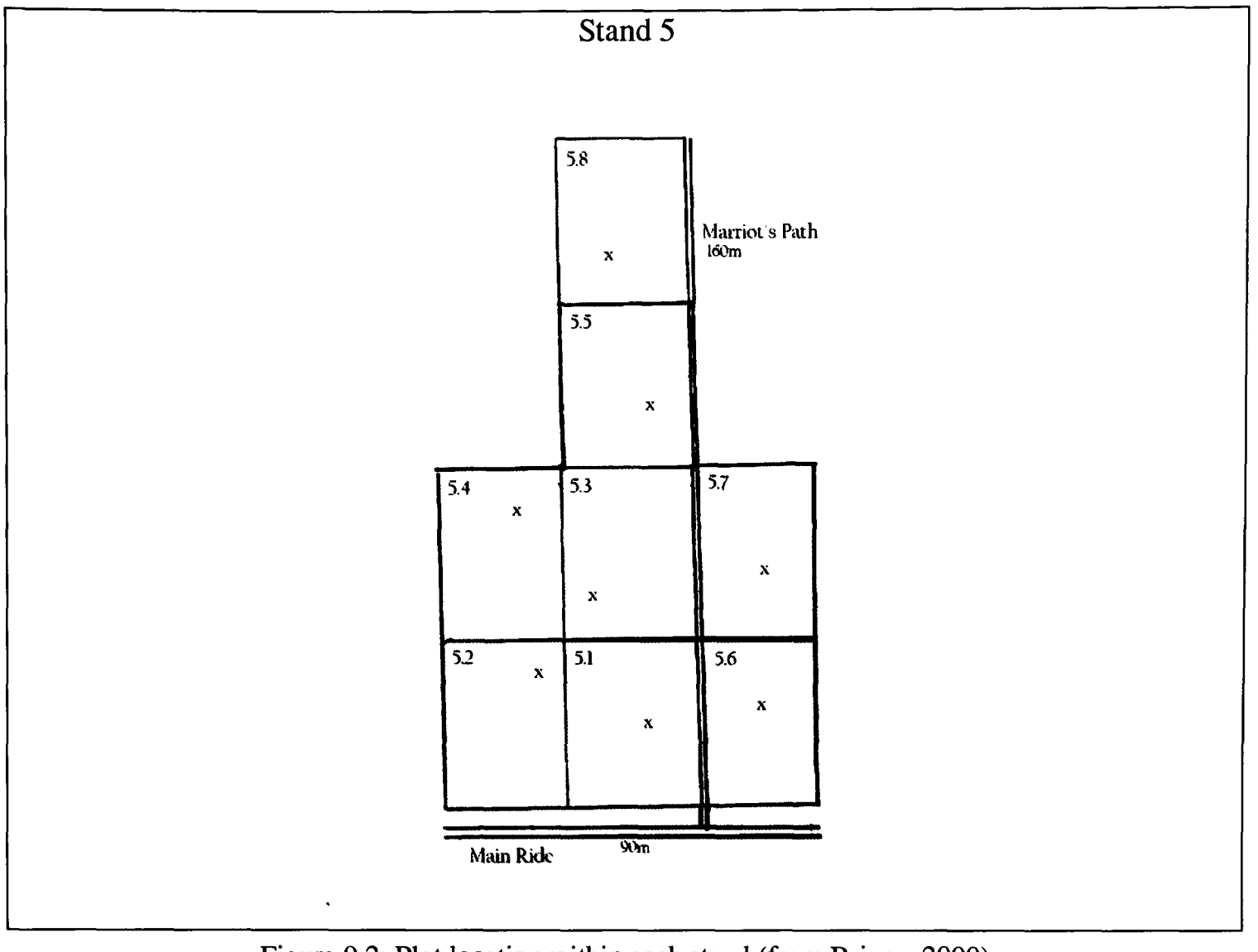


Figure 9.2: Plot location within each stand (from Briggs, 2000)

9.3 Propagation of uncertainties

In this section, the overall uncertainty to the above-ground overstorey component of Stand 1 is estimated through the propagation of errors from individual components. The purpose of this exercise is to demonstrate the incertitude in the results presented in Chapter 3.

In estimating the overall uncertainty, a number of assumptions have been made:

a- The errors are assumed independent.

b- The parameters to the regressions derived from Crockford (1987) are errorless.

c- The relative uncertainties in the conversion factors are: 30% for basic density and 10% for carbon content.

d- The absolute error on the DBH instrument is 0.5 cm.

The propagation of errors was estimated in a 3 steps procedure:

1- The estimation of the AG total volume on a per tree basis is estimated from an equation of the form:

$y = ax+bx^2+c$

Where y is above ground volume (m^3) per tree and x is DBH (cm). Different equations were provided per species (Table 3.2). As stated in the GPG for LULUCF (IPCC, 2005), the resulting relative error on y, $\partial y/y$, is estimated as:

$$\partial y/y = \frac{\text{sqrt}\left((a * \partial x/x)^2 + (\text{sqrt}(2) * \partial x/x * b)^2\right)}{|\, a + b \,|}$$

Where a and b are parameters to the regression, and $\partial x/x$, the relative error to x.

2- The total volume per stand is estimated from the sum of the volumes per plot scaled up to the stand. The overall error in total volume per stand ($\partial z/z$) was therefore estimated as :

$$\partial z/z = \text{sqrt}\ \left((\partial y_1/y_1)^2 + (\partial y_2/y_2)^2 + (\partial y_3/y_3)^2 \ldots + (\partial y_n/y_n)^2 \right)$$

Where $(\partial y_i/y_i)$ is the relative uncertainty associated with each tree total volume, $i=1,\ldots, n$.
The resulting relative uncertainty, $\partial z/z$, was 0.1886.

3- Conversion to carbon content was achieved using multipliers, each with its associated uncertainty. The overall uncertainty in overstorey above ground carbon content ($\partial w/w$) was estimated as:

$$\partial w/w = \text{sqrt}\ \left((\partial z/z)^2 + (\partial d/d)^2 + (\partial c/c)^2 \right)$$

Where $\partial d/d$ is the relative uncertainty to basic density and $\partial c/c$, to carbon content.
The resulting relative uncertainty in overstorey above ground carbon content per stand, $\partial w/w$, was 0.3682, thus 37%

Table 3.3 provides carbon content values of all stand components. The value for Woody Above Ground (WAG) carbon content in stand 1 should be read 85 t ha^{-1} ± 37%.

Appendix C

Additonal information for Chapter 4

10.1 Introduction

This appendix presents information complementary to Chapter 4 and is divided into 4 sections. The first section explores some of the basic assumptions for using stands as the principal unit of investigation. Spatially exhaustive remote sensing data enables the exploration of intra and inter stand variability, thereby testing the assumption under which stands represent relatively homogeneous spatial units.

The second section presents the selected method for locating the field surveyed plots on the LiDAR digital canopy height map (DCHM). Here, an important distinction is made between plots and parcels. For clarity, the term plot refers to the field-based areas for which data were collected on the ground. These are 20x20m^2 rectangular plots. Parcels refer 20m diameter circular areas located on the LiDAR DCHM which correspond spatially to the field-based ground plots.

The third section presents the investigation leading to the use of LiDAR height metrics as a basis to estimate above-ground carbon content (AGCC). Once the plots were located on the DCHM, an investigation of relationships between field-based tree height measurements and AGCC was made. If no relationships had been found between these field-based variables, then the use of LiDAR to extract height metrics as means to obtain AGCC would have been difficult to justify. Correlation was found to exist between field-based tree height measurements and field-based estimates of AGCC. Therefore, LiDAR height metrics were compared to ground-based height measurements. The rationale follows that of Magnussen and Bourdewyn (1998) who suggest that height quantiles per stand derived from LiDAR can be good estimators of stand height metrics. The successful correlation "LiDAR and field-based heights" leaded a search for a suitable model serving as a basis to derive a carbon model. The data available for the selection of this model and ancillary information relevant to the selection of a height metric are provided below.

Finally, the last section to this appendix addresses sources of uncertainties, which define the reliability of the results presented in Chapter 4. A particular attention is given to the calibration of the DCHM using reference canopy height measurements taken with a laser theodolite. The overall quantification of these sources of errors forms the basis for further research.

10.2 The importance of scale: stands as homogeneous forest units

One advantage of remote sensing over field-based surveys is that it enables extensive spatial coverage of the woodland. This provides a means by which some field-based assumptions can be either tested or validated. Here, the basis for selecting stands as relatively homogeneous spatial units was tested.

The following approach was used (Woodcock and Strahler, 1987). The DCHM was degraded from the 1m x1m spatial resolution to coarser resolutions. The local standard deviation (calculated from 3x3 windows), averaged over the image, was used as an indication of spatial variability (Figure 10.2): small standard deviations indicate that neighbouring pixels are highly similar, while large standard deviations indicate a strong contrast between the pixels. As clearly stated by Woodcock and Strahler (1987, p.313):

> *" If the spatial resolution is considerably finer than the objects in the scene, most of the measurements in the image will be highly correlated with their neighbours and a measure of local variance will be low. If the objects approximate the size of the resolution cells, then the likelihood of neighbours being similar decreases and the local variance rises. As the size of the resolution cells increase and many objects are found in a single resolution cell, the local variance decreases."*

Thus, if stands are homogeneous and constitute each a population of its own, intra stand variability should be small while inter stand variability should be largest. Figure 10.1 shows the LiDAR DCHM degraded at various spatial scales. In Figure 10.2, the overall mean local standard deviation is plotted against pixel resolution. The peak area (150-300 m) indicates the resolution with largest standard deviation between pixels. This resolution coincides with the selected stand size (see Table 4.1 in Chapter 4).

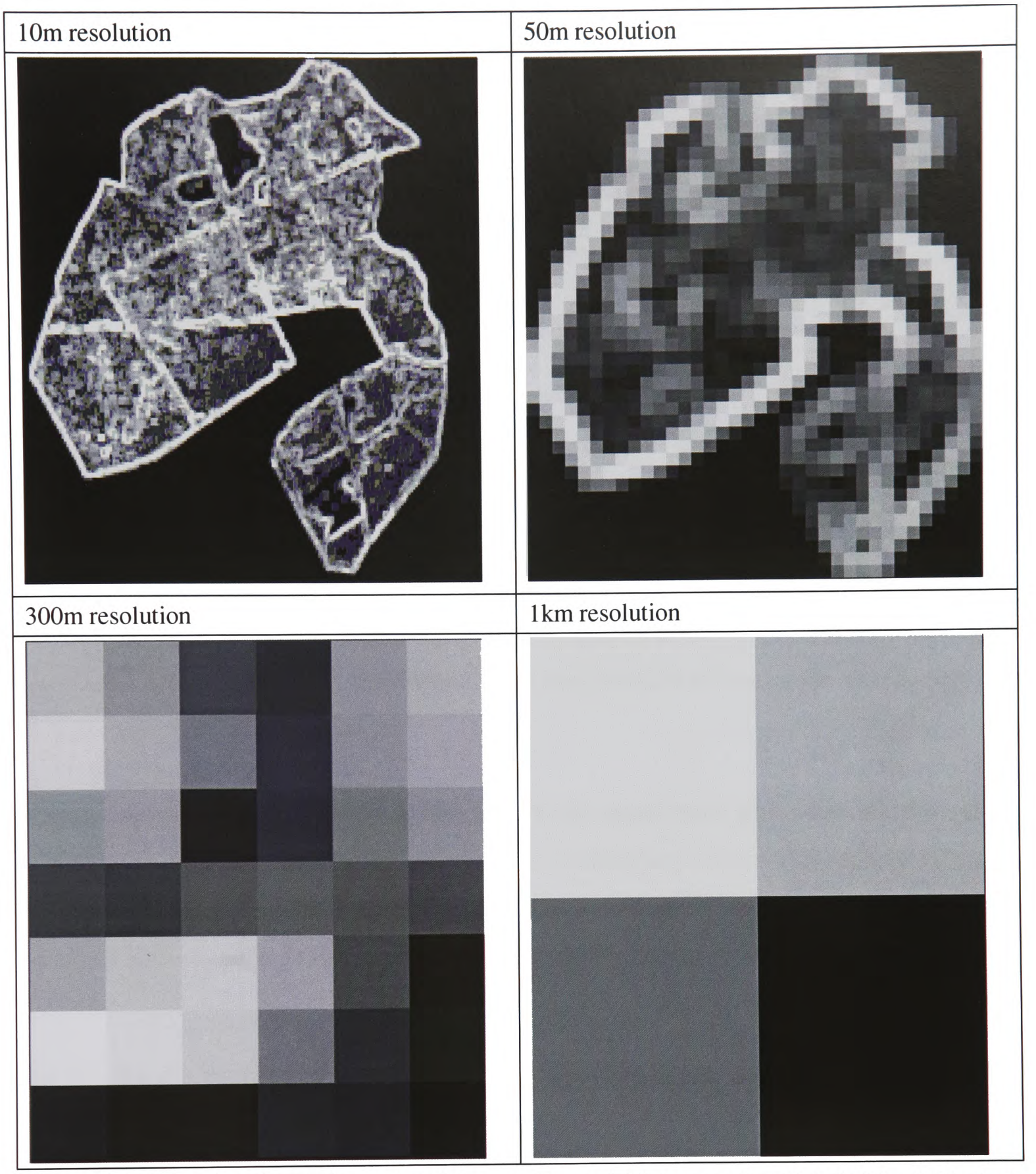


Figure 10.1: Examples of resolutions selected to assess the spatial heterogeneity of Monks Wood. All pixels located outside the woodland were excluded in the analysis.

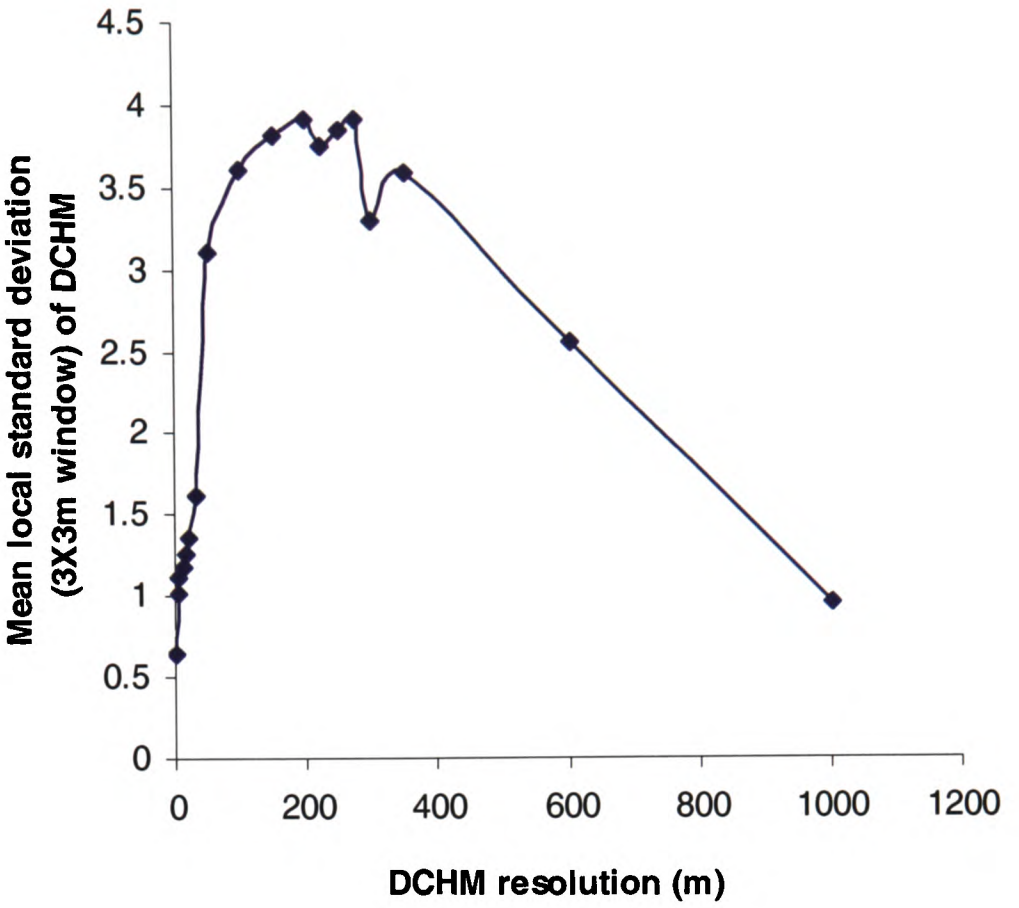


Figure 10.2 Spatial heterogeneity within Monks Wood (based on LiDAR canopy height measurements only)

This illustrate that spatial scales below that of the stand show little intra stand variability while spatial scales around that of the stands size show larger variability. Above 300 metres spatial resolutions, the stands are merged together, and thus the variability between pixels is reduced. This supports the selection of stands as relatively homogeneous forest units.

10.3 Plots location on the digital canopy height model

The following describes the information available to guide the location of the plots on the LiDAR canopy height map.

Field survey

- The plots were square and oriented randomly. No records to the orientation of the squares were made.
- In each plot, dominant tree height (H_{dom}) was measured for approximately 5 trees per plots. Dominant tree height is defined as the height of the tree specimens with largest DBH per plot (height being the vertical distance from the base of the tree to its uppermost point).
- Dominant heights were measured using a clinometer. Distances from observation point to the measured trees were estimated using a tape measurer.

- Schematic maps of the location of the plots, rides, ride intersections, ride length and stand sizes were provided. Estimates of distances between plot centres and rides were also available.
- Each plot was marked in the field using coloured poles (for each plot, the centre and its four corners were signposted).
- After the field work, a single pole per plot was left standing. In most cases, the centre pole was left on site. In some unspecified cases, the pole to one of the four plot corners was left standing instead of the centre pole.

GPS point measurements of plot centre location

- GPS measurements of the poles were taken two years after the fieldwork was conducted. The GPS has a stated maximum error of 15-m but in use, the error was found to average 7-m (15-m max, 4-m min).
- During this second survey, 32 out of 48 poles were found.
- Of the 32 poles found, some were ambiguous and could have belonged to either one of two consecutive plots.

Making use of these available datasets, different approaches to locate the plots on the DCHM were tested:

1. Using the GPS measurements only
2. Using the GPS measurements combined with measurements of dominant tree heights in each plot
3. Using the schematic description of plot location and distances from rides.

10.3.1 Approach 1 - Parcel location using GPS data points

All GPS recordings were overlaid to the DCHM raster layer to visualise their position. Each GPS point measurement was assumed to represent the centre of a plot. Schematic maps of the location of the plots (Figure 9.2, Appendix B) provided guidance for the identification of each GPS points in relation to the others. This approach was however disregarded as it generated too much uncertainty. In stands where only a few GPS point measurements were available, the attribution of plot numbers to GPS point measurements became really subjective. Thus, ancillary data were sought.

10.3.2 Approach 2 - Parcel location using dominant tree heights and GPS data points

In Table 10.1, the average field-based dominant tree height (~5 trees), along with the maximum height and the average from the three tallest heights are presented for each plot. These field-based height metrics were used as ancillary data for locating the plots on the DCHM. For a given plot, it was assumed that heights statistics per parcel, derived from the LiDAR DCHM, should be equal or below field-based height estimates. Chapter 4 provides a discussion on height underestimation from LiDAR measurements.

Table 10.1: Field-based metrics of dominant tree heights per plot

Stand and Plot no.	Average H_{dom}	3 tallest H_{dom}	Maximum H_{dom}
1.1	16	17	18
1.2	14	18	19
1.3	15	18	19
1.4	14	17	17
1.5	17	17	18
1.6	13	16	18
1.7	16	17	18
1.8	15	19	20
1.9	15	16	17
1.10	18	19	20
2.1	18	20	21
2.2	17	17	19
2.3	19	22	24
2.4	20	23	23
2.5	18	18	19
2.6	18	19	20
2.7	21	21	21
2.8	14	15	17
2.9	18	18	20
2.10	17	18	19
3.1	15	16	17
3.2	15	18	21
3.3	10	10	10
3.4	15	15	15
3.5	16	17	18
3.6	13	13	20
3.7	13	14	15
3.8	14	14	14
3.9	13	13	14
3.10	13	15	16
4.1	15	17	16
4.2	19	22	23
4.3	14	14	15
4.4	16	18	22
4.5	16	17	18
4.6	17	17	18
4.7	15	15	16
4.8	18	19	20
4.9	17	17	18
4.10	16	17	18
5.1	19	20	20

5.2	22	22	23
5.3	21	21	22
5.4	20	21	22
5.5	21	21	21
5.6	24	25	26
5.7	22	23	24
5.8	17	19	20

Code was written in C++ to automatically draw circular parcels around and surrounding each GPS point on the DCHM. Only the parcels for which all pixel heights were below or equal to the maximum field-based dominant tree height were selected (Table 10.1). For instance, the maximum field-based dominant tree height for plot 1 of stand 1 (plot 1.1) being 18 m, the parcel drawn in Figure 10.3 would not have been selected, as the maximum pixel height (18.5 m) is above that measured on the ground.

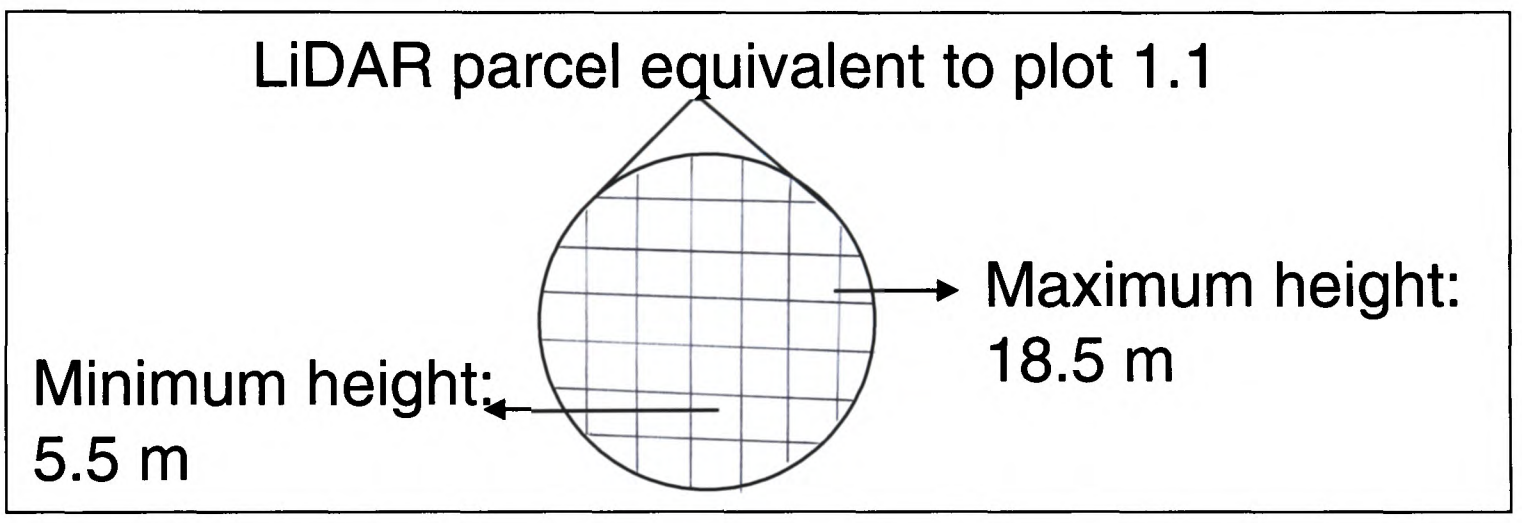


Figure 10.3: Height per pixel within a circular parcel on the DCHM. The pixels of maximum and minimum heights are shown.

A description of the C++ program follows. At first, each GPS co-ordinate is assumed to be the centre of a plot. No orientation to the field-based rectangular plots were provided, thus parcels on the DCHM were drawn circular, with a diameter equal to the length of the side of the square plots (i.e. 20 metres, Figure 10.4).

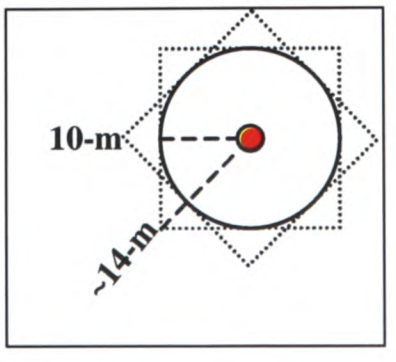


Figure 10.4: Selection of a suitable shape for the parcels. Since no data on the orientation of the field-based plots were given, the parcels were drawn as circles of diameter equal to 20m.

Ambiguous GPS points, for which it was difficult to assign a unique plot number, were tested for all possible matches. For instance, if the GPS coordinate was thought to belong either to plot X or to plot Y, the coordinate was tested both for X, and Y.

Since no orientation of the square plots were provided and because the GPS points could be from plot corners (Section 10.3), the actual centre of the parcel could be located anywhere on the circumference of a circle referred to as the enclosing ring (symbolised by the arrow in Figure 10.5). This ring has the GPS coordinate as centre point and its radius is equal to the distance between the centre of the square plot to one of its corners (see longest distance in Figure 10.4). Figure 10.5 illustrates more clearly these possibilities.

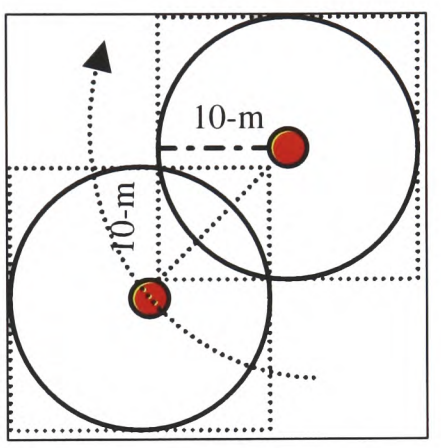


Figure 10.5: Location of the centre of the parcels

Consequently, the program locates circular parcels of 20-m diameter on each GPS point on the DCHM. Thereafter, several adjacent circles, with their centre located on the circumference of the enclosing ring are also located as illustrated in Figure 10.5. Finally, only the parcels with all pixel heights smaller or equal to the maximum field-based dominant tree height were selected (Figure 10.3).

For all parcels for which this approach did not yield results, the stated error by Garmin for its GPS instrument was considered. The GPS point could be located anywhere within a circle of radius equal to the 15 m stated instrument error (Garmin Corporation, 1997). Thus, the grouping of parcels (centre and adjacent circles, see Figure 10.6) is displaced along a 15-m axis and rotated around the 15-m radius circle). In the event that the model gave several solutions, the centre one was always selected.

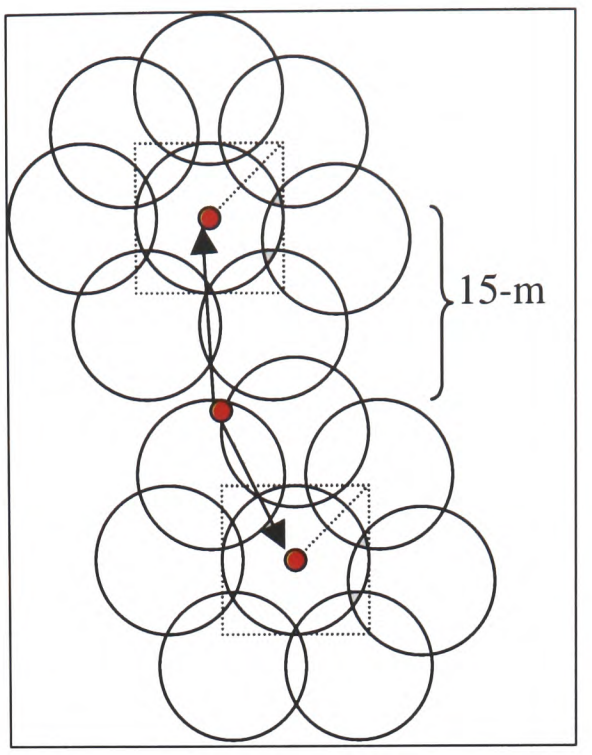


Figure 10.6 The sampling procedures for the selection of the parcel considering the GPS stated error.

Finally, this approach yielded so many results that the solutions often overlapped. Thus the objective selection of the parcels best matching the corresponding plots became impracticable. Consequently, this approach was rejected.

10.3.3 Approach 3 - Parcel location using field-mapping

In this approach, field-based schemas of the stands (Appendix B), exhibiting plot centre points, rides, intersections and dominant features were scanned, registered and geometrically corrected using the rubber sheeting function in Erdas Imagine. Geometric correction was required, as although the distance between the centre plots and the rides was available, no distances along the rides were given: i.e. assuming that ride intersection is the origin, the x axis, the axis along the ride and the y axis, that perpendicular to the ride, then for each plot, only the y coordinate was available.

A vector layer was therefore created from each stand schema (Appendix B) and plot centres were mapped as vector points. The geometric correction was achieved using the rubber sheeting function: "after a triangulated irregular network (TIN) is formed over all the control points, the image area covered by each triangle in the network is rectified by the first (linear) or fifth (nonlinear) order polynomials". The linear model was selected here as it requires less ground control points (GCP) to achieve the transformation (the number of GCP required increases per order of transformation). The LiDAR DCHM image was used as reference. Easily identifiable features and ride intersections on both maps were used as GCPs. In the case where rides were difficult to locate on the DCHM, GPS point

measurements collected along the rides were included. This approach enabled the retrieval of the x coordinate for all plots per stand.

Monks Wood is an intensively studied site and the use of markers to localise transects or research plots is common (Hill, personal communication, 2003). Thus, the poles found, and thereby the GPS coordinates used to locate the plots in Approach 1 and 2, could have mistakenly been from other studies. The approach selected is therefore assumed best, given the information available. The coordinates of the parcel centres on the DCHM, assumed to correspond spatially to the field surveyed plot centres, are presented in Table 10.2. These coordinates and the corresponding circular parcels form the basic units for the carbon accounting using the LiDAR canopy height map.

Table 10.2: British National Grid coordinates of parcel centres on the LiDAR DCHM. The parcel coordinates correspond to the field surveyed plots.

Stand and plot no.		
1.1	520543	279752
1.2	520588	279757
1.3	520645	279770
1.4	520605	279743
1.5	520693	279742
1.6	520666	279721
1.7	520472	279793
1.8	520538	279792
1.9	520583	279813
1.10	520476	279842
2.1	519211	280166
2.2	519217	280217
2.3	519253	280281
2.4	519310	280312
2.5	519330	280365
2.6	519251	280112
2.7	519291	280156
2.8	519307	280220
2.9	519339	280269
2.10	519378	280337
3.1	519830	280187
3.2	519765	280199
3.3	519698	280165
3.4	519666	280139
3.5	519781	280132
3.6	519722	280115
3.7	519684	280100
3.8	519622	280079
3.9	519626	279998
3.10	519618	279997
4.1	519983	279787
4.2	519868	279752
4.3	519794	279710
4.4	519728	279672
4.5	519988	279745
4.6	519907	279716
4.7	519849	279658
4.8	519787	279624
4.9	519870	279633
4.10	519836	279612

5.1	520199	280431
5.2	520171	280437
5.3	520174	280457
5.4	520155	280476
5.5	520165	280498
5.6	520219	280451
5.7	520206	280490
5.8	520143	280543

10.4 Height as a surrogate for volume: validation of the assumption

Once the parcels were located on the LiDAR canopy height map, a preliminary analysis of the approaches for deriving AGCC from tree height estimates was conducted, as although tree height-volume regressions are widely used in even-aged and single species forest stands as predictive tools, tree height may not be a suitable surrogate variable for stemwood volume in heterogeneous woodlands.

Firstly, the strength of association between field-based measurements of dominant tree heights (maximum dominant tree height, average from the three largest and average from all dominant tree heights, Table 10.5) with field-based AGCC was investigated. If a relationship exists between tree heights measured on the ground and carbon content, then the use of LiDAR heights to estimate the carbon content of the stands can be justified. Field-based AGCC was correlated against all dominant tree heights metrics described above. The correlation between the overall average, the average from the three largest, and the maximum height with AGCC were, at the plot level, 0.65, 0.66 and 0.54 (all $p < 0.01$, $n=48$) and at the stand level, 0.87, 0.91 and 0.89 ($0.1 > p > 0.05$, $n=5$), respectively. Figure 10.7 presents an example of these correlations (a.) per plot and (b.) per stand.

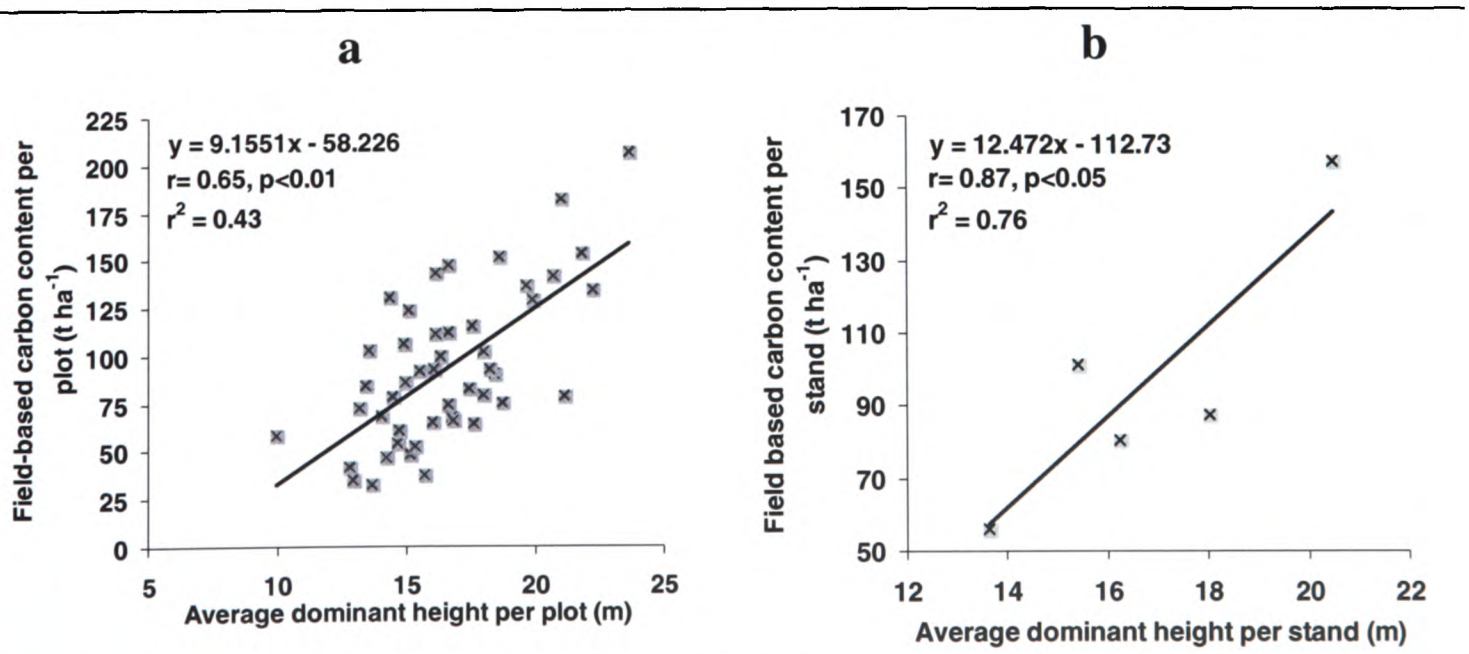


Figure 10.7 Field-based above-ground carbon content against field-based average dominant tree height (a) per plot and (b) per stand

Here, although both X and Y were measured with error, field-based AGCC was also regressed against average dominant tree height to explore their intervariability, rather than to provide a regression for prediction purposes. As shown in Figure 10.7, 43% of the variance in AGCC is explained by the regression model at the plot level and 76% at the stand level. This suggests that height metrics can account for some of the variability of AGCC.

10.4.1 Comparison between average field-based dominant tree heights and LiDAR height metrics

Field-based dominant tree heights per plot were thereafter compared to height metrics derived from the Lidar DCHM parcels. For each 20x20 m^2 parcel corresponding to the ground plots, various LiDAR height metrics were extracted (average height, maximum height, and various height percentiles). Figure 10.8 and Table 10.3 explore the strength of association between these height metrics and the average field-based dominant tree heights.

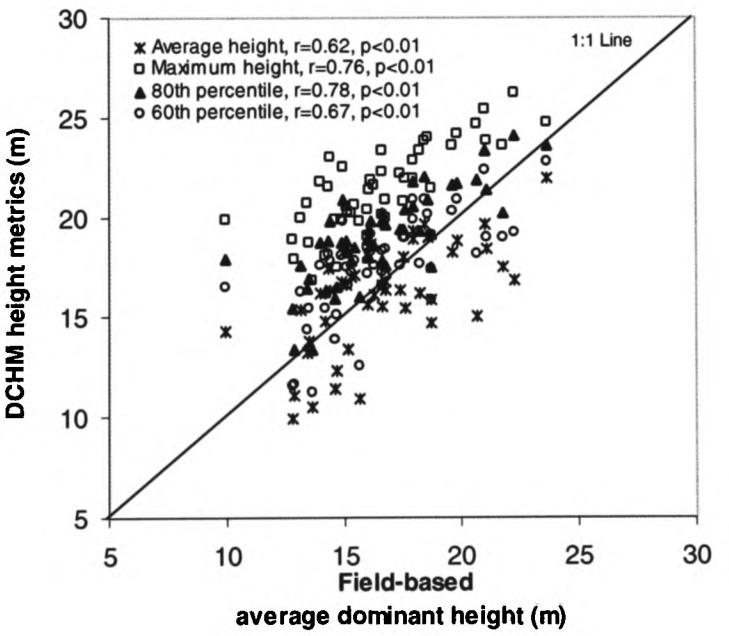


Figure 10.8: DCHM height metrics derived from the 20m diameter circular parcels against field-based average dominant tree height per plot.

Table 10.3: RMSE and bias calculated between DCHM height metrics and field-based average dominant tree height [a.] Negative/positive signs indicate height over/under estimation respectively, of field-based average dominant tree height by the DCHM height metrics

Field-based average H_{dom} and:	RMSE (m)	Bias (m) [a.]
DCHM average height	17	22
DCHM maximum height	35	-230
DCHM 80th height percentile	21	-117
DCHM 60th height percentile	16	267

The strength of association presented in Figure 10.8 is a function of the height statistic elected. The highest correlation is obtained with the 80th percentile (0.78, $p<0.01$) and the poorest, with the average height (0.62, $p<0.01$). In addition to generating the highest correlation, the 80th percentile generated the second lowest bias (Table 10.3). These results supported the search for a mathematical model to derive above-ground carbon content from LiDAR height metrics.

10.5 Yield models as a basis for carbon model

Yield tables provided guidance for exploring size relationships between various stand variables, including tree height and volume. The Sycamore-Ash-Birch (SAB) yield tables were selected as a basis to derive the model for Monks Wood on the following basis:

- Ash is by far the most dominant species in the wood. As shown in Table 4.1, Chapter 4, it contributes to more than 34% of the total basal area in the 48 plots, all trees considered, and to nearly 37% of the population of all trees larger or equal to 7 cm DBH.
- Sycamore is considered an acceptable proxy for maple (Edwards and Christie, 1981).
- Maple is a dominant species and nearly half of the total tree population in the 48 plots is composed of ash and maple alone.

As shown in Figure 10.9, the growth patterns of the oaks found in Monks wood are also well represented by the SAB tables. Within a yield table, several productivity classes are available. Thus, additionally to the selection of a model suitable for the species found in Monks Wood, an assessment of the productivity in Monks wood was required. To do so, a total of 49 dominant trees were cored. The sampled trees were selected so that their DBH was roughly that of 25 ± 10 cm DBH, corresponding approximately to the DBH of SAB trees aged 70-80 years, the average tree age in Monks Wood, if unmanaged condition and

low productivity are assumed (Edwards and Christie, 1981). For all 49 trees, tree rings were counted to estimate age. Age-DBH point samples from the cored trees are presented in Figure 10.9. Averages with standard errors per species are also presented. These were used to construct an overall weighted mean and overall weighted standard deviation of means (error bars) for the whole wood. The basal area of each dominant species was used as weight (Table 4.1, Chapter 4). Figure 10.9 shows the 49 tree samples, averages and standard errors superimposed to the SAB model YC 4, 6 and 8. The yield class 4 model passing through error bars of the weighted average was selected to be the most suitable basis for the modelling (Chapter 4).

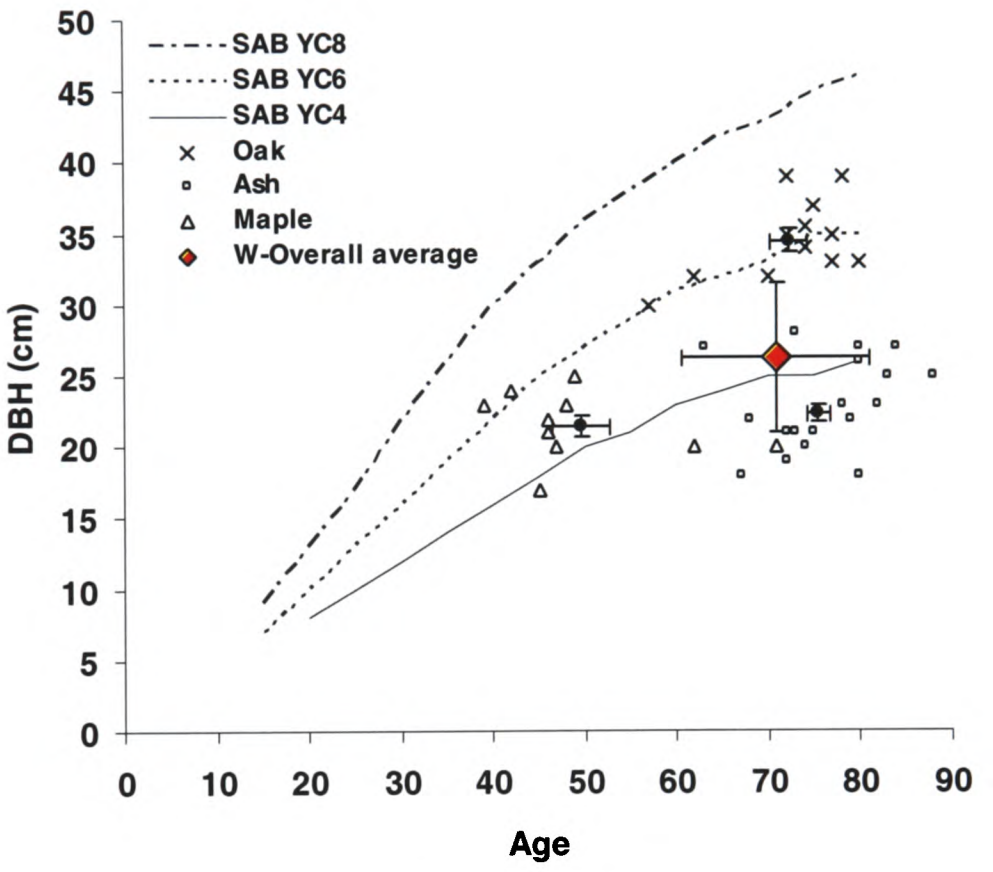


Figure 10.9: Yield model selection based on DBH-age comparison between field collected tree cores and the SAB empirical yield models YC 4, 6 and 8. Standard errors are shown for each per species average. The overall average, estimated by weighting the species average per basal area, shows the correspondence of the field data with the SAB YC4 model. Models were derived from Edwards and Christie (1981).

10.6 Wood density

Drymass densities were also estimated from the 49 cores (Figure 10.10). The resulting overall weighted average was used to convert total above-ground volume to drymass.

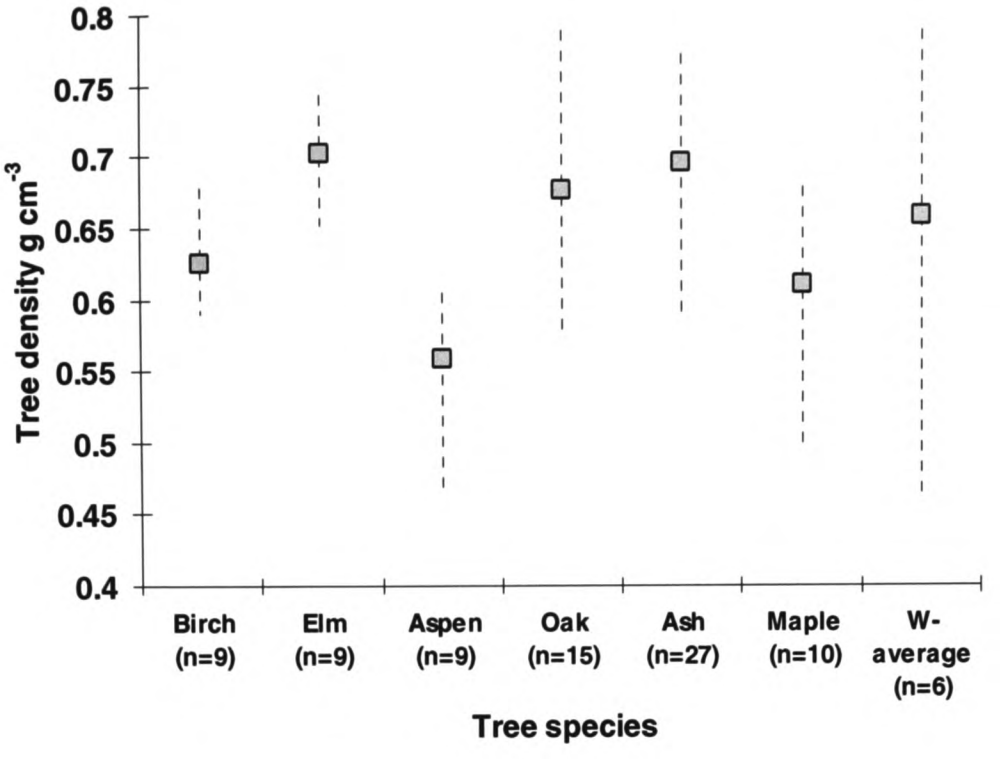


Figure 10.10: Dry mass density from tree species in Monks Wood. All averages per species are shown. The dotted line shows the range of densities measured per species (minimum and maximum values). W-average stands for weighted average of the means 0.66 ± 0.03 (n=6). Standard deviations are given in Table 4.1, Chapter 4.

10.7 Quantifying carbon content from LiDAR height metrics

The AGCC model and parameters derived from the original SAB YC4 table are presented in Equation 2 and Table 4.5, Chapter 4 and are reproduced here:

$$AGCC = k\ a\ e^{b\ H_{\%}}$$

Where $H_{\%}$ is the dependent variable, a LiDAR height metric derived from the DCHM parcels. The parameter k converts stemwood volume to AGCC and is derived directly from the literature and field-based measurements. Similarly, a regulates the amount of biomass volume found on the ground when canopy height is equal to zero. In Monks Wood, the AGCC from ground vegetation and litter ranges between 2.3 and 4.6 t ha^{-1} (Table 3.3, Chapter 3), roughly corresponding to a biomass volume of 12 m^3 ha^{-1} when the same biomass expansion factors as in Table 4.5, Chapter 4 are used. Both parameters k and a have a specific physical meaning. While k is fixed, a should only take up values within the acceptable range mentioned above. Conversely, b is a calibrated parameter.

Two approaches for the calibration of the AGCC model (Equation 2) were tested. In approach 1, the AGCC model was applied to all the pixels within a parcel (Figure 10.3). The AGCC from all pixels was averaged over the parcel. In approach 2, a single height

metric considered representative of the entire parcel was extracted to estimate AGCC for the parcel.

10.7.1 AGCC from all pixels per parcel

A program was written in C++ to extract all pixel canopy heights per parcel. AGCC was then estimated per pixel and all pixels AGCC averaged per parcel. The calibration of the model was then achieved by minimising the difference between the field-based estimates of AGCC per plot from the average AGCC per parcel.

To minimise the Sum of Square Error (SSE) between the average AGCC per parcel and the field-based AGCC, parameters *a* and *b* to

Equation 2 were varied using the solver function in Microsoft Excel. By varying the parameters and recalculating the AGCC per pixel, the function allows searching for the parameters that generate the lowest SSE between the two datasets.

Using this approach, when *b* was kept constant, *a* would vary less than 6% from the SAB YC4 original parameter. The calibration did not produce a considerable improvement over the original parameters derived from the SAB yield table. When both parameters were allowed to vary, *a* reached values beyond its acceptable range. The AGCC resulting from the un-calibrated and calibrated model are presented in Figure 10.11 against field-based estimates per plot. The parameters to the calibrated model yielding the lowest SSE are also presented Table 10.4. Note the unrealistically high value for parameter *a*.

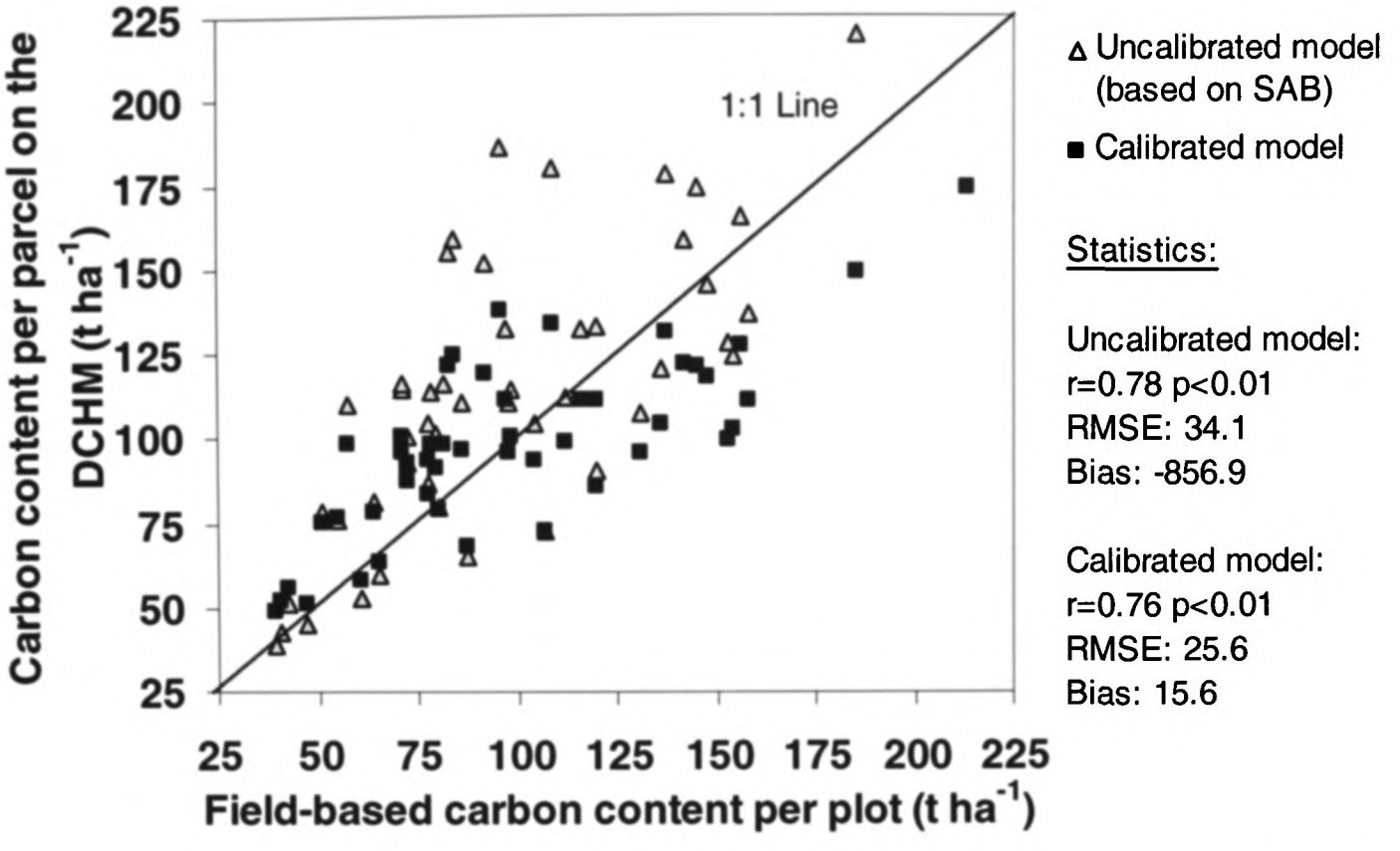


Figure 10.11: AGCC per parcel against AGCC per plot. The AGCC per parcel is obtained from averaging the AGCC per pixel over the entire parcel. Two AGCC per parcel datasets are shown. The grey triangles show the AGCC obtained from the uncalibrated model. The parameters to the model are derived solely from the SAB yield table. The black squares show the resulting AGCC from the calibrated model.

Table 10.4: Parameters and SSE to the calibrated model at the pixel scale. SSE is the sum of square errors between the ground and LiDAR derived AGCC.

Parameters	
a	30.721
b	0.115
SSE	44,870

10.7.2 AGCC from a single DCHM canopy heights metric per parcel

The second approach makes use of a single height metric per parcel as input into the AGCC model. This implied searching for a height statistic representative of the heights per plot. Various height metrics (mode, maximum, percentiles, median, mean). were extracted per parcel from the DCHM. Since height is a continuous variable, the mode per parcel was obtained by classifying all height in two metres height classes (13 classes), enabling the observation of the most frequently occurring height class in each parcel.

Table 10.5 presents a selection these height metrics extracted per parcel. For conciseness, the data for 5 instead of 48 parcels are shown. Each one of the 5 parcels presented belongs to different stands.

Table 10.5: Height statistics extracted per parcel. 5 parcels out of 48 are presented. Each one of the five parcels presented is from a different stand.

Parcel corresponding to:	**Descriptive height Statistics**	**Height (m)**
Plot 1.1	Approximate mode	19
	Maximum	21.61
	80th percentile	18.58
	Median	16.99
	Mean	16.11
Plot 2.1	Approximate mode	23
	Maximum	23.84
	80th percentile	22.00
	Median	20.39
	Mean	19.64
Plot 3.1	Approximate mode	Bi-modal
	Maximum	19.88
	80th percentile	15.92
	Median	12.05
	Mean	11.41
Plot 4.1	Approximate mode	21
	Maximum	19.88
	80th percentile	18.73
	Median	17.73
	Mean	16.80
Plot 5.1	Approximate mode	23
	Maximum	24.00
	80th percentile	20.88
	Median	19.56
	Mean	19.015

The majority of the 48 parcels on the DCHM are characterised by few pixels with small canopy heights and many with larger heights. This leads to height distributions per parcel that are skewed to the left. An example of such distribution is presented in Figure 10.12. Other distributions are presented in Figure 4.3, Chapter 4.

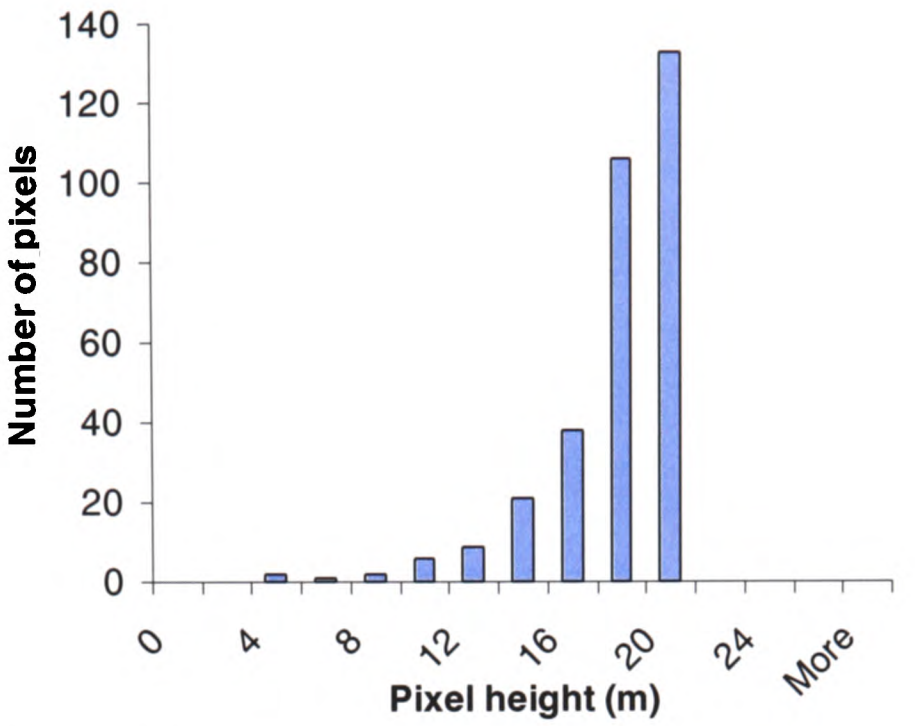


Figure 10.12: Distribution of pixel heights in a 20x20m^2 circular parcel on the DCHM. This parcel corresponds to plot no. 1 in stand 4. See also Figure 4.3 in Chapter 4.

In such non-Gaussian frequency distribution, the average and median are located below the mode. Whereas the two former statistics would underestimate the importance of larger trees on AGCC, the mode is also inappropriate since modal values depend on the resolution of the class interval selected. For instance, if the pixels are grouped in two meters intervals to locate a mode, some parcels (3.1, Figure 4.3) exhibit multi-modal or bimodal distributions. Thus other statistics need to be acquired. Various percentiles were thus extracted and tested.

Of all height metrics tested, the 80th percentile yielded the smallest sum of square errors and was thus selected (Table 10.6). Additionally, this metric provides larger weight to larger trees.

Table 10.6: Parameters and sum of square errors resulting from the calibration of the carbon model with the given height statistic.

Height statistics	**Average Height**	**60th**	**80th**	**Max**
a	30.99	23.90	19.19	12.42
b	0.118	0.123	0.125	0.132
SSE	35798	33765	32981	34757

The AGCC results derived from using the 80th percentile per parcel are shown in Chapter 4. The results from the parcel level were then upscaled to the entire woodland using two different approaches (Figure 10.13). Firstly, the results at the plot level were upscaled to the stand level and from the five stands to the entire woodland. The second approach makes use of the LiDAR dataset covering the entire woodland. The woodland is divided into rectangular grids cells of 20x20 m^2 and the AGCC is estimated on a per grid cell basis.

These two contrasting approaches are schematised in Figure 10.13. The results and a discussion of the implications of using the different approaches are presented in Chapter 4.

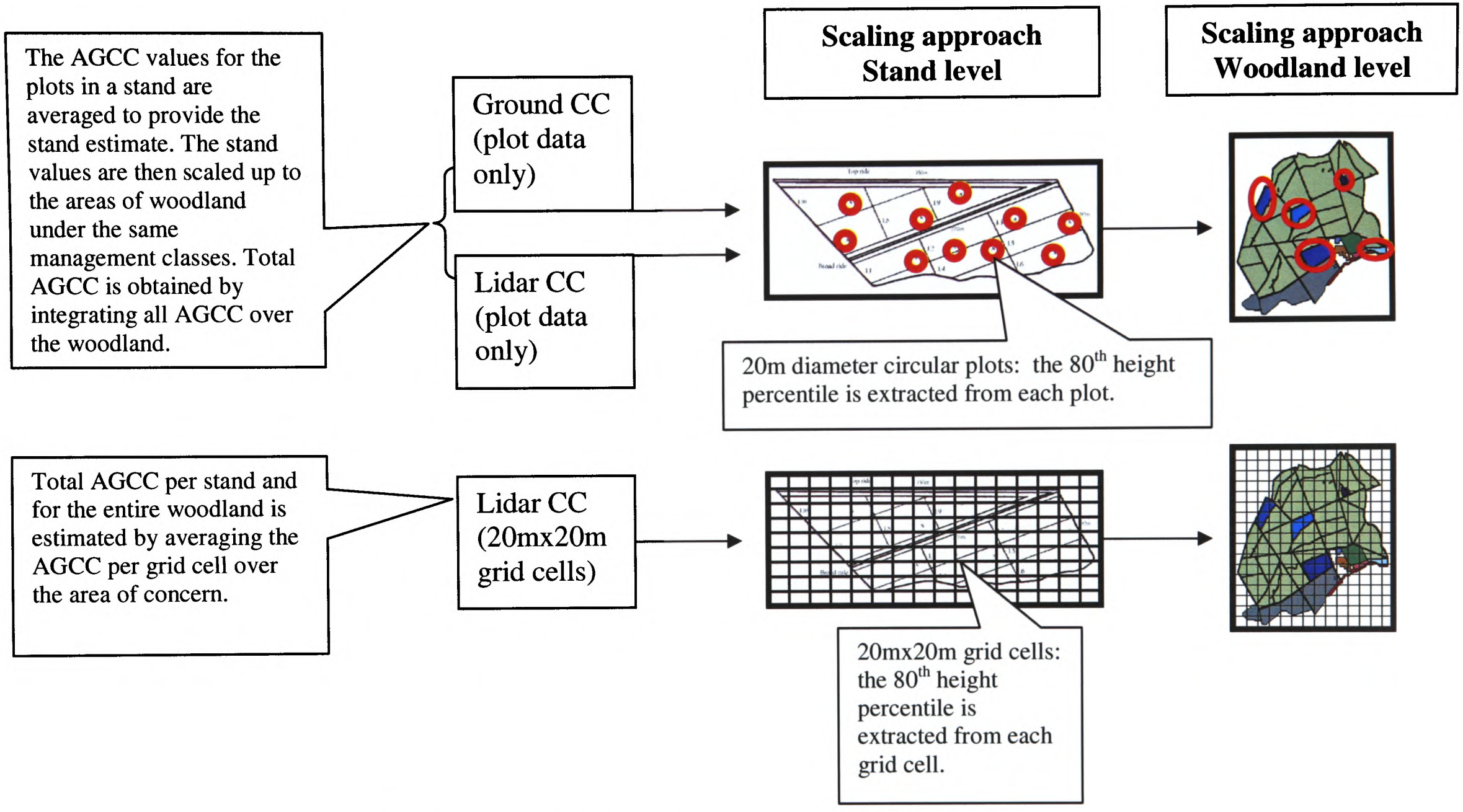


Figure 10.13: Approaches for scaling up the results to the woodland level

Prior to recommending such an approach as a potential technique for future verification of carbon stocks in forest ecosystems, further research on uncertainty is required. The principal sources of uncertainties were categorised as:

(i) The precision of the LiDAR instrument.

(ii) Interpolating LiDAR sample points to a 1x1 m^2 raster surface

(iii)Differentiating between LiDAR returns from the ground to returns arising from ground vegetation or above-ground surfaces.

(iv)Matching spatially the location of the field plots to the circular parcels drawn on the DCHM

(v) Selecting a single height metric as surrogate for the total above-ground carbon content of a plot

(vi)Using a generic model and conversion factors for estimating above-ground carbon content from canopy height estimates.

Although an exhaustive quantification of uncertainty has not yet been conducted, measures were taken to reduce these as far as practicable. Uncertainty sources (i), (ii) and (iii) were reduced by calibrating the DCHM with elevation measurements taken using an electronic total station (laser theodolite, Section 4.2.4, Chapter 4). These reference measurements with an electronic total station were of higher precision than that collected with the LiDAR instrument (see Chapter 4). A total of 82 canopy heights measurements were collected across the woodland. It is important to note that these height measurements were taken independently from the field-based dominant heights measured per plots. The reference height measurements were taken outside the plots and across the woodland in order to test the accuracy of the LiDAR DCHM and to calibrate this dataset.

The results presented in Chapter 4, Sections 4.3.1 and 4.3.2 show that the LiDAR DCHM underestimated reference canopy heights by 2.12 and 1.02 metres in average for trees and shrubs respectively. The following model was therefore used to calibrate the DCHM, thereby removing the average error in LiDAR tree and shrub canopy height estimates (Equation 1, Figure 4.2, Chapter 4): $H_{DCHM}' = bH_{DCHM}$

Where:

$b = 1.19 = \sum H_R / \sum H_{DCHM}$

H_{DCHM}' = Calibrated pixel height

H_{DCHM} = Pixel height

H_R = Theodolite canopy height

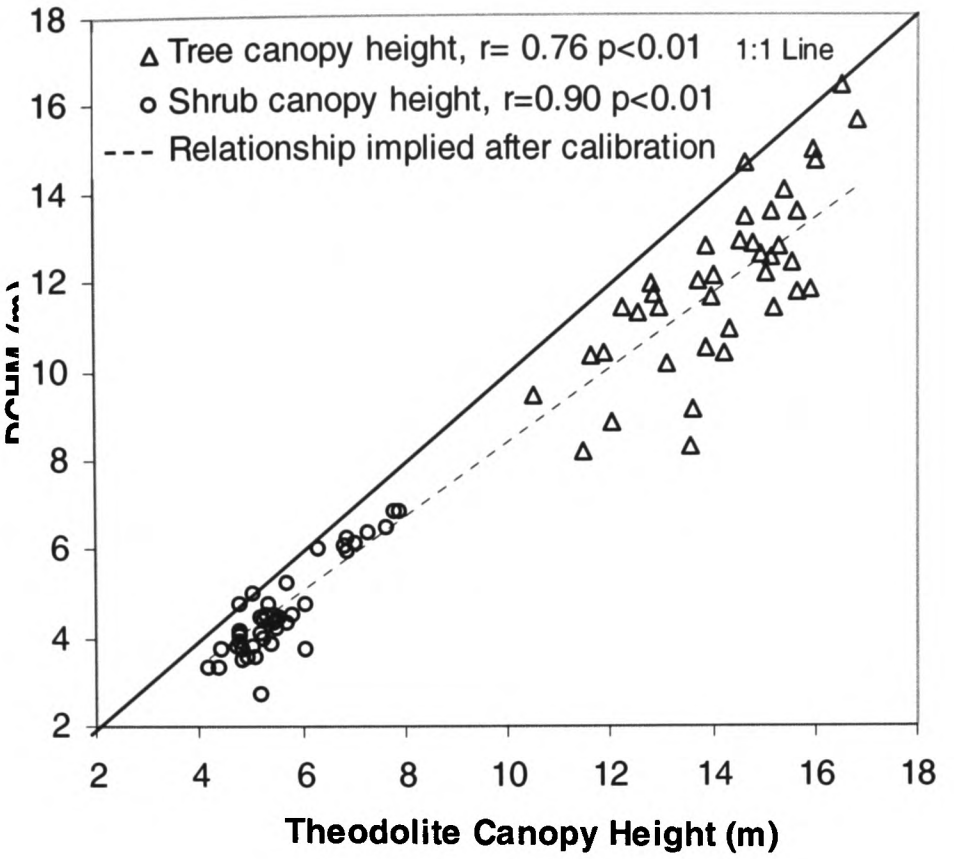


Figure 10.14: Replica of Figure 4.2, Chapter 4: Lidar against reference canopy height estimates (m).

This model was applied to all pixels in the DCHM. However, further analysis of the residuals between reference and LiDAR canopy heights revealed an additional non-random component of the error of unknown origin. This is shown more explicitly in Figure 10.15 below. The calibration procedure described above enabled the removal of the average residual. However, a linear relationship between residuals and DCHM canopy height was found to remain for trees and shrubs. After calibration, the DCHM underestimates reference canopy height of small trees and shrubs. Conversely, as canopy height increases, DCHM overestimates reference height.

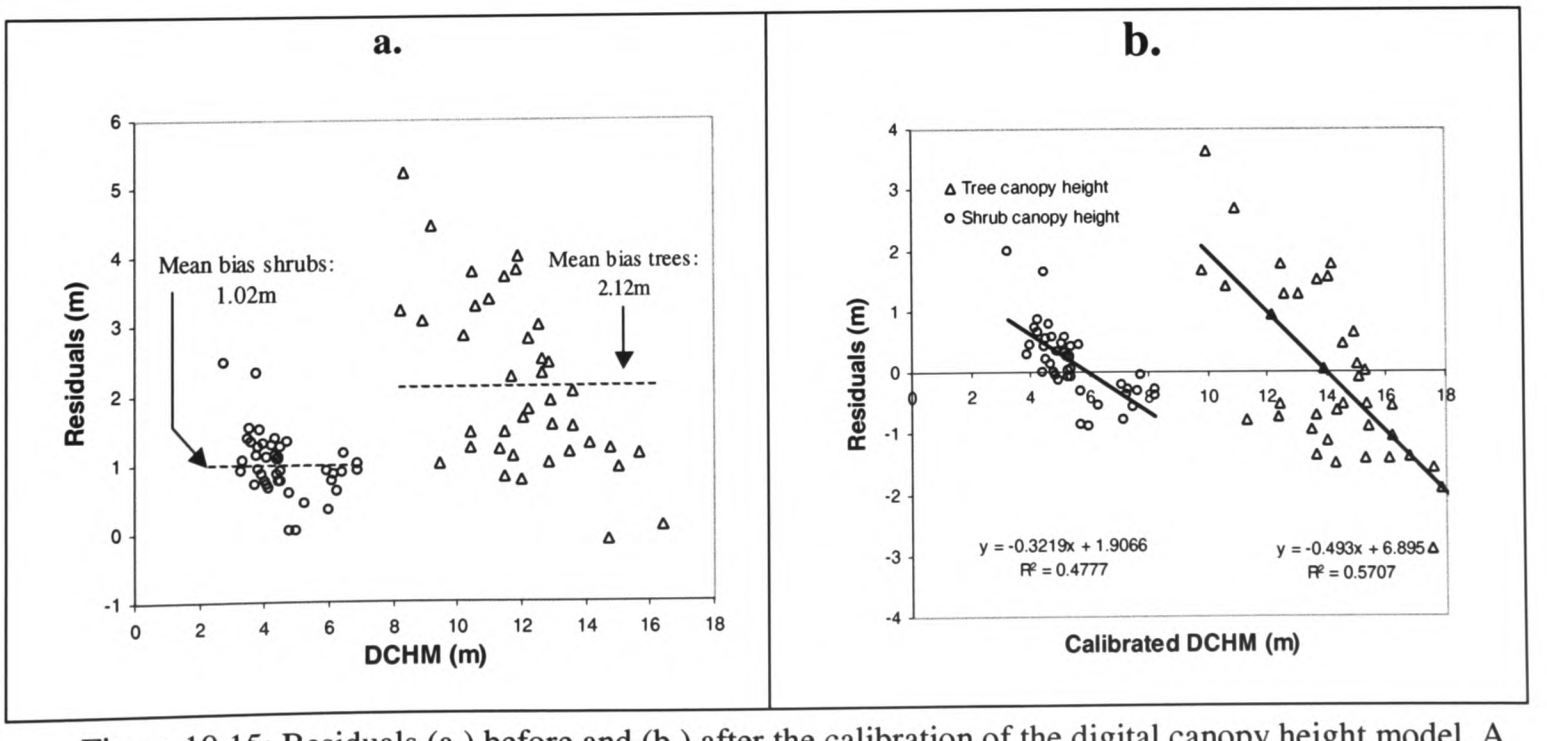


Figure 10.15: Residuals (a.) before and (b.) after the calibration of the digital canopy height model. A remaining systematic error can be observed in (b.) for both shrubs and tree canopy heights.

Further investigation is required to identify the origins of this pattern as the source of this remaining systematic error remains unknown.

Uncertainties arising from (iv) and (v) were minimised by adopting the following strategies. To address (iv), various methods for locating the plots as accurately as practicable on the DCHM were tested (Section 10.3). The most coherent approach given the available data was selected. For (v), several height metrics were tested and that providing the least sum of square errors was selected (Section 10.7). Finally, to tackle (vi), the biomass expansion and conversion factors were either derived from data collected in Monks Wood or from studies conducted in woodland of similar species composition and structure as Monks Wood. A complete uncertainty assessment integrating all these sources of errors nevertheless remains to be completed and forms the basis for future research.

Appendix D

Some useful definitions

DEFINITIONS	
Accuracy	Degree to which the mean of a sample approaches the true mean of the population (Watson *et al.* 2000).
Allometry	Relationship between a dependant variable and an independent variable (e.g. Y= aX + B ; where Y is the dependant variable, a and b are the parameters and X is the independent variable).
Autotrophic respiration	Release of CO_2 by plants.
Bandwidth	The wavelength interval recorded by a detector. Also called spectral resolution.
Basal area/ ha	The sum of the overbark cross-sectional area of the stems of all live trees measured at breast height and given in square meters per hectare.
Baseline	A reference scenario against which a change in greenhouse gas emissions or removal is measured (Watson *et al.* 2000).
Basic density	Weight of oven dry wood expressed relative to its volume. Volume multiplied by basic density gives dry weight.
Carbon flux	Transfer of carbon from one carbon pool to another in units of measurements of mass per unit area and time (e.g. t C ha^{-1} yr^{-1}) (Watson *et al.* 2000).
Carbon pool or reservoir	A system which has the the capacity to accumulate of release carbon. Examples of carbon pools are forest biomass, wood products, soils and atmosphere. The units are mass (e.g. t C) (Watson *et al.* 2000).
Carbon sink	Any process or mechanism which removes a greenhouse gas, and aerosol or a precursor of a greenhouse gas from the atmosphere. A given pool or reservoir can be a sink for atmospheric carbon if during a given time interval, more carbon is flowing into it than is flowing out (Watson *et al.* 2000).
Carbon source	Opposite of sink. A carbon pool (reservoir) can be a source of carbon to the atmosphere if less carbon is flowing into it thank is flowing out of it (Watson *et al.* 2000).
Carbon-trading	Domestic and international trading in emission reduction units, including the specification of trading in carbon credits by accumulating carbon in biomass. Trading in options to buy credits has already begun and mostly involves large plantation owners (mainly state government organisations) and large emitters of carbon (e.g. electricity generators). Price estimates per tonne CO_2 equivalent (CO_{2e}) vary from $8 to $48 per tonne CO_2.
Coppice	Young trees that are cut back to ground level on a regular cycle (traditionally 7-25 years) encouraging the growth of multiple shoots.

Cropland Management	The system of practices on land on which agricultural crops are grown and on land that is set aside of temporarily not being used for crop productions (FCCC/CP/2001/13/Add.1 p.59, UNFCCC, 2001)
Diameter at Breast height	The diameter of a stem at approximately 1.4 m above-ground level.
Dry weight	See basic density.
Forest Management	A system of practices for stewardship and use of forest land aimed at fulfilling relevant ecological (including biological diversity), economic and social functions of the forest in a sustainable manner (FCCC/CP/2001/13/Add.1 P.59) (UNFCCC, 2001).
Gap fraction	The portion of unobstructed sky.
Grassland Management	The system of practices on land-used for livestock production aimed at manipulating the amount and type of vegetation and livestock produced (FCCC/CP/2001/13/Add.1 P.59) (UNFCCC, 2001).
Gross Primary Productivity	Uptake of carbon by plants without taking into account autotrophic respiration.
Heterotrophic respiration	Release of CO_2 by substrate through decomposition of organic matter.
Hyperspectral scanners	A Special type of multispectral scanner that records many tens of bands of imagery at very narrow bandwidth.
Multispectral scanner	Remote sensing system that acquires simultaneously images of the same scene at different wavelengths.
Net Primary Productivity	Uptake of carbon by plants minus autotrophic respiration.
Plot	The smallest experimental sampling unit (a square of area $20m^2$ in this study), presented as evidence from the larger whole (the stand) from which it is taken.
Precision	The repeatability of a measurement (e.g. the standard error of the sample mean) (Watson *et al.* 2000).
Reflectance	Ratio of the radiant energy reflected by a body to the energy incident on it.
Spectral resolution	See bandwidth.
Ride	A forest track or path.
Rotation	The time between planting and harvesting of a forest stand.
Stand	An identifiable compartment of trees occurring in a particular area, which is relatively homogeneous in species composition and structure, and cannot be subdivided into more homogeneous and mappable units.
Standard	A mature tree with single stem (i.e. of non-coppice origin) growing above coppice.

Timber volume	The merchantable volume of wood in a tree, i.e. the main stem up to a height at which it is only 7cm DBH overbark, or to the point at which no main stem is distinguishable, whichever comes first.
Top height	A measure of the height of a stand, defined as the average total height of the 100 trees of the largest DBH per hectare.
Total height	The vertical distance from the base of the tree to the upper most point.
Total volume	Total volume of wood in a tree including all branchwood.
Uptake, storage or sequestration	The addition of carbon to a pool (other than the atmosphere) (Watson *et al.* 2000).
Waveband	A subdivision within an electromagnetic region. For example, the visible region is subdivided into the blue, green and red bands.